

INHIBITORY ACTIVITY OF METABOLITES FROM MANGOSTEEN ROOTS *Garcinia mangostana* L. ON HEPATOCELLULAR CARCINOMA AND COLON CANCER CELL GROWTH



A Thesis Submitted in Partial Fulfillment of the Requirements
for the Degree of Master of Science in Biotechnology
Common Course
FACULTY OF SCIENCE
Chulalongkorn University
Academic Year 2020
Copyright of Chulalongkorn University

ฤทธิ์ยับยั้งของสารเมทาบอลิต์จากรากมังคุด *Garcinia mangostana* L. ต่อการเจริญของ
เซลล์มะเร็งตับและมะเร็งลำไส้



วิทยานิพนธ์นี้เป็นส่วนหนึ่งของการศึกษาตามหลักสูตรปริญญาวิทยาศาสตรมหาบัณฑิต
สาขาวิชาเทคโนโลยีชีวภาพ ไม่สังกัดภาควิชา/เทียบเท่า
คณะวิทยาศาสตร์ จุฬาลงกรณ์มหาวิทยาลัย
ปีการศึกษา 2563
ลิขสิทธิ์ของจุฬาลงกรณ์มหาวิทยาลัย

Thesis Title	INHIBITORY ACTIVITY OF METABOLITES FROM MANGOSTEEN ROOTS <i>Garcinia mangostana</i> L. ON HEPATOCELLULAR CARCINOMA AND COLON CANCER CELL GROWTH
By	Miss Kedkran Koopklang
Field of Study	Biotechnology
Thesis Advisor	Professor KHANITHA PUDHOM, Ph.D.
Thesis Co Advisor	NATTHAYA CHUAYPEN, Ph.D.

Accepted by the FACULTY OF SCIENCE, Chulalongkorn University in Partial
Fulfillment of the Requirement for the Master of Science

..... Dean of the FACULTY OF SCIENCE
(Professor POLKIT SANGVANICH, Ph.D.)

THESIS COMMITTEE

..... Chairman
(Professor VUDHICHAJ PARASUK, Ph.D.)

..... Thesis Advisor
(Professor KHANITHA PUDHOM, Ph.D.)

..... Thesis Co-Advisor
(NATTHAYA CHUAYPEN, Ph.D.)

..... Examiner
(Associate Professor NATTAYA NGAMROJANAVANICH,
Ph.D.)

..... External Examiner
(Associate Professor Prasat Kittakoop, Ph.D.)

เกตุกานต์ ภูปกกลาง : ฤทธิ์ยับยั้งของสารเมทาบอลิต์จากรากมังคุด *Garcinia mangostana* L. ต่อการเจริญของเซลล์มะเร็งตับและมะเร็งลำไส้. (INHIBITORY ACTIVITY OF METABOLITES FROM MANGOSTEEN ROOTS *Garcinia mangostana* L. ON HEPATOCELLULAR CARCINOMA AND COLON CANCER CELL GROWTH) อ.ที่ปรึกษาหลัก : ศ. ดร.ชนิษฐา พุดหอม, อ.ที่ปรึกษาร่วม : อ. ดร.ณัฐธยาน์ ช่วยเพ็ญ

มะเร็งตับถือเป็นหนึ่งในโรคที่ก่อให้เกิดการเสียชีวิตมากที่สุดทั้งทั่วโลกและในประเทศไทย เนื่องจากตับเป็นอวัยวะที่มีเลือดหล่อเลี้ยงเป็นจำนวนมาก เนื่องจากที่เพิ่มขึ้นในบริเวณตับจึงสามารถเจริญเติบโตและลุกลามไปยังอวัยวะข้างเคียงได้อย่างรวดเร็ว โดยกระบวนการที่เกิดขึ้นนี้เรียกว่ากระบวนการแพร่กระจายของเซลล์ มังคุด (*Garcinia mangostana* L.) หรือที่รู้จักกันโดยทั่วไปในชื่อราซินแห้งผลไม้ จัดเป็นพืชผลที่มีการศึกษาอย่างกว้างขวางเกี่ยวกับคุณสมบัติทางการแพทย์อย่างยาวนานนับตั้งแต่อดีต เนื่องจากมีองค์ประกอบกลุ่มหลัก xanthone เป็นเมทาบอลิต์ที่มีฤทธิ์ทางชีวภาพ อย่างไรก็ตาม รายงานเกี่ยวกับการศึกษาฤทธิ์ของสารประกอบกลุ่มอื่น ๆ ที่พบยังมีค่อนข้างน้อย ในการศึกษาครั้งนี้ สารเมทาบอลิต์ที่แยกได้จากรากมังคุดจะถูกนำไปวิเคราะห์ความเป็นพิษ ฤทธิ์ต่อการเจริญและการลุกลามของเซลล์มะเร็งตับ (HepG2 และ Huh7) และมะเร็งลำไส้ (Caco2 และ HCT-116) จากนั้น สารประกอบที่มีฤทธิ์ที่น่าสนใจจะถูกนำไปศึกษาต่อในระดับอนุชีววิทยาอย่างการยับยั้งการลุกลามของเซลล์มะเร็ง การศึกษาการตายแบบอะพอพโตซิส และ การวิเคราะห์ western blot

จากผลการศึกษา ส่วนสกัดหยาบเอทิลอะซิเตทจากรากมังคุดพบสารประกอบใหม่ 4 ตัว ได้แก่ mangostanone I – IV (สารประกอบ 1, 12, 13 และ 18) และสารประกอบที่มีการรายงานโครงสร้างแล้วอีก 18 ตัว ได้แก่ *a*-mangostin (2), *b*-mangostin (3), *g*-mangostin (4), mangostanaxanthone IV (5), dulxanthone D (6), toxyloxanthone B (7), 1,7-dihydroxy-3-methoxy-2-prenylxanthone (8), euxanthone (9), norathyriol (10), 8-deoxygartanin (11), maclurin (14), 2,3',4,6-tetrahydroxybenzophenone (15), mangaphenone (16), (2-hydroxy-4,6-dimethoxyphenyl)(3-hydroxy-4-methoxyphenyl)methanone (17), garciosine A (19), 4,5-dimethoxy[1,1'-biphenyl]-3-ol (20), 3-hydroxy-4-geranyl-5-methoxybiphenyl (21) และ epicatechin (22) จากการทดลองพบว่าสารประกอบหมายเลข 1, 2, 3, 5, 6, 11 และ 21 มีคุณสมบัติเหมาะสมในการยับยั้งการเกิดมะเร็ง เมื่อทดสอบกับเซลล์มะเร็งที่สนใจด้วยค่า IC₅₀ น้อยกว่า 50 mM และมีฤทธิ์ในการยับยั้งการลุกลามกับเซลล์มะเร็ง Huh-7 เมื่อใช้ชุดทดสอบอะพอพโตซิส Annexin V พบว่าสารประกอบ 1, 6 และ 11 มีความสามารถในการเหนี่ยวนำให้เกิดการตายแบบอะพอพโตซิสในเซลล์ Huh-7 ที่ความเข้มข้นแตกต่างกัน นอกจากนี้ จากการวิเคราะห์ western blot พบว่า การกระตุ้นการตายแบบอะพอพโตซิสของ 21 ในเซลล์ HepG2 เกิดจากการยับยั้งการแสดงออกของ Bcl-2

สาขาวิชา เทคโนโลยีชีวภาพ
ปีการศึกษา 2563

ลายมือชื่อนิสิต
ลายมือชื่อ อ.ที่ปรึกษาหลัก
ลายมือชื่อ อ.ที่ปรึกษาร่วม

6171917023 : MAJOR BIOTECHNOLOGY

KEYWORD: *Garcinia mangostana* L., hepatocellular carcinoma, colon cancer, antiproliferation, cytotoxicity

Kedkran Koopklang : INHIBITORY ACTIVITY OF METABOLITES FROM MANGOSTEEN ROOTS *Garcinia mangostana* L. ON HEPATOCELLULAR CARCINOMA AND COLON CANCER CELL GROWTH. Advisor: Prof. KHANITHA PUDHOM, Ph.D. Co-advisor: NATTHAYA CHUAYPEN, Ph.D.

Liver cancer is one of the most common deadliest diseases both worldwide and in Thailand. Because of its rich and dual blood supply, malignant tumors in the liver could grow proliferative and rapidly spread to another organ. This process was called Metastasis, the major cause of human death. Mangosteen (*Garcinia mangostana* L.) generally known as a queen of fruits, has been widely studied in medicinal applications for many decades, due to plenty of bioactive metabolites such as xanthenes as a major component. Nonetheless, reports about bioactivities of minor components were barely known. In this study, metabolites isolated from mangosteen roots were evaluated their cytotoxic property and antiproliferative against hepatocellular carcinoma (HepG2 and Huh-7) and colon (Caco2 and HCT-116) cancer cells. The remarkable compounds were further investigated in molecular biology, including cell migration, apoptosis assessment and western blot analyses.

As results, the EtOAc crude extract of mangosteen roots was afforded four new compounds: mangostanone I – IV (compounds 1, 12, 13 and 18) and eighteen known compounds: *a*-mangostin (2), *b*-mangostin (3), *g*-mangostin (4), mangostanaxanthone IV (5), dulxanthone D (6), toxylloxanthone B (7), 1,7-dihydroxy-3-methoxy-2-prenylxanthone (8), euxanthone (9), norathyriol (10), 8-deoxygartanin (11), maclurin (14), 2,3',4,6-tetrahydroxybenzophenone (15), mangaphenone (16), (2-hydroxy-4,6-dimethoxyphenyl)(3-hydroxy-4-methoxyphenyl)methanone (17), garciosine A (19), 4,5-dimethoxy[1,1'-biphenyl]-3-ol (20), 3-hydroxy-4-geranyl-5-methoxybiphenyl (21) and epicatechin (22). It was showed that compound 1, 2, 3, 5, 6, 11 and 21 accommodated potential effects in anticancer properties against investigated cell lines with IC₅₀ less than 50 mM and considerable anti-migration effects against Huh-7. Using Annexin V apoptosis kit, found out that compounds 1, 6 and 11 have an ability to increase apoptosis rate of cell Huh-7 in dose-dependent manner. In addition, western blot analysis revealed that apoptotic activation of 21 in HepG2 was mediated by selective suppression of Bcl-2 expression.

Field of Study: Biotechnology

Academic Year: 2020

Student's Signature

Advisor's Signature

Co-advisor's Signature

ACKNOWLEDGEMENTS

I would like to express my gratitude towards my advisor, Professor Dr. Khanitha Pudhom, Department of Chemistry, Faculty of Science, Chulalongkorn University and my co-advisor, Dr. Natthaya Chuaypen, Department of Biochemistry, Faculty of Medicine, Chulalongkorn University for all of their instructions and immense knowledge. Their guidance helps me to pass through this research successfully.

Besides, I would like to thank my thesis committees: Associate Professor Dr. Vudhichai Parasuk from Department of Chemistry, Faculty of Science, Chulalongkorn University as my Chairperson, Associate Professor Dr. Nattaya Ngamrojanavanich from Department of Chemistry, Faculty of Science, Chulalongkorn University and Associate Professor Dr. Prasat Kittakoop from Chulabhorn Graduate Institute as my examiners, for their encouragement, insightful comments and suggestions.

I am really grateful and appreciate every member in KP lab for their kind friendship especially our postdoc, Dr. Siwattra Choodej for willingly helping and sharing valuable knowledge in the field of study I never knew.

Lastly, thanks to the 90th Anniversary of Chulalongkorn University Fund for financial support to conduct this research.

จุฬาลงกรณ์มหาวิทยาลัย
CHULALONGKORN UNIVERSITY

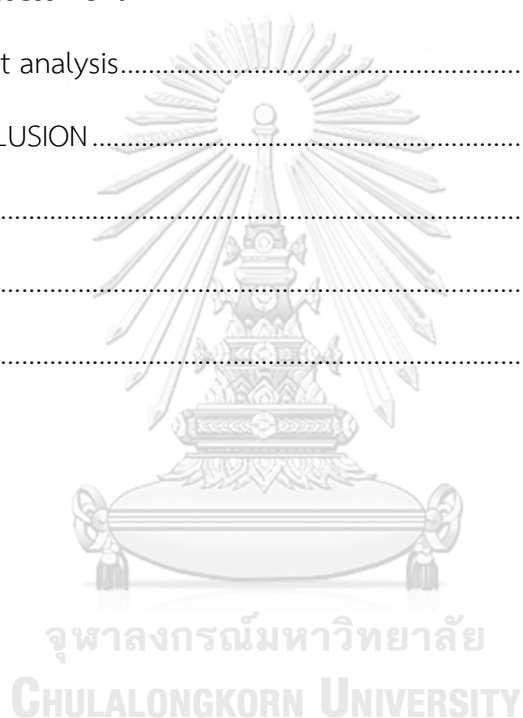
Kedkran Koopklang

TABLE OF CONTENTS

	Page
ABSTRACT (THAI).....	iii
ABSTRACT (ENGLISH).....	iv
ACKNOWLEDGEMENTS	v
TABLE OF CONTENTS	vi
LIST OF FIGURES	ix
LIST OF SCHEMES	xi
LIST OF TABLES	xii
LIST OF ABBREVIATIONS	xiii
CHAPTER I INTRODUCTION.....	1
1.1 Introduction of cancer.....	1
1.2 Introduction of <i>Garcinia mangostana</i> L.....	3
1.3 Literature reviews.....	6
1.4 Objectives of the present study.....	7
CHAPTER II EXPERIMENTAL.....	9
2.1 Plant Materials	9
2.2 General Experimental Procedures	9
2.2.1 Thin-layer chromatography (TLC).....	9
2.2.2 Column chromatography (CC).....	9
2.2.3 High performance liquid chromatography (HPLC).....	9
2.2.4 Nuclear magnetic resonance spectroscopy (NMR).....	9
2.2.5 Mass spectrometry (MS)	9

2.2.6 Fourier transforms infrared spectrophotometer (FT-IR).....	10
2.2.7 Melting point.....	10
2.2.8 Microplate reader	10
2.3 Chemicals and reagents.....	10
2.3.1 Solvents	10
2.4 Extraction and Isolation	10
2.5 Cell culture.....	17
2.6 Cytotoxicity assay.....	17
2.7 Migration analysis	17
2.8 Apoptosis assessment.....	18
2.9 Western blot assay.....	18
2.10 Statistical analysis	19
CHAPTER III RESULTS AND DISCUSSION.....	20
3.1 Isolated compounds from mangosteen (<i>G. mangostana</i>) roots.....	20
3.2 Structure elucidation of isolated compounds.....	21
3.2.1 Structure elucidation of compound 1	21
3.2.2 Structure elucidation of compounds 2, 3 and 4	23
3.2.3 Structure elucidation of compound 5	24
3.2.4 Structure elucidation of compound 6	25
3.2.5 Structure elucidation of compound 7	28
3.2.6 Structure elucidation of compound 8	29
3.2.7 Structure elucidation of compounds 9 and 10.....	29
3.2.8 Structure elucidation of compound 11	30
3.2.9 Structure elucidation of compounds 12 – 17	33

3.2.10	Structure elucidation of compounds 18 – 20.....	38
3.2.11	Structure elucidation of compound 21.....	40
3.2.12	Structure elucidation of compound 22.....	43
3.3	Cytotoxic activity of isolated compounds.....	44
3.4	Anti-migration effect of compounds 1, 2, 3, 5, 6, 11 and 21 against HCC cell (Huh7).....	46
3.5	Apoptosis assessment.....	53
3.6	Western blot analysis.....	57
CHAPTER IV	CONCLUSION.....	59
REFERENCES	61
APPENDIX	66
VITA	130



LIST OF FIGURES

	Page
Figure 1.1 Start of cells multiplies and becoming cancer	1
Figure 1.2 Clinical algorithm of hepatocellular carcinoma.....	2
Figure 1.3 Characteristic of mangosteen (<i>Garcinia mangostana</i> L.).....	3
Figure 1.4 Classification of <i>Garcinia mangostana</i> L.....	4
Figure 1.5 Structures of isolated xanthenes from mangosteen.....	5
Figure 1.6 Structure of isolated flavonoid from mangosteen.....	5
Figure 1.7 Structures of isolated anthocyanins from mangosteen.....	6
Figure 1.8 Structures of isolated benzophenones from mangosteen.....	6
Figure 3.1 Structures of isolated compounds from mangosteen roots.....	20
Figure 3.2 Structure of compound 1.....	21
Figure 3.3 selected HMBC correlations ($^1\text{H} \rightarrow ^{13}\text{C}$) of compound 1.....	22
Figure 3.4 Structures of compounds 2, 3 and 4.....	23
Figure 3.5 Structure of compound 5.....	24
Figure 3.6 Structure of compound 6.....	25
Figure 3.7 Structure of compound 7.....	28
Figure 3.8 Structure of compound 8.....	29
Figure 3.9 Structures of compounds 9 and 10.....	29
Figure 3.10 Structure of compound 11.....	30
Figure 3.11 Structures of compounds 12 – 17.....	33
Figure 3.12 Selected HMBC correlations ($^1\text{H} \rightarrow ^{13}\text{C}$) of compound 12.....	34
Figure 3.13 Selected HMBC correlations ($^1\text{H} \rightarrow ^{13}\text{C}$) of compound 13.....	35
Figure 3.14 Structures of compounds 18 – 20.....	38
Figure 3.15 Selected HMBC correlations ($^1\text{H} \rightarrow ^{13}\text{C}$) of compound 18.....	39
Figure 3.16 Selected HMBC correlations ($^1\text{H} \rightarrow ^{13}\text{C}$) of compound 20.....	40
Figure 3.17 Structure of compound 21.....	40
Figure 3.18 Structure of compound 22.....	43
Figure 3.19 Wound closure of untreated cells and cells treated with sorafenib	

(3 μM) at 0, 24 and 48 h.....	47
Figure 3.20 Effect of compound 1 on wound closure at 0, 24 and 48 h (a), graph correlation between times and %tissue repair (b).....	48
Figure 3.21 Effect of compound 2 on wound closure at 0, 24 and 48 h (a), graph correlation between times and %tissue repair (b).....	49
Figure 3.22 Effect of compound 3 on wound closure at 0, 24 and 48 h (a), graph correlation between times and %tissue repair (b).....	50
Figure 3.23 Effect of compound 5 on wound closure at 0, 24 and 48 h (a), graph correlation between times and %tissue repair (b).....	50
Figure 3.24 Effect of compound 6 on wound closure at 0, 24 and 48 h (a), graph correlation between times and %tissue repair (b).....	51
Figure 3.25 Effect of compound 11 on wound closure at 0, 24 and 48 h (a), graph correlation between times and %tissue repair (b).....	52
Figure 3.26 Effect of compound 21 on wound closure at 0, 24 and 48 h (a), graph correlation between times and %tissue repair (b).....	53
Figure 3.27 Apoptosis profile (a) and apoptosis rate (%) (b) of compound 1 on Huh-7 cells in 12 and 24 μM	54
Figure 3.28 Apoptosis profile (a) and apoptosis rate (%) (b) of compound 5 on Huh-7 cells in 12 and 24 μM	55
Figure 3.29 Apoptosis profile (a) and apoptosis rate (%) (b) of compound 6 on Huh-7 cells in 12 and 24 μM	56
Figure 3.30 Apoptosis profile (a) and apoptosis rate (%) (b) of compound 21 on Huh-7 cells in 12 and 24 μM	57
Figure 3.31 Effect of compound 21 on Bcl-2 and Bcl-XL protein expression.....	58

LIST OF SCHEMES

	Page
Scheme 2.1 The extraction procedure of powdered mangosteen roots.....	11
Scheme 2.2 The isolation procedure of fraction H.....	12
Scheme 2.3 The isolation procedure of fractions B, C, and E.....	13
Scheme 2.4 The isolation procedure of fractions G and J.....	14
Scheme 2.5 The isolation procedure of fraction F.....	15
Scheme 2.6 The isolation procedure of fraction D.....	16



LIST OF TABLES

	Page
Table 3.1 ^1H NMR data of compounds 1 – 6	26
Table 3.2 ^{13}C NMR data of compounds 1 – 6	27
Table 3.3 ^1H NMR data of compounds 7 – 11	31
Table 3.4 ^{13}C NMR data of compounds 7 – 11	32
Table 3.5 ^1H NMR data of compounds 12 – 17	36
Table 3.6 ^{13}C NMR data of compounds 12 – 17	37
Table 3.7 ^1H NMR data of compounds 18 – 21	41
Table 3.8 ^{13}C NMR data of compounds 18 – 21	42
Table 3.9 NMR spectral data of compound 22 in acetone- d_6	43
Table 3.10 Cytotoxic activity of compounds 1 – 22 against HCC and colon cancer cells.....	45
Table 3.11 Concentrations used for wound healing analysis of compound 1, 2, 3, 5, 6, 11 and 21	47
Table 3.12 Tissue repair percentage value (%) of compound 1	48
Table 3.13 Tissue repair percentage value (%) of compound 2	49
Table 3.14 Tissue repair percentage value (%) of compound 3	50
Table 3.15 Tissue repair percentage value (%) of compound 5	51
Table 3.16 Tissue repair percentage value (%) of compound 6	51
Table 3.17 Tissue repair percentage value (%) of compound 11	52
Table 3.18 Tissue repair percentage value (%) of compound 21	53
Table 4.1 Data summaries of compounds 1, 2, 3, 5, 6, 11 and 21	60

LIST OF ABBREVIATIONS

J	Coupling constant
δ	Chemical shift
δ_{H}	Chemical shift of proton
δ_{C}	Chemical shift of carbon
s	Singlet (for NMR spectra)
d	Doublet (for NMR spectra)
dd	Doublet of doublet (for NMR spectra)
t	Triplet (for NMR spectra)
m	Multiplet (for NMR spectra)
q	Quartet (for NMR spectra)
brs	Broad singlet (for NMR spectra)
calcd.	Calculated
^1H NMR	Proton nuclear magnetic resonance
^{13}C NMR	Carbon-13 nuclear magnetic resonance
2D NMR	Two dimensional nuclear magnetic resonance
^1H - ^1H COSY	Homonuclear (proton-proton) correlation spectroscopy
NOESY	Nuclear overhauser effect spectroscopy
HSQC	Heteronuclear single quantum coherence
HMBC	Heteronuclear multiple bond correlation
HRESIMS	High resolution electrospray ionization mass spectrometry
CC	Column chromatography
TLC	Thin layer chromatography
IC ₅₀	Half maximal inhibitory concentration
CDCl ₃	Deuterated chloroform

MeOH	Methanol
EtOH	Ethanol
CH ₂ Cl ₂	Dichloromethane
EtOAc	Ethyl acetate
DMSO	Dimethylsulfoxide
(NH ₄) ₆ Mo ₇ O ₂₄	Ammonium molybdate
H ₂ SO ₄	Sulfuric acid
SiO ₂	Silicon dioxide
g	Gram (s)
mg	Milligram (s)
ml	Milliliter (s)
μg	Microgram (s)
μl	Microliter (s)
μM	Micromolar
mM	Millimolar
L	Liter (s)
M	Molar
min	Minute
h	Hour
m	Meter (s)
mm	Millimeter (s)
cm	Centimeter (s)
nm	Nanometer
Hz	Hertz
cm ⁻¹	Reciprocal centimeter (unit of wave number)
NMR	Nuclear magnetic resonance
MS	Mass spectrometry

IR	Infrared
UV	Ultraviolet
$[M+Na]^+$	Pseudomolecular ion
λ_{\max}	Wavelength of maximum absorption
ϵ	Molar extinction coefficient
$^{\circ}\text{C}$	Degree celcius
spp.	Species



CHAPTER I

INTRODUCTION

1.1 Introduction of cancer

Cancer is a disease refers to abnormal cells develop and multiply uncontrollable rapidly. The abnormal cells then form a mass and become malignant tumor which could spread to other organs via blood and lymphatic system. According to World Health Organization (WHO), cancer is the second leading cause of human death worldwide. The number of death estimated 9.6 million deaths in 2018 and still increase in every year. Nowadays, there are many ways to prevent cancer but the treatment to cure completely is still none exist.

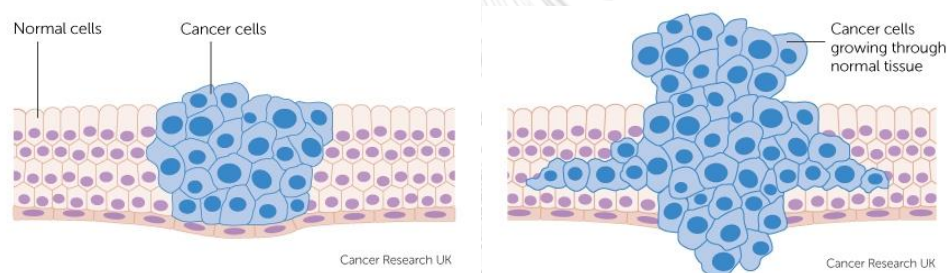


Figure 1.1 Start of cells multiplies and becoming *cancer*

(Courtesy to <https://www.cancerresearchuk.org/about-cancer/what-is-cancer>)

Hepatocellular carcinoma (HCC) is number one deadliest disease in Thailand from the report of Ministry of Public Health. The risk factors for cancer are various, it could be from environment, life routine and human genetic. Interestingly, carcinogenic infection from human papillomavirus (HPV), hepatitis B and C virus could lead approximately 25% to 40% to HCC even though the mechanism underlying progression still remains unclear. According to Thailand-based Cancer Registry reported, in 2015, liver cancer accounted for 15,912 patients out of 20,617 new cancer cases to deaths. Moreover, it occurs more often in men than women. Despite metastatic liver cancer being the most frequently seen type, for instance, spreading from breasts or colons, hepatocellular carcinoma (HCC) is also the most common

primary cancer account for 80% of all primary liver cancers. This is due to the typically late diagnosis with a median survival following diagnosis of approximately 6 to 20 months [1]. Currently, general drugs approved by the Food and Drug Administration (FDA) for liver cancer are extensively depends on patient's symptoms. For examples, sorafenib tosylate, a kinase inhibitor drug is used with the HCC that cannot be removed by surgery, and bevacizumab, an angiogenesis inhibitor is given to patients who have not received systemic therapy or in metastatic stage [2].

In addition, liver cancer has been grouping into five stages to prevent medical intervention harms in patients with cirrhosis. As **Figure 1.2** showed, liver cancer metastasis appears in fourth of five stages classified as Advanced stage. This meaning that liver cancer could spread from origin to other organs. For explanation, metastasis occurs when the primary cancer travels from its original place through the bloodstream and lymph node, then forms a secondary or metastatic tumor in the nearest organs. More importantly, HCC has a high recurrent rate of intrahepatic metastatic spread [3] as well as extrahepatic metastasis to the colon [4]. Thus, this could estimate lessen of survival time in patient with around 11 – 13 months in nearly last stage.

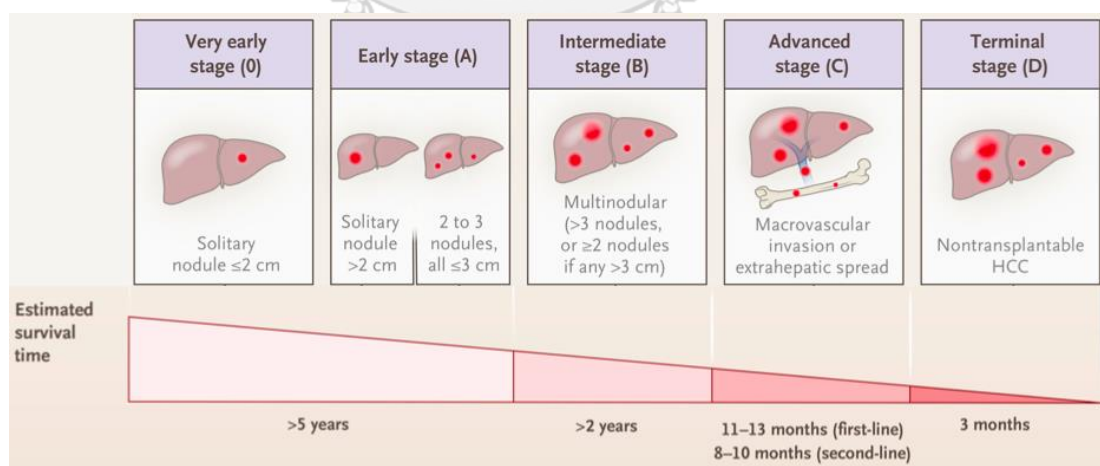


Figure 1.2 Clinical algorithm of hepatocellular carcinoma

(Courtesy to <https://www.nejm.org/doi/full/10.1056/NEJMra1713263>)

Nowadays, there are many treatments use to fight cancer, such as immunotherapy, radiation therapy, or targeted therapy. However, among various treatments, chemotherapy is the most often use to treat cancers. In addition, more than 50% of chemotherapeutic drugs are natural compounds. This is due to a fewer toxicity and side-effects against normal cells [5].

1.2 Introduction of *Garcinia mangostana* L.

Mangosteen (*Garcinia mangostana* L.), a large perennial plant with lushes of leathery thick leaves, grown well and widely in tropical weather countries specially in Southeast Asia. It is known as ‘Queen of fruits’ due to the unique sweet-but-sour taste and the round, dark purplish appearance with thick green sepals arranged like a crown [6].



Figure 1.3 Characteristic of mangosteen (*Garcinia mangostana* L.)
(Courtesy to <https://lunti.ph/products/mangosteen-grafted-seedling>)

The taxonomy hierarchy of mangosteen was classified by scientist as **Figure 1.4** described below.

Kingdom: Plantae
Division: Tracheophyta
Class: Magnoliopsida
Order: Malpighiales
Family: Clusiaceae
Genus: *Garcinia* L.
Species: *Garcinia mangostana* L.

Figure 1.4 Classification of *Garcinia mangostana* L.

Additionally, not only a flavor that makes mangosteen becomes well known but also because of its variety in medicinal applications. In many countries including Thailand, mangosteen has been used as a traditional medicine for recent past. Various parts from the mangosteen plant can be used in numerous ways. For instance, extracts of ripening fruits were used for diarrhea treatment, whereas stem barks were used for wound infection treatment [7]. Nowadays, there are prevalent researches and studies about metabolite compositions from mangosteen. The most common classes found are xanthenes with α - and β -mangostin as major components (**Figure 1.5**). These compounds have been reported with many beneficial bioactivities such as anti-oxidation, anti-inflammatory, antimicrobial and anticancer [8]. Mangosteen also contains other class compositions, for examples, flavonoids (**Figure 1.6**), anthocyanins (**Figure 1.7**) and benzophenones (**Figure 1.8**) [9].

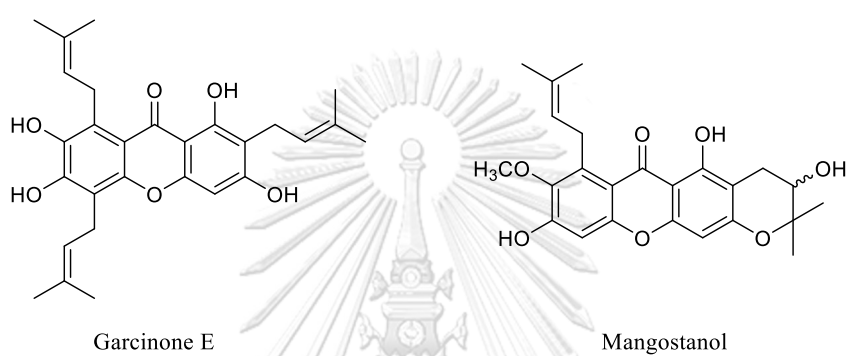
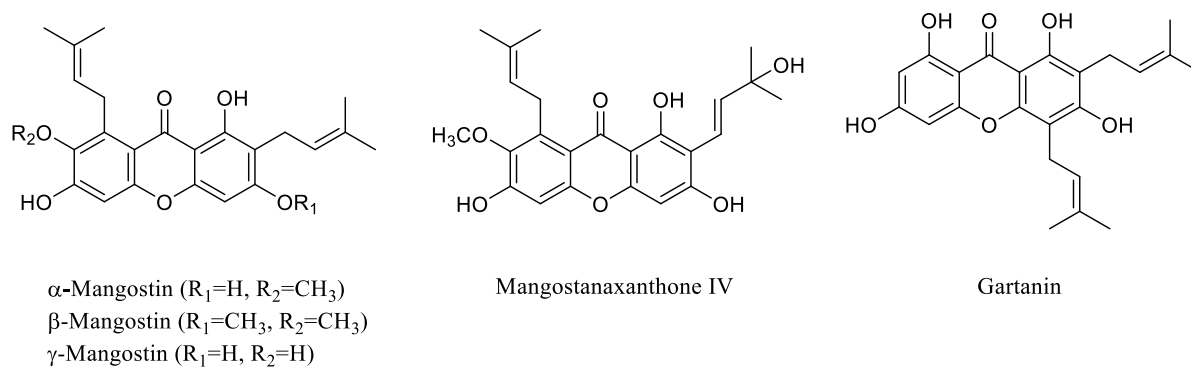


Figure 1.5 Structures of isolated xanthones from mangosteen

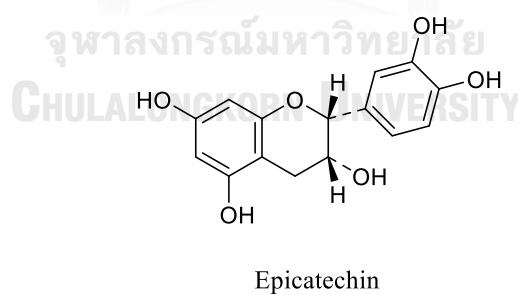


Figure 1.6 Structure of isolated flavonoid from mangosteen

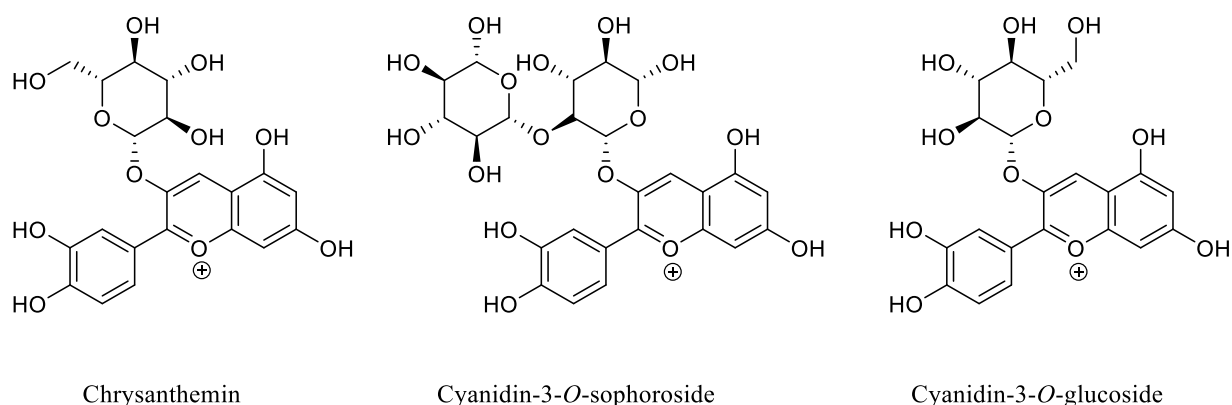


Figure 1.7 Structures of isolated anthocyanins from mangosteen

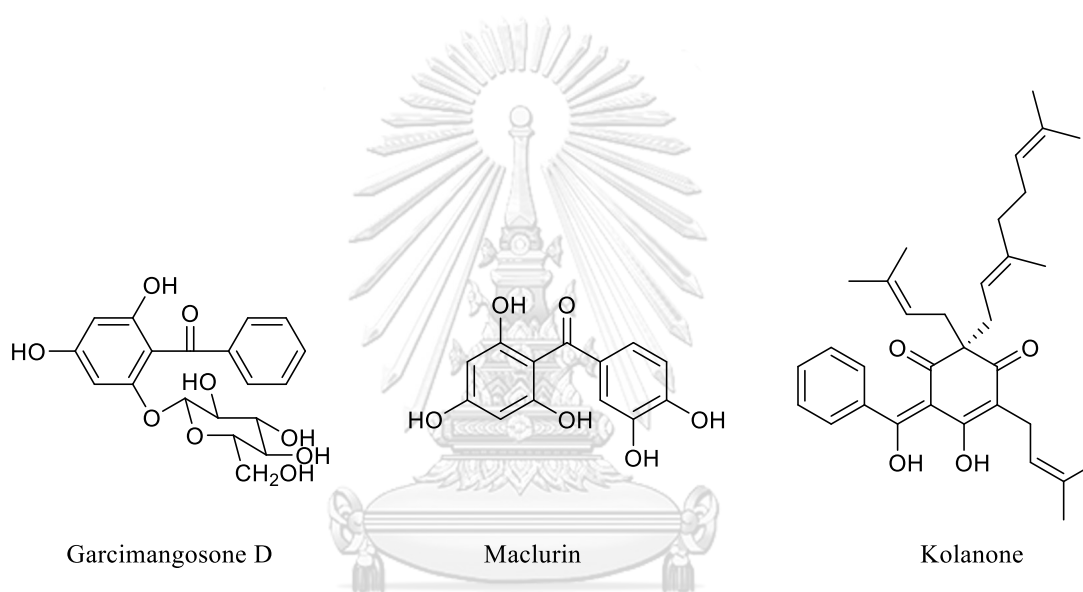


Figure 1.8 Structures of isolated benzophenones from mangosteen

1.3 Literature reviews

Many previous researches have been studied about the bioactivities of xanthenes especially with α -mangostin. Because of it being easily found, this largest constituent α -mangostin was used to study for medicinal usages. One of the common study is anticancer activity. To demonstrate that, α -mangostin was applied with various cancer cell lines. As a result, α -mangostin could prevent and inhibit proliferation of many cancer cells such as colorectal, hepatocellular, and breast cancer cells [10].

Hung et al. (2009) reported that α -mangostin could reduce matrix metalloproteinase-2 (MMP-2), matrix metalloproteinase-9 (MMP-9) and urokinase-

plasminogen activator (u-PA) expression by suppressing JNK1/2 signaling pathway and inhibiting NF- κ B and AP-1 binding activity. Hence, it could moderate PC-3 cells metastasis.

In 2010, Shih et al. studied correlation between α -mangostin and FAK/ERK/NF- κ B signaling pathway. The reported showed that α -mangostin could decrease matrix metalloproteinase-2 (MMP-2) and matrix metalloproteinase-9 (MMP-9) expressions through the α v β 3 integrin receptor. Thus, α -mangostin was able to inhibit the PMA-induced invasion and migration of A549 human lung adenocarcinoma cell.

Lee et al. (2010) reported the metastatic inhibition in MCF-7 breast cancer cells by α -mangostin. The antimetastatic activity happened via inactivated the phosphorylation of ERK1/2 and reduced AP-1 and NF- κ B DNA binding activities, leading to the down-regulation of matrix metalloproteinase-2 (MMP-2) and matrix metalloproteinase-9 (MMP-9) expressions.

Yoo et al. (2011) reported that α -mangostin had antiproliferation ability against colon cancer cells by inhibiting the transcriptional activity of TCF/ β -catenin in Wnt/ β -catenin signaling.

In 2011, Shibata et al. reported the metastasis inhibition of α -mangostin against mammary carcinoma cells with p53 mutation. It could induce mitochondria-mediated apoptosis along with S-phase and G1-phase arrest. Moreover, α -mangostin was able to decrease the levels of phospho-Akt-threonine 308 (Thr308) significantly.

Wudtiwai et al. (2017) reported that HepG2, a hepatocellular carcinoma (HCC) significantly sensitized α -mangostin at the anoikis-resistance state through the inhibition of cell survival by induced caspase-9, caspase-8 and caspase-3 activities. Furthermore, it could suppress AKT and ERK signaling pathways excellently.

1.4 Objectives of the present study

Apart from α -mangostin and other xanthenes, the study in bioactivity of other metabolites with anticancer activities are still lack and barely known. Although there were some reports, most were only preliminary investigation. In addition, study on metabolites from mangosteen roots is still less.

Because of this, this study aims to isolate secondary metabolites from mangosteen roots and to study effect of these metabolites against hepatocellular carcinoma and colon cancer cell growth as well as their efficacy on cell migration.



CHAPTER II

EXPERIMENTAL

2.1 Plant Materials

G. mangostana roots were collected in May 2019 from Nakhon Sri Thammarat province, Thailand.

2.2 General Experimental Procedures

2.2.1 Thin-layer chromatography (TLC)

Thin-layer chromatography (TLC) was performed on aluminum foil sheet, coated with silica gel. The TLC was observed under UV light at 256 nm and dipped with ammonium molybdate ((NH₄)₆Mo₇O₂₄) in 5% H₂SO₄/EtOH.

2.2.2 Column chromatography (CC)

Column chromatography was performed using Silica gel 60 (No. 7734 and No. 9385, Merck), Sephadex LH-20 (Pharmacia), and Octadecyl-silica (ODS, C-18) as packing materials.

2.2.3 High performance liquid chromatography (HPLC)

High performance liquid chromatography (HPLC) was performed using Thermo Scientific Spectra System (Thermo Scientific P200 pump and Thermo Scientific UV6000LP detector). Column VertiSep™ UPD C18 (4.6 × 150 mm, 5 μM) was used for analysis and Column GL Sciences (20 × 250 mm, 5 μM) was used for separation.

2.2.4 Nuclear magnetic resonance spectroscopy (NMR)

The NMR spectra was recorded in chloroform - *d* (CDCl₃) and acetone - *d*₆ ((CD₃)₂CO) using Varian Mercury 400 plus (400 MHz for ¹H NMR) and Bruker AV400 (400 MHz for ¹H NMR, 100 MHz for ¹³C).

2.2.5 Mass spectrometry (MS)

HRESIMS spectra was obtained with a Bruker micrOTOF.

2.2.6 Fourier transforms infrared spectrophotometer (FT-IR)

Perkin-Elmer Model 1760X Fourier Transform Infrared Spectrophotometer was performed to recode FT-IR spectra.

2.2.7 Melting point

Melting point was recorded using Fisher-Johns melting point apparatus.

2.2.8 Microplate reader

BioTek™ ELx800™ Absorbance Microplate Reader was used to measure absorbance at 540 and 570 nm.

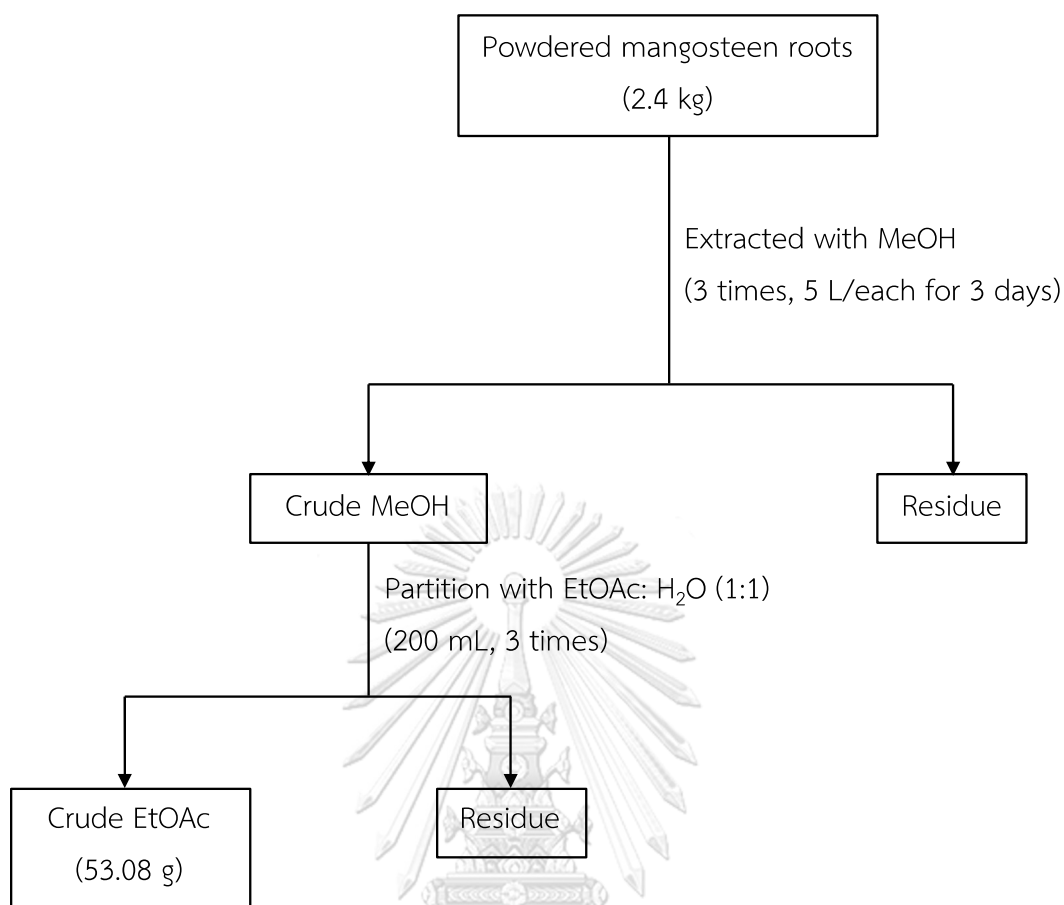
2.3 Chemicals and reagents

2.3.1 Solvents

Chemicals used in this experiment were classified into two types. Commercial grade solvents including methanol (MeOH), acetone, ethyl acetate (EtOAc), dichloromethane (CH₂Cl₂) and n-hexane were purified by distillation prior to use. HPLC grade solvents, Milli-Q water, MeOH, and acetonitrile were used for HPLC purification.

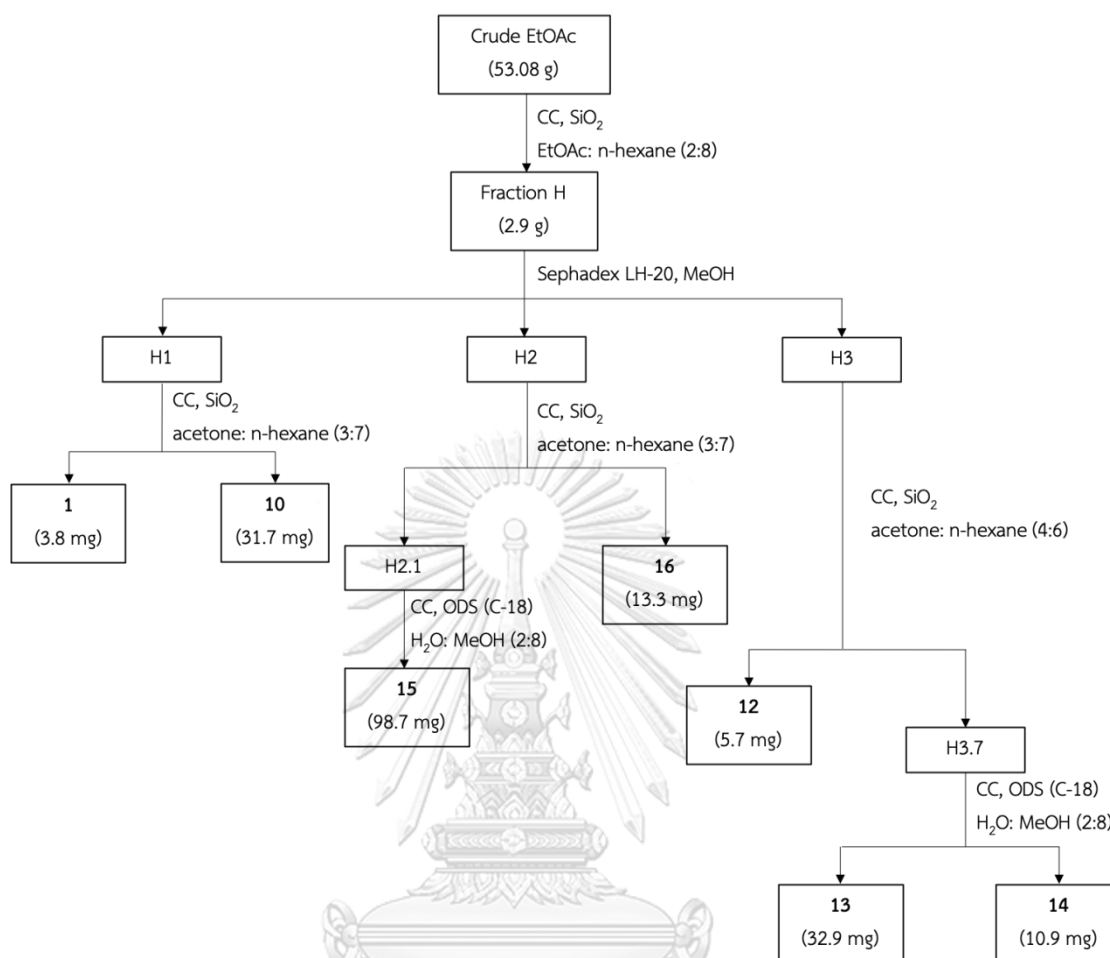
2.4 Extraction and Isolation

The powdered mangosteen roots (2.4 kg) were extracted 3 times with MeOH for 3 days (5 L each per time) at room temperature to obtain dark purple residue. After concentrated under reduced pressure, the latter was partitioned between H₂O and EtOAc in equal amount for 3 times. The EtOAc layer was concentrated with rotary evaporator under reduced pressure to get the EtOAc crude extract (53.08 g). The extraction procedure is shown in **Scheme 2.1**.



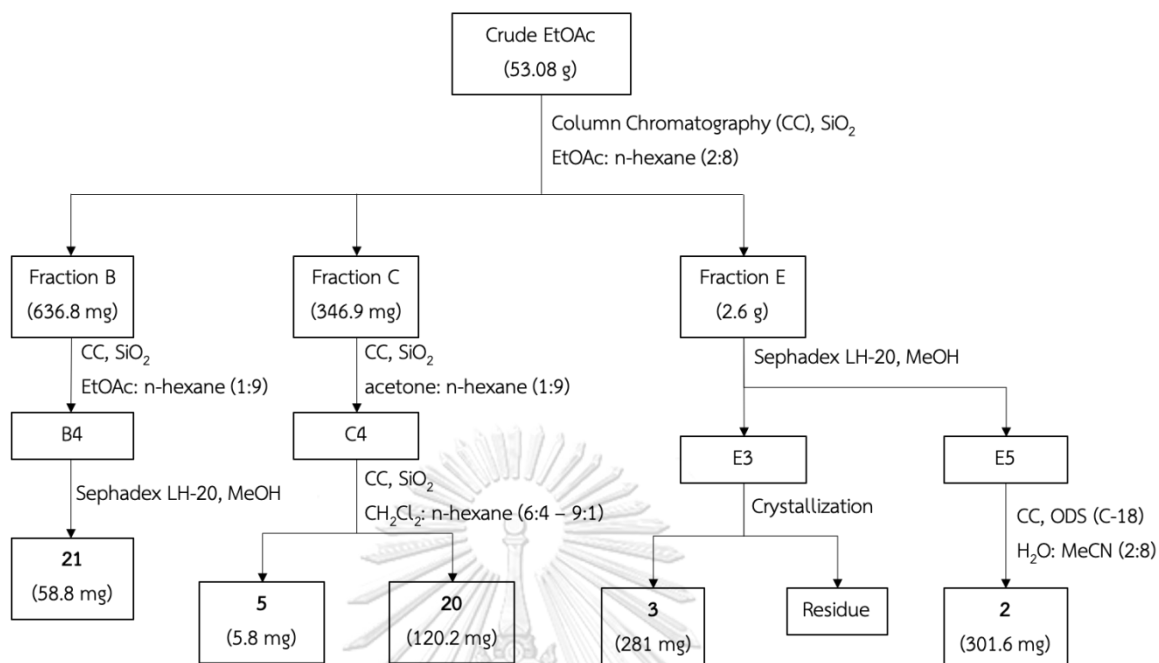
Scheme 2.1 The extraction procedure of powdered mangosteen roots

The EtOAc crude extract was chromatographed on SiO_2 column using EtOAc: n-hexane (2:8) to give ten fractions (A-J). Fraction H (2.9 g) was separated by Sephadex LH-20 CC (MeOH) to gain three subfractions (H1-H3). Subfraction H1 was meticulously separated with SiO_2 CC using acetone: n-hexane (3:7) to afford compounds **1** and **10** (3.8 mg and 31.7 mg respectively). The solvent used for subfraction H3 separation was 4:6 ratio of acetone: n-hexane to yield compound **12** (5.7 mg) together with H3.7. Later, subfraction H3.7 was re-chromatographed over ODS (C-18) using H_2O : MeOH (2:8) to provide compounds **13** (32.9 mg) and **14** (10.9 mg). Subfraction H2 was treated similarly to subfraction H1 to obtain compound **16** (13.3 mg) with another subfraction H2.1. The subfraction H2.1 was then subjected to ODS (C-18) CC with H_2O : MeOH (2:8) as eluent, gave out compound **15** (98.7 mg). The isolation of fraction F is shown in **Scheme 2.2**.



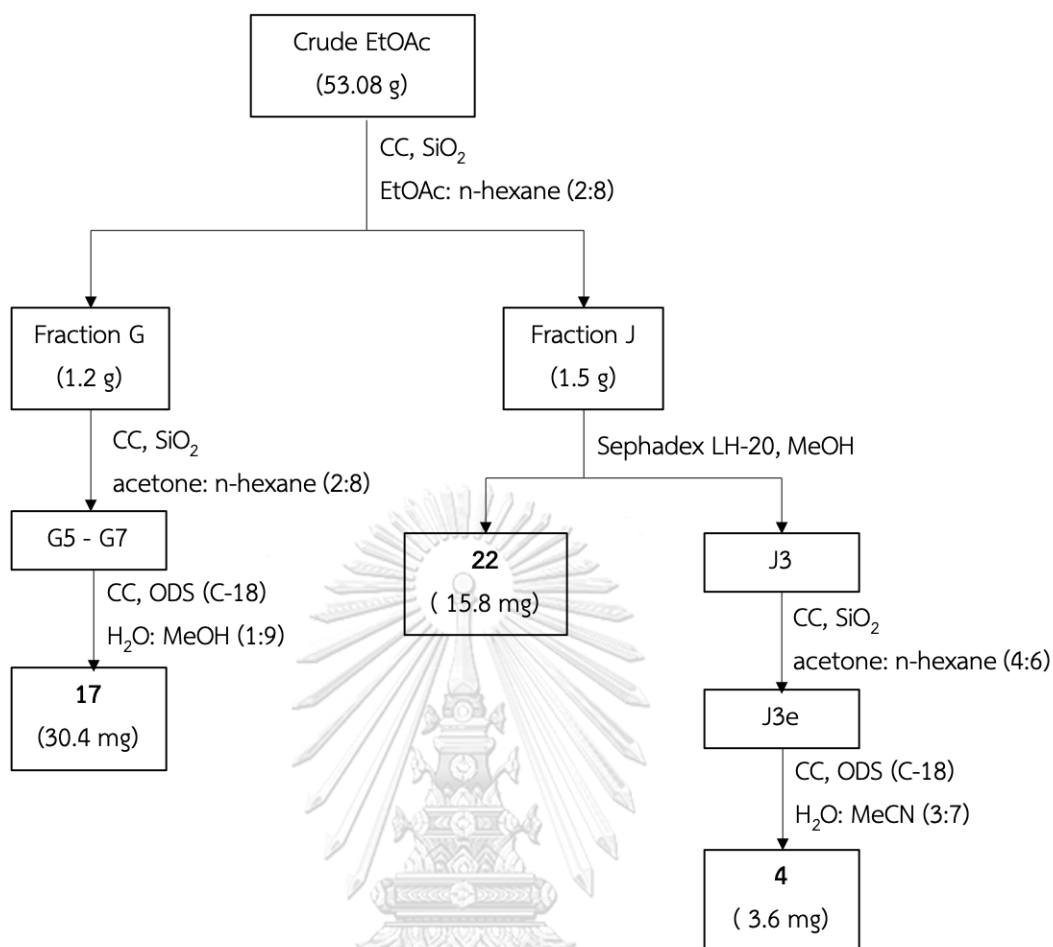
Scheme 2.2 The isolation procedure of fraction H

Subsequently, Fraction E (2.6 g) was separated by Sephadex LH-20 CC with MeOH and gave six subfractions (E1-E6) which E3 was crystallized and yielded compound **3** (281 mg). Fraction E5 was further purified by reversed-phase ODS (C-18) CC using H₂O: MeCN (2:8) to obtain compound **2** (301.6 mg). Following by fraction C (346.9 mg), was submitted to SiO₂ CC utilizing acetone: n-hexane (1:9) to obtain six subfractions (C1-C6). Subfraction C4 then was subjected to SiO₂ CC using CH₂Cl₂: n-hexane gradient from 6:4 – 9:1 and gave compounds **5** and **20** with weight 5.8 and 120.2 mg, respectively. Fraction B was separated by SiO₂ CC using EtOAc: n-hexane (1:9) to give nine subfractions (B1-B9). Subfraction B4 was picked to separate with Sephadex LH-20 CC using MeOH and gave out compound **21** (58.8 mg). The isolation procedure of these compounds is shown in **Scheme 2.3**.



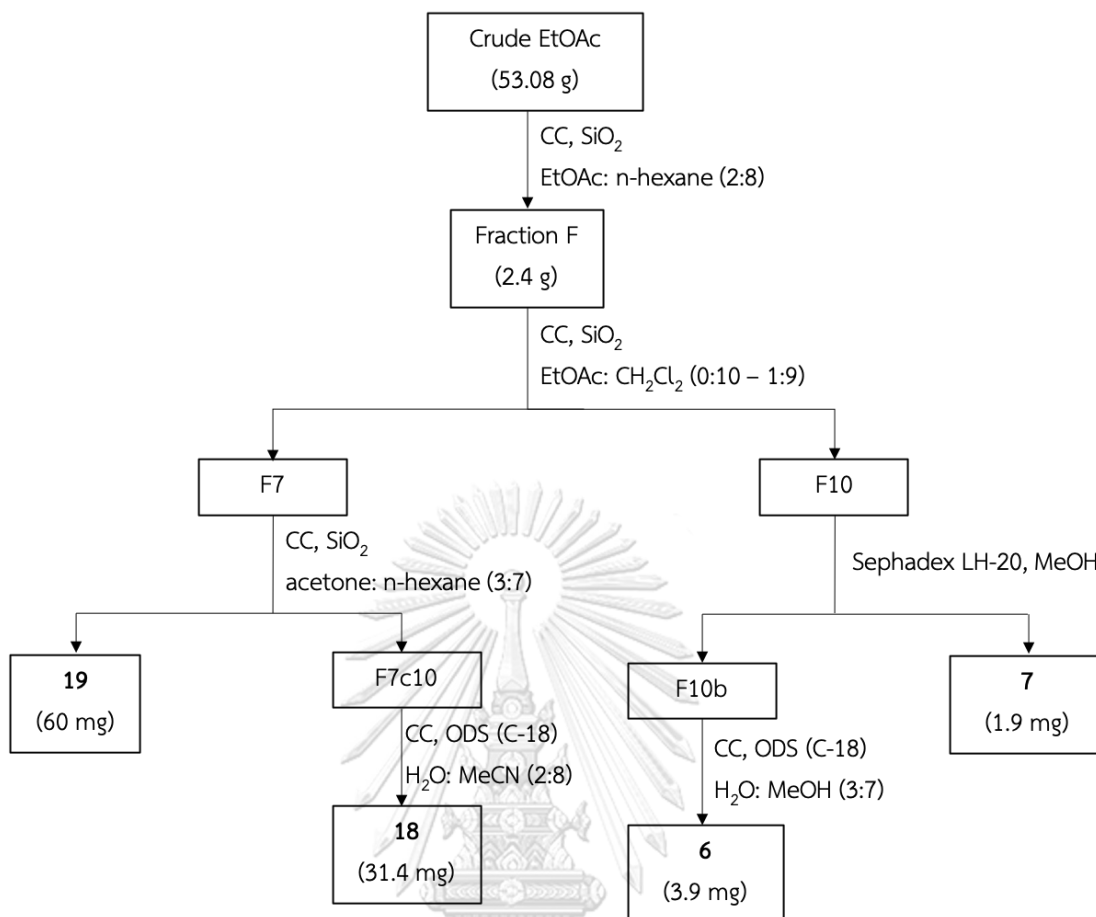
Scheme 2.3 The isolation procedure of fractions B, C, and E

Furthermore, fraction G was subjected with acetone: n-hexane (2:8) elution on SiO_2 column. The fraction provided many subfractions included impure G5 – G7. Subfraction was then purified by ODS (C-18) CC with H_2O : MeOH (1:9) to yield compound **17** (30.4 mg). Fraction J was eluted over Sephadex LH-20 with MeOH to obtain seven subfractions (J1 – J7). One of these became compound **22** (15.8 mg), whereas subfraction J3 was continually chromatographed with SiO_2 CC utilizing acetone: n-hexane (4:6). Lastly, ODS (C-18) column chromatography of J3e afforded compound **4** (3.6 mg). The isolation of fraction D is shown in **Scheme 2.4**.



Scheme 2.4 The isolation procedure of fractions G and J

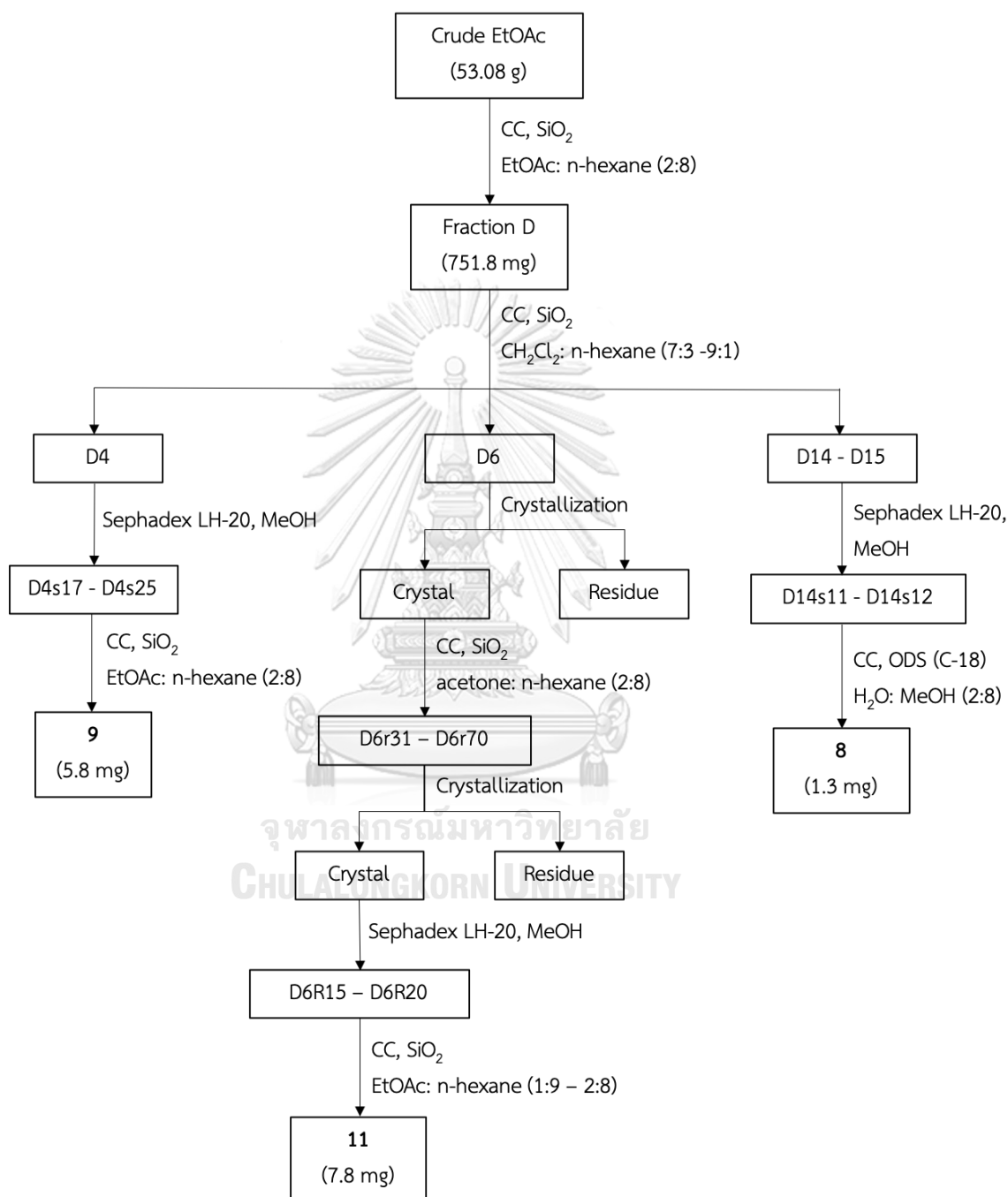
Fraction F was subjected to SiO_2 CC utilizing EtOAc: CH_2Cl_2 gradients from 0:10 to 1:9 to obtain ten subfractions (F1-F10). Compound **19** (60 mg) was obtained by separating subfraction F7 with SiO_2 CC using acetone: n-hexane (3:7) together with impure compound 18. The impure compound was further purified by ODS (C-18) column utilizing H_2O : MeCN (2:8) to yield compound **18** (31.4 mg). Subfraction F10 was isolated by Sephadex LH-20 CC using MeOH to afford compound **7** (1.9 mg) and impure major subfraction F10b. ODS (C-18) CC eluted with H_2O : MeOH (3:7) provided compound **6** (3.9 mg). The isolation of fraction F is shown in **Scheme 2.5**.



Scheme 2.5 The isolation procedure of fraction F

Last but not least, fraction D, the chromatography was performed using SiO₂ CC with CH₂Cl₂: n-hexane from 7:3 to 9:1 gradient elution to yield fifteen subfractions (D1-D15). Subfractions D4, D14 and D15 were treated similarly by fractionation with Sephadex LH-20 CC using MeOH elution. The D14s11 – D14s12 obtained from subfractions D14 and D15 were purified by ODS (C-18) CC with H₂O: MeOH (20%) to give compound **8** (1.3 mg). Minor subfractions D4s17 – D4s25, which had been obtained from subfraction D4 was then separated again by SiO₂ CC utilizing EtOAc: n-hexane (2:8) to yield compound **9** (5.8 mg). Major subfraction D6, being crystal pellets, was subjected to SiO₂ CC with acetone: n-hexane (2:8) to give minor subfractions D6r31 – D6r70 which also been crystalized and submitted to Sephadex LH-20 CC using MeOH elution to obtain another subfractions D6R15 – D6R20. Lately,

SiO₂ CC with EtOAc: n-hexane with 1:9 to 2:8 gradients was performed to yield compound **11** (7.8 mg). The isolation of fraction D is shown in **Scheme 2.6**.



Scheme 2.6 The isolation procedure of fraction D

2.5 Cell culture

Human hepatocellular carcinoma (HCC) cell lines including HepG2, Huh7 and colon cancer cell lines Caco2 and HCT-116 were cultured in Dulbecco's Modified Eagle's medium (DMEM) supplemented with 10% fetal bovine serum (FBS) and 1% penicillin/streptomycin (P/S) at 37°C in a 5% CO₂ humidified incubator.

2.6 Cytotoxicity assay

Cytotoxicity activity was performed to quantify the cell viability in cell treated with active compounds using MTT assay. Briefly, HCC and colon cancer cells were seeded in 96-well plate with a density of 4.5×10^4 and 5×10^4 cells/200 μ l/well, respectively. Then, the cells were incubated at 37°C with 5% CO₂ for 24 h. After that removed the supernatant, the cells were treated for 48 h with serial dilution of the tested compounds along with sorafenib and doxorubicin as standard drug control in the presence of serum-free DMEM media. MTT solution (0.5 mg/ml DMEM) was added to each well and then incubated for 4 h in a humidified atmosphere. After the incubation period, the supernatant was removed and DMSO 100 μ l was added to dissolve formazan crystals. The absorbance was measured at 570 nm using microplate reader. The results were calculated by using GraphPad Prism™ (version 8.0) and presented as the percentage of cells viability and half-maximal inhibitory concentration (IC₅₀).

2.7 Migration analysis

Wound healing assay was performed to identify cell migration. Huh7 monolayer cells were prepared in 12-well plate with density of 5.5×10^5 cells/well. The wound was created by scratching with micropipette tip (1 mm diameter). The medium was removed and replaced with serum-free DMEM containing compound **1**, **2**, **3**, **5**, **6**, **11** and **21** (at IC₅₀, <IC₅₀ and >IC₅₀ concentrations for each compound). Sorafenib (3 μ M) was used as a positive control and cells treated only with serum-free medium were used as standard control. The cells were observed and

photographed using microscope at 0, 24 and 48 h. The wound healing progression was calculated and presented as percentage of tissue repair (%Tissue repair)

$$\% \text{Tissue repair} = \frac{\text{Wound space}_{0\text{ h}} - \text{Wound space}_{n\text{ h}}}{\text{Wound space}_{0\text{ h}}} \times 100$$

Where Wound space_{0 h}: length of gap between scratched cells (μm) at 0 h

Wound space_{n h}: length of gap between scratched cells (μm) at n h

2.8 Apoptosis assessment

Apoptosis was determined by measuring external phosphatidylserine, which located on the outer of cell membrane. Huh7 and HepG2 were seeded in 24-well plate with density of 2.5×10^5 cells/well and incubated for 24 h with 5% CO₂ at 37°C. Huh7 cells were treated with compound **1**, **6**, and **11** and HepG2 were treated with compound **21** (using IC₅₀ value and 2 times above of IC₅₀ value) for 24 h. Then, cells were detached with trypsin and collected to wash with PBS and resuspended in 1 ml of DMEM. Then, Annexin V – 7AAD reagent (Luminex Corp., Austin, TX, USA) was added in the cell's suspension with 1:1 ratio and stained for 30 minutes at room temperature in the dark. Live, dead, and apoptosis cell populations were determined using Muse[®] Cell Analyzer. The results were analyzed and calculated as apoptosis profile.

2.9 Western blot assay

For further molecular biology analysis, western blot was performed to identify interested apoptotic proteins. After treated HepG2 with compound **21** using IC₅₀ and double in value for 24 h with density of 2.5×10^5 cells/well in 24 wells-plate, cells were harvested at time-depended and total protein were collected using ice cold lysis buffer. Protein samples then calculated and loaded in SDS-PAGE to separate using electrophoresis. Later, Protein were transferred from gel to polyvinylidene fluoride (PVDF) transmembrane and blocked with 5% skimmed milk. The primary

antibodies then added and incubated for 24 h in 4^oc. Membrane was washed with PBST afterward, then secondary antibodies were added and incubated with in optimal times. Membrane was washed again with PBST and performed color developer to visualize in the dark room. The results were photographed and analyze using Image J program.

2.10 Statistical analysis

Data are presented as mean \pm SD values. GraphPad prismTM ver. 8 program with one-way analysis of variation was used for testing the significance, P-value (p) < 0.05 was considered as statistically significance.

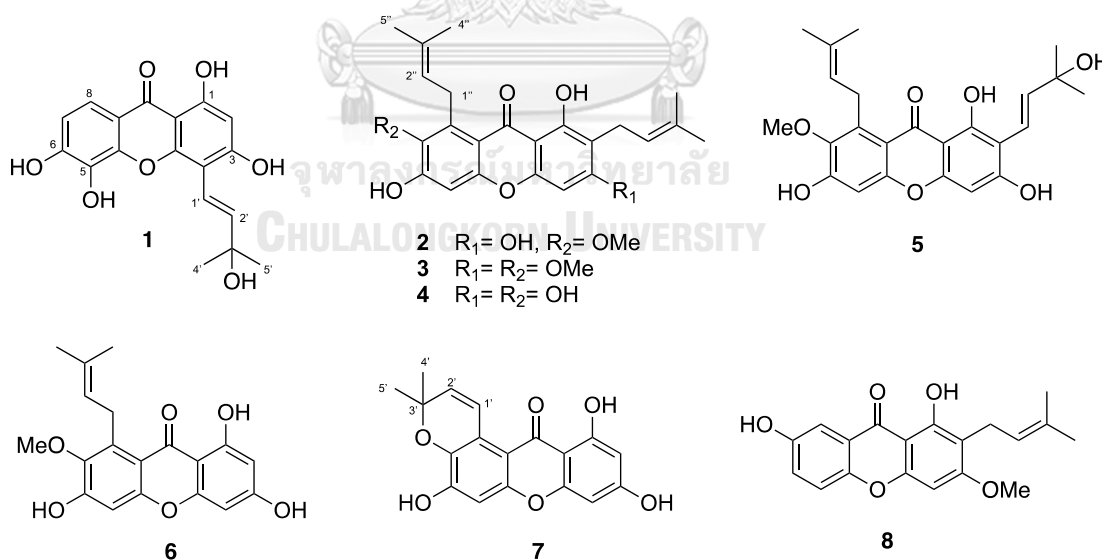


CHAPTER III

RESULTS AND DISCUSSION

3.1 Isolated compounds from mangosteen (*G. mangostana*) roots

Chemical investigation of EtOAc crude extract of mangosteen roots afforded four new compounds: mangostanone I – IV (compounds **1**, **12**, **13**, and **18**), and one new found in naturally occurring, 4,5-dimethoxy[1,1'-biphenyl]-3-ol (**20**), along with seventeen known compounds: α -mangostin (**2**), β -mangostin (**3**), γ -mangostin (**4**), mangostanaxanthone IV (**5**), dulxanthone D (**6**), toxyloxanthone B (**7**), 1,7-dihydroxy-3-methoxy-2-prenylxanthone (**8**), euxanthone (**9**), norathyriol (**10**), 8-deoxygartanin (**11**), maclurin (**14**), 2,3',4,6-tetrahydroxybenzophenone (**15**), mangaphenone (**16**), (2-hydroxy-4,6-dimethoxyphenyl)(3-hydroxy-4-methoxyphenyl)methanone (**17**), garciosine A (**19**), 3-hydroxy-4-geranyl-5-methoxybiphenyl (**21**) and epicatechin (**22**).



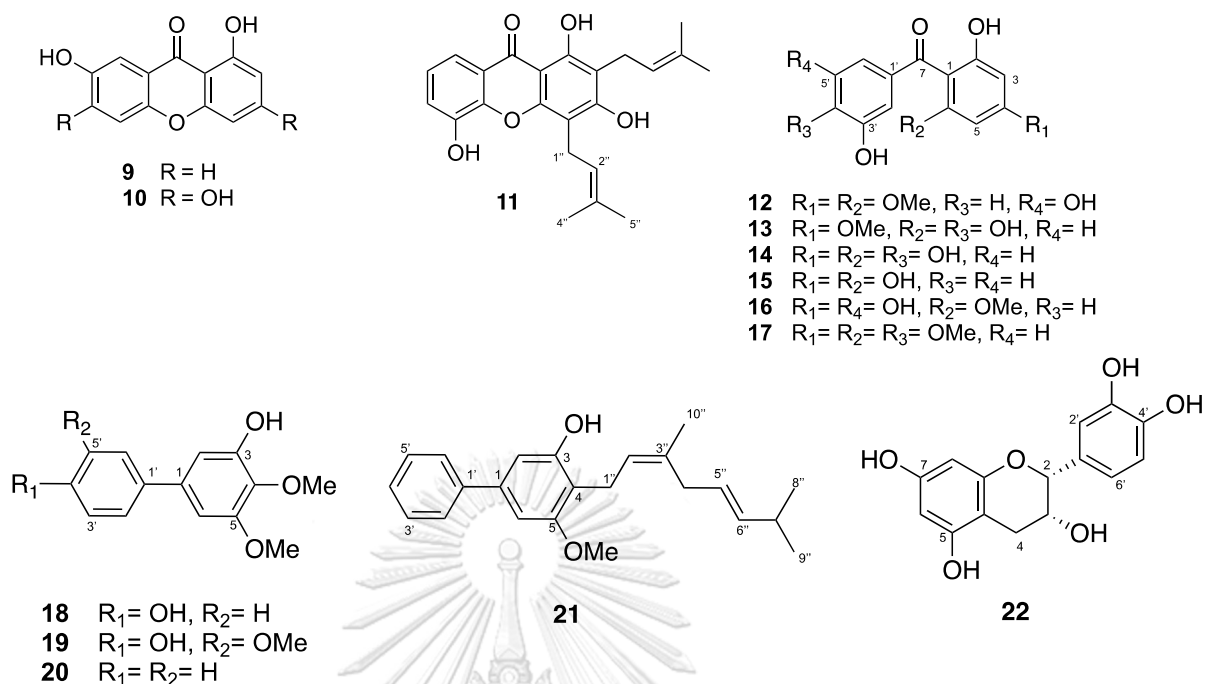


Figure 3.1 Structures of isolated compounds from mangosteen roots

3.2 Structure elucidation of isolated compounds

3.2.1 Structure elucidation of compound 1

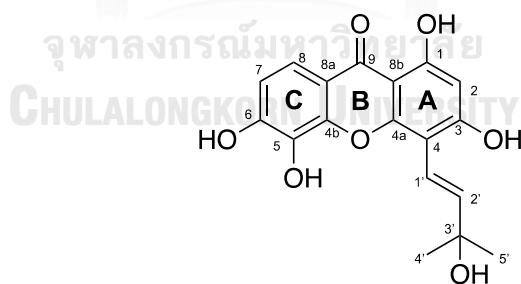


Figure 3.2 Structure of compound 1

Compound **1** was obtained as dark yellow solid (mp 213-220 °C) that gave a $[M + H]^+$ ion at m/z 349.0679 in the HRESIMS, consistent with a molecular formula $C_{18}H_{15}O_7$ (calcd for $C_{18}H_{16}O_7$, m/z 349.0674). The UV spectrum showed absorption bands at λ_{max} 256 and 329 nm (logE= 2.768 and 2.528), which are typical of a xanthone chromophore [11]. The IR spectrum showed stretching bands for hydroxy

(3304 cm^{-1}) and carbonyl (1624 cm^{-1}) functional groups. The ^1H (Table 3.1) and ^{13}C (Table 3.2) NMR spectroscopic data displayed resonances for a H-bonded hydroxy proton (δ_{H} 13.31 (1H, s, OH-1)), two ortho-coupled aromatic protons [$\delta_{\text{H}}/\delta_{\text{C}}$ 7.01 (1H, d, $J = 8.0$ Hz, H-7)/113.7 (C-7) and 7.64 (1H, d, $J = 12$ Hz, H-8)/117.5 (C-8)], one singlet aromatic proton [$\delta_{\text{H}}/\delta_{\text{C}}$ 6.17 (1H, s, H-2)/99.4 (C-2)], and a set of (*E*)-3-hydroxy-3-methylbutyl-1-en unit [$\delta_{\text{H}}/\delta_{\text{C}}$ 5.74 (1H, d, $J = 8.0$ Hz, H-1')/127.9 (C-1'), 7.06 (1H, d, $J = 8.0$ Hz, H-2')/115.8 (C-2'), 1.48 (6H, s, H-4' and H-5')/28.3 (C-4' and C-5'), and an oxygen-bonded aliphatic carbon at δ_{C} 78.8 (C-3')]. The correlation of H-1' (δ_{H} 5.74) to C-3 (δ_{C} 161.1), C-4 (δ_{C} 102.0), and C-4a (δ_{C} 152.7) in the HMBC spectrum (Figure 3.3) confirmed the location of the (*E*)-3-hydroxy-3-methylbutyl-1-en unit at C-4. The locations of the hydroxy groups at C-1, C-3, C-5 and C-6 were indicated by the HMBC correlations of OH-1 to C-1 (δ_{C} 164.1), C-2 (δ_{C} 99.4) and C-8b (δ_{C} 109.1), for OH-3 confirm by the correlations between H-1' (δ_{H} 5.74) to C-3 (δ_{C} 161.1) and H-2 (δ_{H} 6.17) to C-3 (δ_{C} 161.1), OH-5 confirm by the 3J HMBC correlations of H-7 (δ_{H} 7.01) to C-5 (δ_{C} 133.3) and C-8a (δ_{C} 114.6). The HMBC correlations observed between H-8 (δ_{H} 7.64) to C-6 (δ_{C} 152.6), C-4b (δ_{C} 152.6), and C-9 (δ_{C} 181.3) confirmed the location of OH-6. Thus compound **1** was identified as a new compound, namely mangostanone I.

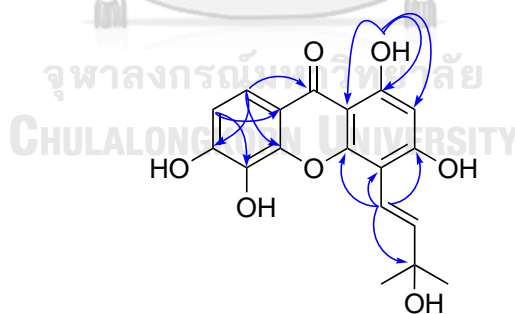
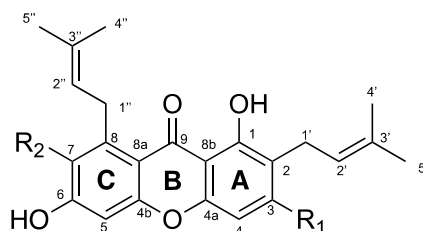


Figure 3.3 Selected HMBC correlations ($^1\text{H} \rightarrow ^{13}\text{C}$) of compound **1**

3.2.2 Structure elucidation of compounds **2**, **3** and **4**

- 2** $R_1 = \text{OH}, R_2 = \text{OMe}$
3 $R_1 = \text{OMe}, R_2 = \text{OMe}$
4 $R_1 = R_2 = \text{OH}$

Figure 3.4 Structures of compounds **2**, **3** and **4**

Compound **2** was isolated as yellow crystals and had molecular formula $\text{C}_{24}\text{H}_{26}\text{O}_6$ as determined by NMR data. The ^1H and ^{13}C NMR spectral data of compound **2** (Tables 3.1 and 3.2) showed the signals of twelve aromatic carbons at δ_c 160.7, 109.2, 161.8, 93.2, 152.9, 154.9, 101.8, 155.8, 142.8, 137.3, 112.2, and 104.1 constituted the xanthone skeleton [12] and one carbonyl group (δ_c 182.1), the presence of isopropenyl units at ring A [δ_H/δ_c 4.08 (*d*, $J = 8.0$ Hz, H-1')/26.6 (C-1'), 5.27 (*d*, $J = 8.0$ Hz, H-2')/121.9 (C-2'), 1.72 and 1.67 (*s*, H-4')/25.9 (C-4'); δ_c 131.5 (C-3') and 17.9 (C-5')] and ring C [δ_H/δ_c 3.41 (*d*, $J = 8.5$ Hz, H-1'')/21.6 (C-1''), 5.25 (*d*, $J = 8.5$ Hz, H-2'')/123.4 (C-2''), 1.79 (*d*, $J = 8.0$ Hz, H-5'')/18.3 (C-5''); δ_c 132.0 (C-3'') and 25.8 (C-4'')] were confirmed position by HMBC correlations of H-1' (δ_H 4.08, *d*, $J = 8.0$ Hz) to C-2 (δ_c 109.2) and H-1'' (δ_H 3.41, *d*, $J = 8.5$ Hz) to C-8 (δ_c 137.3). Three phenolic hydroxyl groups were located at C-1 (δ_c 160.7), C-3 (δ_c 161.8), and C-6 (δ_c 155.8) and one methoxy group at (δ_H/δ_c 3.78 (*s*, OMe-7)/61.9). The NMR data was compared with the previous study, compound **2** was identified as α -mangostin [13].

Compound **3** was isolated as yellow crystals with the molecular formula of $\text{C}_{25}\text{H}_{28}\text{O}_6$ as determined by 1D and 2D NMR data. The ^1H (Table 3.1) and ^{13}C (Table 3.2) NMR spectroscopic data showed the presence of a xanthone derivative having a

H-bonded hydroxy proton (δ_{H} 13.41 (1H, s, OH-1)), two isoprenyl units [$(\delta_{\text{H}}/\delta_{\text{C}}$ 3.35 (2H, *d*, $J= 8.0$ Hz, H-1')/21.5 (C-1'), 5.23 (1H, *m*, H-2')/122.5 (C-2'), 1.68 (3H, *s*, H-4')/26.0 (C-4'), 1.80 (3H, *s*, H-5')/17.9 (C-5'); δ_{C} 131.8 (C-3'') and $(\delta_{\text{H}}/\delta_{\text{C}}$ 4.10 (2H, *d*, $J= 8.0$ Hz, H-1'')/26.7 (C-1''), 5.27 (1H, *m*, H-2'')/123.4 (C-2''), 1.69 (3H, *s*, H-4'')/26.0 (C-4''), 1.83 (3H, *s*, H-5'')/18.4 (C-5''); δ_{C} 132.2 (C-3'')], and two singlet aromatic protons [$\delta_{\text{H}}/\delta_{\text{C}}$ 6.35 (1H, *s*, H-4)/89.0 (C-4) and 6.84 (1H, *s*, H-5)/101.6 (C-5)]. The data were quite similar to compound **2** except for the presence of two methoxy groups at ring A and C [$\delta_{\text{H}}/\delta_{\text{C}}$ 3.90 (3H, *s*, OMe-3)/56.0 and 3.82 (3H, *s*, OMe-7)/62.2, respectively] instead of one. To confirm the structure, its NMR data were compared to those previously reported and it was identified as β -mangostin [14].

Compound **4** was isolated as light-yellow powder. The molecular formula determined using 1D and 2D NMR was $\text{C}_{23}\text{H}_{24}\text{O}_6$. The comparison of NMR data (Tables 3.1 and 3.2) between compound **4** and previous compound **2** suggested that these two compounds have similar structures, except for the absence of methoxy group at ring C was replaced by phenolic hydroxyl group at δ_{H} 8.92 (*s*, OH-7). This was confirmed by the HMBC correlations of OH-7 to C-6, C-7 and C-8 (δ_{C} 154.0, 142.8 and 137.0, respectively). Thus, this compound was named γ -mangostin as reported in the previous literature [15].

3.2.3 Structure elucidation of compound **5**

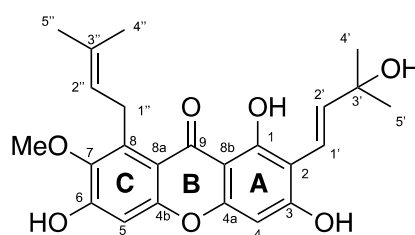


Figure 3.5 Structure of compound **5**

Compound **5** was obtained as dark yellow gum. The molecular formula was identified as $\text{C}_{24}\text{H}_{28}\text{O}_7$ by its NMR data. The NMR spectra both ^1H and ^{13}C were

appeared in **Tables 3.1** and **3.2** suggested that compound **5** have a nearly similar structure as compound **2** in the presence of xanthone structure core displayed by twelve aromatic carbons and one carbonyl, three hydroxy groups located at C-1, C-3, and C-6 were confirmed by HMBC correlations as well as methoxy group at C-7. The only different was a replacement of signals of one *di*-substituted olefinic bonds at $\delta_{\text{H}}/\delta_{\text{C}}$ 5.57 (*d*, $J= 8.0$ Hz, H-1'/125.1 (C-1') and 6.73 (*d*, $J= 12.0$ Hz, H-2')/115.7 (C-2') by an oxygenated quaternary carbon at δ_{C} 77.9 (C-3') at ring A, whereas isoprenyl group at ring C remain the same ($\delta_{\text{H}}/\delta_{\text{C}}$ 4.11 (*d*, $J= 8.0$ Hz, H-1'')/26.5, 5.27 (*d*, $J= 4.0$ Hz, H-2'')/123.1, 1.71 (*s*, H-4'')/25.7, 1.84 (*s*, H-5'')/18.2; δ_{C} 132.1 (C-3'')). The structure was identified as mangostanaxanthone IV as compared with the previous literature [16].

3.2.4 Structure elucidation of compound **6**

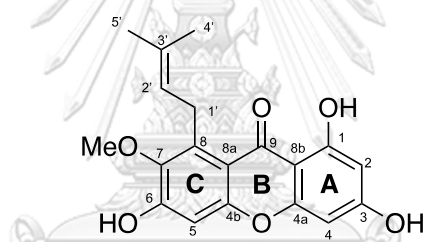


Figure 3.6 Structure of compound **6**

Compound **6** was obtained as yellowish gum and the molecular formula of $\text{C}_{19}\text{H}_{18}\text{O}_6$ was determined by analysis of ^1H - and ^{13}C -NMR data. From NMR spectra data (**Tables 3.1** and **3.2**), compound **6** also showed a close similarity structure with compound **2** in term of xanthone derivative with the presence of methoxy signal at $\delta_{\text{H}}/\delta_{\text{C}}$ 4.60 (*s*, OMe-7)/61.5, phenyl side chain signals at $\delta_{\text{H}}/\delta_{\text{C}}$ 5.84 (*d*, $J= 6.0$ Hz, H-1'')/27.3, 7.37 (*d*, $J= 8.0$ Hz, H-2'')/125.2, 1.51 (*s*, H-4'')/26.2, 1.46 (*s*, H-5'')/18.5; δ_{C} 132.1 (C-3'), chelated hydroxy signal at δ_{H} 13.52 (*s*, OH-1), and two aromatic singlet protons at δ_{H} 6.23 (*s*, H-4) and 6.73 (*s*, H-5), except for the disappearance of isoprenyl group in ring A as the signal of aromatic singlet proton appeared at δ_{H} 6.11 (*s*, H-2). The

structure was confirmed by the comparison between their NMR data and previously reported, resulted as dulxanthone D [17].

Table 3.1 ^1H NMR data of compounds **1** - **6**

Position	δ_{H} , mult. (<i>J</i> in Hz)					
	1 ^(b)	2 ^(a)	3 ^(a)	4 ^(b)	5 ^(a)	6 ^(c)
1	-	-	-	-	-	-
2	6.17 s	-	-	-	-	6.11 s
3	-	-	-	-	-	-
4	-	6.31 s	6.35 s	6.31 s	6.25 s	6.23 s
4a	-	-	-	-	-	-
4b	-	-	-	-	-	-
5	-	6.80 s	6.84 s	6.73 s	6.85 s	6.73 s
6	-	-	-	-	-	-
7	7.01 d, 8.0	-	-	-	-	-
8	7.64 d, 12.0	-	-	-	-	-
8a	-	-	-	-	-	-
8b	-	-	-	-	-	-
9	-	-	-	-	-	-
1'	5.74 d, 8.0	4.08 d, 8.0	3.35 d, 8.0	4.03 d, 8.0	5.57 d, 8.0	5.84 d, 6.0
2'	7.06 d, 8.0	5.27 d, 8.0	5.23 m	5.19 t, 8.0	6.73 d, 12.0	7.37 d, 8.0
3'	-	-	-	-	-	-
4'	1.48 s	1.72 s 1.67 s	1.68 s	1.73 s	-	1.51 s
5'	1.48 s	-	1.80 s	-	1.48 s	1.46 s
1''	-	3.41 d, 8.5	4.10 d, 8.0	3.21 d, 4.0	4.11 d, 8.0	-
2''	-	5.25 d, 8.5	5.27 m	5.17 t, 8.0	5.27 d, 4.0	-
3''	-	-	-	-	-	-
4''	-	-	1.69 s	-	1.71 s	-
5''	-	1.79 d, 8.0	1.83 s	1.77 s	1.84 s	-
OH-1	13.31 s	-	13.41 s	13.85 s	13.70 s	13.52 s

OMe-3	-	3.90 s	-	-
OH-6	-	-	6.32 s	5.86 s
OH-7	-	-	8.92 s	-
OMe-7	3.78 s	3.82 s	3.82 s	4.60

(a) measured in CDCl₃; (b) measured in acetone-d₆; (c) measured in methanol-d₄

Table 3.2 ¹³C NMR data of compounds **1 - 6**

Position	δ_c					
	1 ^(b)	2 ^(a)	3 ^(a)	4 ^(b)	5 ^(a)	6 ^(c)
1	164.1	160.7	160.0	159.6	157.9	158.4
2	99.4	109.2	111.7	109.2	104.5	99.0
3	161.1	161.8	163.7	161.8	159.9	162.2
4	102.0	93.2	89.0	92.0	94.1	94.2
4a	152.7	152.9	155.9	151.7	156.3	153.4
4b	152.6	154.9	154.5	152.3	103.7	153.9
5	133.3	101.8	101.6	101.9	101.6	101.5
6	152.6	155.8	155.4	154.0	155.7	154.7
7	113.7	142.8	142.7	140.7	142.6	145.2
8	117.5	137.3	137.2	137.0	137.0	137.1
8a	114.6	112.2	112.7	112.4	112.2	112.5
8b	103.4	103.5	104.0	104.1	103.7	103.6
9	181.3	182.1	182.1	181.3	181.9	182.3
1'	127.9	26.6	21.5	21.0	125.1	27.3
2'	115.8	121.9	122.5	122.5	115.7	125.2
3'	78.8	131.5	131.8	129.9	77.9	132.1
4'	28.3	25.9	26.0	25.7	28.3	26.2
5'	28.3	17.9	17.9	17.7	28.3	18.5
1''	-	21.6	26.7	25.4	26.5	-
2''	-	123.4	123.4	123.6	123.1	-
3''	-	132.0	132.2	130.1	132.1	-

4"	-	25.8	26.0	25.5	25.7	-
5"	-	18.3	18.4	18.1	18.2	-
OMe-3	-	-	56.0	-	-	-
OMe-7	-	61.9	62.2	-	62.0	61.5

(a) measured in CDCl₃; (b) measured in acetone-d₆; (c) measured in methanol-d₄

3.2.5 Structure elucidation of compound 7

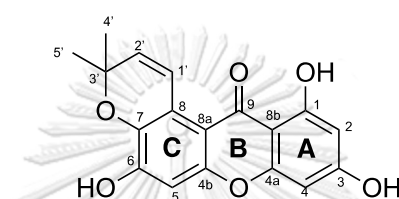


Figure 3.7 Structure of compound 7

Compound **7** was obtained as yellow powder. The molecular formula established by 1D and 2D NMR was C₁₈H₁₄O₆. This compound appeared a structure core of xanthone similarly with previous compounds provided by the twelve aromatic carbons showed in ¹³C NMR spectral data (**Tables 3.4**). From ¹H NMR data (**Tables 3.3**), chelated hydroxy proton showed signal at δ_{H} 13.12 (*s*, OH-1) with a notable difference of signals for two *gem*-dimethyl groups at δ_{H} 1.67 *s* (H-4' and H-5') appeared in ring C. Signals of *ortho*-*di*-substituted olefinic bonds at $\delta_{\text{H}}/\delta_{\text{C}}$ 6.20 (*d*, *J*= 4.0 Hz, H-1'/124.6) and 6.27 (*s*, H-2')/117.5) revealed the structure of compound **7** to contain dimethylchromene ring attached at C-7 (δ_{C} 140.7) and C-8 (δ_{C} 138.8) by correlation obtained from HMBC. To confirmed the structure, its NMR data were compared to those previously reported and its was identified as toxyloxanthone B [18].

3.2.6 Structure elucidation of compound 8

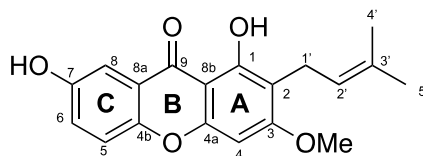
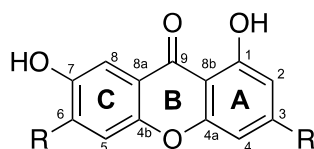


Figure 3.8 Structure of compound 8

Compound **8** was obtained as light-yellow powder with the molecular formula of $C_{19}H_{18}O_5$ determined by 1D and 2D NMR data. All the NMR data were showed in **Tables 3.3** and **3.4** which quite similar when compared with compound **3**. This compound appears signals of isoprenyl group in ring A with δ_H/δ_C 3.42 (*d*, $J= 8.0$ Hz, H-1')/21.9 (C-1'), 5.22 (*t*, $J= 8.0$ Hz, H-2')/123.2 (C-2'), 1.64 (*s*, H-4')/25.9 (C-4'), 1.78 (*s*, H-5')/17.9 (C-5'); δ_C 131.8 (C-3'), one methoxy group at δ_H/δ_C 3.99 (*s*, OMe-3)/56.8. However, the absence in signals of isoprenyl group at ring C (position at C-8) and hydroxy group at C-6 make the different. In addition, the methoxy group at ring C was replaced with hydroxy group located at C-7 (δ_C 155.0). The structure was then identified as 1,7-dihydroxy-3-methoxy-2-prenylxanthone as previously reported by mahabusarakam et al [19].

3.2.7 Structure elucidation of compounds 9 and 10



9 R = H

10 R = OH

Figure 3.9 Structures of compounds 9 and 10

Compound **9** was obtained as pale yellow solid. The molecular formula determined by ^1H - and ^{13}C -NMR data analysis was $\text{C}_{13}\text{H}_8\text{O}_4$. The ^1H NMR data (**Table 3.3**) showed signals of six aromatic protons at δ_{H} 6.74 (*d*, $J = 8.0$ Hz, H-2), 7.67 (*t*, $J = 8.0$ Hz, H-3), 6.98 (*d*, $J = 8.0$ Hz, H-4), 7.49 (*d*, $J = 4.0$ Hz, H-5), 7.41 (*dd*, $J = 4.0, 12.0$ Hz, H-6) and 7.59 (*d*, $J = 4.0$ Hz, H-8). The ^{13}C NMR data from **Table 3.4** confirmed a xanthone skeleton with twelve aromatic carbons at δ_{C} 162.8, 110.6, 137.8, 107.8, 157.4, 150.6, 120.2, 126.2, 155.1, 109.2, 121.8 and 109.1 and one conjugated carbonyl carbon at δ_{C} 183.1 (C-9). The structure was identified as euxanthone by comparison with reported literature [20].

Compound **10** was obtained as marigold powder with molecular formula of $\text{C}_{13}\text{H}_8\text{O}_6$ established by NMR data analysis. ^1H and ^{13}C NMR data were showed in **Tables 3.3** and **3.4** respectively results that structure of compound **10** was very similar to compound **9**. For further explanation, one signal of chelated aromatic proton at δ_{H} 13.00 (*s*, OH-1) was appeared, follow by the signals of twelve aromatic carbons and one carbonyl. Except for the replacement of two hydroxyl groups located in ring A $\delta_{\text{H}}/\delta_{\text{C}}$ 13.16 (*s*, OH-3)/165.2 (C-3) and ring C (δ_{C} 153.9) instead of aromatic protons. Compound **10** was identified as norathyriol by comparing the NMR data to those previously reported [21].

3.2.8 Structure elucidation of compound **11**

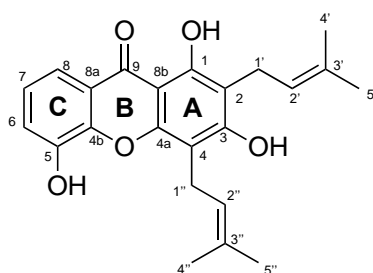


Figure 3.10 Structure of compound **11**

Compound **11** was obtained as light-yellow powder. The molecular structure was established by NMR spectral data as $\text{C}_{23}\text{H}_{24}\text{O}_5$ (**Table 3.3** and **3.4**). ^1H and ^{13}C

NMR data of compound **11** provided its xanthone skeleton structure. ^1H NMR data displayed signals of two olefinic protons at δ_{H} 5.27 (s, H-2') and 5.29 (s, H-2''), four allylic methyls at δ_{H} 1.76 (s, H-4'), 1.86 (s, H-5'), 1.87 (s, H-4''), and 1.79 (s, H-5''), and two methylene protons at δ_{H} 3.47 (d, $J = 8.0$ Hz, H-1') and 3.54 (d, $J = 8.0$ Hz, H-1''). By HMBC observed, connectivity at C-2 (δ_{C} 109.3) was confirmed by correlations of proton at δ_{H} 3.47 (d, $J = 8.0$ Hz, H-1') with aromatic carbons at δ_{C} 158.9 (C-1), 109.3 (C-2) and 161.1 (C-3) and another connectivity at C-4 (δ_{C} 105.6) also confirmed by correlations of proton at δ_{H} 3.54 (d, $J = 8.0$ Hz, H-1'') with aromatic carbons at δ_{C} 161.1 (C-3), 105.6 (C-4) and 152.6 (C-4a) suggested the existence of two 3-methylbut-2-enyl moieties in ring A. Compound **11** was identified as 8-deoxygartanin as previous reported [22].

Table 3.3 ^1H NMR data of compounds **7 - 11**

Position	δ_{H} , mult. (J in Hz)				
	7 ^(b)	8 ^(b)	9 ^(b)	10 ^(b)	11 ^(a)
1	-	-	-	-	-
2	6.34 s	-	6.74 d, 8.0	6.20 s	-
3	-	-	7.67 t, 8.0	-	-
4	6.31 s	6.24 s	6.98 d, 8.0	6.34 s	-
4a	-	-	-	-	-
4b	-	-	-	-	-
5	6.82 s	7.46 d, 8.0	7.49 d, 4.0	6.88 s	-
6	-	7.36 dd, 12.0	7.41 dd, 4.0, 9.0	-	7.28 s
7	-	-	-	-	7.21 s
8	-	7.58 d, 4.0	7.59 d, 4.0	7.52 s	7.76 d, 8.0
8a	-	-	-	-	-
8b	-	-	-	-	-
9	-	-	-	-	-
1'	6.20 d, 4.0	3.42 d, 8.0	-	-	3.47 d, 8.0
2'	6.27 s	5.22 t, 8.0	-	-	5.27 s

3'	-	-	-	-	-
4'	1.67 s	1.64 s	-	-	1.76 s
5'	1.67 s	1.78 s	-	-	1.86 s
1"	-	-	-	-	3.54 d, 8.0
2"	-	-	-	-	5.29 s
3"	-	-	-	-	-
4"	-	-	-	-	1.87 s
5"	-	-	-	-	1.79 s
OH-1	13.12 s	-	-	13.00 s	13.19 s
OH-3	-	-	-	13.16 s	6.52 s
Ome-3	-	3.99 s	-	-	-
OH-5	-	-	-	-	5.71 s

(a) measured in CDCl₃; (b) measured in acetone-d₆

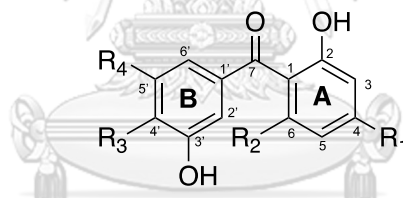
Table 3.4 ¹³C NMR data of compounds 7 - 11

Position	δ_c				
	7 ^(b)	8 ^(b)	9 ^(b)	10 ^(b)	11 ^(a)
1	160.8	160.3	162.8	164.1	158.9
2	110.5	112.1	110.6	98.2	109.3
3	165.6	165.6	137.8	165.2	161.1
4	91.4	90.8	107.8	94.1	105.6
4a	151.7	157.4	157.4	158.5	152.6
4b	153.8	150.9	150.6	152.2	144.5
5	100.9	119.9	120.2	103.1	144.6
6	156.4	125.3	126.2	153.9	119.9
7	140.7	155.0	155.1	143.7	123.9
8	138.8	109.4	109.2	108.9	117.1
8a	112.2	122.1	121.8	113.4	121.1
8b	104.2	104.4	109.1	102.8	103.5
9	183.1	181.5	183.1	180.1	180.3

1'	124.6	21.9	-	-	21.8
2'	117.5	123.2	-	-	121.4
3'	132.0	131.8	-	-	136.4
4'	27.8	25.9	-	-	25.8
5'	27.8	17.9	-	-	18.1
1''	-	-	-	-	22.3
2''	-	-	-	-	122.4
3''	-	-	-	-	133.7
4''	-	-	-	-	18.1
5''	-	-	-	-	26.0
Ome-3	-	56.8	-	-	-

(a) measured in CDCl₃; (b) measured in acetone-d₆

3.2.9 Structure elucidation of compounds **12** – **17**



12 R₁= R₂= OMe, R₃= H, R₄= OH

13 R₁= OMe, R₂= R₃= OH, R₄= H

14 R₁= R₂= R₃= OH, R₄= H

15 R₁= R₂= OH, R₃= R₄= H

16 R₁= R₄= OH, R₂= OMe, R₃= H

17 R₁= R₂= R₃= OMe, R₄= H

Figure 3.11 Structures of compounds **12** – **17**

Compound **12** was obtained as dark-yellow solid. The molecular formula C₁₅H₁₃O₆ was determined by HRESIMS ion at *m/z* 313.0690 [M + Na]⁺ (calcd 313.0688)

with melting point 176-180 °C. The FT-IR shown absorption band of hydroxyl group from ν_{\max} 3151 cm^{-1} . UV spectrum showed absorption bands at λ_{\max} 208 (logE= 2.727) and 305 (logE= 2.441) nm suggested that compound **12** had a benzophenone skeleton [23]. The ^1H NMR spectroscopic data (**Table 3.5**) displayed signals of five aromatic protons at δ_{H} 6.13 (*d*, $J= 4.0$ Hz, H-2), 6.15 (*d*, $J= 4.0$ Hz, H-5), 6.60 (*d*, $J= 4.0$ Hz, H-2'), 6.51 (*t*, $J= 4.0$ Hz, H-4'), and 6.60 (*d*, $J= 4.0$ Hz, H-6'). Added data from ^{13}C NMR spectral provide *meta-di*-substituted methoxy located at $\delta_{\text{H}}/\delta_{\text{C}}$ 3.86 (*s*, OMe-4)/166.3 (C-4) and 3.59 (*s*, OMe-6)/162.5 (C-6) in ring A confirmed by HMBC correlation as showed in **Figure 3.12**. Moreover, NMR data in ring B also suggested the *meta* relationship of the two hydroxyl groups located at δ_{C} 159.1 (C-3' and C-5') due to the correlation of HMBC of H-6' to C-2' (δ_{C} 106.7), C-4' (δ_{C} 105.0), and C-7 (δ_{C} 198.4), and H-4' to C-2'. Thus compound **12** was identified as a new compound, namely mangostanone II.

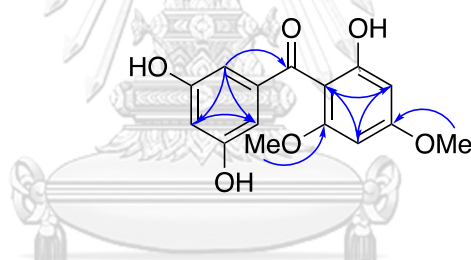


Figure 3.12 Selected HMBC correlations ($^1\text{H} \rightarrow ^{13}\text{C}$) of compound **12**

Compound **13** was obtained as brown-yellow solid with the molecular formula of $\text{C}_{15}\text{H}_{14}\text{O}_6$ determined by HRESIMS at m/z 299.0537 [$\text{M} + \text{Na}$] $^+$ (calcd 299.0532) and melting point of 180-200 °C. The FT-IR exhibited absorption band for O-H stretching at ν_{\max} 3471 cm^{-1} and conjugate of C=O at 1634 cm^{-1} . UV absorption band at 210 and 305 nm (logE= 2.757 and 2.451 respectively). The ^1H (**Table 3.5**) NMR spectroscopic data contained a singlet signal for one methoxy groups at δ_{H} 3.58 *s*, 6H, which attached to two equivalent C-4 (δ_{C} 161.4) according to the HMBC correlations (**Figure 3.13**). Furthermore, two duplets aromatic protons at H-3 and H-5 (δ_{H} 6.08 *s* and 6.08 *s*) both showed correlation to C-1 (δ_{C} 106.2) and C-7 (δ_{C} 196.1) indicated that compound **13** had a 4-hydroxy-2,6-dimethoxybenzoyl moiety in ring A.

The ^{13}C NMR spectra data displayed two hydroxyl group at δ_{C} 144.3 (C-3') and δ_{C} 149.3 (C-4') suggest the *ortho* relationship in ring A as provide by the HMBC correlation of [H-2' (7.23 d, $J= 2.0$ Hz)/C-7, C-3', C-4', C-6'], [H-5' (6.85 d, $J= 8.4$ Hz)/C-1', C-3',and C-4'] and [H-6' (7.09 dd, $J= 2.0, 8.4$ Hz) /C-7, C-2', and C-4']. Finally, the structure of **13** was confirmed by COSY and HMBC correlations as shown in **Figure 3.13**, and it was identified as a new compound and named as mangostanone III.

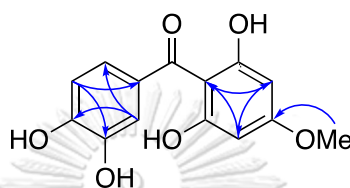


Figure 3.13 Selected HMBC correlations ($^1\text{H} \rightarrow ^{13}\text{C}$) of compound **13**

Compound **14** was obtained as macaron yellow solid with molecular formula of $\text{C}_{13}\text{H}_{10}\text{O}_6$ determined by NMR data. When comparing ^1H and ^{13}C NMR data (**Table 3.5 and 3.6**) with previous compound, it suggested that compound **14** also have similar benzophenone structure. Signals of five aromatic protons were appeared at δ_{H} 5.98 (s, H-3 and H-5), 7.24 (brs, $J= 4.0$ Hz, H-2'), 6.84 (d, $J= 4.0$ Hz, H-5'), and 7.16 (d, $J= 4.0$ Hz, H-6'). From HMBC correlations, ring A showed 1,3,5-*tri*-substituted hydroxyl groups located C-2 (δ_{C} 162.8), C-4 (δ_{C} 164.5), and C-6 (δ_{C} 162.8) along with *ortho* relationship of two hydroxyl groups at C-3' (δ_{C} 145.1) and C-4' (δ_{C} 150.0). After compared NMR data with previous reported, compound **17** was identified as maclurin [24].

Compound **15** was obtained as yellowish solid. The molecular formula was obtained by NMR spectra data as $\text{C}_{13}\text{H}_{10}\text{O}_5$. ^1H and ^{13}C NMR (**Tables 3.5 and 3.6**) provided the typical signals of benzophenone compared with previous compound **14**. Form HMBC spectra, hydroxy group at C-3' was confirmed by the correlation of H-2' (δ_{H} 7.08 s, 1H), H-4' (δ_{H} 7.06 s, 1H), H-5' (δ_{H} 7.23 t, $J= 8.0$ Hz, 1H), and H-6' (δ_{H} 7.08 d, $J= 12$ Hz, 1H) in ring B. Whereas H-3 (5.97 s) and H-5 (5.97 s) indicated *meta* aromatic

relationship in ring A. The structure was identified as 2,3',4,6-tetrahydroxybenzophenone as described in previous report [25].

Compound **16** was obtained as beige solid with molecular formula of $C_{14}H_{11}O_6$ established by 1H and ^{13}C NMR data. Compared with others previous compound, NMR data suggested that compound **16** was a benzophenone derivative. The data showed resonances of four hydroxyl groups located at δ_c 165.1 (C-2), 164.7 (C-4), 159.2 (C-3'), and 159.2 (C-5') and one methoxy group at δ_c 56.1 (OMe-6) confirmed by HMBC correlations. This compound was identified as mangaphenone as compared with the data from previous research [26].

Compound **17** was obtained as pearl-white solid. The molecular formula was $C_{16}H_{15}O_6$ obtained from NMR data analysis. By comparing data of 1H and ^{13}C NMR spectra between compound **16** and **17**, the signals of five aromatic protons appear at δ_H 6.15 (*d*, $J= 4.0$ Hz, H-3), 5.95 (*d*, $J= 8.0$ Hz, H-5), 7.17 (*brs*, $J= 4.0$ Hz, H-2'), 6.82 (*d*, $J= 4.0$ Hz, H-5'), and 7.18 (*d*, $J= 4.0$ Hz, H-6'). It suggested that these two compounds have nearly similar benzophenone core structure, except for the replacement of methoxyl groups at C-4 (δ_c 165.9) and C-4' (δ_c 149.4). Compound **17** structure was identified as (2-hydroxy-4,6-dimethoxyphenyl)(3-hydroxy-4-methoxyphenyl)methanone by comparison of reported study [27].

Table 3.5 1H NMR data of compounds **12** - **17**

Position	δ_H , mult. (J in Hz)					
	12 ^(b)	13 ^(b)	14 ^(b)	15 ^(b)	16 ^(b)	17 ^(a)
1	-	-	-	-	-	-
2	-	-	-	-	-	-
3	6.13 d, 2.0	6.08 s	5.98 s	5.97 s	6.08 s	6.15 d, 8.0
4	-	-	-	-	-	-
5	6.15 d, 2.0	6.08 s	5.98 s	5.97 s	6.06 s	5.95 d, 8.0
6	-	-	-	-	-	-
7	-	-	-	-	-	-
1'	-	-	-	-	-	-

2'	6.60 d, 2.1	7.23 d, 2.0	7.24 4.0	brs, 7.08 s	-	7.17 4.0	brs, 4.0
3'	-	-	-	-	-	-	-
4'	6.51 t, 2.1	-	-	7.06 s	6.50 t, 4.0	-	-
5'	-	6.85 d, 8.4	6.84 d, 4.0	7.23 t, 8.0	-	6.82 d, 4.0	-
6'	6.60 d, 2.1	7.09 2.0, 8.4	dd, 7.16 d, 4.0	6.96 d, 12.0	6.57 d, 4.0	7.18 d, 4.0	-
OH-2	-	-	-	-	-	-	11.74 s
OH-4	-	-	-	-	3.07 s	-	-
OMe-4	3.86 s	3.58 s	-	-	-	3.83 s	-
OMe-6	3.59 s	-	-	-	3.55 s	3.53 s	-
OH-3'	-	-	-	-	-	5.69 s	-
OMe-4'	-	-	-	-	-	3.94 s	-

(a) measured in CDCl₃; (b) measured in acetone-d₆

Table 3.6 ¹³C NMR data of compounds **12** - **17**

Position	δ_c					
	12 ^(b)	13 ^(b)	14 ^(b)	15 ^(b)	16 ^(b)	17 ^(a)
1	107.9	106.2	105.0	105.4	107.1	105.9
2	163.8	163.1	162.8	163.8	165.1	165.1
3	94.7	95.8	96.0	95.9	96.9	93.6
4	166.3	161.4	164.5	165.4	164.7	165.9
5	91.9	91.5	96.0	95.9	92.8	91.7
6	162.5	162.2	162.8	163.8	163.4	161.7
7	198.4	196.1	197.9	199.6	198.9	198.2
1'	144.0	132.8	133.9	144.0	144.7	134.0
2'	106.7	115.9	117.2	120.2	107.6	7.17
3'	159.1	144.3	145.1	157.7	159.2	144.6
4'	105.0	149.3	150.0	115.6	106.6	149.4
5'	159.1	114.2	115.1	129.5	159.2	109.3
6'	106.7	122.7	123.4	118.7	107.6	115.0

OMe-4	56.0	54.8	-	-	-	55.5
OMe-6	56.1	-	-	-	56.1	55.3
OMe-4'	-	-	-	-	-	56.0

(a) measured in CDCl₃; (b) measured in acetone-d₆

3.2.10 Structure elucidation of compounds **18** – **20**

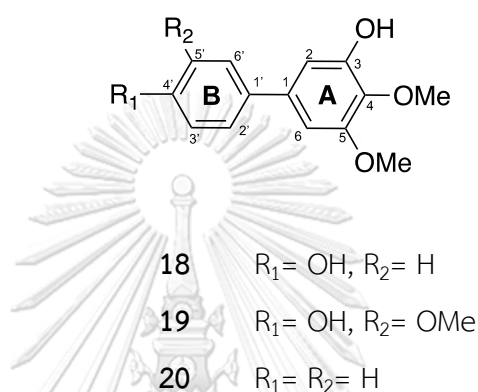


Figure 3.14 Structures of compounds **18** – **20**

New compound **18** was obtained as white powder. The molecular formula was C₁₄H₁₄O₄ as determined by HRESIMS at m/z 269.0799 [M + Na]⁺ (calcd 269.0790). The FT-IR spectral data showed major absorption band at ν_{\max} 3465 cm⁻¹ (O-H stretching) and 1596, 1576 cm⁻¹ (C=C stretching). The UV spectrum displayed absorption band at maximum wavelength λ_{\max} at 221 nm (logE= 2.744) and 267 nm (logE= 2.663) indicated the presence of hydroxygenated benzene derivative [28]. The ¹H (Table 3.7) and ¹³C (Table 3.8) NMR spectroscopic data displayed two *meta*-coupled aromatic protons at δ_{H} 6.78 *d*, *J*=2.0 Hz (H-2) and 6.63 *d*, *J*=2.0 Hz (H-6). The remaining δ_{H} 6.87 *s*, 2H (H-5') and 7.42 *s*, 2H (H-6') suggest a system of two aromatic protons in trisubstituted benzene in ring B. The correlation of OH-3 (δ_{H} 5.84, *s*) to C-2 (δ_{C} 106.7), C-3 (δ_{C} 149.5), and C-4 (δ_{C} 134.9) in the HMBC spectrum (Figure 3.15) confirmed the location of hydroxyl group at C-3. The locations of the methoxy groups at C-4 and C-5 were indicated by the HMBC correlations of OMe-4 to C-4 (δ_{C} 134.9) and C-5 (δ_{C} 152.6) and OMe-5 to C-4 and C-5 similarly. In comparison with the

NMR data of compound **18** with previous biphenyl, the common features were observed quite similar except for the additional hydroxy group (OH-4') in ring B. These suggest that compound **18** could be identified as a new compound, namely mangostanone IV.

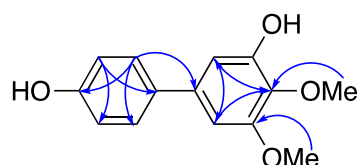


Figure 3.15 Selected HMBC correlations ($^1\text{H} \rightarrow ^{13}\text{C}$) of compound **18**

Compound **19** was obtained as light-yellow powder and a molecular formula as $\text{C}_{15}\text{H}_{16}\text{O}_5$ determined using 1D and 2D NMR spectra. HMBC correlations suggested a structure core as biphenyl derivative. The ^1H NMR spectroscopic data (Table 3.7) showed two doublets of aromatic protons at δ_{H} 6.80 (*d*, $J = 4.0$ Hz, H-2) and 6.64 (*d*, $J = 4.0$ Hz, H-6) in ring A, and three aromatic protons at δ_{H} 7.04 (*d*, $J = 8.0$ Hz, H-2'), 6.96 (*d*, $J = 8.0$ Hz, H-5') and 7.06 (*d*, $J = 4.0$ Hz, H-5') in ring B. Additionally, three methoxy groups were located at C-4 (δ_{C} 134.9), C-5 (δ_{C} 152.6), and C-5' (δ_{C} 114.8) and two hydroxyl groups at C-3 (δ_{C} 149.5) and C-4' (δ_{C} 145.4). Compound **19** was identified as garciosine A as comparison to the reported data from literature [29].

Compound **20** was obtained as light-yellow gum and a molecular formula of $\text{C}_{14}\text{H}_{14}\text{O}_3$ was determined by ^1H - and ^{13}C -NMR data analysis. NMR data of compound **20** (Tables 3.7 and 3.8) ^1H NMR spectroscopic data showed two doublets of aromatic proton at δ_{H} 6.85, $J = 4.0$ Hz, H-2 and δ_{H} 6.69, $J = 4.0$ Hz, H-6 with the correlation observed by HMBC of [H-2/C-3, C-4, and C-6 (δ_{H} 6.85 *d*, $J = 4.0$ Hz)/ δ_{C} 149.6, 135.1, and 103.6] and H-6/C-2, C-4, and C-5 (δ_{H} 6.69 *d*, $J = 4.0$ Hz)/ δ_{C} 107.2, 135.1, and 152.6]. This pattern was similar to compound **18** and suggest that compound **20** might have same biphenyl core. In addition, correlations showed the absence of hydroxyl group at C-4' (δ_{C} 127.4). The structure was compared and identified as 4,5-dimethoxy[1,1'-biphenyl]-3-ol as described in the previous reported

which occur by synthesis [30], this conclude that compound **20** is new found in naturally occur.

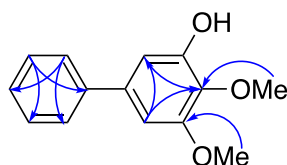


Figure 3.16 Selected HMBC correlations ($^1\text{H} \rightarrow ^{13}\text{C}$) of compound **20**

3.2.11 Structure elucidation of compound **21**

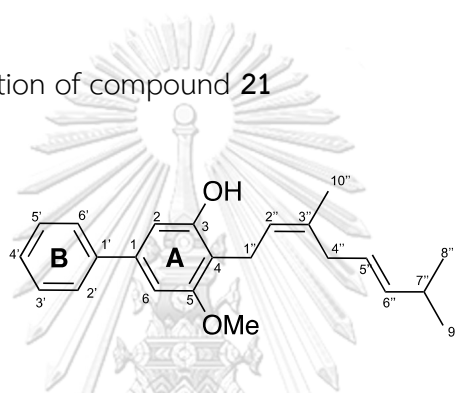


Figure 3.17 Structure of compound **21**

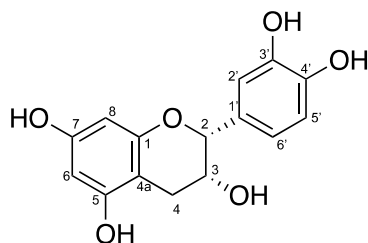
Compound **21** was obtained as yellow gum with molecular formula $\text{C}_{23}\text{H}_{28}\text{O}_2$ determined by 1D and 2D NMR spectral data. The ^1H and ^{13}C NMR data showed the similar structural core of hydroxygenated benzene as previous compound, except for the replacement of geranyl group with signals appeared at $\delta_{\text{H}}/\delta_{\text{C}}$ 3.50 (*t*, $J= 8.0$ Hz, H-1'')/22.3, 5.32 (*t*, $J= 8.0$ Hz, H-2'')/122.0, 2.09 (*m*, H-4'')/39.9, 2.11 (*m*, H-5'')/26.6, 5.11 (*t*, $J= 8.0$ Hz, H-6'')/124.1, 1.63 (*s*, H-8'')/17.8, 1.71 (*s*, H-9'')/25.8, 1.86 (*s*, H-10'')/16.3; δ_{C} 138.3 (C-3'') and 131.9 (C-7'') located at δ_{C} 114.6 (C-4) confirmed by HMBC correlations of H-1'' to C-4. The structure was elucidated based on comparison to its NMR data to the literature, it was identified as 3-hydroxy-4-geranyl-5-methoxybiphenyl [31].

Table 3.7 ^1H NMR data of compounds **18** – **21** in CDCl_3

Position	δ_{H} , mult. (<i>J</i> in Hz)			
	18	19	20	21
1	-	-	-	-
2	6.78 d, 2.0	6.80 d, 4.0	6.85 d, 4.0	6.76 s
3	-	-	-	-
4	-	-	-	-
5	-	-	-	-
6	6.63 d, 2.0	6.64 d, 4.0	6.69 d, 4.0	6.73 s
1'	-	-	-	-
2'	-	7.04 d, 8.0	-	-
3'	-	6.96 d, 8.0	-	-
4'	-	-	7.33 d, 8.0	7.36 t, 8.0
5'	6.87 dt, 8.0, 2.0	-	7.42 t, 8.0	7.44 t, 8.0
6'	7.42 dt, 8.0, 2.0	7.06 d, 4.0	7.53 d, 8.0	7.58 d, 8.0
1''	-	-	-	3.50 t, 8.0
2''	-	-	-	5.32 t, 8.0
3''	-	-	-	-
4''	-	-	-	2.09 m
5''	-	-	-	2.11 m
6''	-	-	-	5.11 t, 8.0
7''	-	-	-	-
8''	-	-	-	1.63 s
9''	-	-	-	1.71 s
10''	-	-	-	1.86 s
OH-3	5.84 s	6.07 s	5.83 s	5.52 s
OMe-4	3.93 s	3.92 s	3.94 s	-
OMe-5	3.92 s	3.93 s	3.39 s	3.90 s
OMe-5'	-	3.93 s	-	-
OH-4'	-	5.85 s	-	-

Table 3.8 ^{13}C NMR data of compounds **18** - **21** in CDCl_3

Position	δ_{c}			
	18	19	20	21
1	137.4	137.7	137.8	140.8
2	106.7	106.9	107.2	108.1
3	149.5	149.5	149.6	155.9
4	134.9	134.9	135.1	114.6
5	152.6	152.6	152.6	158.3
6	103.2	103.2	103.6	102.6
1'	133.9	133.6	141.2	141.4
2'	128.4	109.9	127.2	127.1
3'	115.7	146.8	128.8	128.9
4'	155.4	145.4	127.4	127.4
5'	115.7	114.8	128.8	128.9
6'	128.4	120.0	127.2	127.1
1''	-	-	-	22.3
2''	-	-	-	122.0
3''	-	-	-	138.3
4''	-	-	-	39.9
5''	-	-	-	26.6
6''	-	-	-	124.1
7''	-	-	-	131.9
8''	-	-	-	17.8
9''	-	-	-	25.8
10''	-	-	-	16.3
OMe-4	61.2	61.1	61.3	-
OMe-5	56.1	56.1	56.1	56.0
OMe-5'	-	56.1	-	-

3.2.12 Structure elucidation of compound **22**Figure 3.18 Structure of compound **22**

Compound **22** was obtained as yellow powder with molecular formula of $C_{15}H_{14}O_6$ determined by NMR data analysis. ^{13}C NMR data (Table 3.9) indicated fifteen carbon signals δ_c 158.9, 109.3, 161.1, 105.6, 152.6, 144.6, 119.9, 123.9, 117.1, 21.8, 121.4, 136.4, 25.8, 18.1, and 22.3 consisted as two benzene rings and one linked with heterocyclic pyran ring and 1H NMR data showed typical signal of chelated hydroxy group at δ_H 13.19 (s, OH-5) lead to the suggestion of flavonoid derivative [32]. Another four hydroxyl groups were located at C-3, C-7, C-3' and C-4' owing to HMBC correlations. The structure was identified as epicatechin after comparison with previous reported.

Table 3.9 NMR spectral data of compound **22** in acetone- d_6

Position	δ_H , mult. (J in Hz)	δ_c
1	-	158.9
2	-	109.3
3	-	161.1
4	-	105.6
4a	-	152.6
5	-	144.6
6	7.28 s	119.9
7	7.21 s	123.9

8	7.76 d, 8.0	117.1
1'	3.47 d, 8.0	21.8
2'	5.27 s	121.4
3'	-	136.4
4'	1.76 s	25.8
5'	1.86 s	18.1
6'	3.54 d, 8.0	22.3
OH-3	6.52 s	-
OH-5	13.19 s	-

3.3 Cytotoxic activity of isolated compounds

Xanthenes are known as one of the largest constituent found in mostly parts of mangosteen. Thus, these compounds have been studied extensively in both structure elucidation and primary bioactivities. Many of them possessed medicinal abilities such as antibacterial, anti-inflammatory and anticancer [33]. In this study, the isolated compounds obtained from mangosteen roots collected from Nakhon Sri Thammarat province, the southern Thailand are classified not only xanthenes but also benzophenones and biphenyls which are barely studied in medicinal applications. To investigate anticancer properties of these compounds, preliminary screening of twenty-two compounds were observed by their cytotoxic ability towards two hepatocellular carcinomas (HepG2 and Huh7) and two colon cancer cells (Caco2 and HCT-116) using MTT assay. Sorafenib and doxorubicin were used as positive drug controls. This assay based on colorimetric analysis using 3-(4,5-dimethylthiazol-2-yl)-2,5-diphenyltetrazolium bromide or MTT, a yellow tetrazolium salt, which is reduced to a purple formazan crystal by mitochondrial dehydrogenase of active cells. In this study, compounds **2**, **3**, **5** and **11** showed considerable activities on all cell lines tested with the IC_{50} values less than 50 μ M. Nonetheless, many previous studies have been reported that compound **2** or α -mangostin, the major xanthone of mangosteen, has a potential effect against various cancer cells. Hence, these results were able to confirm the efficacy of α -mangostin bioactivities with the previous reported. Three-fourth cell lines (HepG2, Huh-7 and Caco2) showed cytotoxicity

affected by compound **21** with IC_{50} 11.87 ± 1.24 , 41.63 ± 1.22 and 10.47 ± 0.68 μM , respectively. Compounds **13** and **16** showed more selective results against one cell line each in two types of cancer, HepG2 and HCT-116 with their cytotoxic ability in dose-dependent manner. In addition, compound **17** showed only significant difference in HCT-116 cells with IC_{50} of 28.28 ± 0.58 μM and compound **19** showed only significant difference in HepG2 cells with IC_{50} value of 19.42 ± 0.88 μM . Interestingly, new compound **1** showed highly effective against Huh7 with IC_{50} of 9.52 ± 1.05 μM and moderate effect on HepG2 and Caco2 cells (38.30 ± 1.19 and 20.20 ± 0.50 μM , respectively). Unfortunately, compounds **4**, **6**, **7** and **22** were unable to conclude cytotoxicity against last investigated cell line due to the problem occur during experiment which led to the loss of HCT-116. Apart from these, other compounds showed weak cytotoxicity to all investigated cell lines.

For further study, compounds which active against both HepG2 and Huh7 with IC_{50} less than 50 μM will be observes in cell migration analysis.

Table 3.10 Cytotoxic activity of compounds **1** – **22** against HCC cells and colon cancer cells

Compound	IC_{50} (μM) \pm S.D.			
	HepG2	Huh-7	Caco2	HCT-116
Sorafenib	2.66 ± 1.86	3.22 ± 1.20	4.98 ± 0.43	N/A
Doxorubicin	3.07 ± 0.62	2.47 ± 0.59	67.83 ± 0.11	1.10 ± 1.34
1	38.30 ± 1.19	9.52 ± 1.05	20.20 ± 0.50	64.55 ± 1.04
2	5.85 ± 1.13	6.84 ± 1.28	6.11 ± 0.60	11.51 ± 1.80
3	12.43 ± 0.99	14.96 ± 1.05	7.79 ± 0.58	32.85 ± 1.22
4	11.30 ± 0.83	11.98 ± 0.68	16.08 ± 0.47	N/A
5	10.43 ± 1.34	7.23 ± 1.25	6.96 ± 0.60	37.83 ± 1.51
6	22.13 ± 0.98	14.20 ± 0.90	29.99 ± 0.51	N/A
7	50.04 ± 0.75	40.08 ± 0.81	67.16 ± 0.40	N/A
8	UD	UD	UD	95.3 ± 0.19
9	UD	50.43 ± 1.30	62.83 ± 0.60	UD
10	99.14 ± 0.66	60.8 ± 1.03	UD	UD

11	15.99 ± 1.39	9.97 ± 1.33	6.39 ± 0.62	30.95 ± 1.65
12	UD	UD	UD	UD
13	19.41 ± 1.19	UD	87.87 ± 0.34	31.43 ± 0.40
14	UD	UD	UD	UD
15	UD	UD	UD	UD
16	9.81 ± 1.26	UD	UD	32.95 ± 0.25
17	UD	UD	UD	28.28 ± 0.58
18	72.62 ± 0.52	87.15 ± 0.56	UD	UD
19	UD	19.42 ± 0.88	83.19 ± 0.32	UD
20	UD	UD	97.02 ± 0.34	UD
21	11.87 ± 1.24	41.63 ± 1.22	10.47 ± 0.68	83.78 ± 1.43
22	UD	UD	UD	N/A

Values are expressed as mean ± standard deviation (n=3), UD (undetectable, IC₅₀ value >100 μM), N/A (Not available)

3.4 Anti-migration effect of compounds 1, 2, 3, 5, 6, 11 and 21 against HCC cell (Huh7)

Cell metastasis is a process of cancer cells spread from primary tumor to the nearest organs via lymphatic and blood circulatory system. Collective cell migration is the major process of tissue regeneration, cancer invasion and cancer metastasis. (Pijuan et al, 2019). This process could lead to poor survival of patients with end-stage of cancer. To assess whether candidate compounds could inhibit cell migration, compounds **1, 2, 3, 5, 6, 11** and **21** were tested in dose- and time-dependent manner for wound healing activity using monolayer Huh7 cells scratch assay. In this experiment, the IC₅₀ values of candidate active compounds were considered in assessing wound healing activity. Dosage for experiments were fixed as μM at IC₅₀, (IC₅₀/2), (IC₅₀*2) and 3 μM following the IC₅₀ value of sorafenib described in previous study [34]. Sorafenib is a standard drug approved to treat many cancer types such as hepatocellular carcinoma, renal cell carcinoma and thyroid cancer [35]. Because of this, 3 μM were used to compare between tested compounds and

standard drug in the same concentration. **Table 3.11** summarize a concentration used for each compound.

Table 3.11 Concentrations used for wound healing analysis of compound **1, 2, 3, 5, 6, 11,** and **21**

Compound	Actual IC ₅₀ (μM) ± S.D. value against Huh7	Treated concentration (μM)			
		Std.	IC ₅₀ /2	IC ₅₀	IC ₅₀ *2
1	9.52 ± 1.05	3	6	12	24
2	6.84 ± 1.28	3	1.5	6	12
3	14.96 ± 1.05	3	6	12	24
5	7.23 ± 1.25	3	4	8	16
6	14.20 ± 0.90	3	6	12	24
11	9.97 ± 1.33	3	6	12	24
21	41.63 ± 1.22	3	15	30	60

As a result, **Figure 3.19** showed wound closure of untreated cells as control and cells treated with sorafenib as positive control. The results indicated that wound closure percentage of untreated control were significantly higher than the 3 μM sorafenib group at 24 and 48 h.

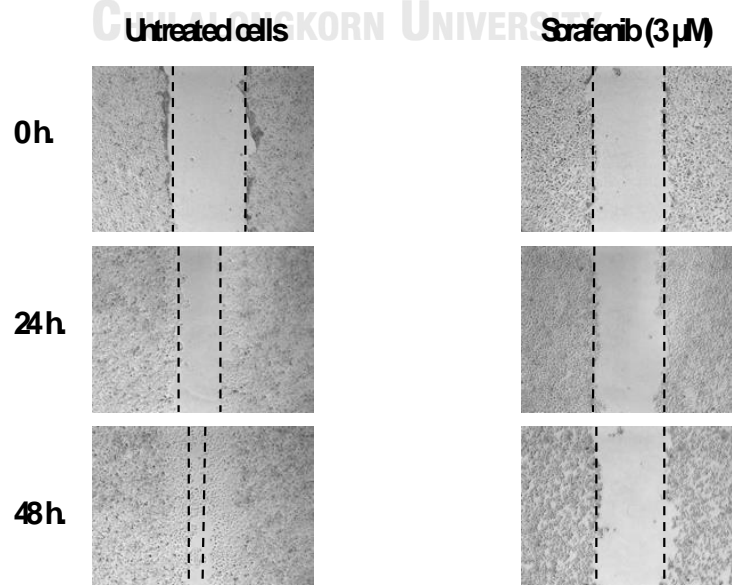


Figure 3.19 Wound closure expression of untreated cells and cells treated with sorafenib (3 μM) at 0, 24 and 48 h

Firstly, compound **1** showed a considerable effect in inhibiting cell migration with IC_{50} value (12 μM) compare with untreated control at 24 h. The percentage of tissue repair was dramatically decreased meaning that the compound was able to retard wound closure. In addition, concentration less than IC_{50} (6 μM) also suggested ability to inhibit migration with the percentage of tissue repair decreasing more than 50% when compared with the percentage of control at 24 h. The higher concentration resulted in same pattern with that at IC_{50} (**Figure 3.20**).

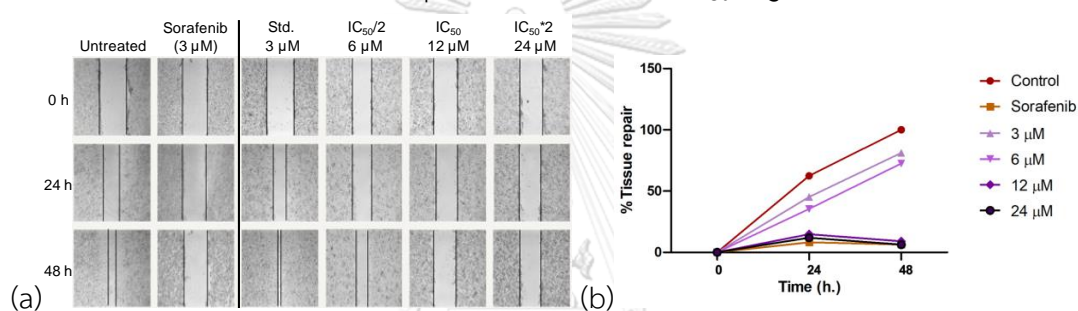


Figure 3.20 Effect of compound **1** on wound closure at 0, 24 and 48 h (a), graph correlation between times and %tissue repair (b)

Table 3.12 Tissue repair percentage value (%) of compound **1**

Time (h)	Percentage of tissue repair (%)					
	Control	Sorafenib	3 μM	6 μM	12 μM	24 μM
0	0	0	0	0	0	0
24	62.42 \pm 2.78	8.15 \pm 3.39	45.19 \pm 1.38	35.38 \pm 4.03	14.76 \pm 4.41	11.98 \pm 1.74
48	100.0 \pm 0.00	6.40 \pm 2.93	81.14 \pm 3.57	72.60 \pm 5.10	9.12 \pm 2.62	6.28 \pm 2.48

Values are expressed as mean \pm standard deviation (n=2)

Next, the results indicated that compound **2** gave significant effect at 24 h (**Figure 3.21 b**). To explain further, 6 μM was able to inhibit wound closing with just 1.78% of tissue repair compared to control at the same period of time. Additionally, with the same concentration at 24 h, compound **2** was able to decrease migration

process with the result close to tissue repair percentage of sorafenib as data shown in **Table 3.13**. Increasing of concentration led cells morphology to change and peel off, it caused wound space area to be unable measure. This suggested that treatment with double in IC_{50} was too strong and toxic to cells.

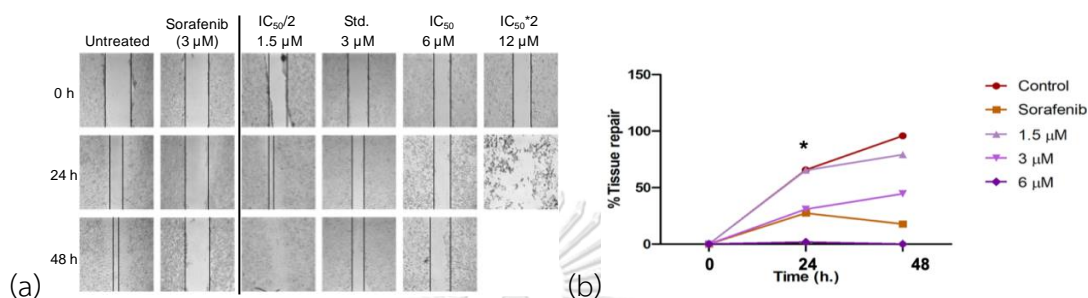


Figure 3.21 Effect of compound 2 on wound closure at 0, 24 and 48 h (a), graph correlation between times and %tissue repair (b)

Table 3.13 Tissue repair percentage value (%) of compound 2

Time (h)	Percentage of tissue repair (%)					
	Control	Sorafenib	1.5 μ M	3 μ M	6 μ M	12 μ M
0	0	0	0	0	0	0
24	65.67 \pm 3.70	27.41 \pm 5.44	65.27 \pm 7.59	30.90 \pm 12.71	1.78 \pm 20.04	UD
48	95.86 \pm 2.85	17.77 \pm 5.07	79.18 \pm 8.64	44.60 \pm 15.61	0	UD

Values are expressed as mean \pm standard deviation (n=2), UD (undetectable)

Compound 3 also gave significant results at 24 h. From **Table 3.14**, considered no increase in tissue repair percentage in cells treated with IC_{50} concentration since 24 h and became toxic as 48 h pass by. Lower concentration (6 μ M) showed decrease in cell migration by compare percentage results with control. Moreover, higher concentration showed cytotoxicity against investigated cells at 24 h due to change in cells morphology and damage. Because of this, gaps between wound cells could not be measured.

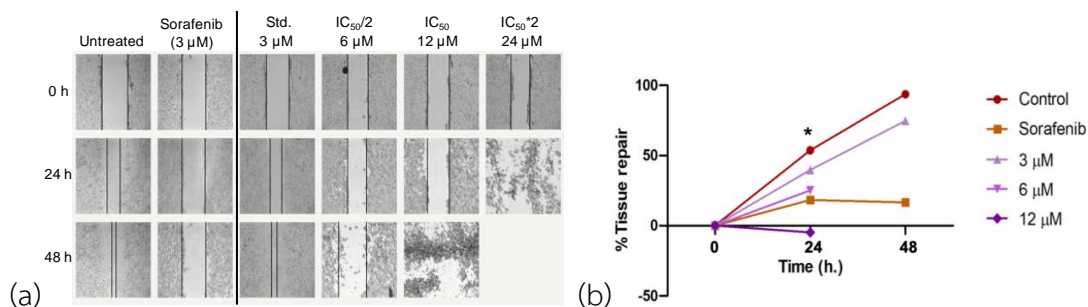


Figure 3.22 Effect of compound **3** on wound closure at 0, 24 and 48 h (a), graph correlation between times and %tissue repair (b)

Table 3.14 Tissue repair percentage value (%) of compound **3**

Time (h)	Percentage of tissue repair (%)					
	Control	Sorafenib	3 μM	6 μM	12 μM	24 μM
0	0	0	0	0	0	0
24	53.71 \pm 7.32	18.34 \pm 6.95	39.74 \pm 3.31	25.23 \pm 3.91	0	UD
48	93.65 \pm 3.67	16.62 \pm 6.48	74.65 \pm 3.53	UD	UD	UD

Values are expressed as mean \pm standard deviation (n=2), UD (undetectable)

Compare between %tissue repair of 8 μM and sorafenib at 24 h (**Table 3.15**), compound **5** showed a similar result of inhibited wound closure and more effectiveness when time increased. In addition, lower concentration (4 μM) at 24 h was able to slowdown migration progress about 50% better than untreated cells when compare with tissue repair percentage at each condition. Results also suggested that, higher concentration was toxic enough to damage cells and not adherent since 24 h. Thus, results could not be calculated.

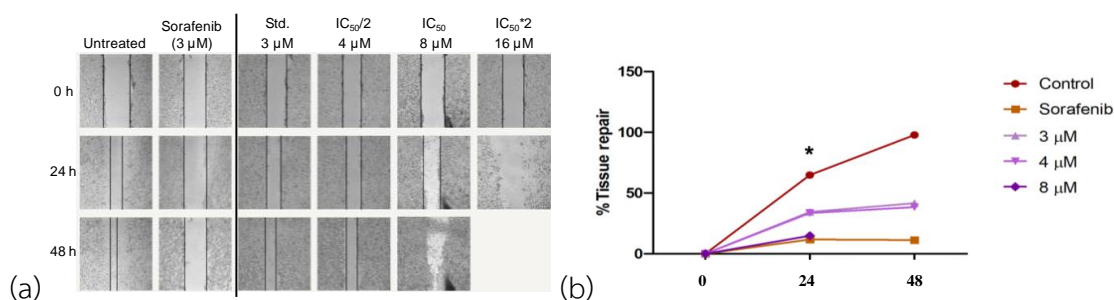


Figure 3.23 Effect of compound **5** on wound closure at 0, 24 and 48 h (a), graph correlation between times and %tissue repair (b)

Table 3.15 Tissue repair percentage value (%) of compound **5**

Time (h)	Percentage of tissue repair (%)					
	Control	Sorafenib	3 μ M	4 μ M	8 μ M	16 μ M
0	0	0	0	0	0	0
24	64.75 \pm 7.97	11.78 \pm 4.12	34.49 \pm 5.11	33.61 \pm 2.14	14.77 \pm 5.25	UD
48	97.85 \pm 3.62	11.36 \pm 3.49	41.63 \pm 7.18	38.45 \pm 3.52	UD	UD

Values are expressed as mean \pm standard deviation (n=2), UD (undetectable)

Compound **6** showed fascinating results in inhibited cells migration. There were no increase of tissue repair percentage in all condition since 24 h (as shown in **Table 3.16**) compared to sorafenib and control. Hence, it gave significant effects at 24 h (**Figure 3.24 b**). Furthermore, in higher concentration we could slightly see a change in morphology which suggested that this compound might not be too toxic.

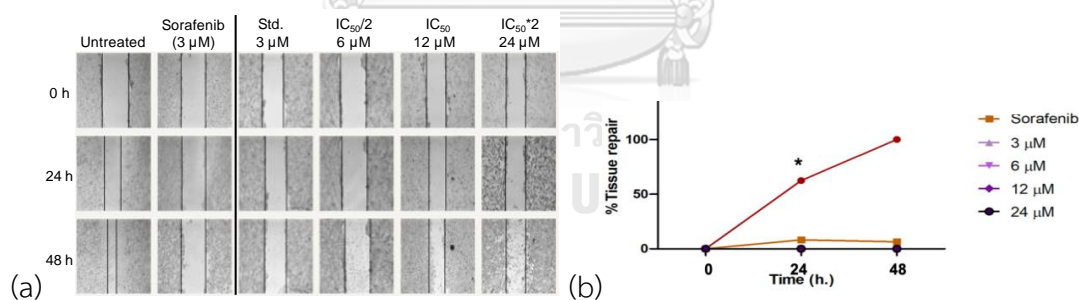


Figure 3.24 Effect of compound **6** on wound closure at 0, 24 and 48 h (a), graph correlation between times and %tissue repair (b)

Table 3.16 Tissue repair percentage value (%) of compound **6**

Time (h)	Percentage of tissue repair (%)					
	Control	Sorafenib	3 μ M	6 μ M	12 μ M	24 μ M
0	0	0	0	0	0	0
24	65.88 \pm 11.11	7.88 \pm 10.70	0	0	0	0

48 96.74 ± 2.15 6.04 ± 2.38 0 0 0 0

Values are expressed as mean \pm standard deviation (n=2)

Compound **11** showed moderately results in cell migrate inhibition. Within IC_{50} concentration (12 μM) at 24 h, this compound could decrease cell motility with $29.89 \pm 2.66\%$ tissue repair compared to control. In higher concentration (24 μM) was able to inhibit wound closure since 24 h. However, in the concentration lower than IC_{50} , this compound showed no effect as tissue repair rates still remained same as untreated cells.

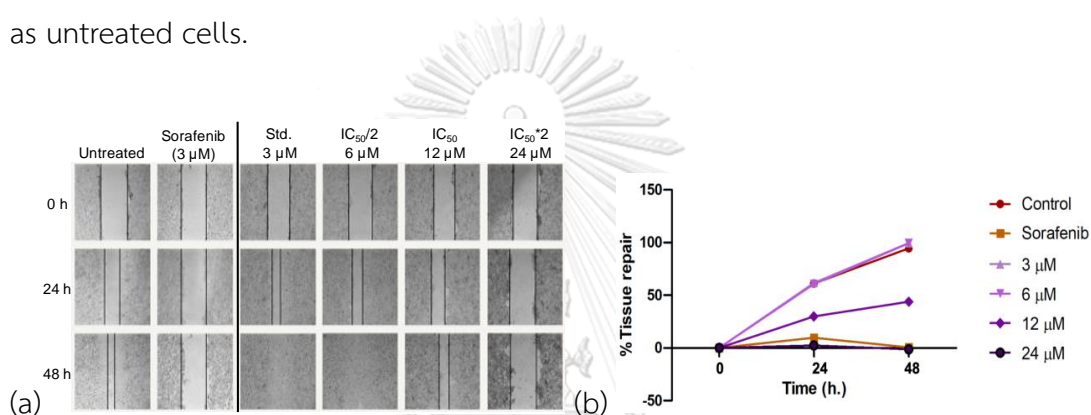


Figure 3.25 Effect of compound **11** on wound closure at 0, 24 and 48 h (a), graph correlation between times and %tissue repair (b)

Table 3.17 Tissue repair percentage value (%) of compound **11**

Time (h)	Percentage of tissue repair (%)					
	Control	Sorafenib	3 μM	6 μM	12 μM	24 μM
0	0	0	0	0	0	0
24	61.05 ± 5.84	9.71 ± 3.03	61.75 ± 1.64	60.53 ± 2.66	29.89 ± 2.66	2.42 ± 4.42
48	94.58 ± 1.90	0.54 ± 4.53	99.50 ± 0.81	99.43 ± 0.77	43.97 ± 2.77	0

Values are expressed as mean \pm standard deviation (n=2)

Lastly, compound **3**, which appears to be only a biphenyl metabolite apart from other candidate compounds, showed significant effect at 24 h (**Figure 3.26 b**). To explain more, compound with IC_{50} concentration at 24 h (30 μM) was able to inhibit wound closure with no increase in tissue repair percentage (**Table 3.18**). In 15

μM at 24 h condition, this compound could decrease tissue repair rate with the percentage closed to sorafenib. As for higher concentration, results showed that it was too toxic to cells which could damage cells perfectly since 24. Thus, this compound gave significant effects at 24 h.

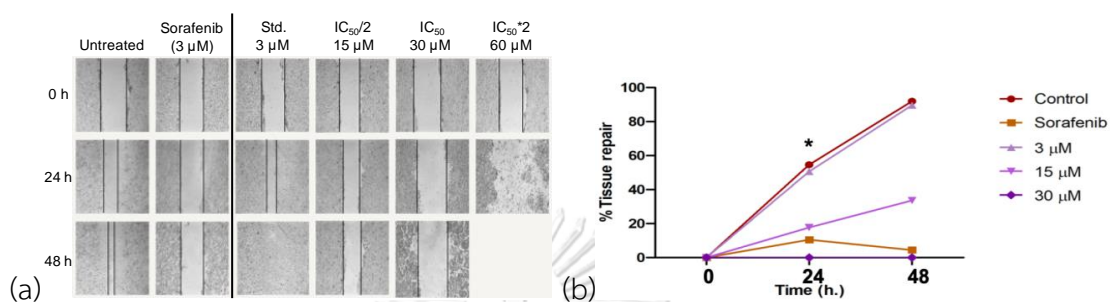


Figure 3.26 Effect of compound **21** on wound closure at 0, 24 and 48 h (a), graph correlation between times and %tissue repair (b)

Table 3.18 Tissue repair percentage value (%) of compound **21**

Time (h)	Percentage of tissue repair (%)					
	Control	Sorafenib	3 μM	15 μM	30 μM	60 μM
0	0	0	0	0	0	0
24	54.59 \pm 3.53	10.50 \pm 3.44	50.66 \pm 3.17	17.73 \pm 3.17	0	UD
48	91.99 \pm 2.18	4.44 \pm 4.98	89.66 \pm 2.39	33.60 \pm 2.19	0	UD

Values are expressed as mean \pm standard deviation (n=2), UD (undetectable)

3.5 Apoptosis assessment

Apoptosis is a programmed cell death, which occurs naturally in multicellular organism. Normally, there are two main pathways of apoptosis including intrinsic and extrinsic pathway. Apoptosis leads to elimination of unnecessary, damaged and infected cells to balance and protect organism. On the other hand, loss of apoptosis pathway could lead to pathological disorder such as cancer. In this study, assessment of apoptosis was performed to analyze whether compounds **1**, **6** and **11** were able to induce apoptosis in Huh7 cell line whereas compound **2**, **3**, and **5** have

already been studied previously [16]. The concentrations of each compounds were similar to those of previous experiment, at IC_{50} and two-folds greater than IC_{50} ($IC_{50} \times 2$). Untreated cells were used as control. The Annexin V/phosphatidylserine (PS) double stain was performed to study apoptotic cells and determined by Muse[®] Cell Analyzer. As results, each quadrant indicated stages of apoptosis profile, explain the mechanism of Annexin V reagent. Generally, phosphatidylserines are found exclusively in the inner membrane in healthy cells. During the early stage of apoptosis, phosphatidylserines are translocated from inner to the outer surface of the cell membrane where Annexin V, a specific phospholipid binding protein, can readily bind them. In addition, damaged nucleus is found in late apoptosis detected by DNA-binding dye.

Compound **1** or mangostanone I, showed a significant in total apoptosis rate. Apoptosis rate were increased to 22.60% in 12 μM and 25.70% in 24 μM comparing with the control. The comparative was shown clearly in **Figure 3.27**.

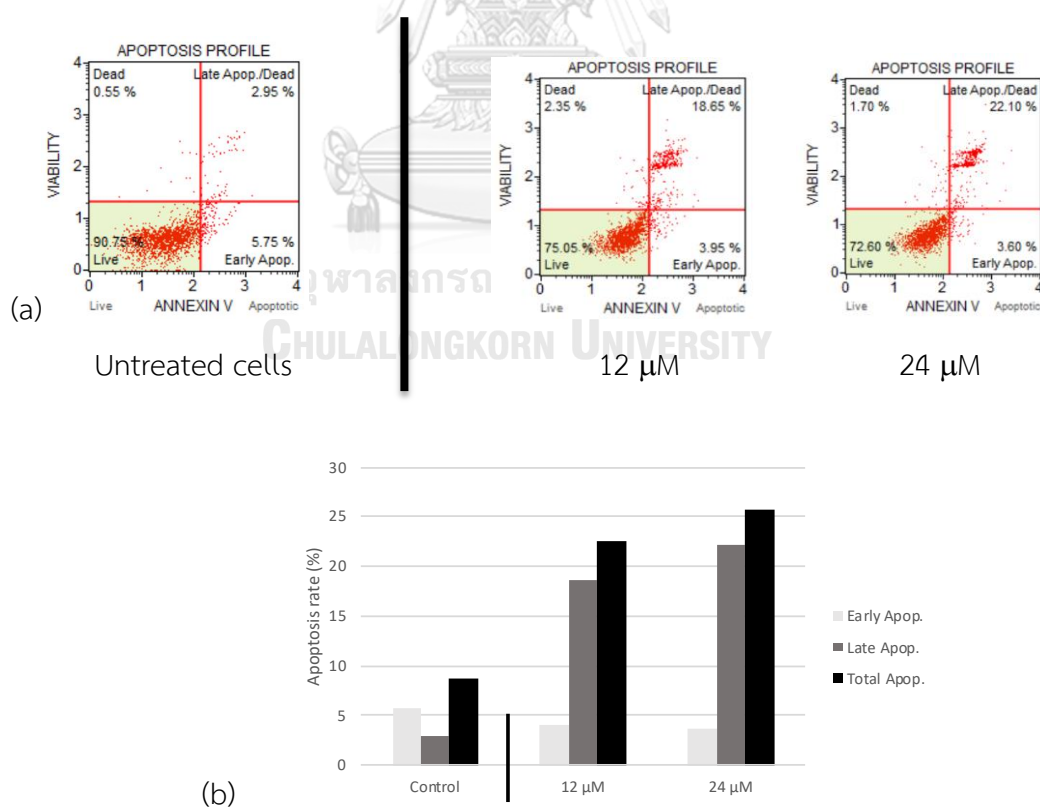


Figure 3.27 Apoptosis profile (a) and apoptosis rate (%) (b) of compound **1** on Huh-7 cells in 12 and 24 μM

Compound **6** (dulxanthone D) was able to enhance apoptosis in 24 μM concentration. It provided the highest rate of apoptotic induction when compared with untreated cells. However, the different between control and 12 μM concentration were barely seen. This result correlated with the previous experiment, explaining the reason that higher concentration was way too toxic and led to the increase of apoptotic cells.

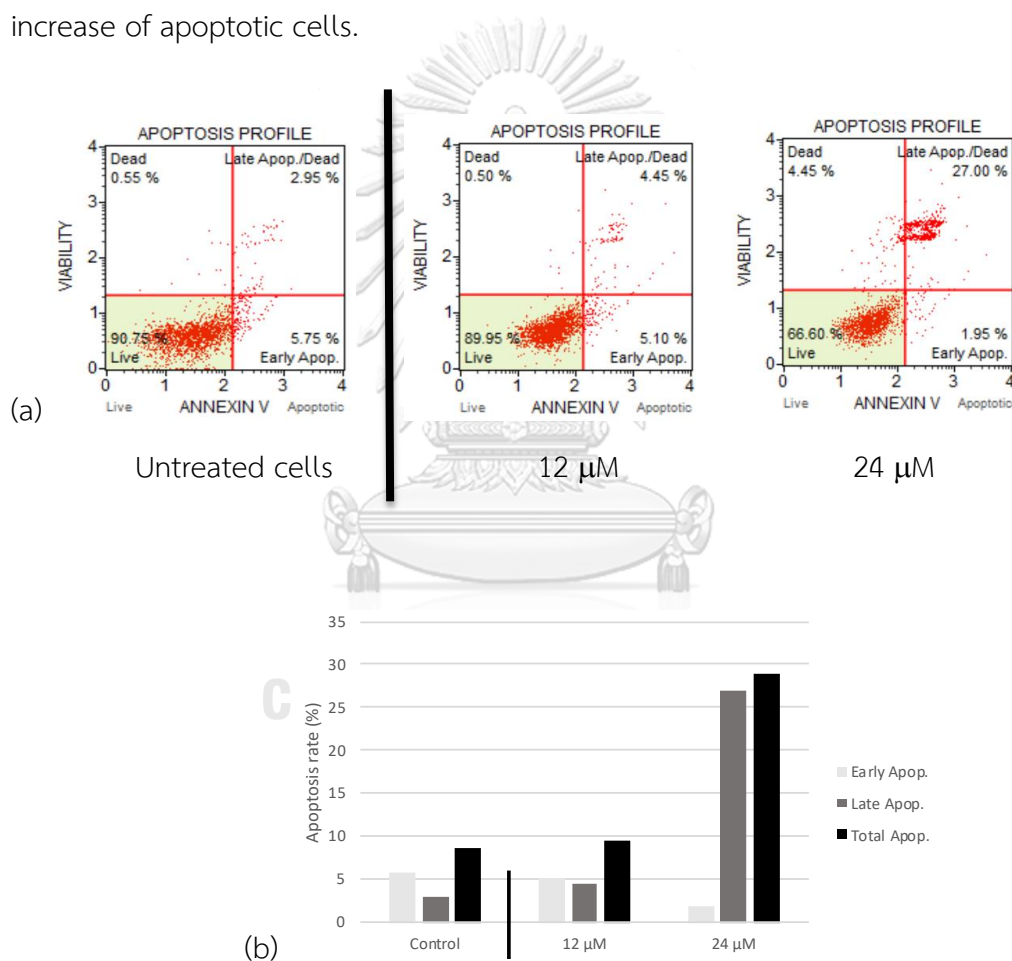


Figure 3.28 Apoptosis profile (a) and apoptosis rate (%) (b) of compound **5** on Huh-7 cells in 12 and 24 μM

Compound **11** or 8-deoxygartanin showed increase of total apoptosis rate moderately compared with the control. Even so, **Figure 3.29** showed that compound **11** was able to induced specifically in late apoptosis stage with 31.06% and 32.48% in 12 and 24 μM respectively.

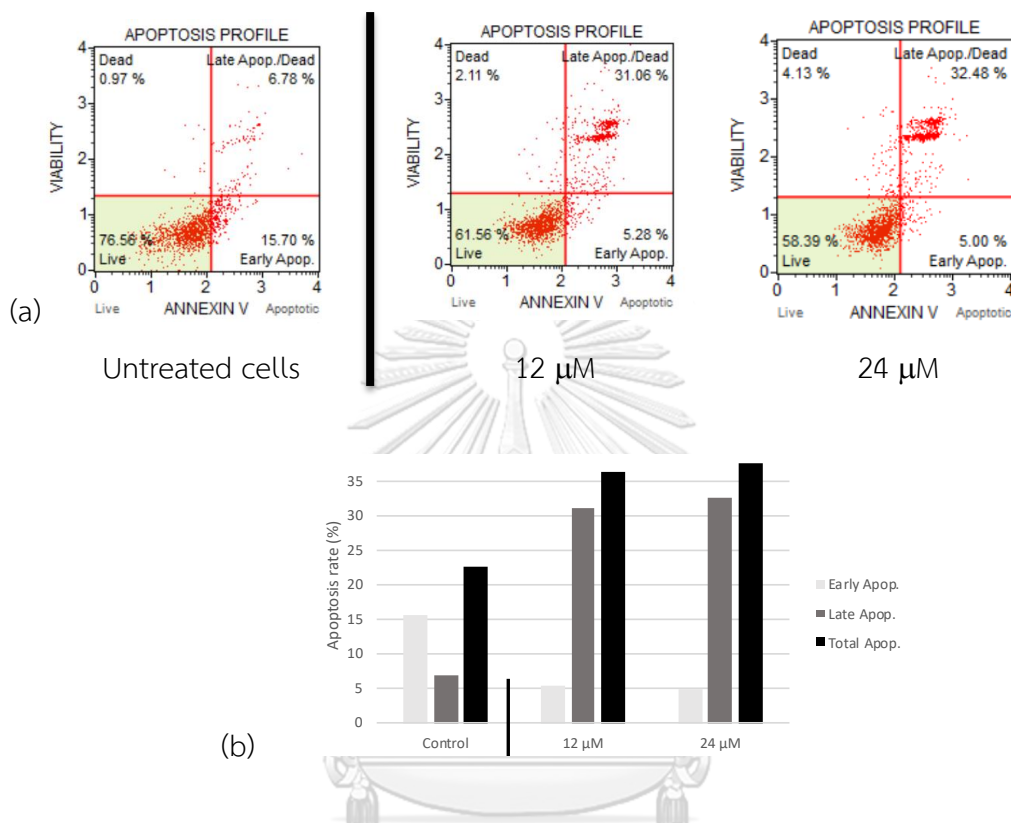


Figure 3.29 Apoptosis profile (a) and apoptosis rate (%) (b) of compound **6** on Huh-7 cells in 12 and 24 μM

Effect of compound **21** (3-hydroxy-4-geranyl-5-methoxybiphenyl) on Huh-7 apoptosis was neglectable due to a high IC_{50} value. However, the cytotoxicity against HepG2 as $11.87 \pm 1.24 \mu\text{M}$ was considered. Only this compound was used to investigate apoptosis assessment with HepG2 with the same condition of concentrations treated (IC_{50} and two-folds greater than IC_{50} ($\text{IC}_{50} \times 2$)). As results, compound **21** showed moderately increase in apoptosis rate compared to control.

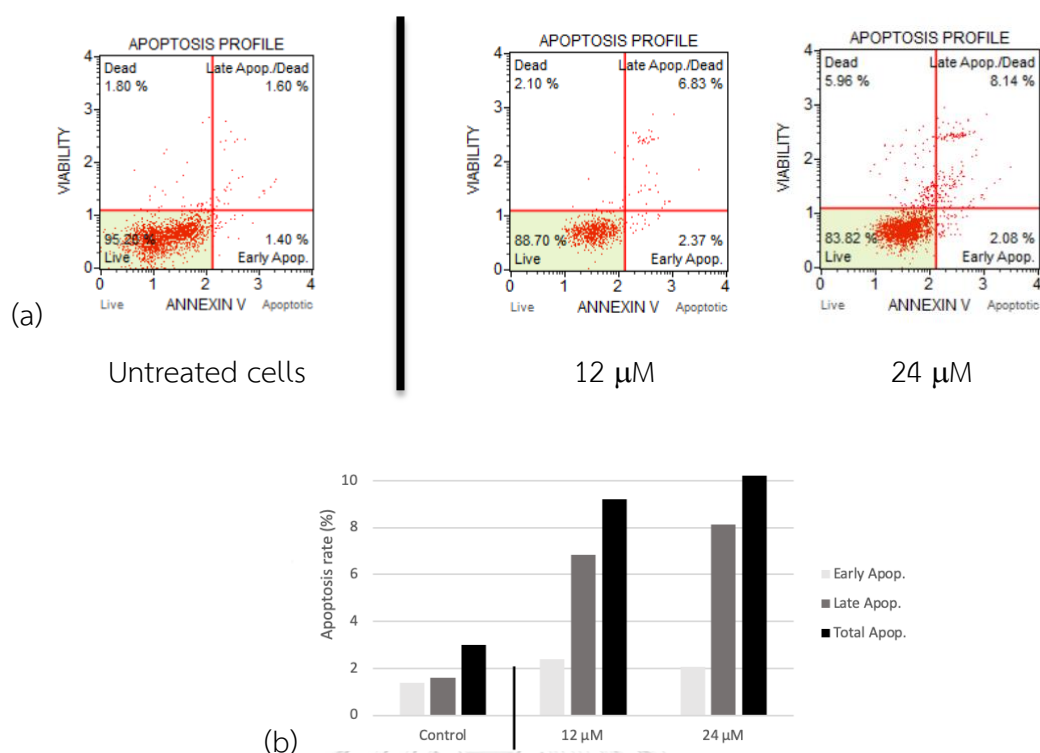


Figure 3.30 Apoptosis profile (a) and apoptosis rate (%) (b) of compound **21** on HepG2 in 12 and 24 μM

3.6 Western blot analysis

For the further study, western blot was performed to investigate targeted proteins by observing ability in suppression or expression of candidate compound. The interest targeted proteins are Bcl-2 and Bcl-XL from B-cell lymphoma-2 (Bcl-2) family. These proteins, mainly found in mitochondrial membrane, are the key regulators of apoptosis including anti-apoptotic and pro-apoptotic members. Normally, the anti-apoptotic proteins Bcl-2 and Bcl-XL will inhibit apoptosis by interacting and sequestering with pro-apoptotic proteins to balance cells in organism. However, in cancer patient, these proteins are increasing numerous and lead to the decreasing of apoptosis process. In this experiment, compound **21** was chosen to determine with HepG2 cell line, and β -actin was used as housekeeping protein. Concentrations used are follow by IC_{50} , $(\text{IC}_{50}/2)$ and $(\text{IC}_{50} \times 2)$ and untreated as control.

As results, compound **21** or 3-hydroxy-4-geranyl-5-methoxybiphenyl was able to suppress Bcl-2 protein with the increasing of concentration as shown in **Figure**

3.31 while Bcl-XL still expressed normally. This meant that apoptotic activation of HepG2 cells by compound **21** was mediated by the down regulation of Bcl-2 protein.

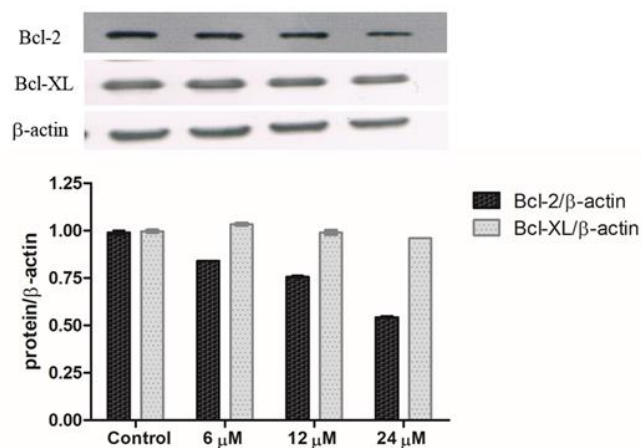


Figure 3.31 Effect of compound **21** on Bcl-2 and Bcl-XL protein expression

CHAPTER IV

CONCLUSION

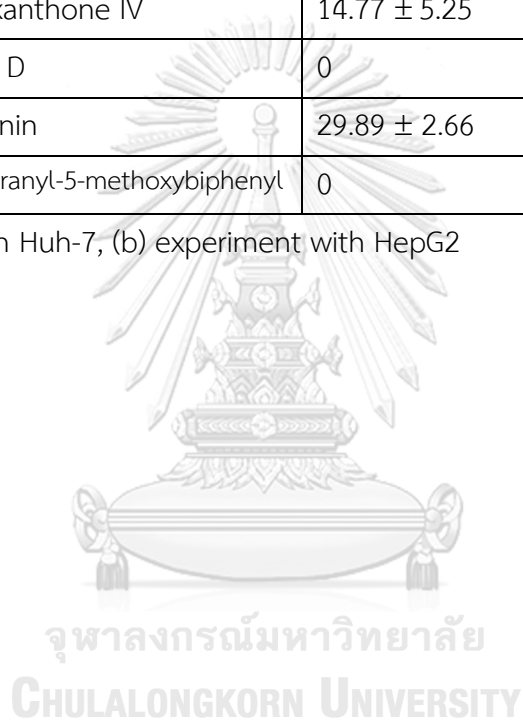
In conclusion, purification of the EtOAc extract of mangosteen (*Garcinia mangostana* L.) roots led to the isolation of four new compounds: mangostanone I – IV (compounds **1**, **12**, **13**, and **18**), and one firstly reported in natural, 4,5-dimethoxy[1,1'-biphenyl]-3-ol (**20**). Moreover, Seventeen known compounds could be identified as ten xanthones: α -mangostin (**2**), β -mangostin (**3**), γ -mangostin (**4**), mangostanaxanthone IV (**5**), dulxanthone D (**6**), toxyloxanthone B (**7**), 1,7-dihydroxy-3-methoxy-2-prenylxanthone (**8**), euxanthone (**9**), norathyriol (**10**), 8-deoxygartanin (**11**), four benzophenones: maclurin (**14**), 2,3',4,6-tetrahydroxybenzophenone (**15**), mangaphenone (**16**), (2-hydroxy-4,6-dimethoxyphenyl)(3-hydroxy-4-methoxyphenyl)methanone (**17**), two biphenyls: garciosine A (**19**), 3-hydroxy-4-geranyl-5-methoxybiphenyl (**21**), and one flavonoid: epicatechin (**22**).

All twenty-two compounds were determined for their cytotoxic activity against HCC (HepG2 and Huh-7) and colon cancer (Caco2 and HCT-116) cell lines by using MTT assay as preliminary screening. The results showed that compounds **1**, **2**, **3**, **5**, **6**, **11** and **21** have a potential effect in anticancer properties. These compounds were then selected for the next investigation in cell migration analysis with Huh-7. As results, most of the compounds showed significantly decrease of wound closure percentage except for compound **11**. Moreover, compounds **1**, **6**, **11** and **21** were further investigated with apoptosis assessment. Results suggested that these four compounds have an ability to increase apoptosis rate in dose-dependent manner. Lastly, compound **21** was chosen for Bcl-2 protein inhibitory activity using Western blot analysis. To summarize, the data obtained from cell migration analysis and apoptosis assessment in considerable condition at 24 h treated with concentrations of IC₅₀ value were shown in **Table 4.1**.

Table 4.1 Data summaries of compound 1, 2, 3, 5, 6, 11 and 21

No.	Compound	Anti-migration activity (% Tissue repair)	Total apoptosis rate (%)	Bcl-2 inhibition
1	mangostanone I	14.76 ± 4.41	22.60 ^(a)	-
2	α -mangostin	1.78 ± 20.04	-	-
3	β -mangostin	0	-	-
5	mangostanaxanthone IV	14.77 ± 5.25	-	-
6	dulxanthone D	0	9.55 ^(a)	-
11	8-deoxygartanin	29.89 ± 2.66	36.34 ^(a)	-
21	3-hydroxy-4-geranyl-5-methoxybiphenyl	0	9.20 ^(b)	✓

(a) experiment with Huh-7, (b) experiment with HepG2



REFERENCES



จุฬาลงกรณ์มหาวิทยาลัย
CHULALONGKORN UNIVERSITY

1. Golabi, P., Fazel, S., Otgonsuren, M., Sayiner, M., Locklear, C.T., & Younossi Z.M (2017). Mortality assessment of patients with hepatocellular carcinoma according to underlying disease and treatment modalities. *Medicine*, 96(9), e5904.
2. National Cancer Institute. Drugs Approved for Liver Cancer. [Online]. 2020. Available from: <https://www.cancer.gov/about-cancer/treatment/drugs/liver> [2020, November 10]
3. Tang Z. Y. (2001). Hepatocellular carcinoma -- cause, treatment and metastasis. *World journal of gastroenterology*, 7(4), 445 – 454.
4. Ou, D.L., Chang, C.J., Jeng, Y.M., Lin, zy.J., Lin, Z.Z., Gandhi, A.K., ... Cheng, A.L. (2014). Potential synergistic anti-tumor activity between lenalidomide and sorafenib in hepatocellular carcinoma. *Journal of Gastroenterology and zhepatology*, 29(12), 2021 – 2031.
5. Cragg, G. M., & Pezzuto, J.M. (2016). Natural Products as a Vital Source for thw Discovery of Cancer Chemotherapeutic and Chemopreventive Agents. *Medical Principles and Practice*, 25(Suppl 2), 41 – 59.
6. Aizat, W.M., Jamil, I.N., Ahmad-Hashim, F.H., & Noor, N.M. (2019). Recent updates on metabolite composition and medicinal benefits of mangosteen plant. *PeerJ*. DOI 10.7717/peerj.6324
7. Ovalle-Magallanes, B., Eugenio-Pérez, D., & Pedraza-Chaverri, J. (2017). Medicinal properties of mangosteen (*Garcinia mangostana* L.): a comprehensive update. *Food and Chemical Toxicology*, 109, 102–122.
8. Tousian Shandiz, H., Razavi, B.M., & Hosseinzadeh, H. (2017). Review of *Garcinia mangostana* and its xanthenes in metabolic syndrome and related complications. *Phytotherapy Research*, 31(8), 1173–1182.
9. Obolskiy, D., Pischel, I., Siriwatanametanon, N., & Heinrich, M. (2009). *Garcinia mangostana* L.: A Phytochemical and Pharmacological Review. *Phytotherapy research*, 23, 1047 – 1065.
10. Mohamed, G.A., Al-Abd, A.M., El-Halawany, A.M., Abdallah, H.M., & Ibrahim, S.R. (2017). New xanthenes and cytotoxic constituents from *Garcinia*

mangostana fruit hulls against human hepatocellular, breast, and colorectal cancer cell lines. *Journal of Ethnopharmacology*, 198, 302–312.

11. Kaennakam, S., Siripong, P., Tip-pyang, S. (2015). Kaennacowanols A–C, three new xanthenes and their cytotoxicity from the roots of *Garcinia cowa*, *Fitoterapia*, 102, 171 – 176.
12. Morel, C., Se´raphin, D., Oger, J-M., Litaudon, M., Se´venet, T., Richomme, P., & Bruneton, J. (2000). New Xanthenes from *Calophyllum caledonicum*. *Journal of Natural products*, 63(11), 1471 – 1474.
13. Liandhajani, Iwo, M.I., Sukrasno, Soemardji, A.A., & Hanafi, M. (2013). Sunscreen Activity of α -mangostin from the Pericarps of *Garcinia mangostana* Linn. *Journal of Applied Pharmaceutical Science*, 3(06), 070 – 073.
14. Yates, P. & Bha, H.B. (1968). Structure of b-mangostin. *Canadian Journal of Chemistry*, 46, 3770 – 3772.
15. Xu, Z., Huang, L., Chen, X. H., Zhu, X. F., Qian, X. J., Feng, G. K., Lan, W. J., & Li, H. J. (2014). Cytotoxic prenylated xanthenes from the pericarps of *Garcinia mangostana*. *Molecules (Basel, Switzerland)*, 19(2), 1820–1827.
16. Abdallah, H. M., El-Bassossy, H. M., Mohamed, G. A., El-Halawany, A. M., Alshali, K. Z., & Banjar, Z. M. (2017). Mangostanaxanthenes III and IV: advanced glycation end-product inhibitors from the pericarp of *Garcinia mangostana*. *Journal of natural medicines*, 71(1), 216–226.
17. Ito, C., Miyamoto, Y., Nakayama, M., Kawai, Y., Rao, K.S., & Furukawa, H. (1997). A Novel Depsidone and Some New Xanthenes from *Garcinia* species. *Chemical and Pharmaceutical Bulletin*, 45(9), 1403 – 1413.
18. Cotterill, P.J., & Scheinmann, F. (1980). Studies in the Xanthone Series. Part 13. Structural and Synthetic Studies on Toxyloxanthone B. *Journal of the Chemical Society, Perkin Transactions 1*, 2353 – 2357.
19. Mahabusarakam, W., & Wlriyachitra, P. (1987). Chemical Constituents of *Garcinia mangostana*. *Journal of Natural Products*, 50(3), 474 – 478.
20. Tocci, N., Simonetti, G., D'Auria, F. D., Panella, S., Palamara, A. T., Valletta, A., & Pasqua, G. (2011). Root cultures of *Hypericum perforatum* subsp. *angustifolium* elicited with chitosan and production of xanthone-rich extracts

- with antifungal activity. *Applied microbiology and biotechnology*, 91(4), 977–987.
21. Noro, T., Ueno, A., Mizutani, M., Hashimoto, T., Miyase, T., Kuroyanagi, M., & Fukushima, S. (1984). Inhibitors of xanthine oxidase from *Athyrium mesosorum*. *Chemical & pharmaceutical bulletin*, 32(11), 4455–4459.
 22. Nguyen, L. H., Vo, H. T., Pham, H. D., Connolly, J. D., & Harrison, L. J. (2003). Xanthones from the bark of *Garcinia merguensis*. *Phytochemistry*, 63(4), 467–470.
 23. Fleischer, E.B., Sung, N., & Hawkinson, S. (1968). Crystal structure of benzophenone. *The Journal of Physical Chemistry A*. 72(12), 4311 – 4312.
 24. Holloway, D.M., & Scheinmann, F. (1975). Phenolic compounds from the heartwood of *Garcinia mangostana*. *Phytochemistry*, 14, 2517-2518.
 25. Chiang, Y. M., Kuo, Y. H., Oota, S., & Fukuyama, Y. (2003). Xanthones and benzophenones from the stems of *Garcinia multiflora*. *Journal of natural products*, 66(8), 1070–1073.
 26. See, I., Ee, G. C., Teh, S. S., Kadir, A. A., & Daud, S. (2014). Two new chemical constituents from the stem bark of *Garcinia mangostana*. *Molecules (Basel, Switzerland)*, 19(6), 7308–7316.
 27. Triana, J., López, M., Pérez, F. J., Platas, J. G., Estévez, F., León, J. F., ... & Bermejo, J. (2009). Chemical constituents of *Tolpis* species. *Fitoterapia*, 80(7), 437–441.
 28. Chen, J. J., Peng, C. F., Huang, H. Y., & Chen, I. S. (2006). Benzopyrans, biphenyls and xanthones from the root of *Garcinia linii* and their activity against *Mycobacterium tuberculosis*. *Planta medica*, 72(5), 473–477.
 29. Pailee, P., Kuhakarn, C., Sangsuwan, C., Hongthong, S., Piyachaturawat, P., Suksen, K., & Reutrakul, V. (2018). Anti-HIV and cytotoxic biphenyls, benzophenones and xanthones from stems, leaves and twigs of *Garcinia speciosa*. *Phytochemistry*, 147, 68–79.
 30. Chittimalla, S.K., Kuppusamy, R., & Akavaram, N. (2014). Palladium-Catalyzed Regioselective Synthesis of Oxygenated Biphenyls. *Synlett*, 26, 613-618.

31. Dharmaratne, H. R., Piyasena, K. G., & Tennakoon, S. B. (2005). A geranylated biphenyl derivative from *Garcinia mangostana*. *Natural product research*, 19(3), 239–243.
32. Rice-Evans, C.A., Miller, N.J., Paganga, G. (1996). Structure-antioxidant activity relationships of flavonoids and phenolic acids. *Free Radical Biology and Medicine*. 20(7), 933-56.
33. Ovalle-Magallanes, B., Eugenio-Pérez, D., & Pedraza-Chaverri, J. (2017). Medicinal properties of mangosteen (*Garcinia mangostana* L.): a comprehensive update. *Food and Chemical Toxicology*, 109, 102–122.
34. Huang, A., Yang, X.R., Chung, W.Y., Dennison, A.R., & Zhou, J. (2020). Targeted therapy for hepatocellular carcinoma. *Signal Transduction and Targeted Therapy*, 5(146),
35. National Cancer Institute. [Sorafenib Tysolate](https://www.cancer.gov/about-cancer/treatment/drugs/liver). [Online]. 2020. Available from: <https://www.cancer.gov/about-cancer/treatment/drugs/liver> [2020, November 10]

APPENDIX

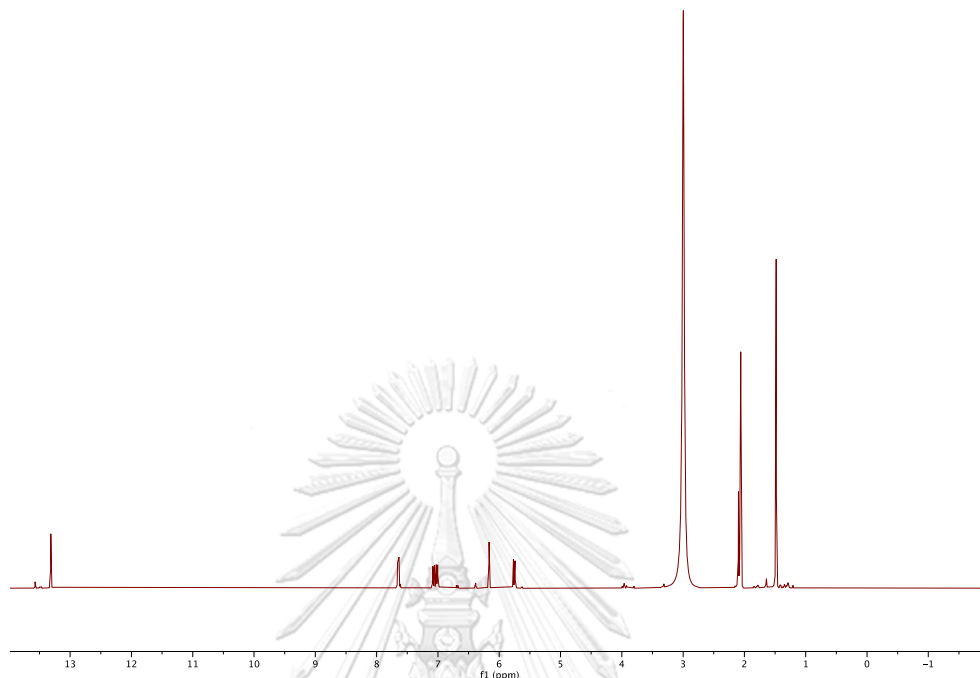


Figure A.1.1 ^1H NMR (400 MHz, acetone- d_6) spectrum of compound **1**

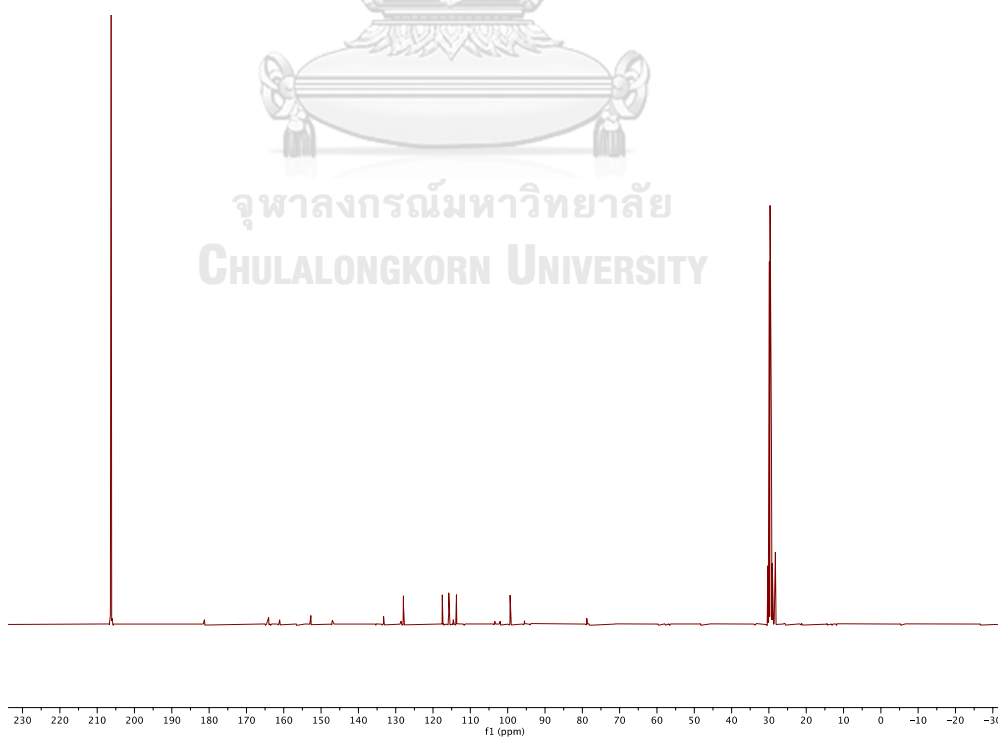


Figure A.1.2 ^{13}C NMR (100 MHz, acetone- d_6) spectrum of compound **1**

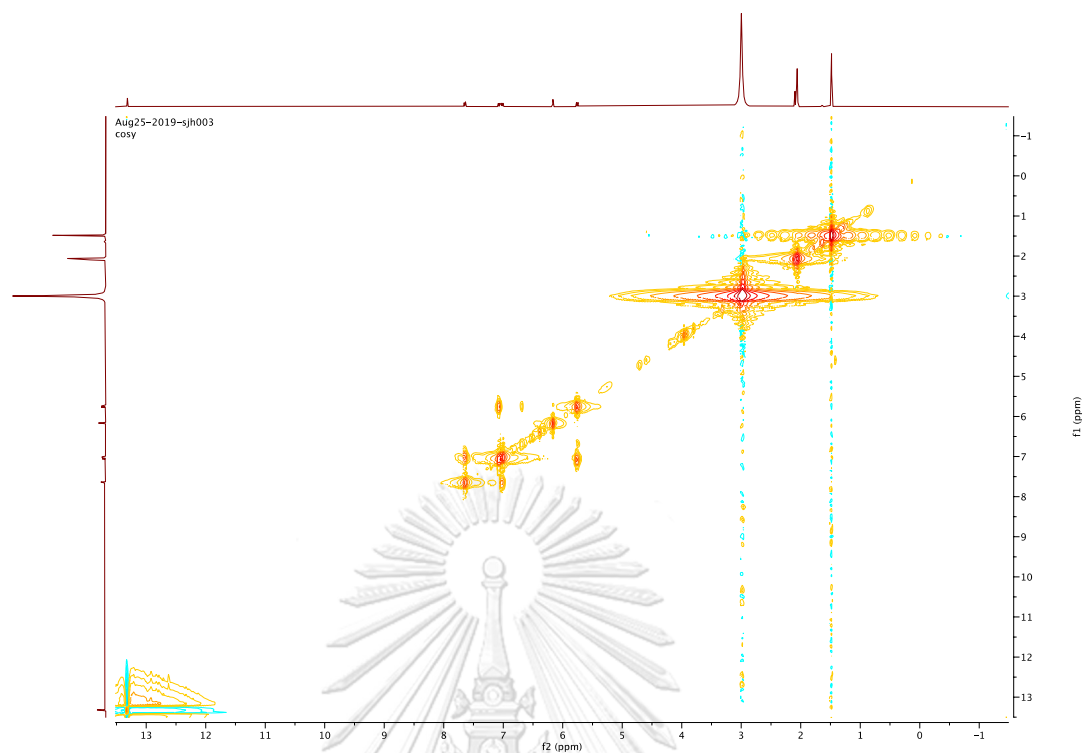


Figure A.1.3 ^1H - ^1H COSY spectrum (acetone- d_6) of compound **1**

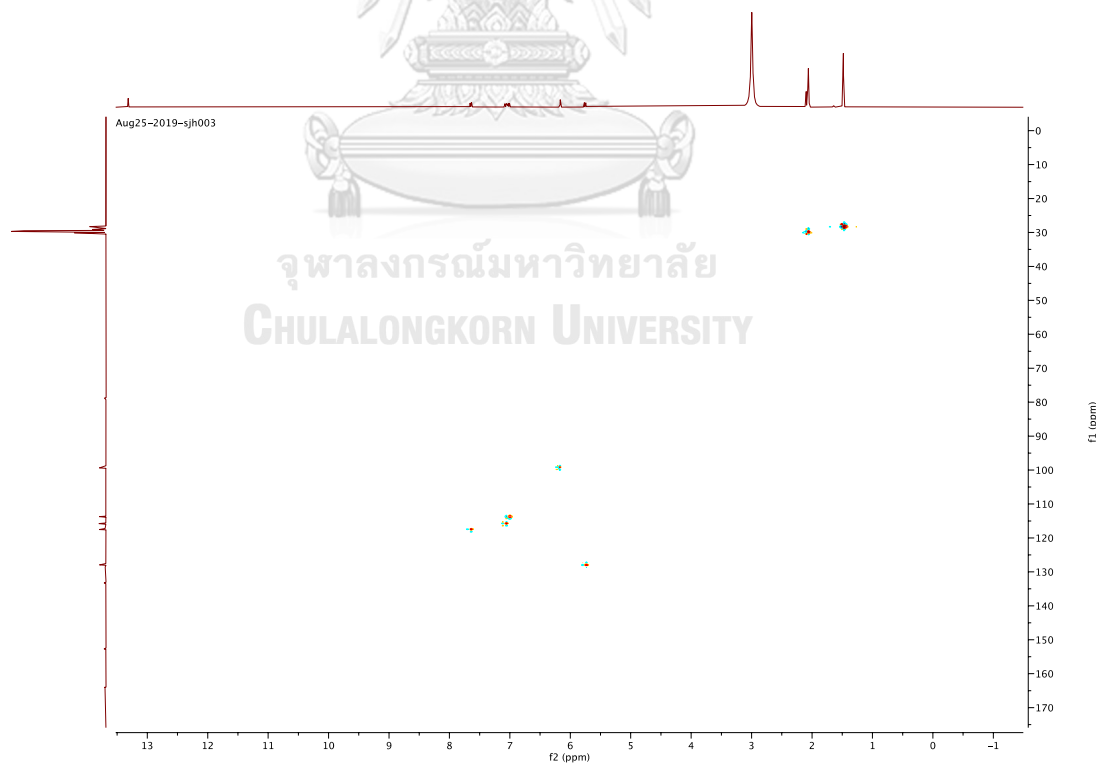


Figure A.1.4 HSQC spectrum (acetone- d_6) of compound **1**

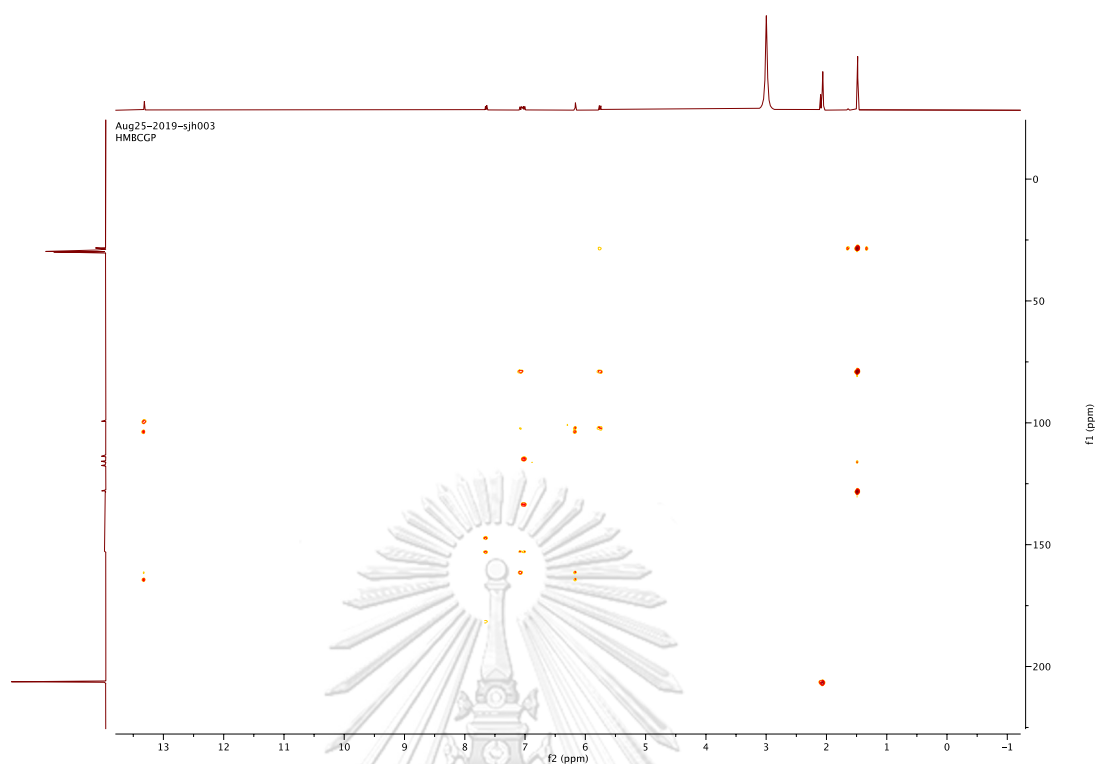


Figure A.1.5 HMBC spectrum (acetone-d₆) of compound 1

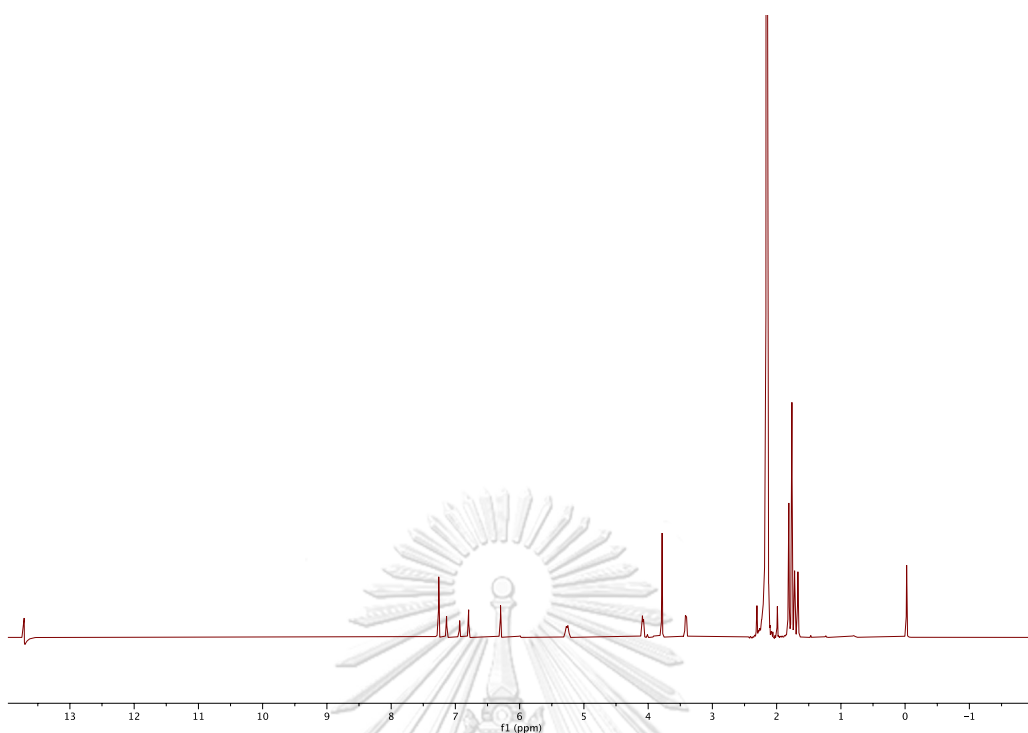


Figure A.2.1 ^1H NMR (400 MHz, CDCl_3) spectrum of compound 2

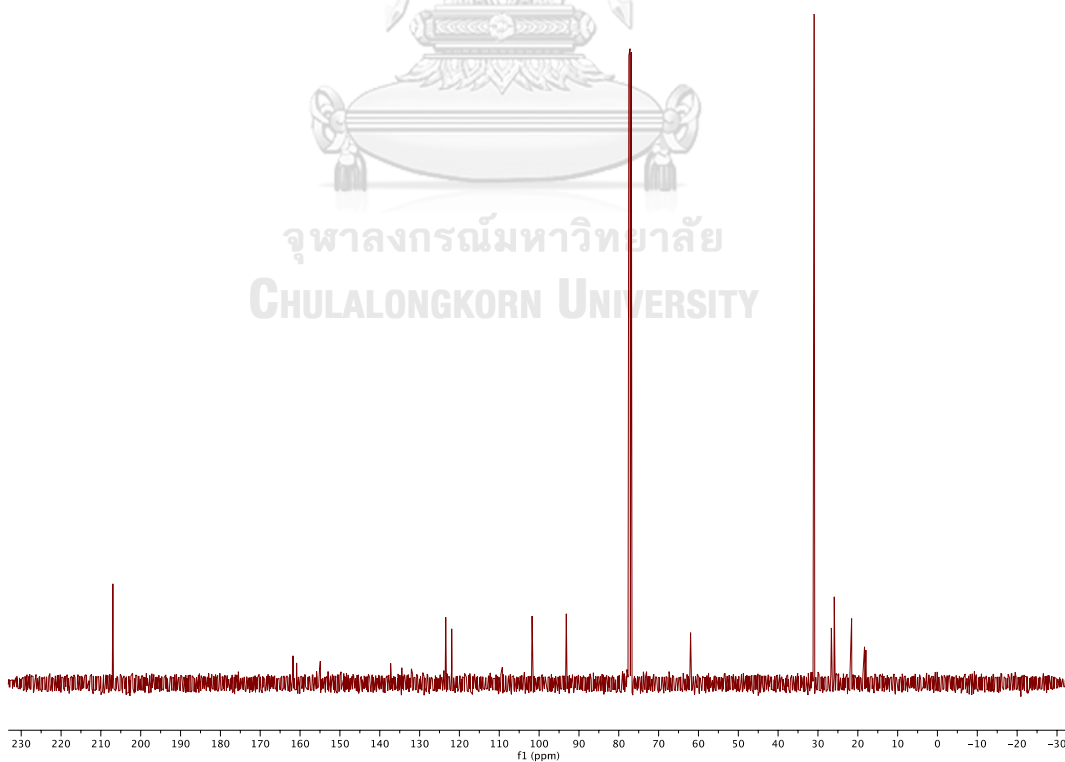


Figure A.2.2 ^{13}C NMR (100 MHz, CDCl_3) spectrum of compound 2

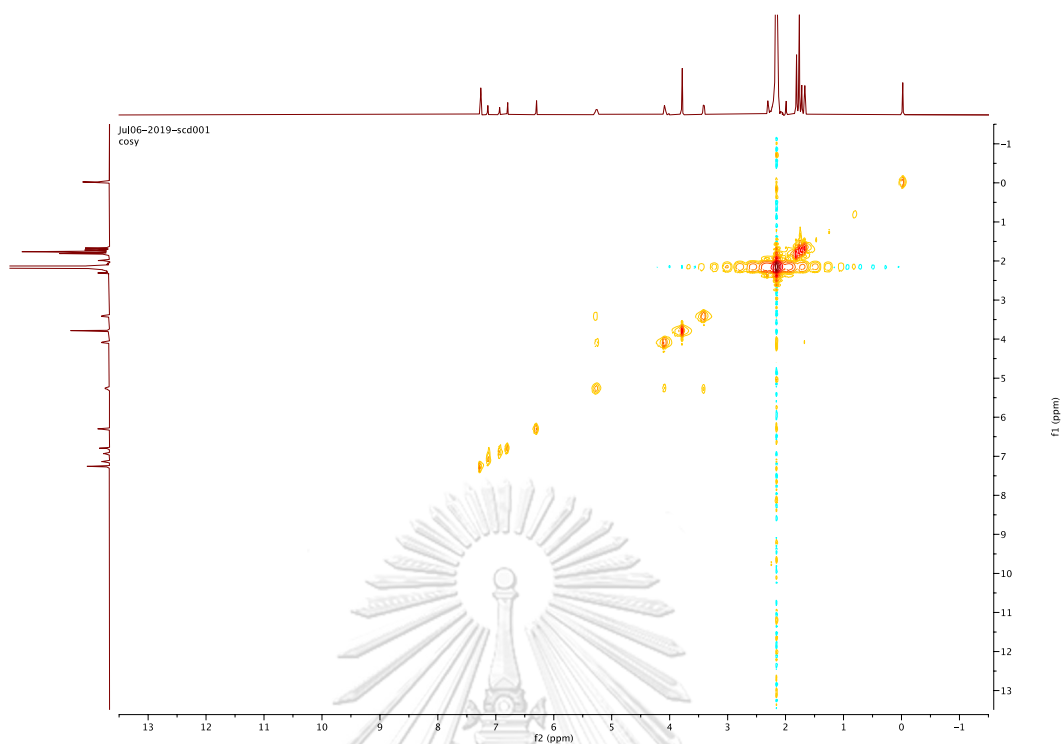


Figure A.2.3 ^1H - ^1H COSY spectrum (CDCl_3) of compound 2

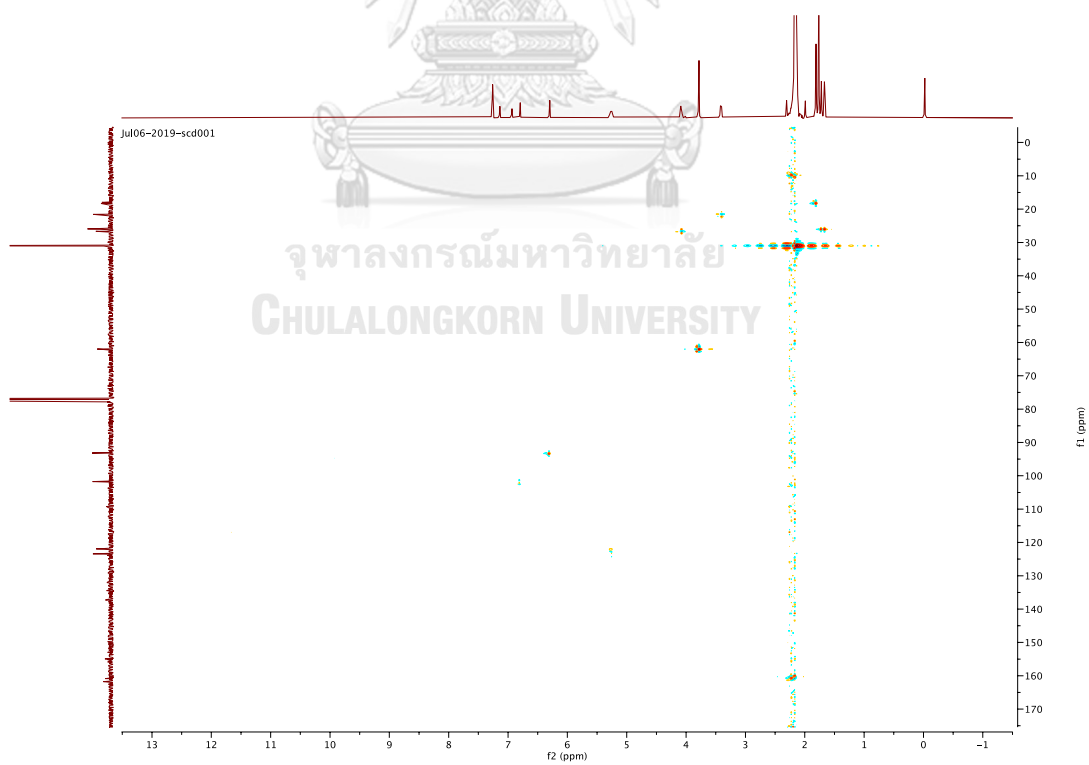


Figure A.2.4 HSQC spectrum (CDCl_3) of compound 2

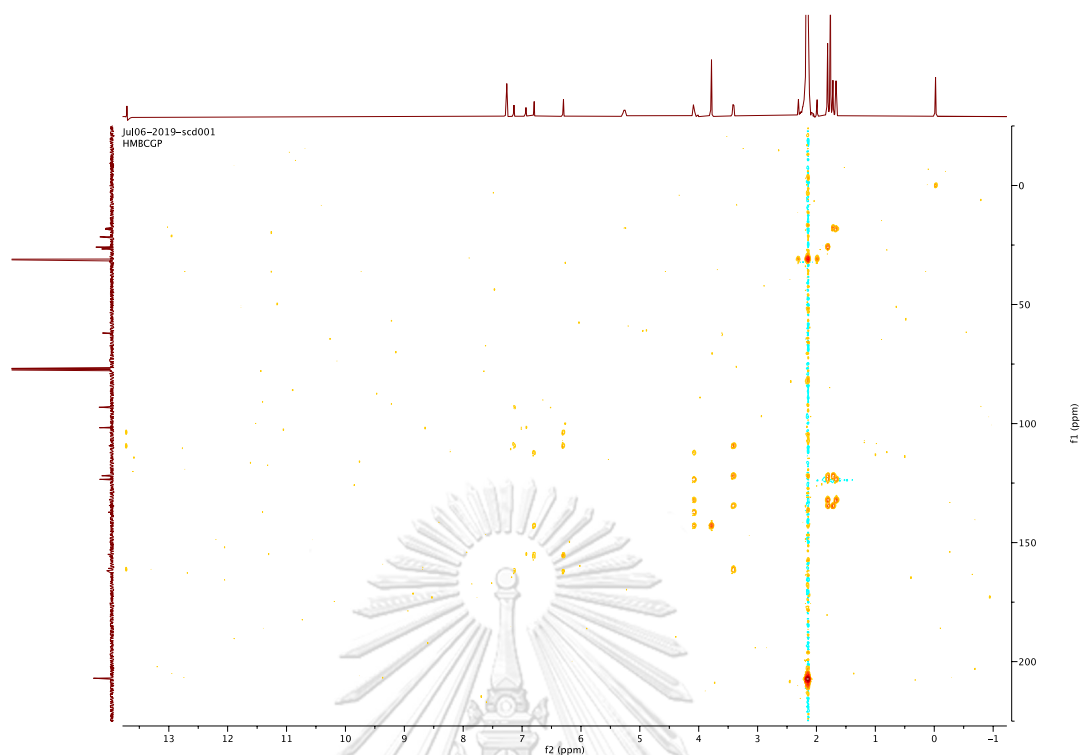


Figure A.2.5 HMBC spectrum (CDCl_3) of compound 2

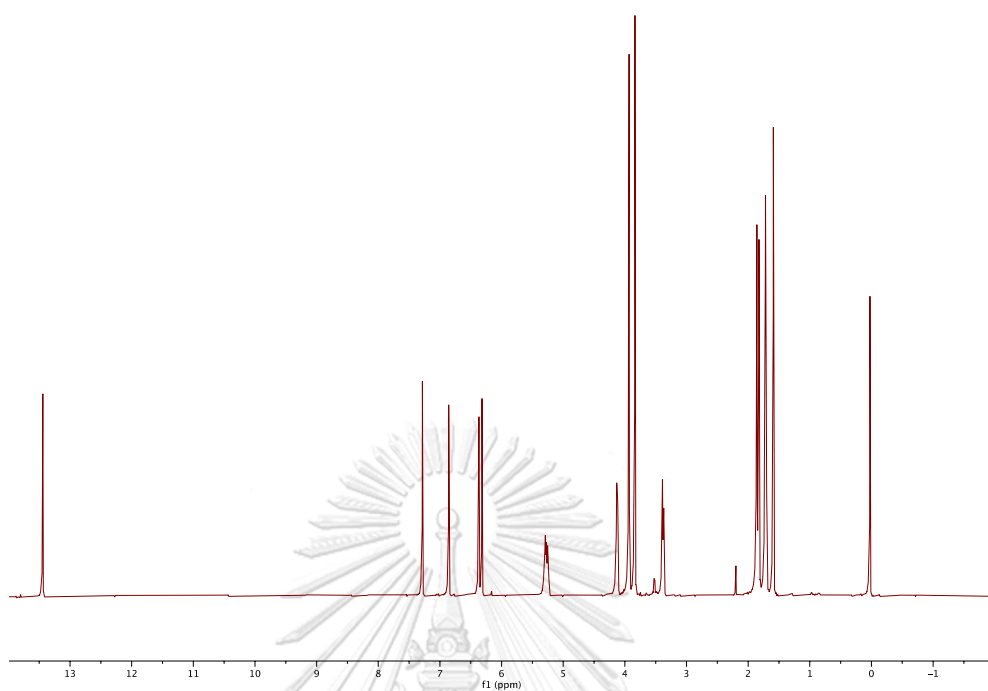


Figure A.3.1 ^1H NMR (400 MHz, CDCl_3) spectrum of compound **3**

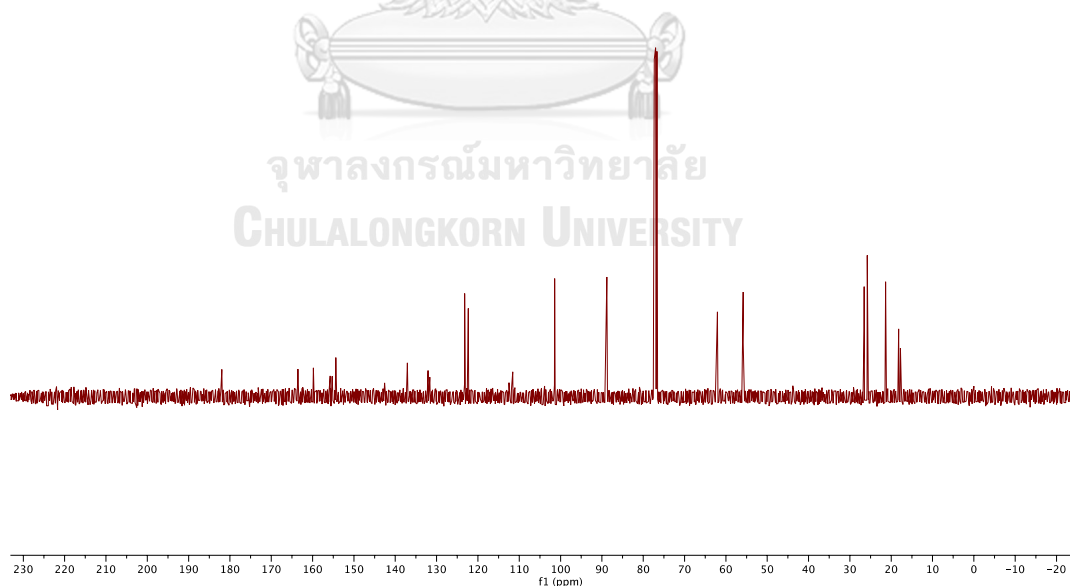


Figure A.3.2 ^{13}C NMR (100 MHz, CDCl_3) spectrum of compound **3**

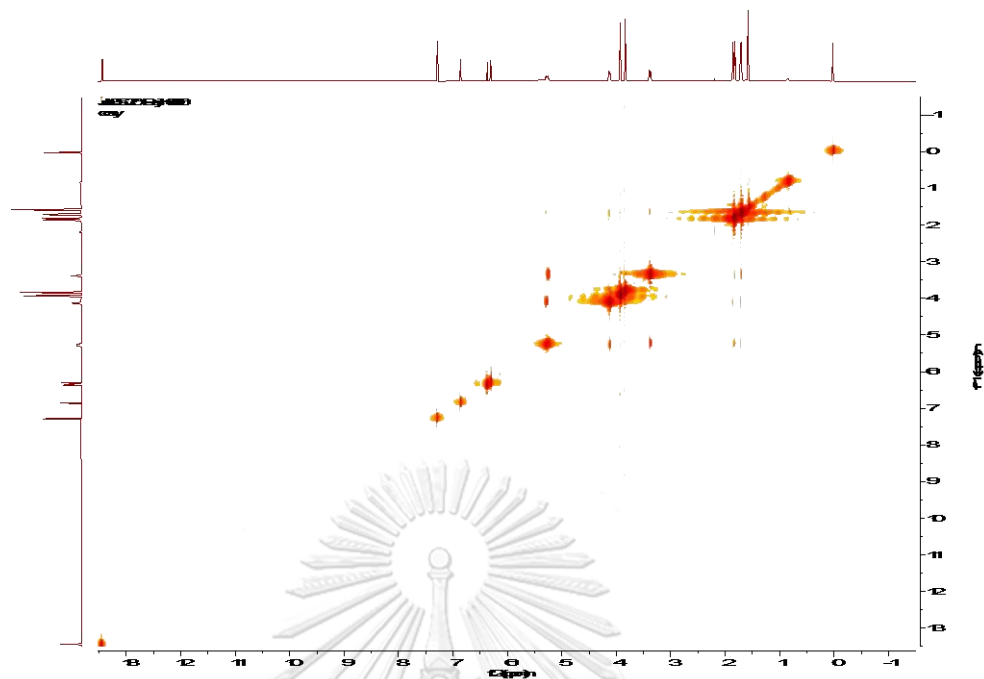


Figure A.3.3 ^1H - ^1H COSY spectrum (CDCl_3) of compound 3

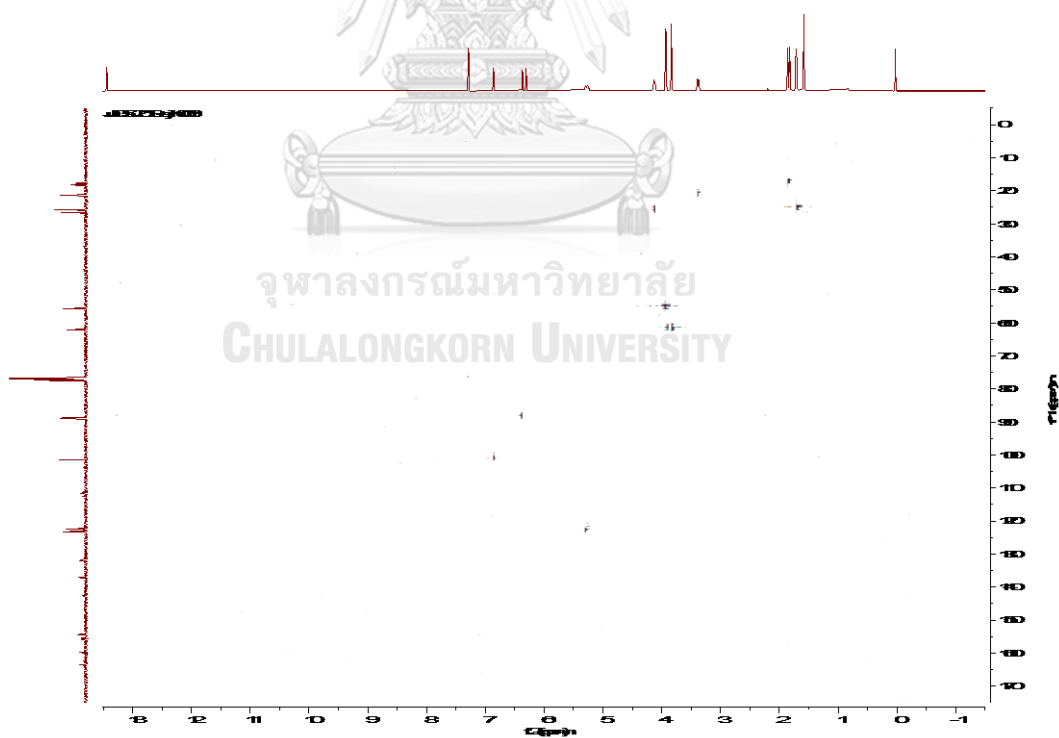


Figure A.3.4 HSQC spectrum (CDCl_3) of compound 3

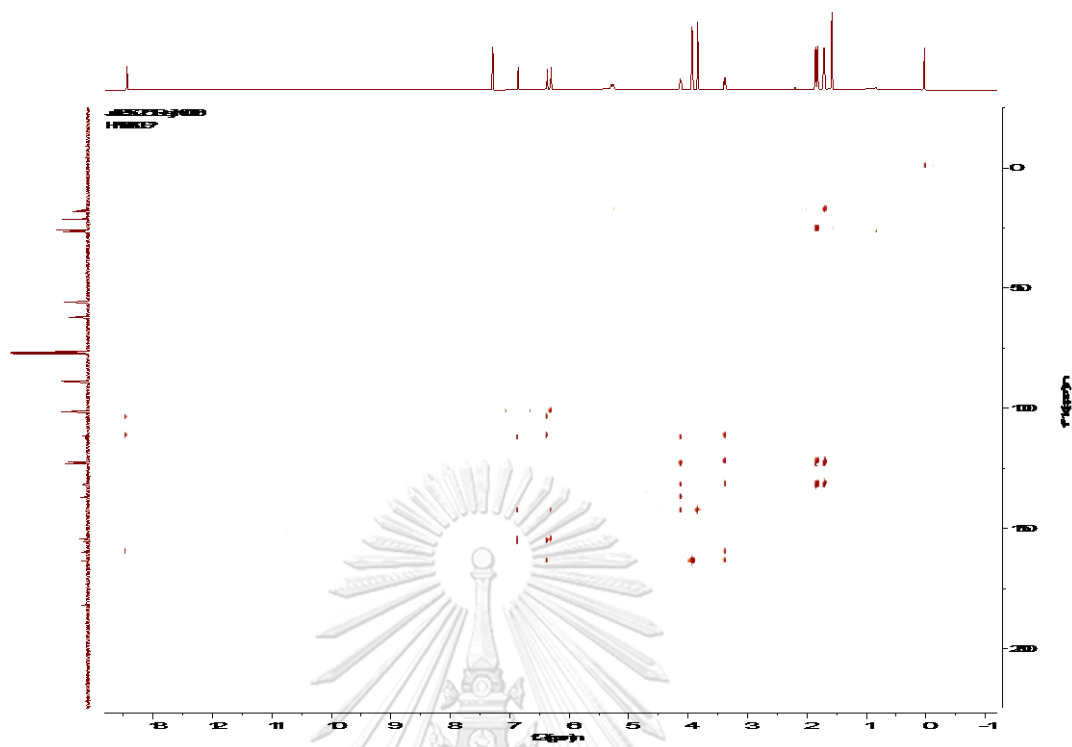


Figure A.3.5 HMBC spectrum (CDCl_3) of compound 3

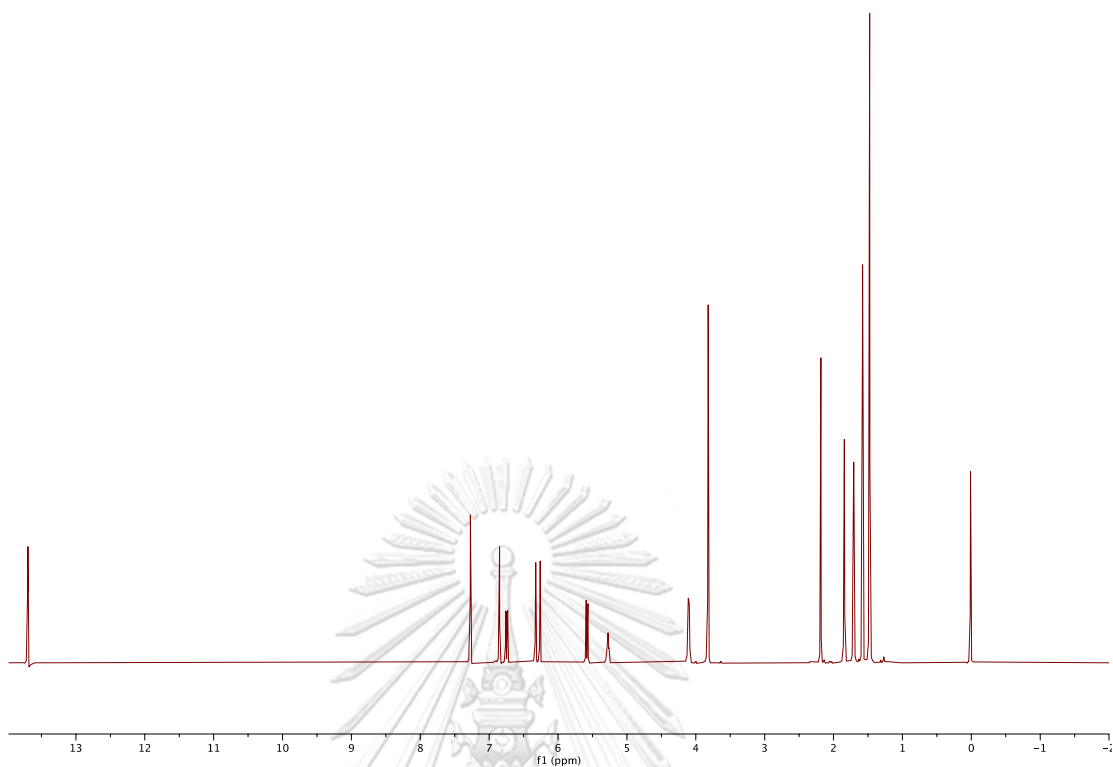


Figure A.5.1 ^1H NMR (400 MHz, CDCl_3) spectrum of compound 5

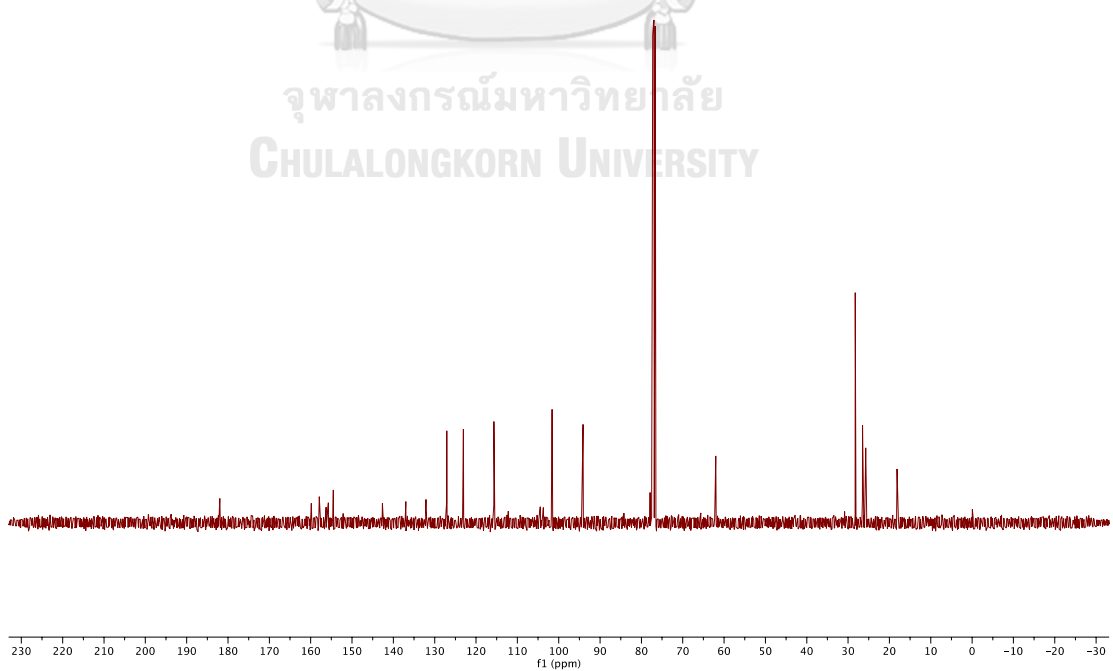


Figure A.5.2 ^{13}C NMR (100 MHz, CDCl_3) spectrum of compound 5

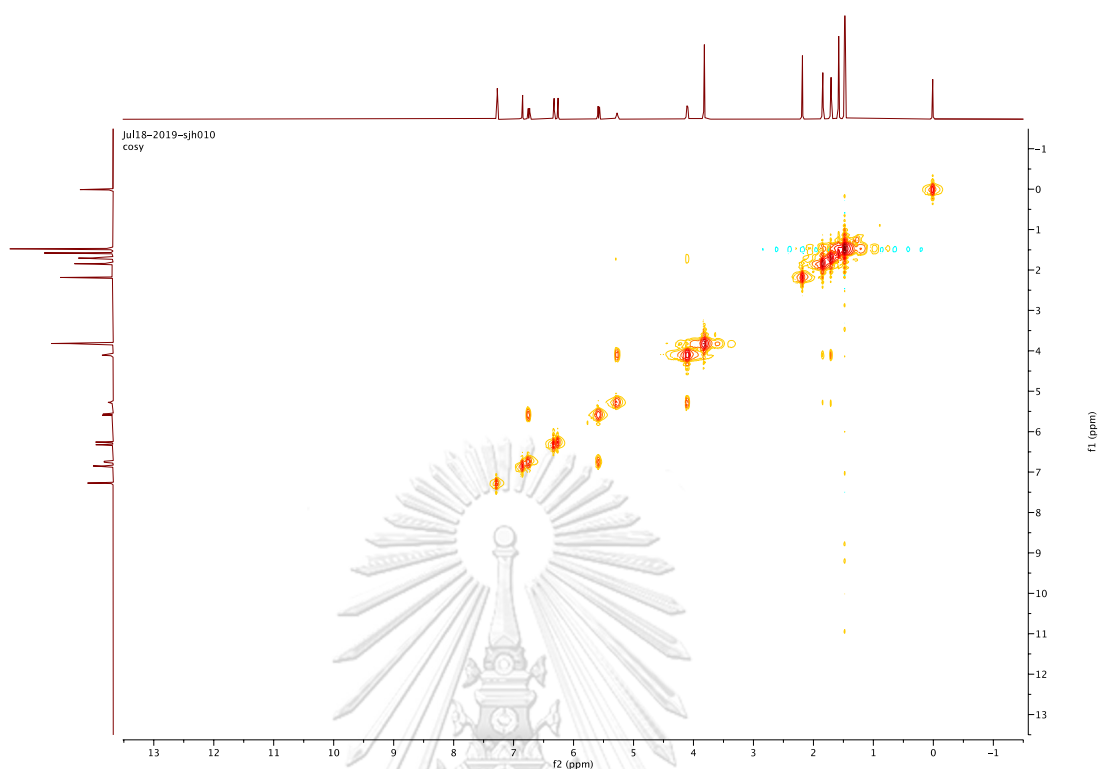


Figure A.5.3 ^1H - ^1H COSY spectrum (CDCl_3) of compound 5

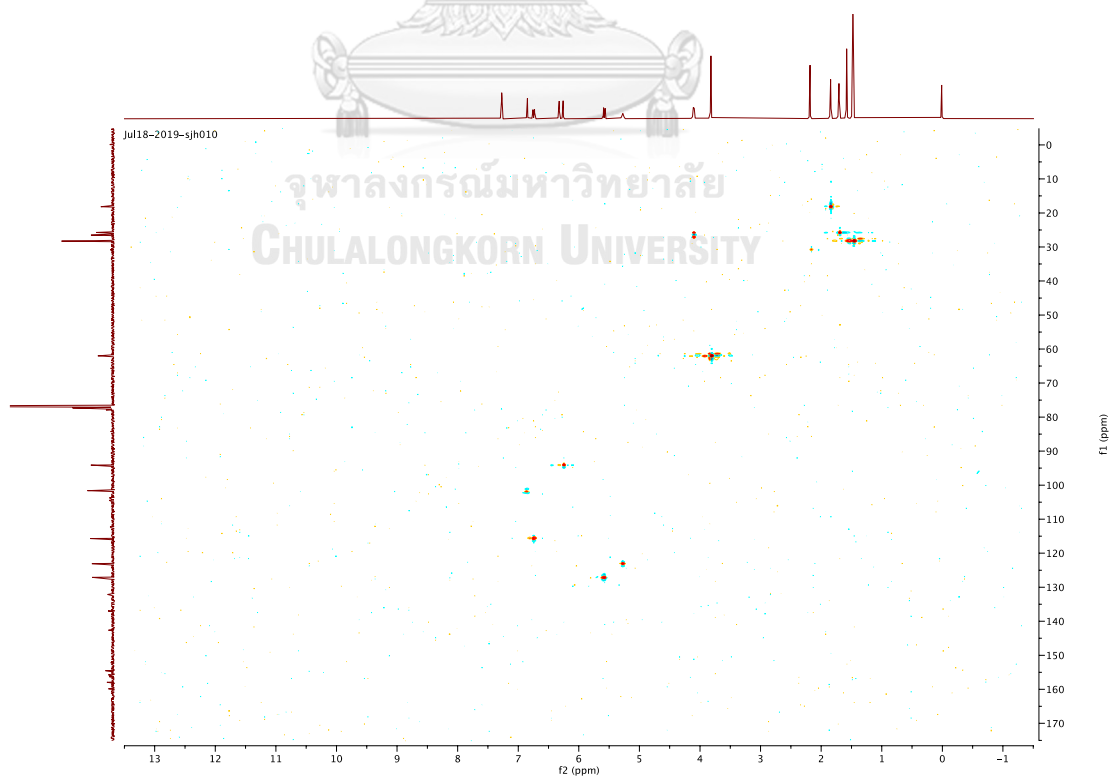


Figure A.5.4 HSQC spectrum (CDCl_3) of compound 5

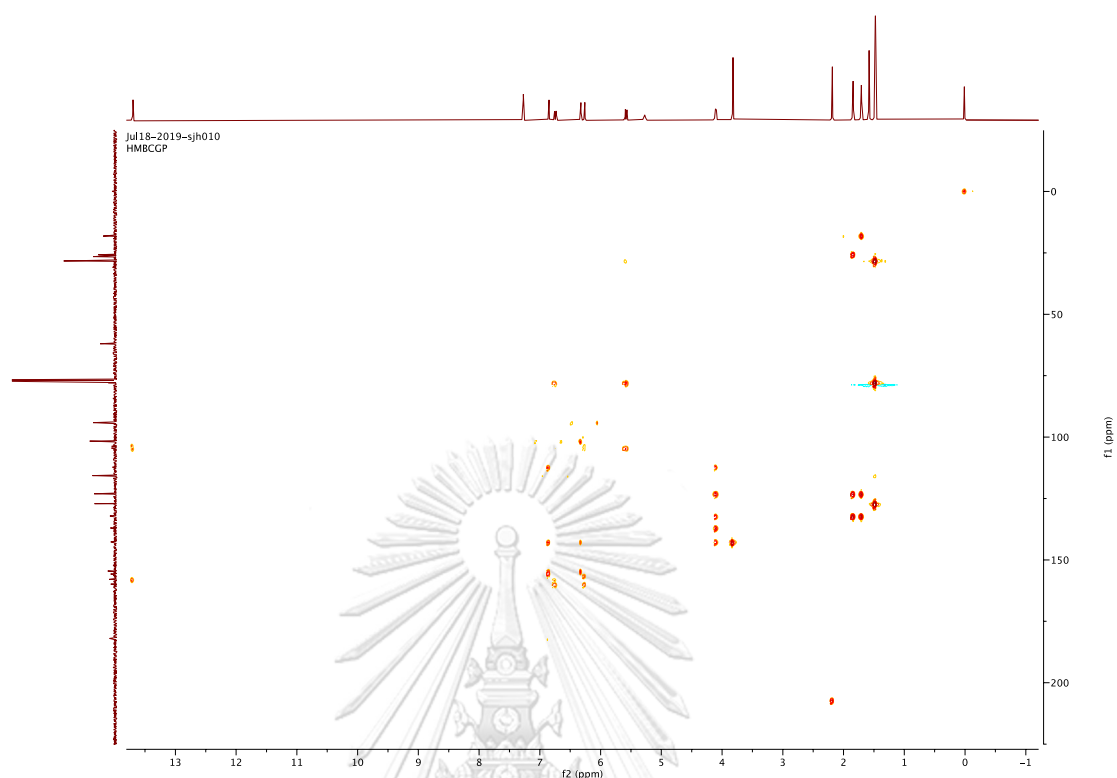


Figure A.5.5 HMBC spectrum (CDCl₃) of compound 5

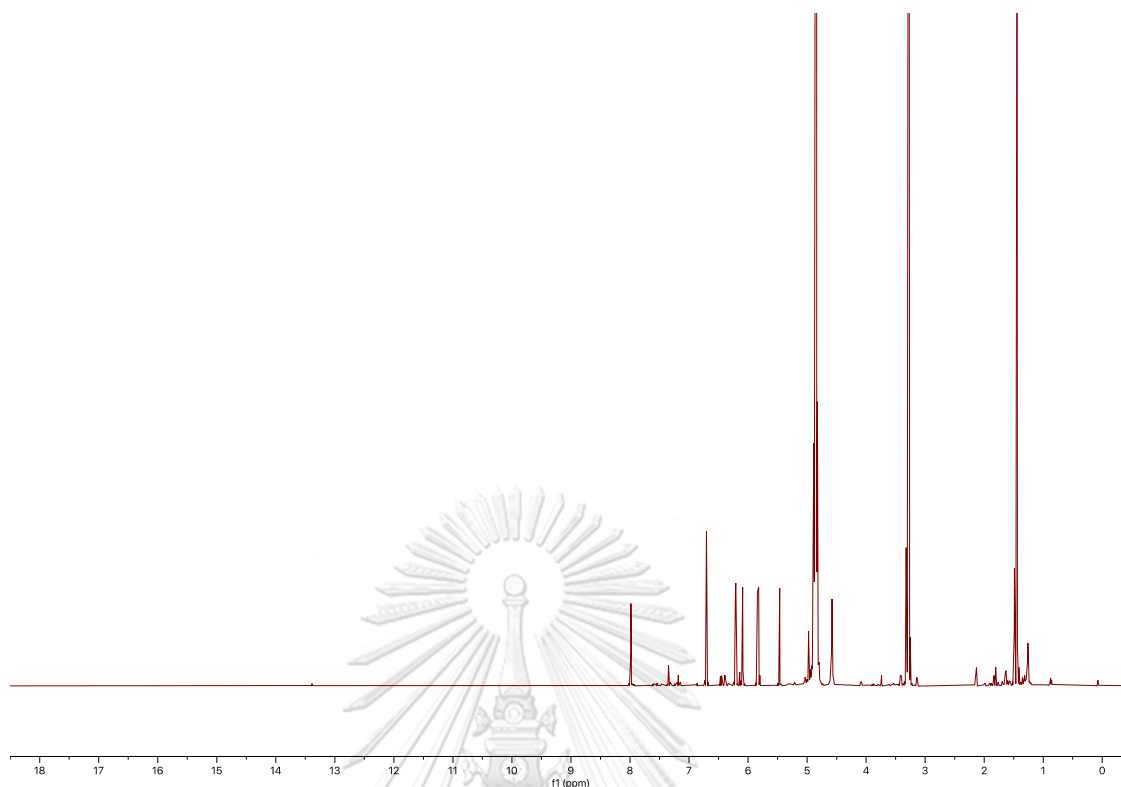


Figure A.6.1 ^1H NMR (400 MHz, methanol- d_4) spectrum of compound **6**

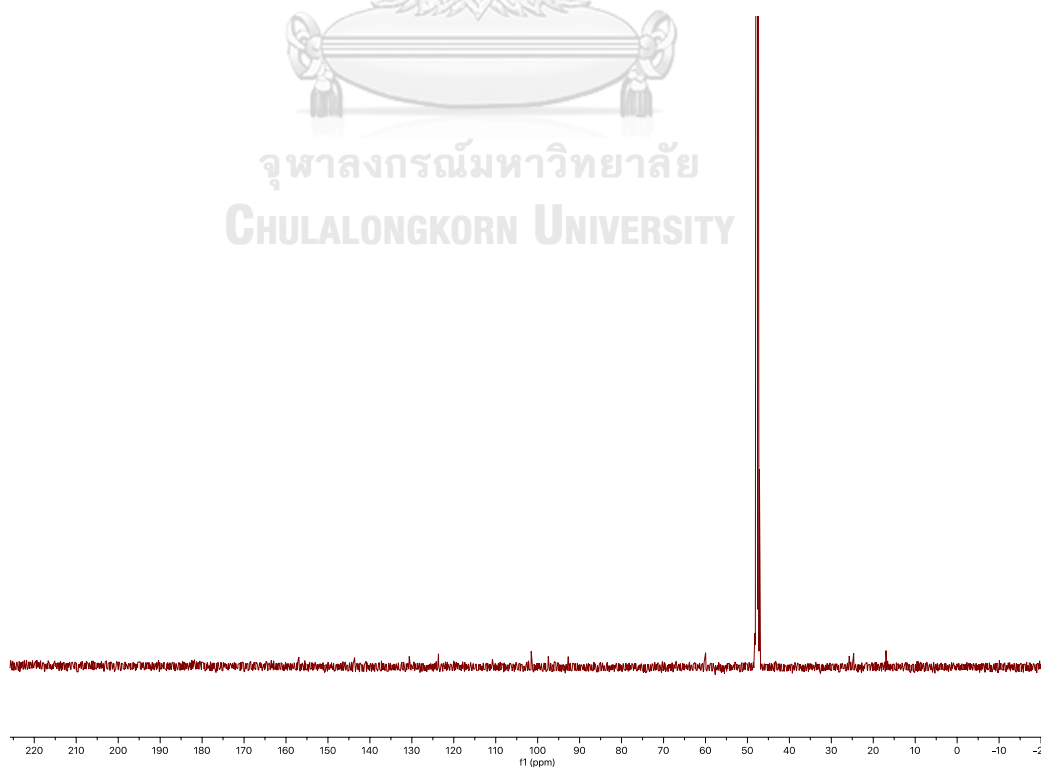


Figure A.6.2 ^{12}C NMR (100 MHz, methanol- d_4) spectrum of compound **6**

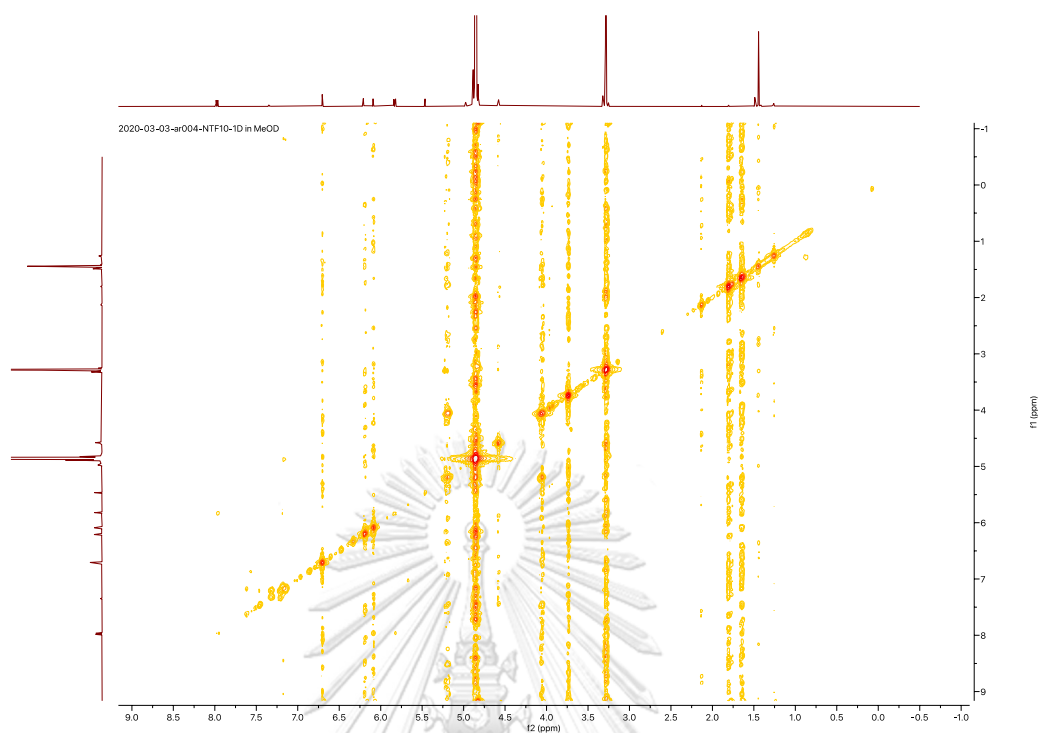


Figure A.6.3 ^1H - ^1H COSY spectrum (methanol- d_4) of compound 6

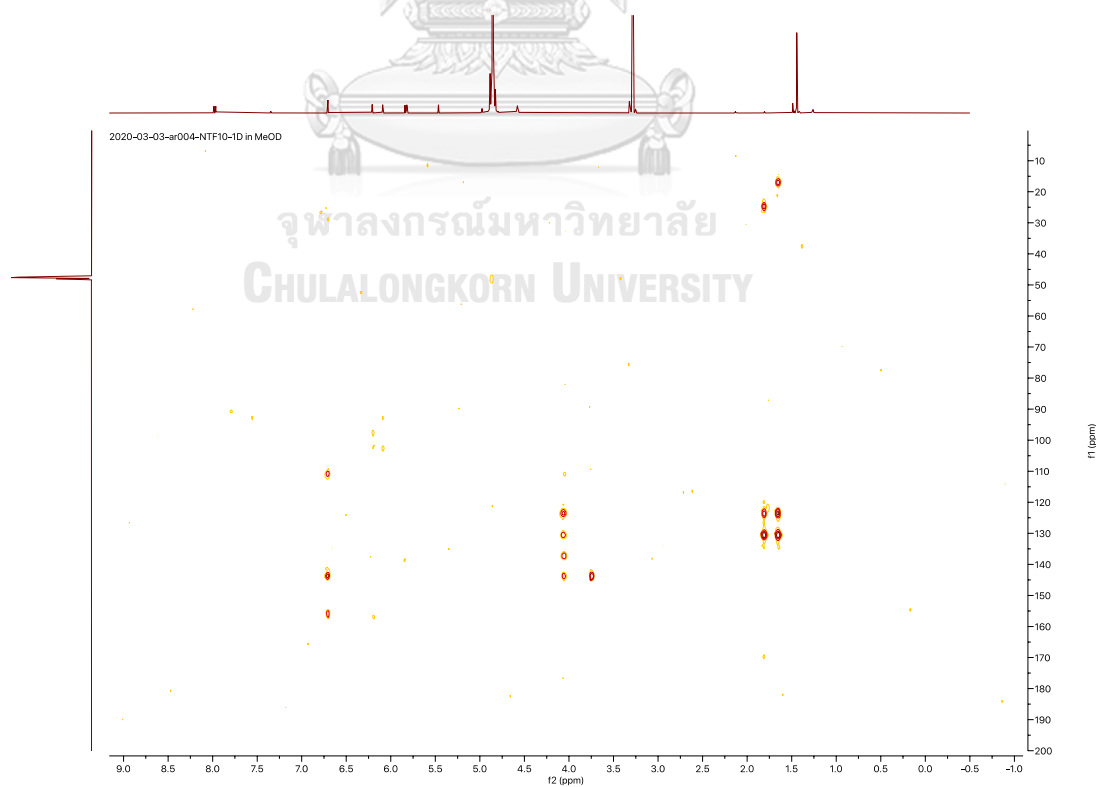


Figure A.6.4 HSQC spectrum (methanol- d_4) of compound 6

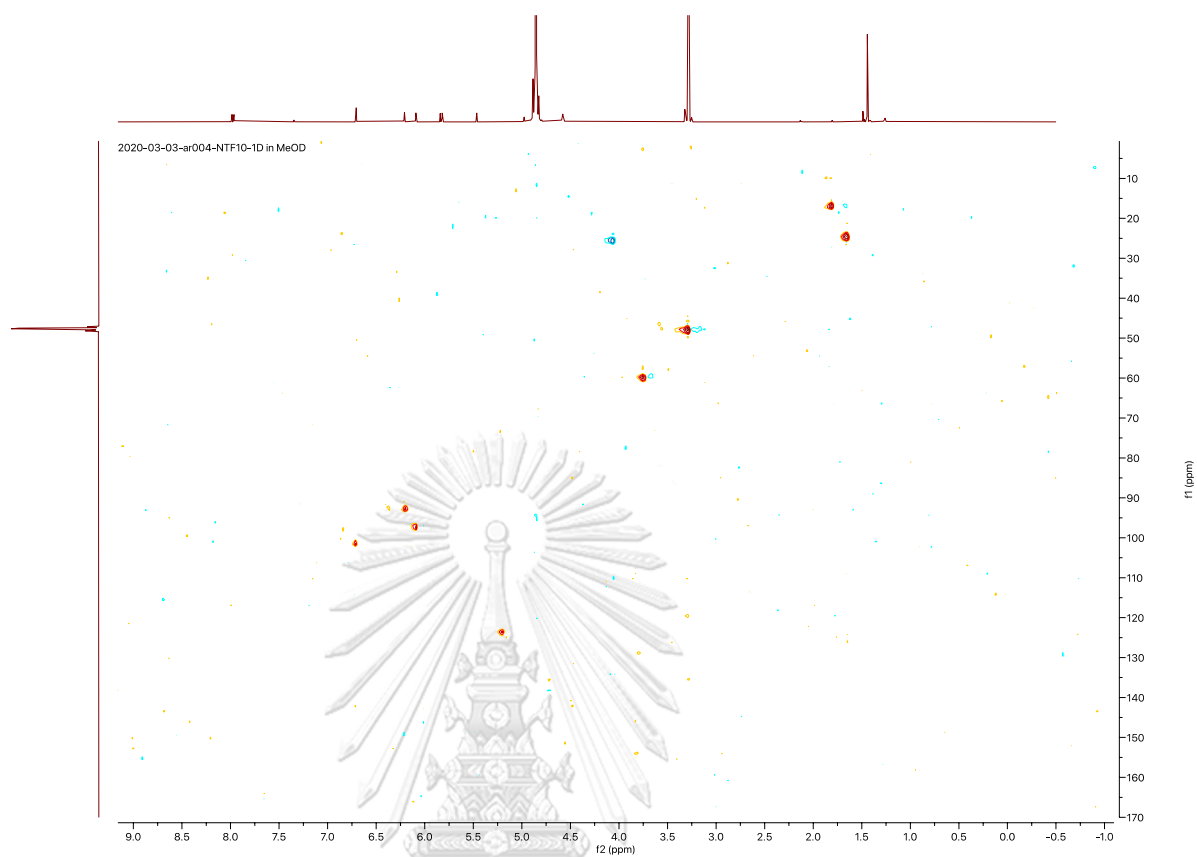


Figure A.6.5 HMBC spectrum (methanol-d₄) of compound **6**

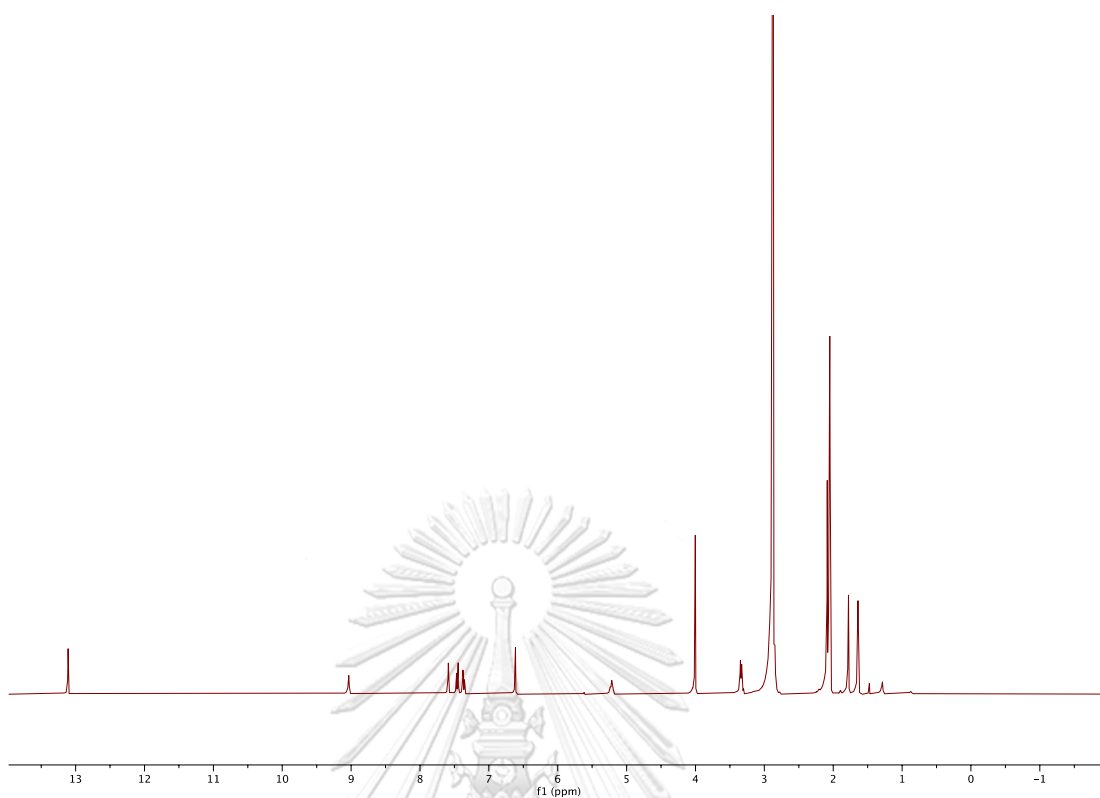


Figure A.8.1 ^1H NMR (400 MHz, acetone- d_6) spectrum of compound **8**

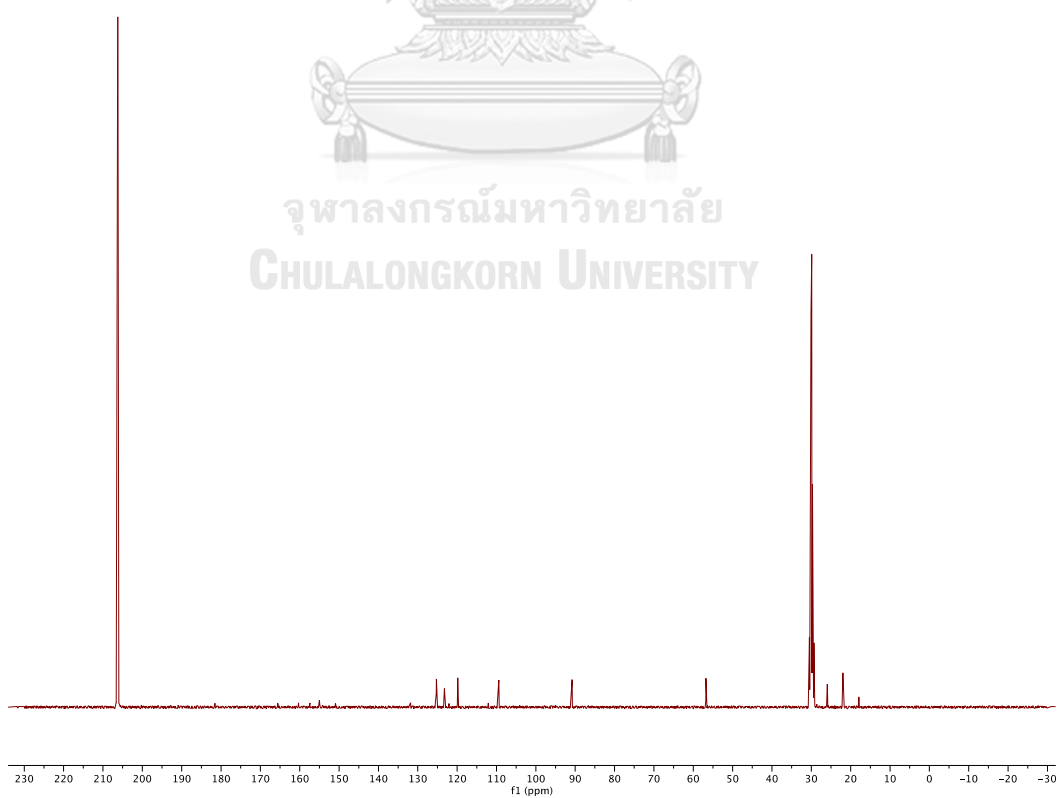


Figure A.8.2 ^{13}C NMR (100 MHz, acetone- d_6) spectrum of compound **8**

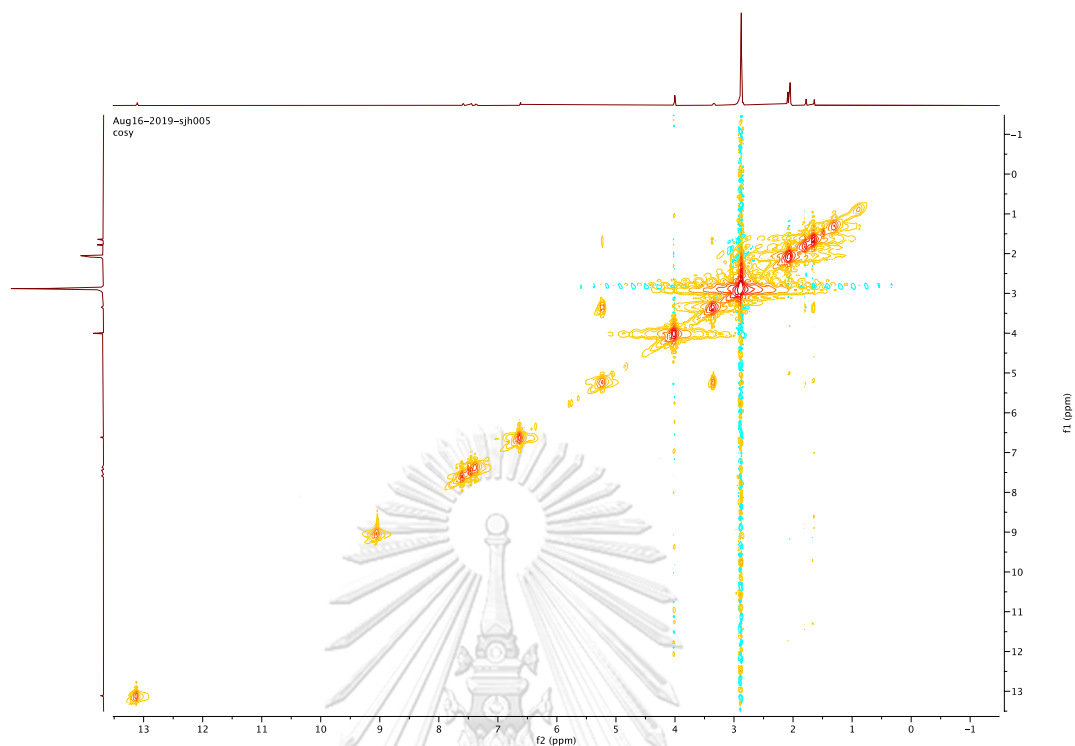


Figure A.8.3 ^1H - ^1H COSY spectrum (acetone- d_6) of compound **8**

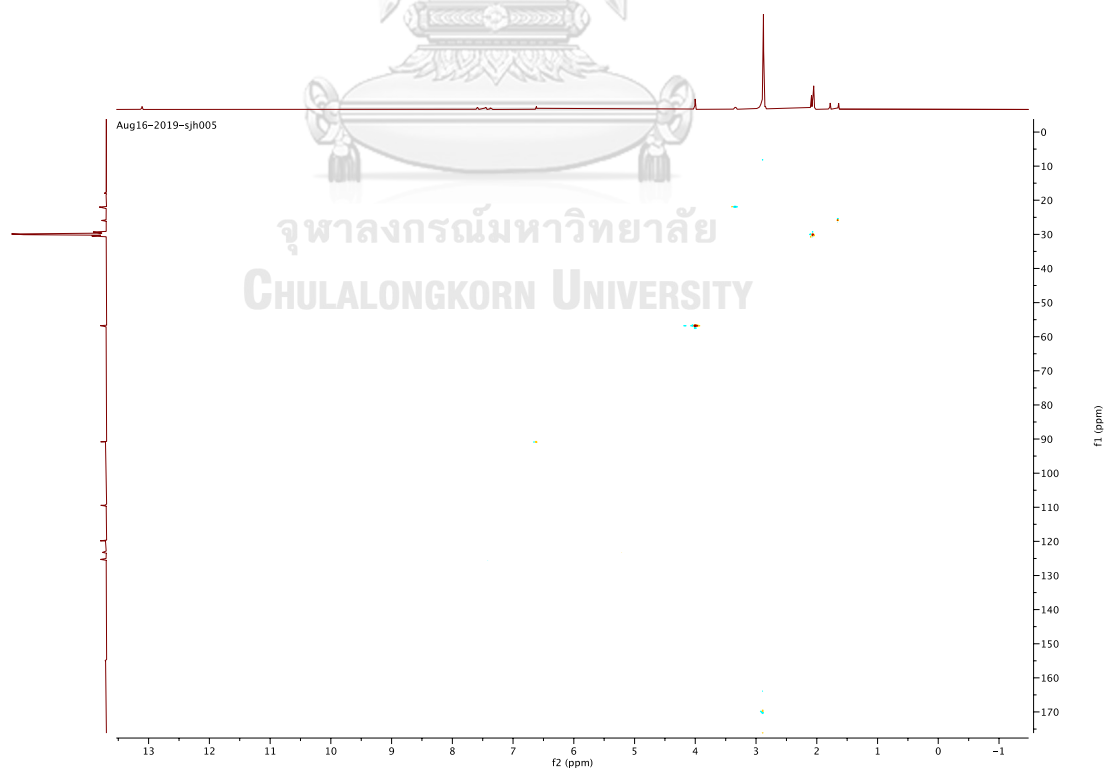


Figure A.8.4 HSQC spectrum (acetone- d_6) of compound **8**

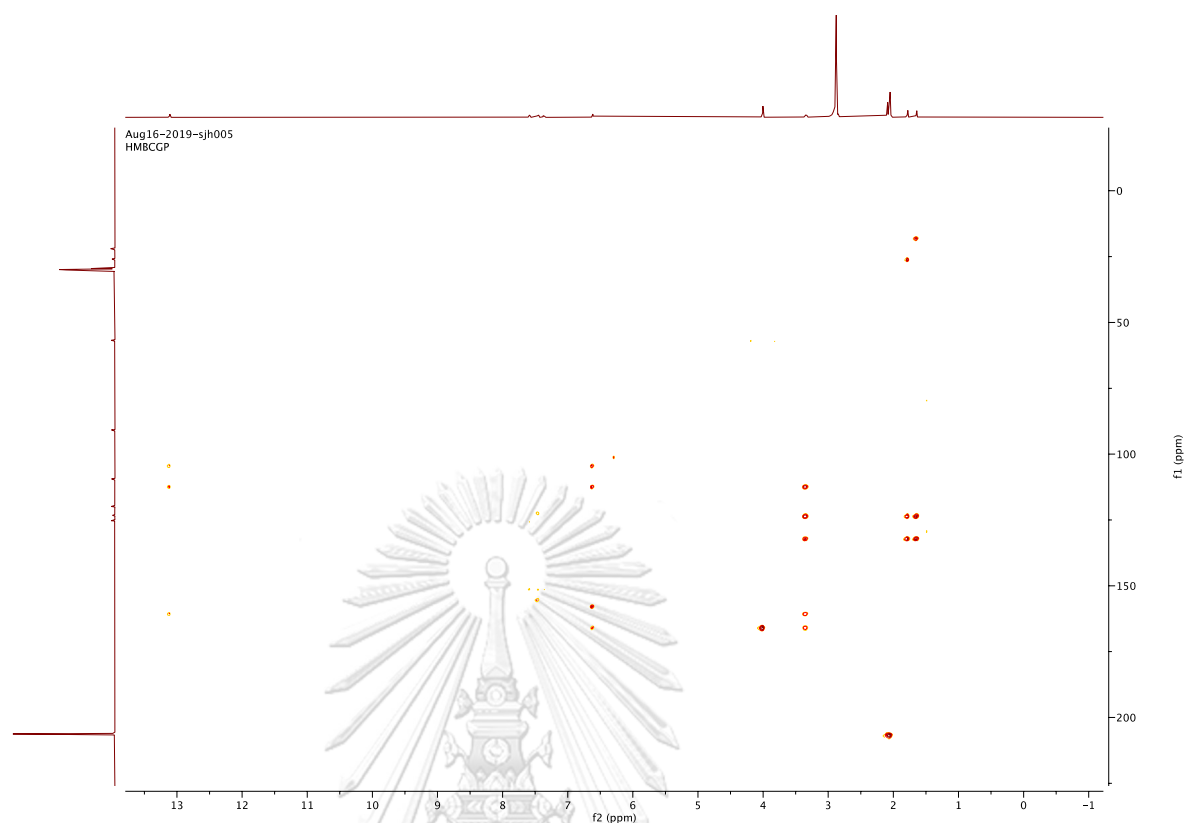


Figure A.8.5 HMBC spectrum (acetone-d₆) of compound 8

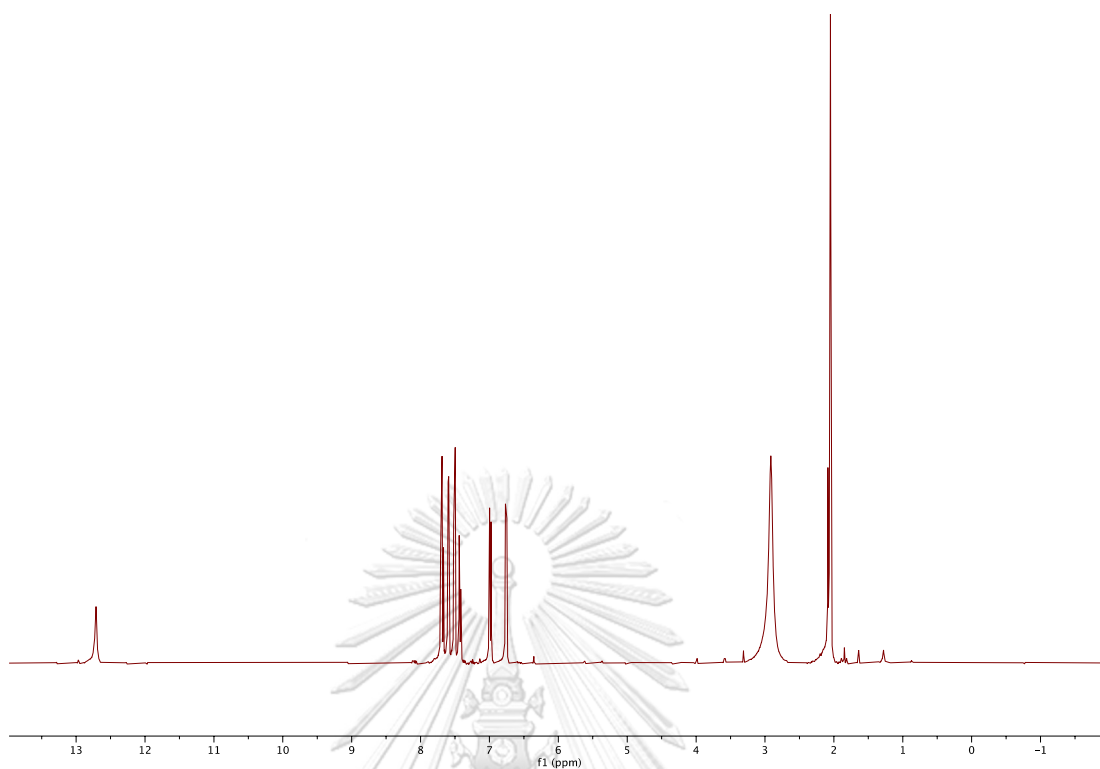


Figure A.9.1 ^1H NMR (400 MHz, CDCl_3) spectrum of compound **9**

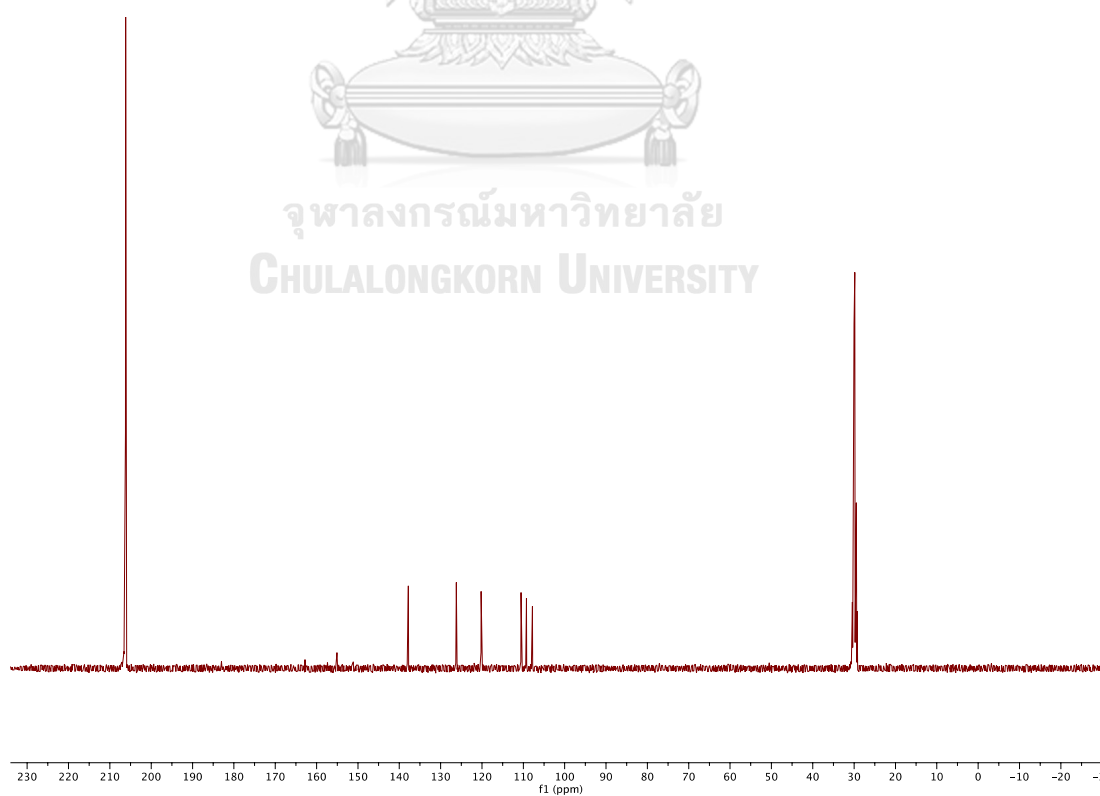


Figure A.9.2 ^{13}C NMR (100 MHz, CDCl_3) spectrum of compound **9**

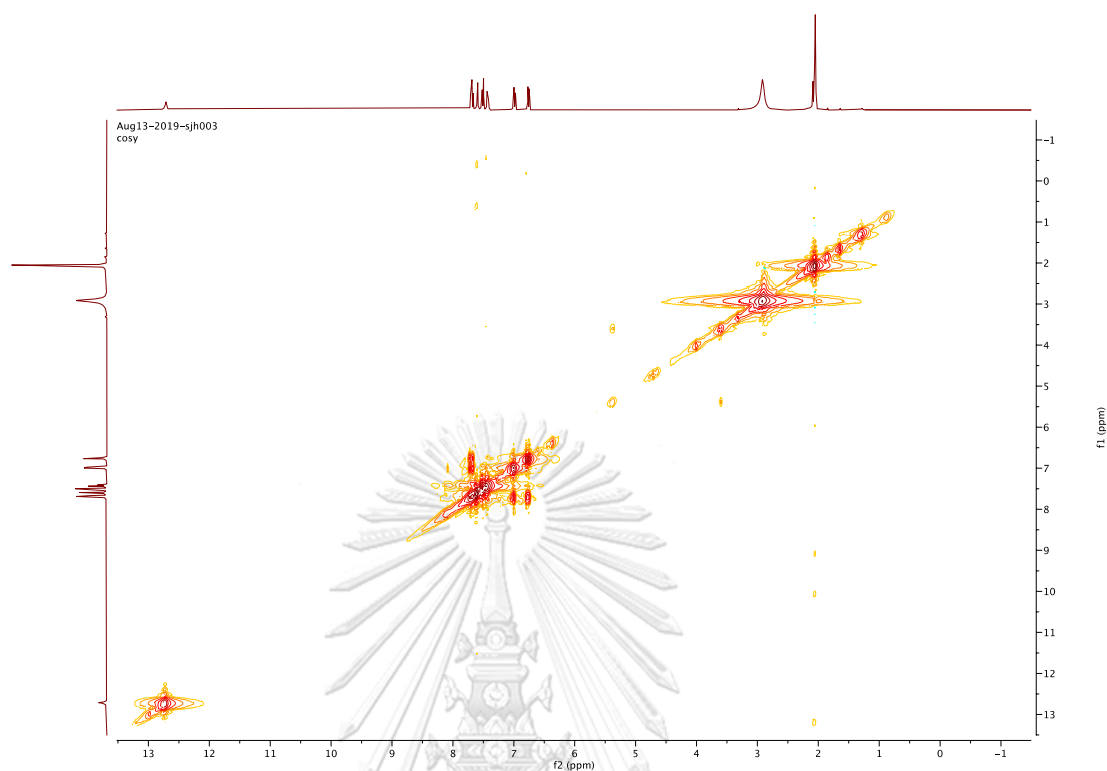


Figure A.9.3 ^1H - ^1H COSY spectrum (CDCl_3) of compound **9**

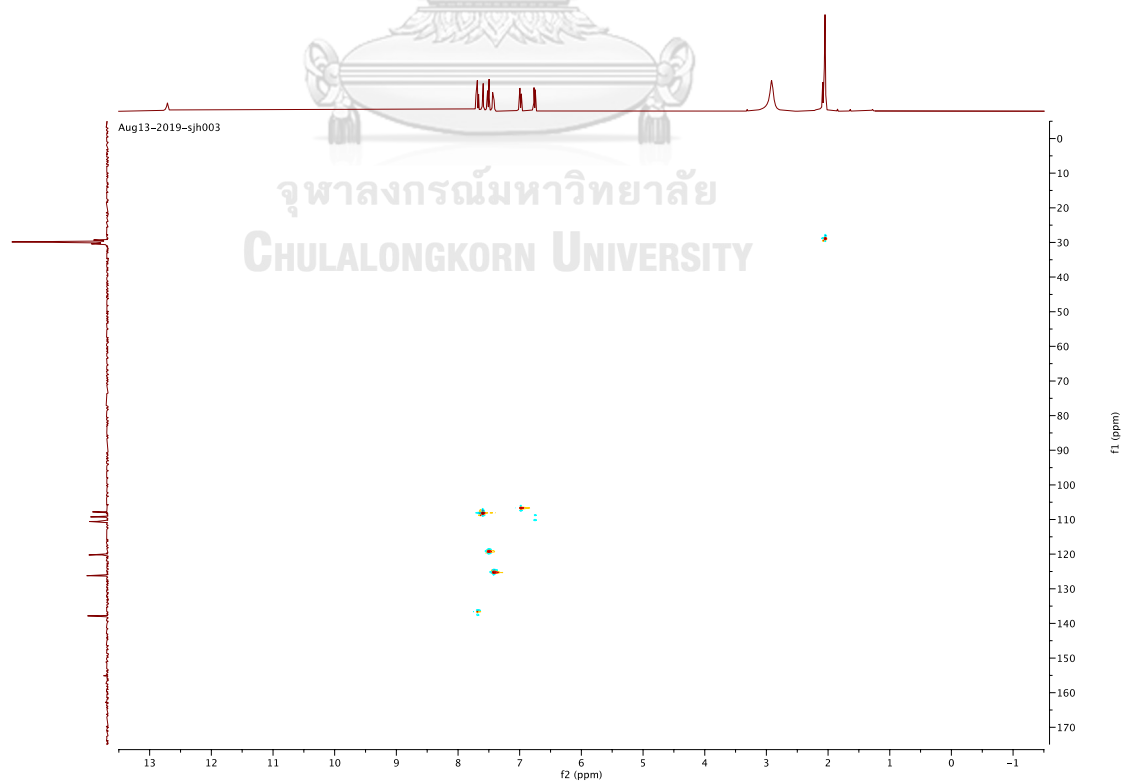


Figure A.9.4 HSQC spectrum (CDCl_3) of compound **9**

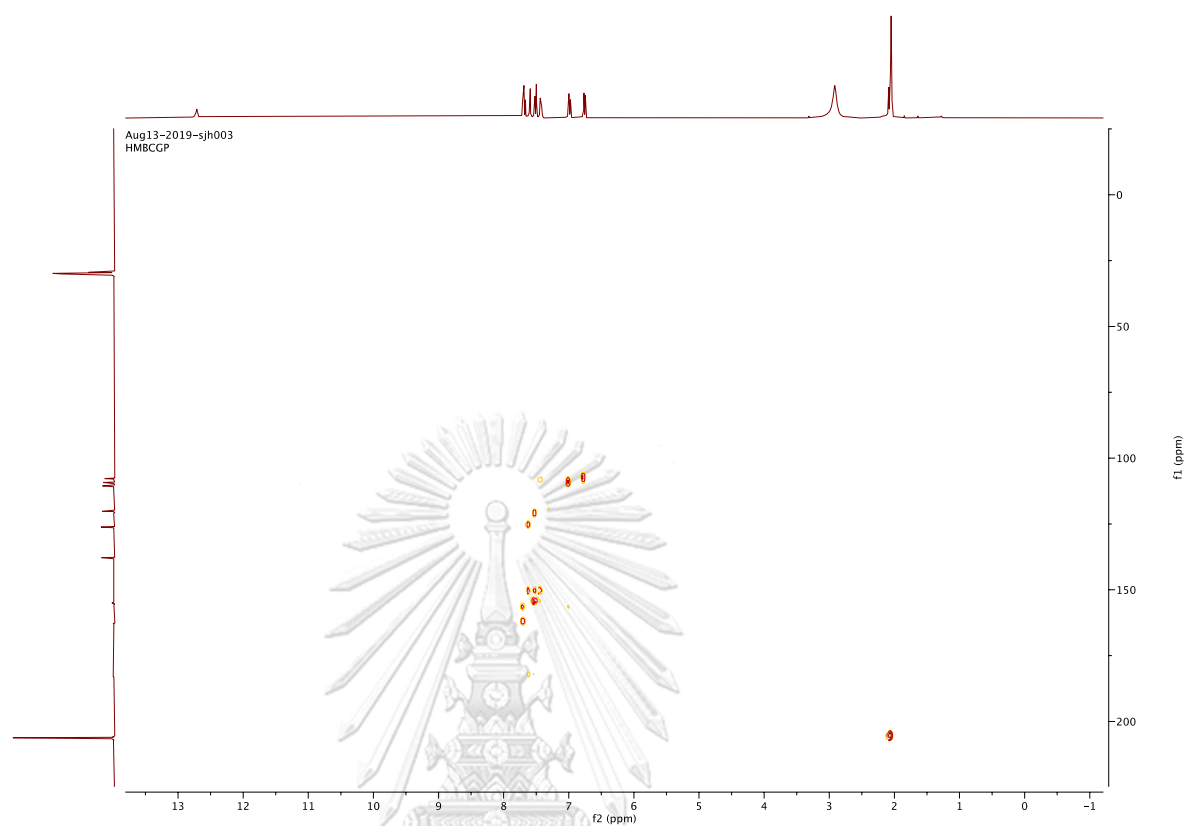


Figure A.9.5 HMBC spectrum (CDCl_3) of compound 9

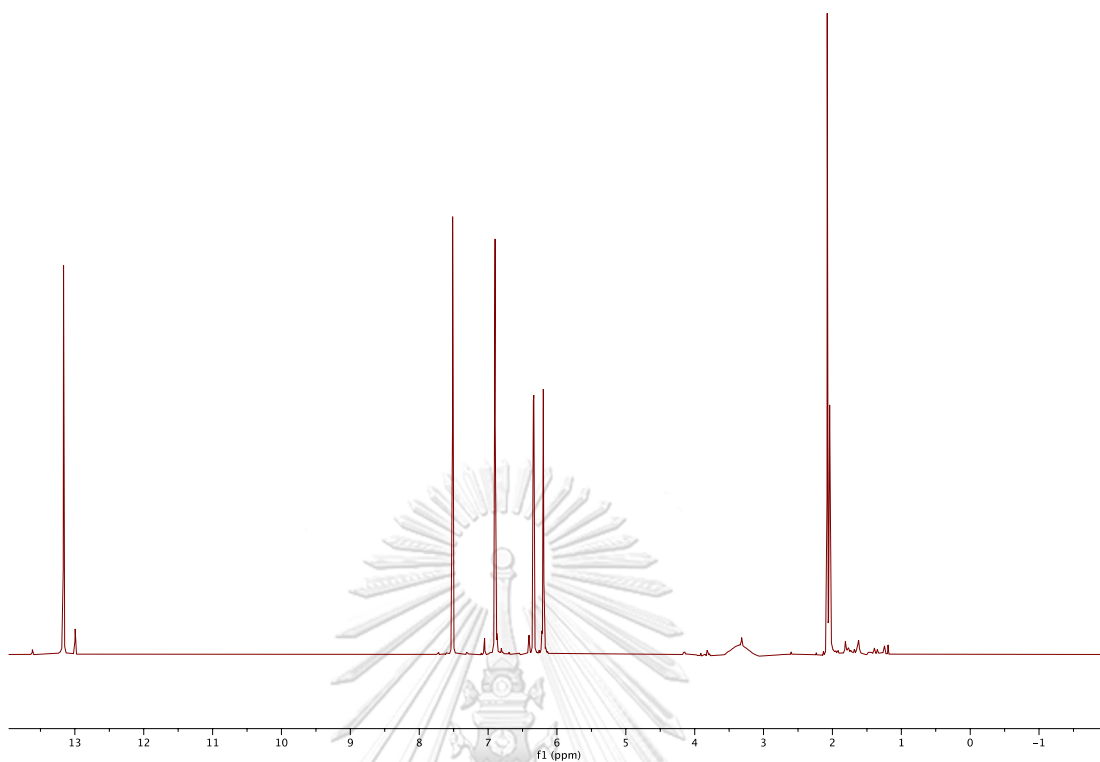


Figure A.10.1 ^1H NMR (400 MHz, CDCl_3) spectrum of compound 10

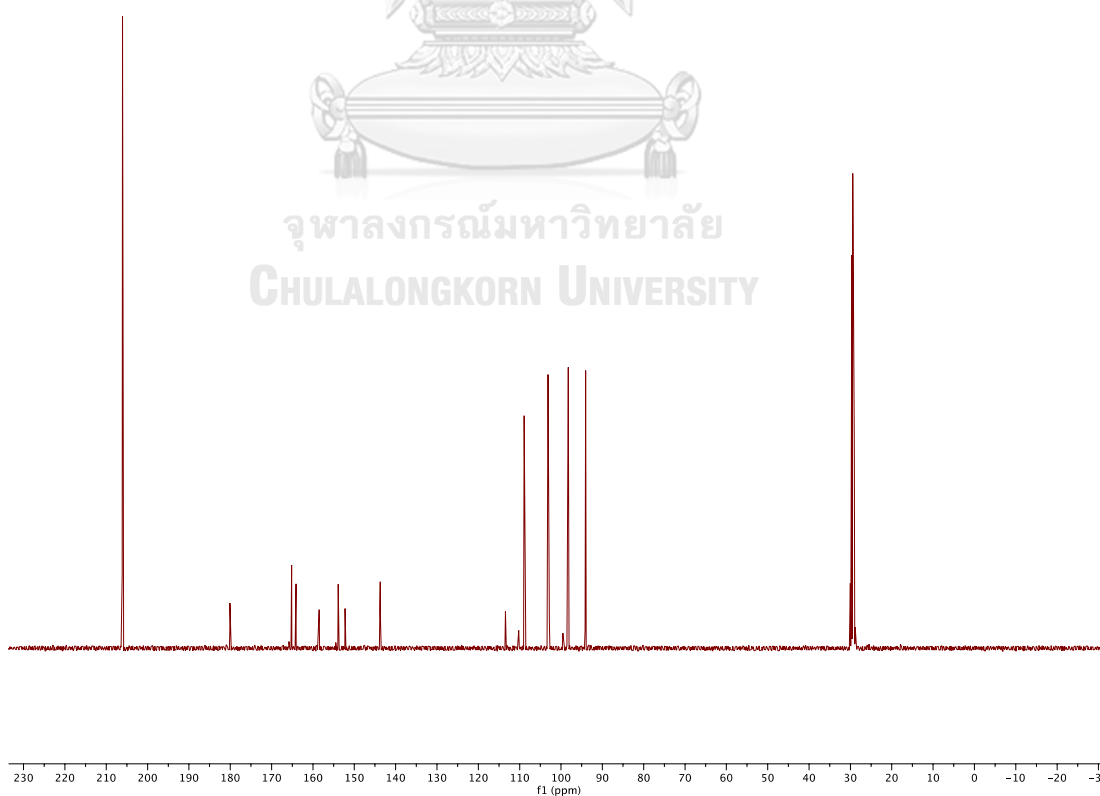


Figure A.10.2 ^{13}C NMR (100 MHz, CDCl_3) spectrum of compound 10

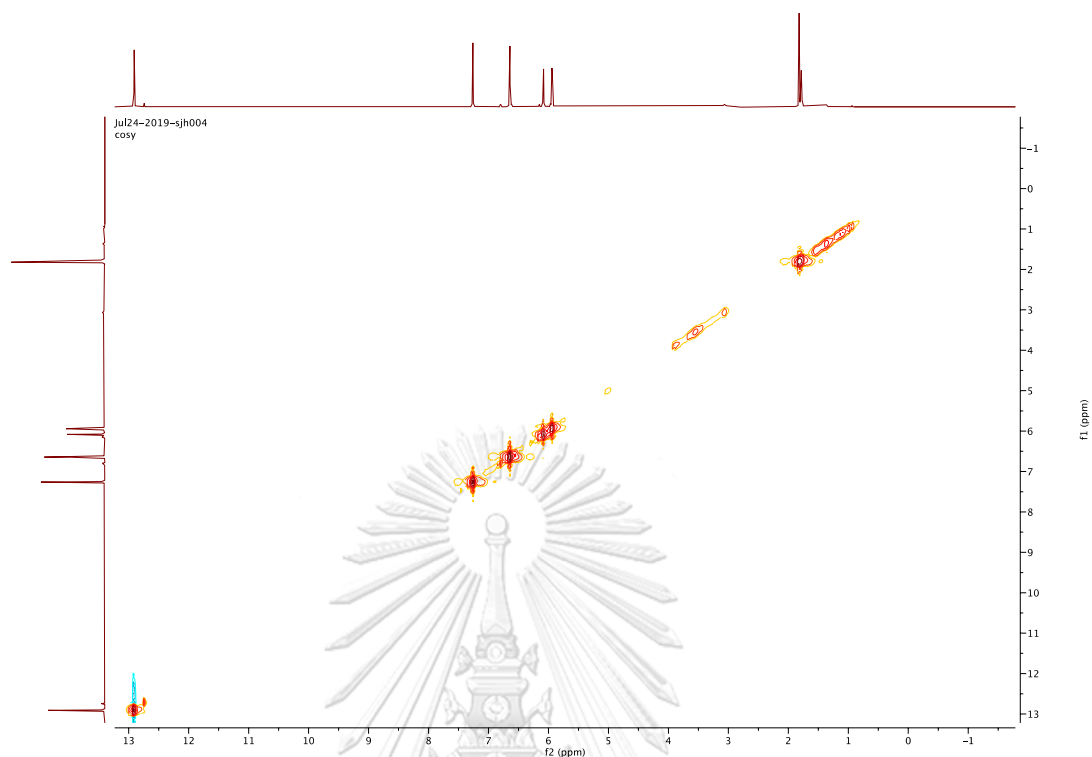


Figure A.10.3 ^1H - ^1H COSY spectrum (CDCl_3) of compound 10

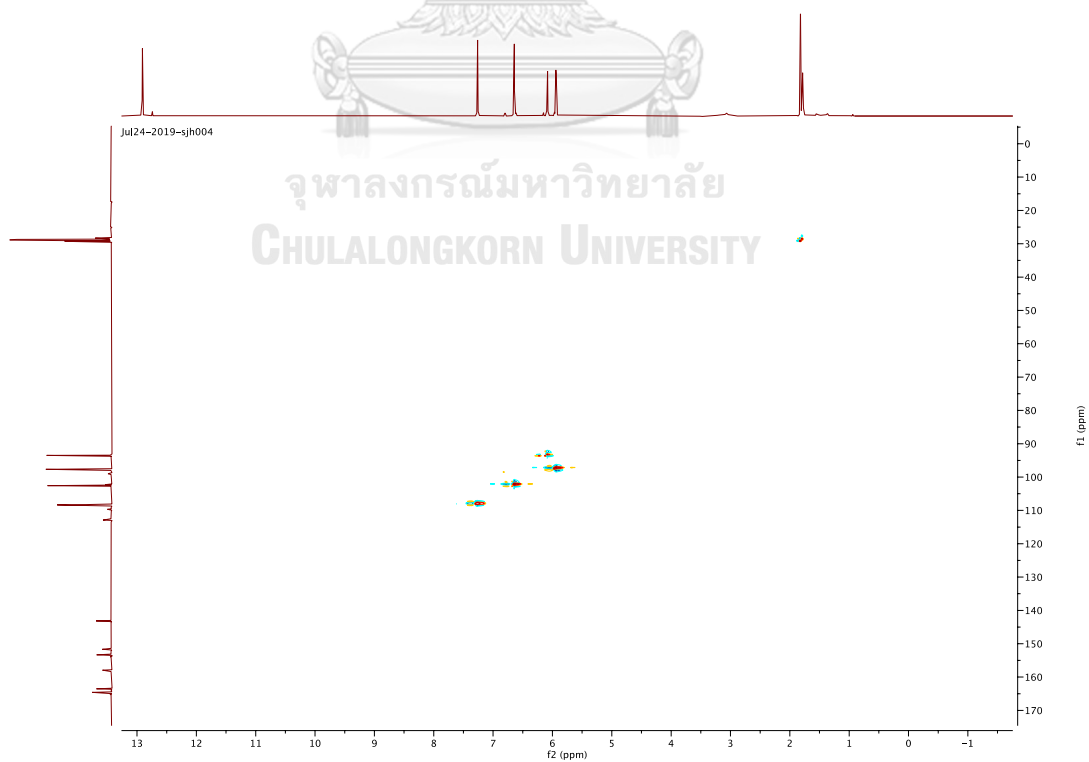


Figure A.10.4 HSQC spectrum (CDCl_3) of compound 10

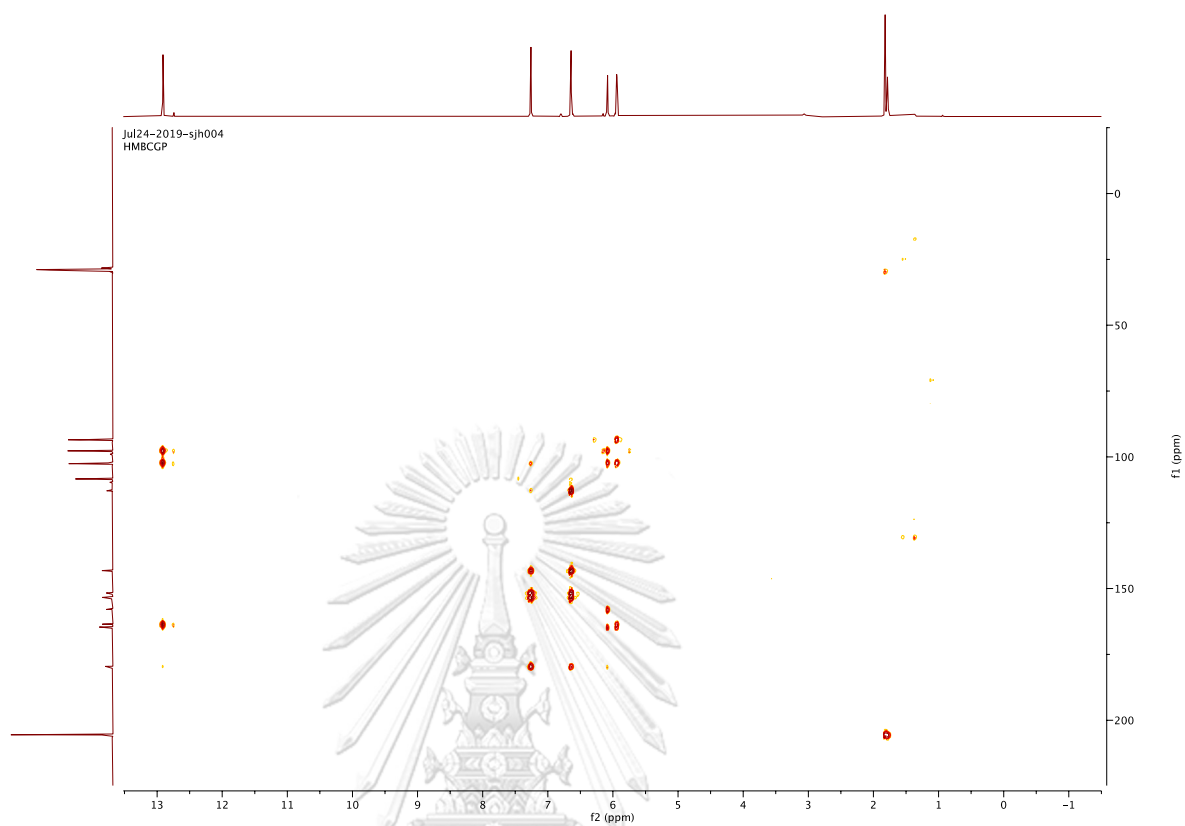


Figure A.10.5 HMBC spectrum (CDCl_3) of compound 10

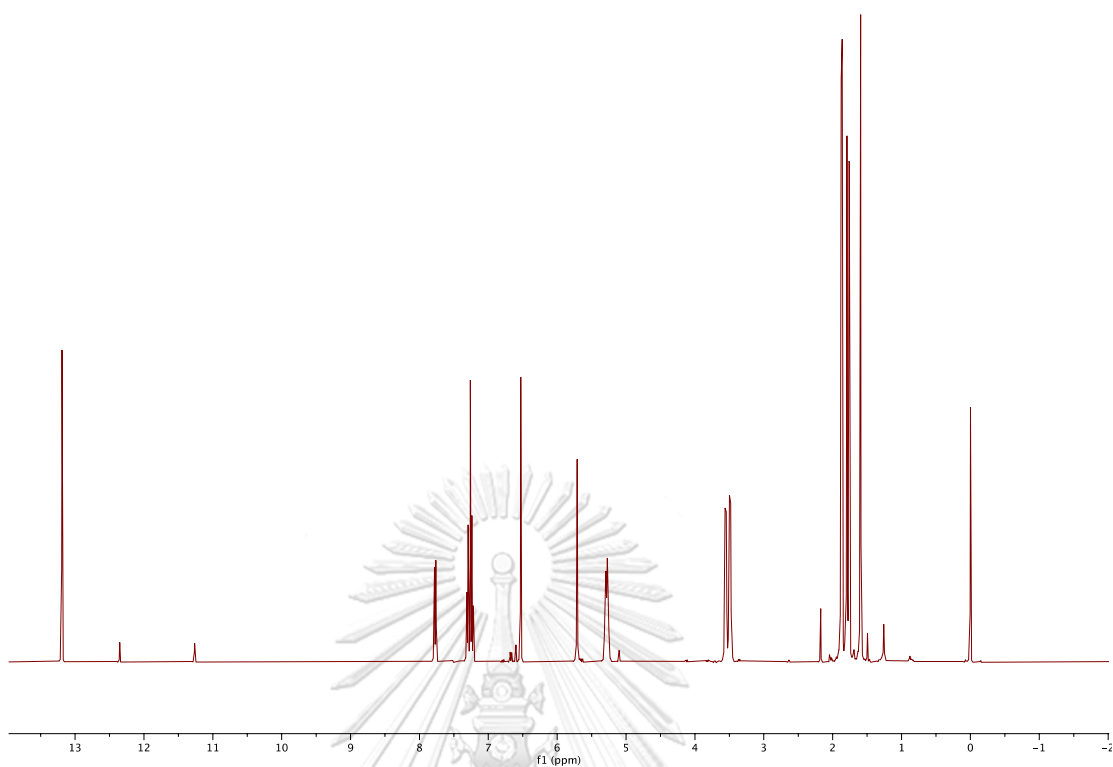


Figure A.11.1 ^1H NMR (400 MHz, CDCl_3) spectrum of compound 11

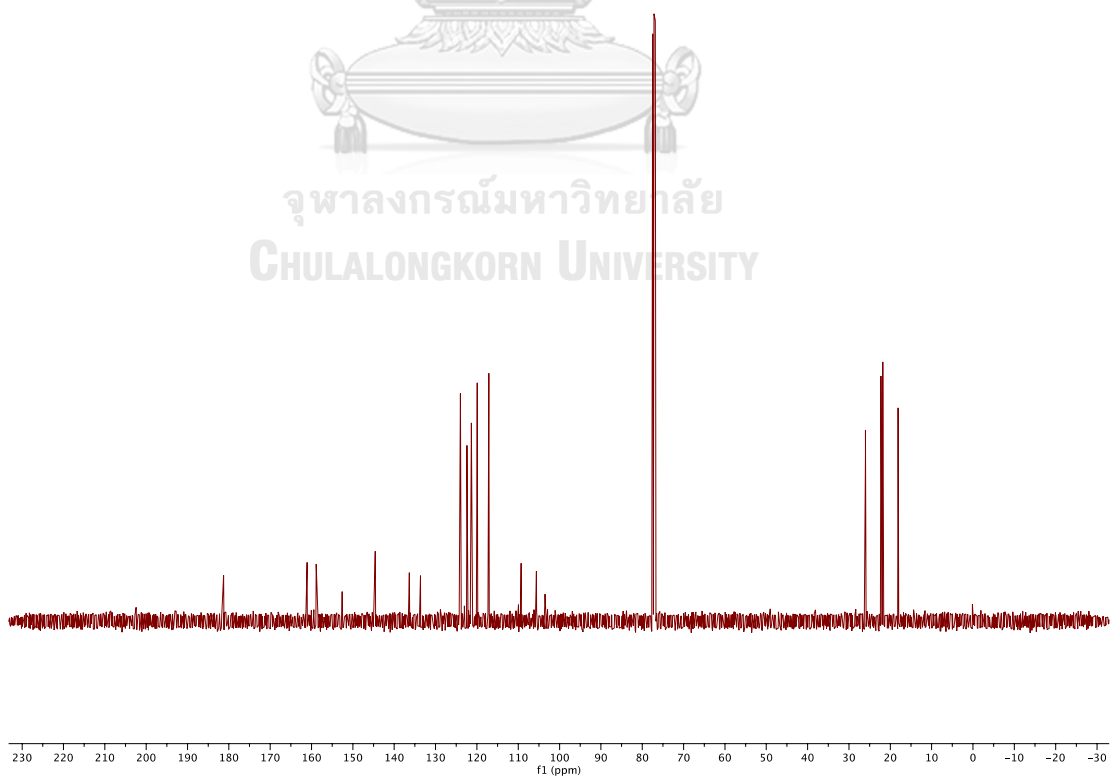


Figure A.11.2 ^{13}C NMR (100 MHz, CDCl_3) spectrum of compound 11

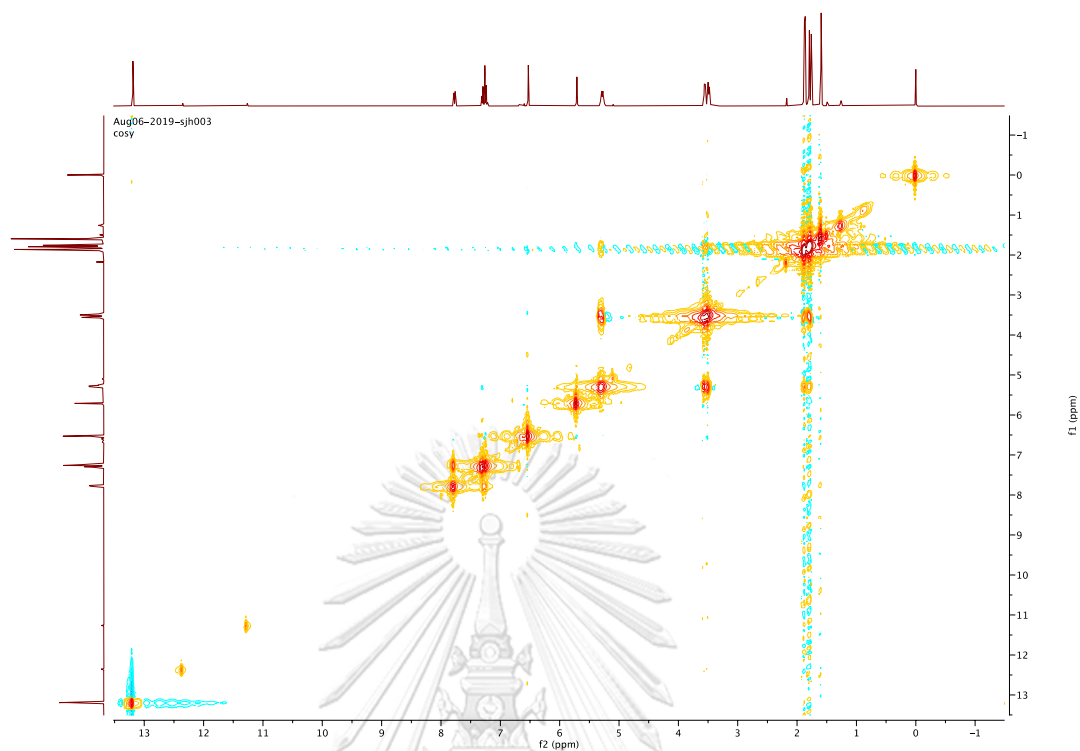


Figure A.11.3 ^1H - ^1H COSY spectrum (CDCl_3) of compound 11

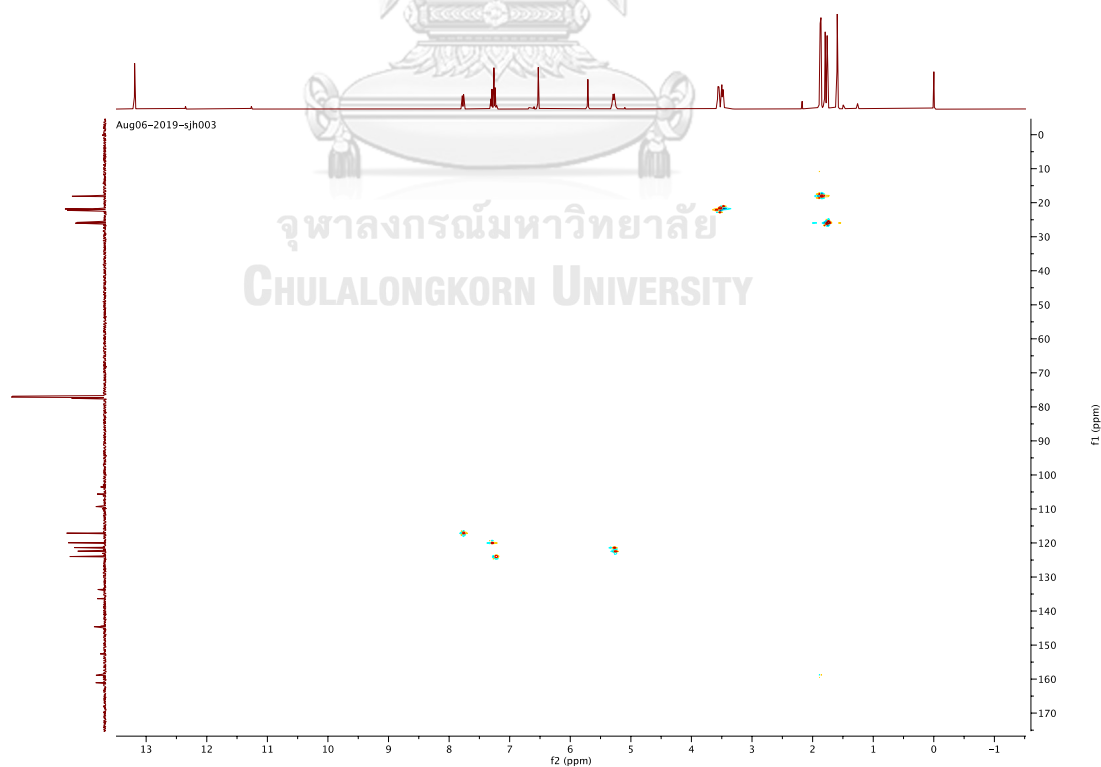


Figure A.11.4 HSQC spectrum (CDCl_3) of compound 11

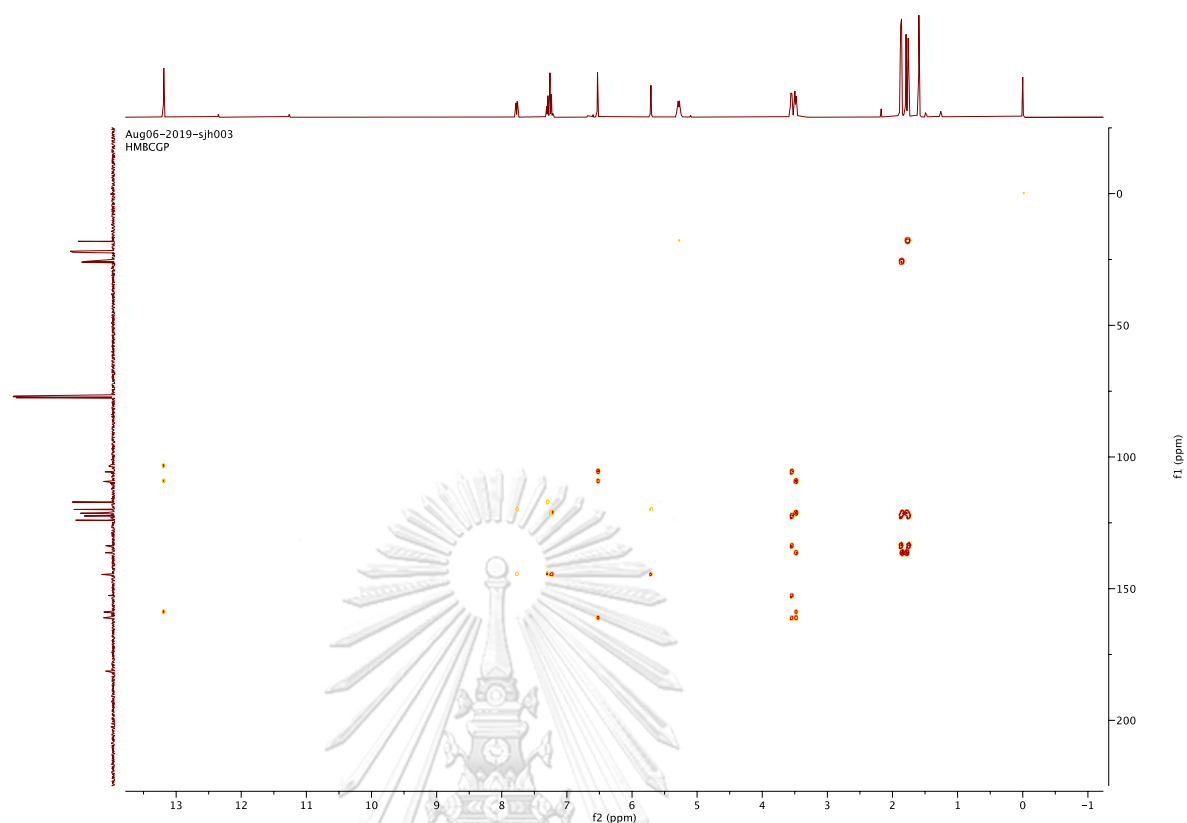


Figure A.11.5 HMBC spectrum (CDCl_3) of compound 11

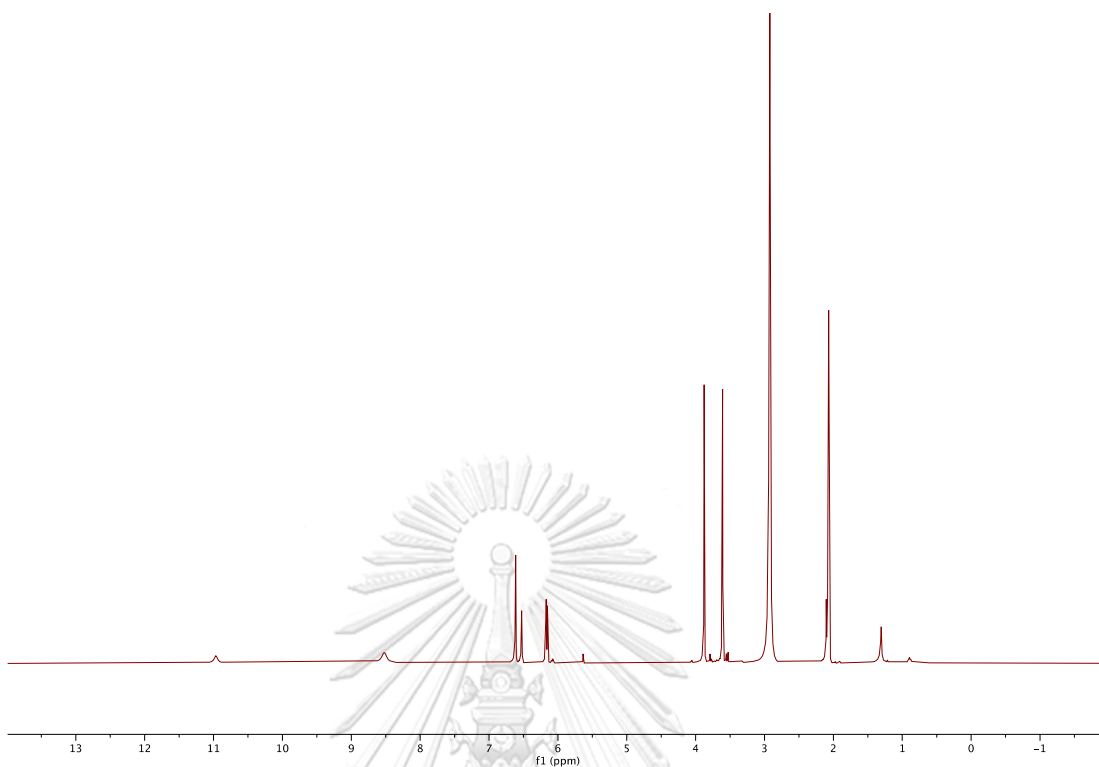


Figure A.12.1 ^1H NMR (400 MHz, acetone- d_6) spectrum of compound 12

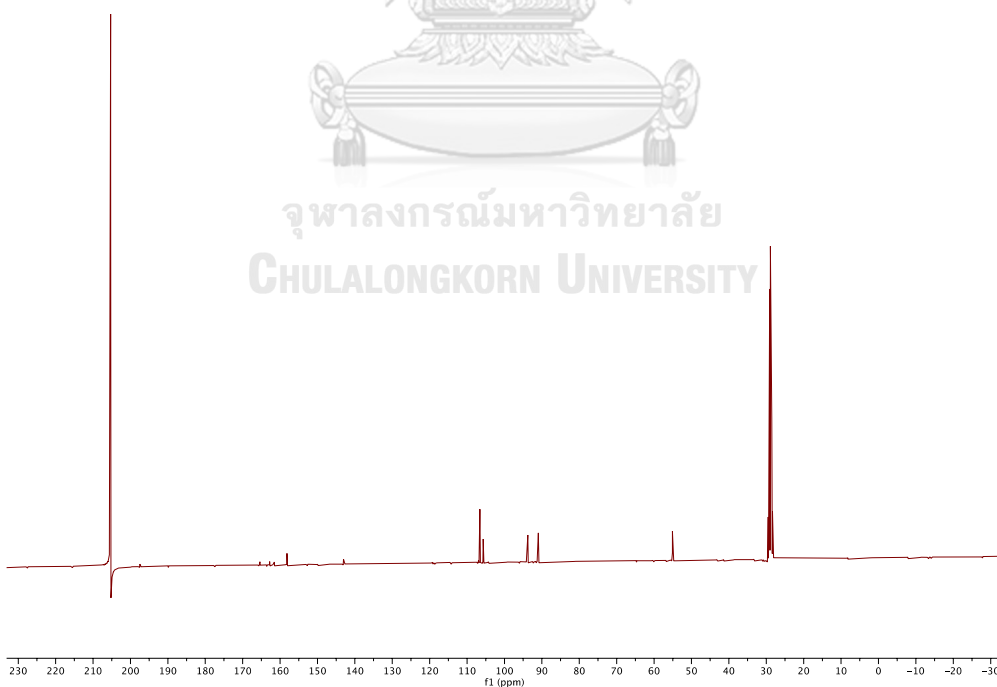


Figure A.12.2 ^{13}C NMR (100 MHz, acetone- d_6) spectrum of compound 12

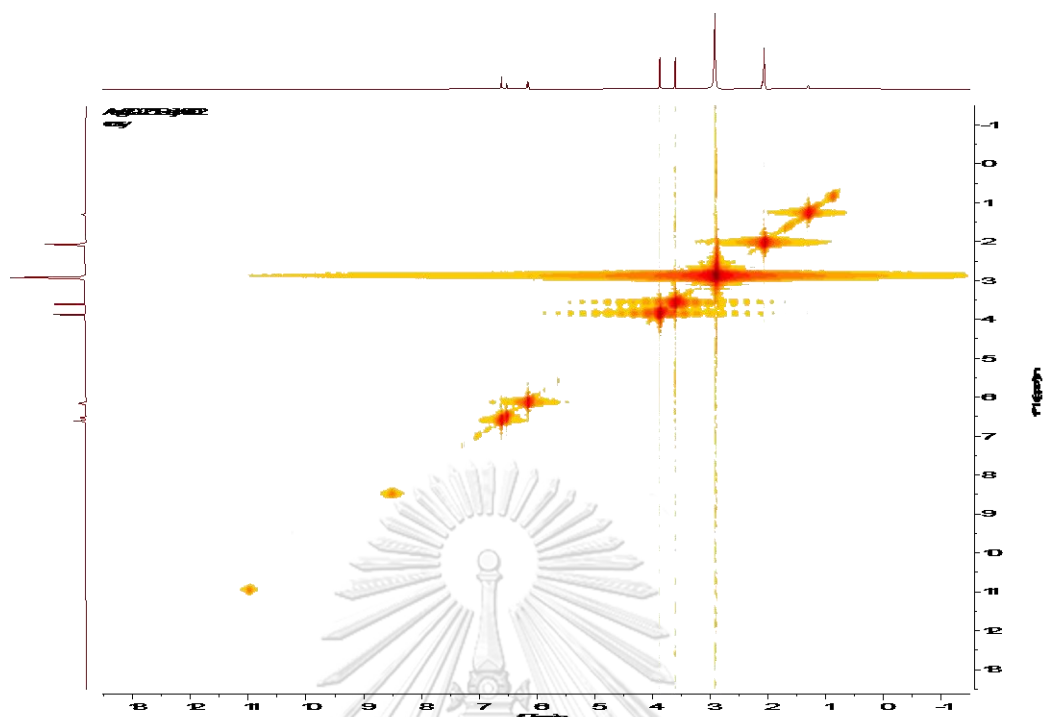


Figure A.12.3 ^1H - ^1H COSY spectrum (acetone- d_6) of compound 12

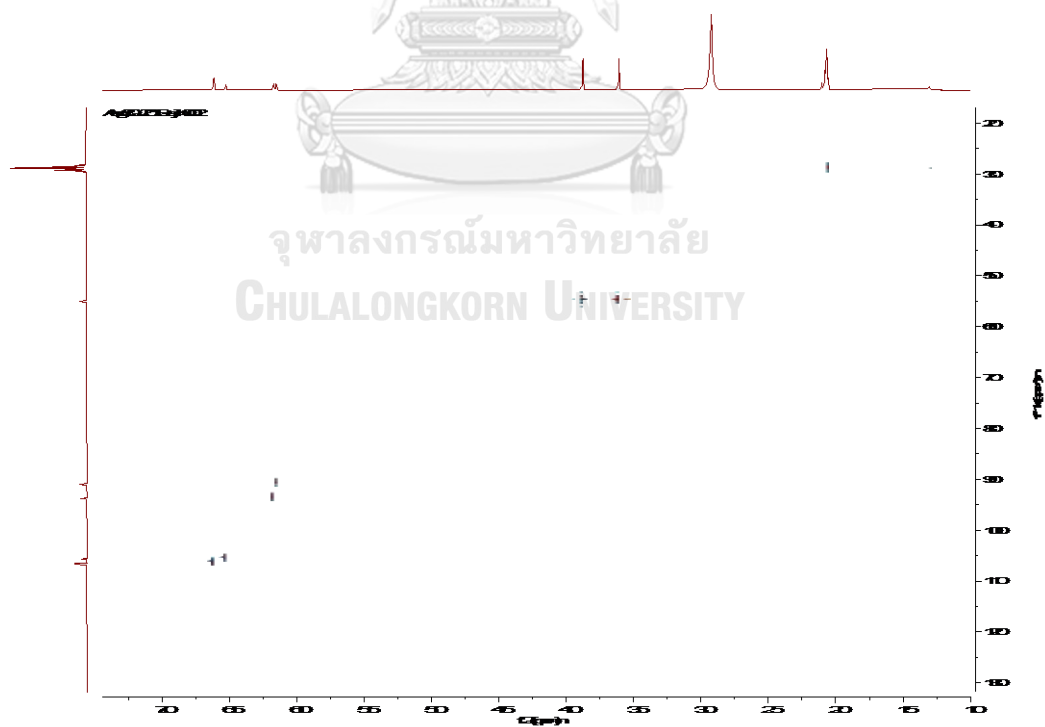


Figure A.12.4 HSQC spectrum (acetone- d_6) of compound 12

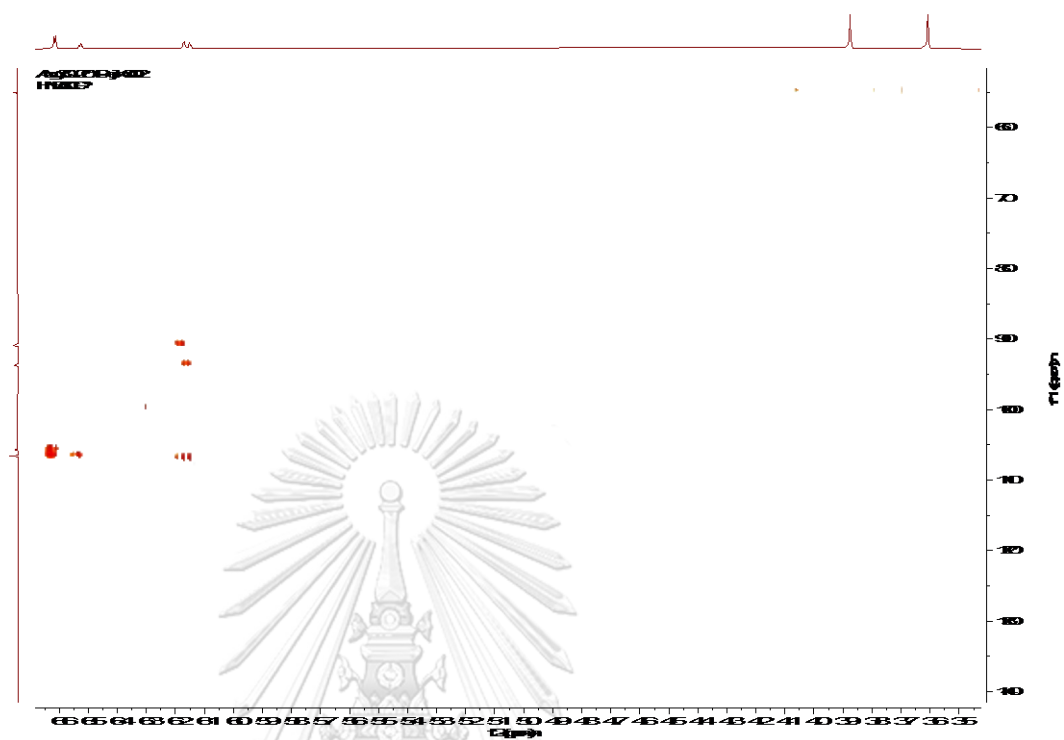


Figure A.12.5 HMBC spectrum (acetone-d6) of compound 12

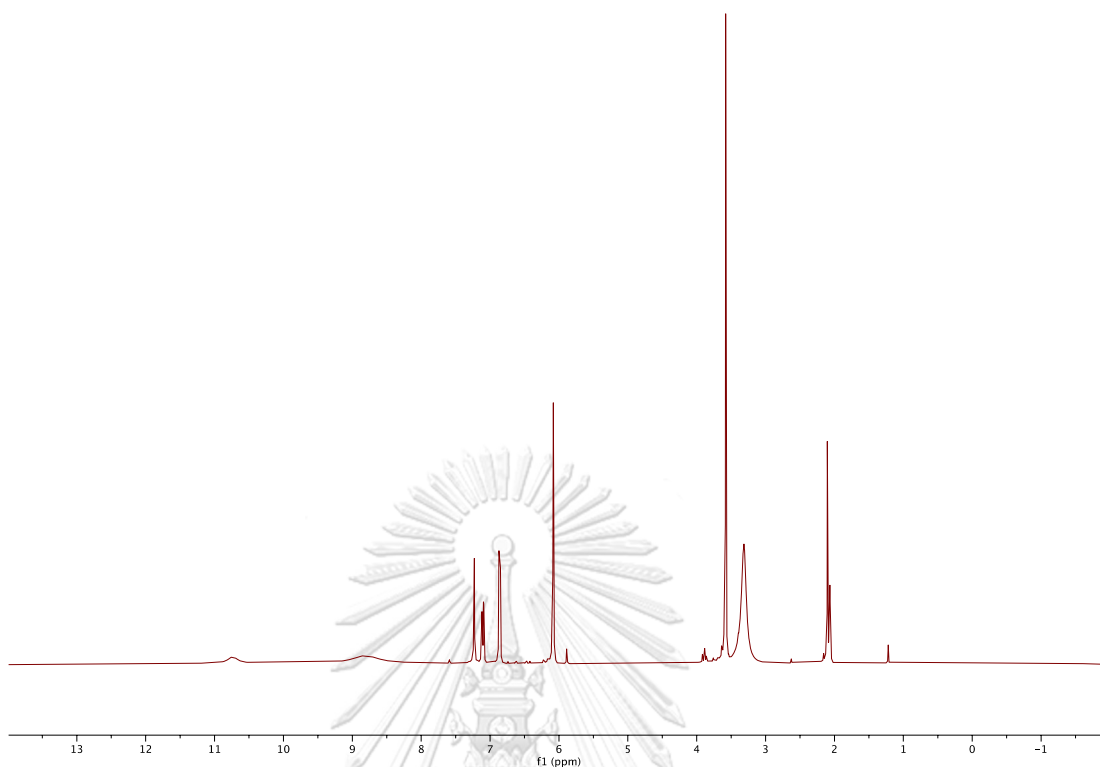


Figure A.13.1 ^1H NMR (400 MHz, acetone- d_6) spectrum of compound **13**

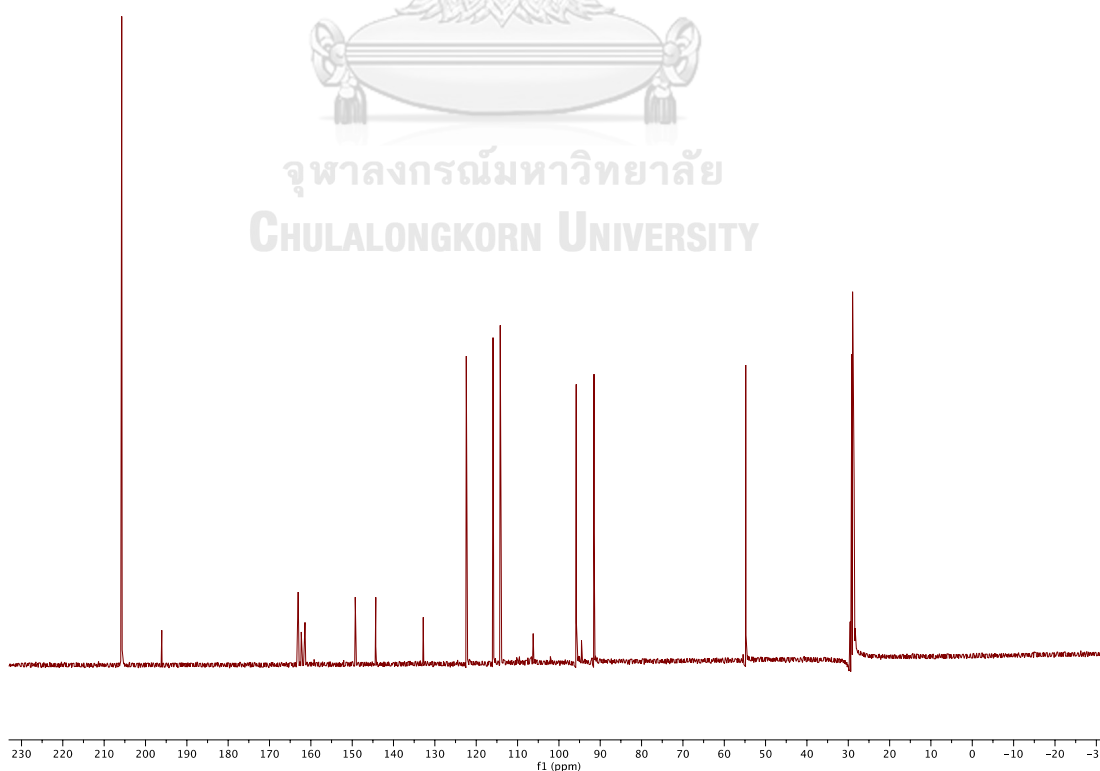


Figure A.13.2 ^{13}C NMR (100 MHz, acetone- d_6) spectrum of compound **13**

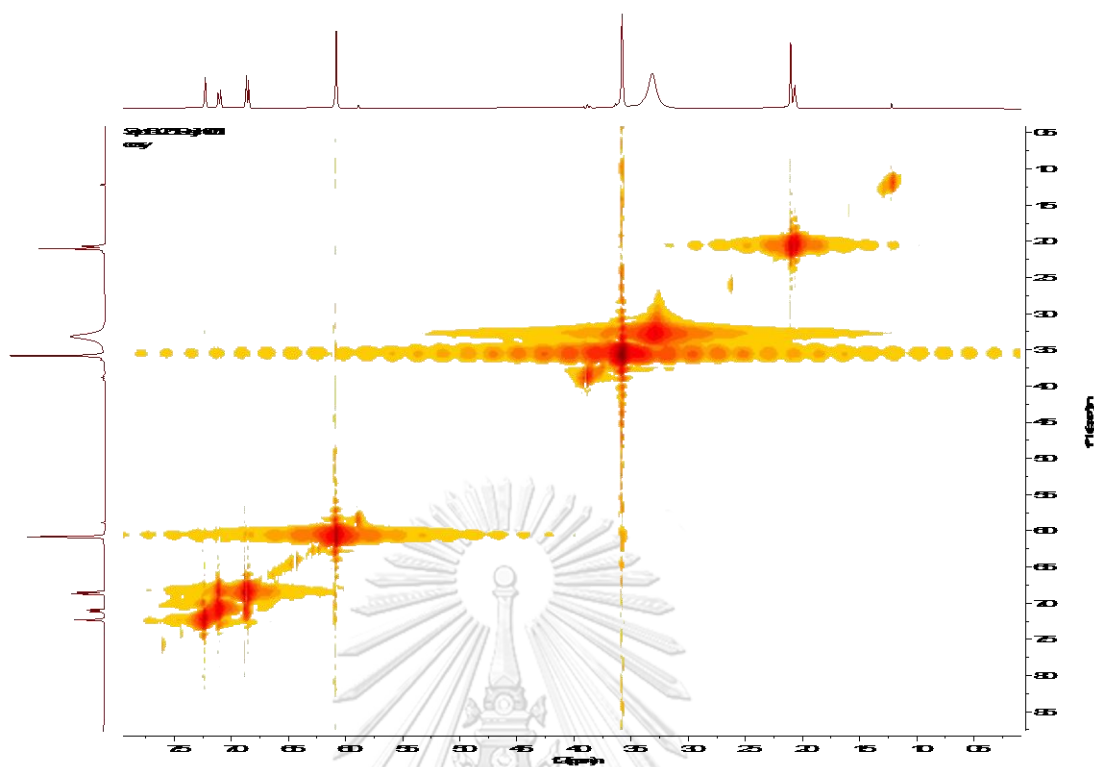


Figure A.13.3 ^1H - ^1H COSY spectrum (acetone- d_6) of compound 13

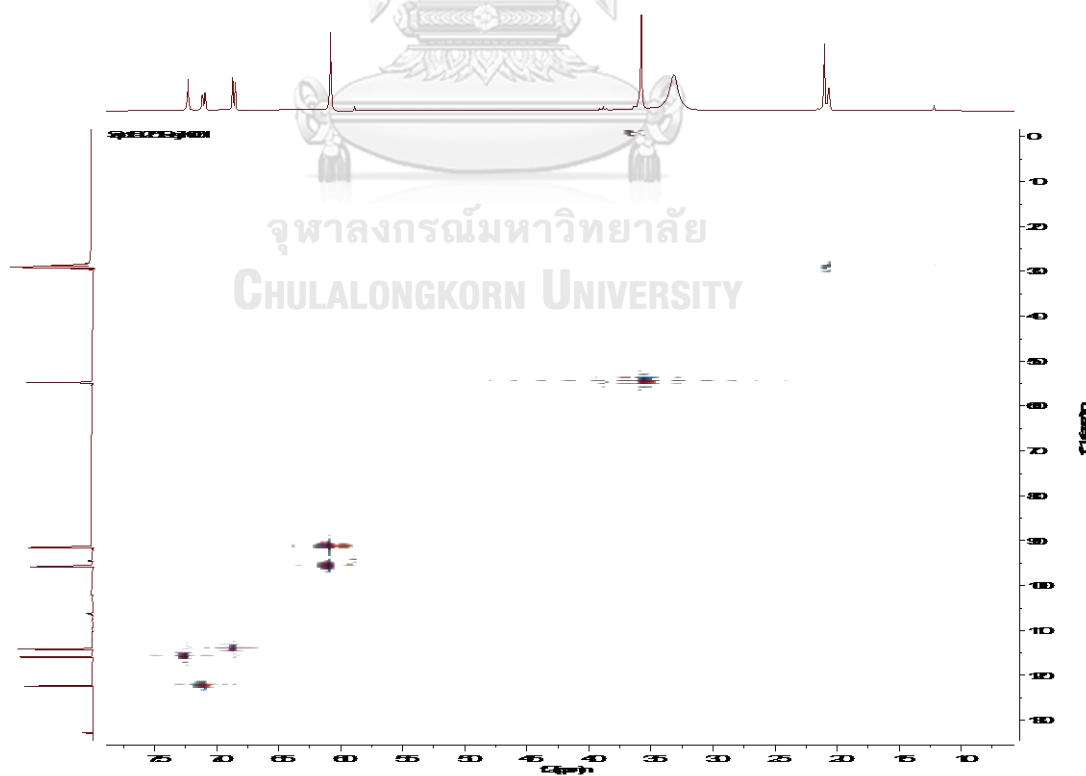


Figure A.13.4 HSQC spectrum (acetone- d_6) of compound 13

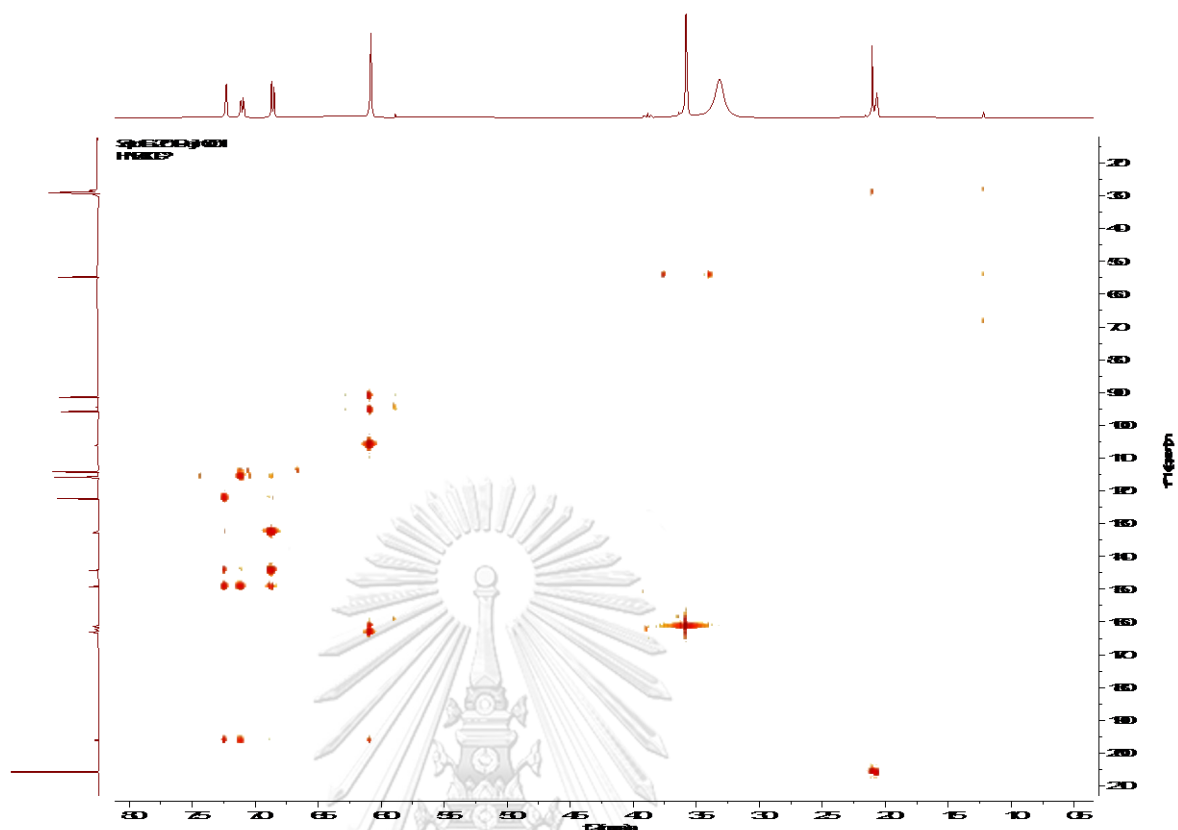


Figure A.13.5 HMBC spectrum (acetone-d₆) of compound 13

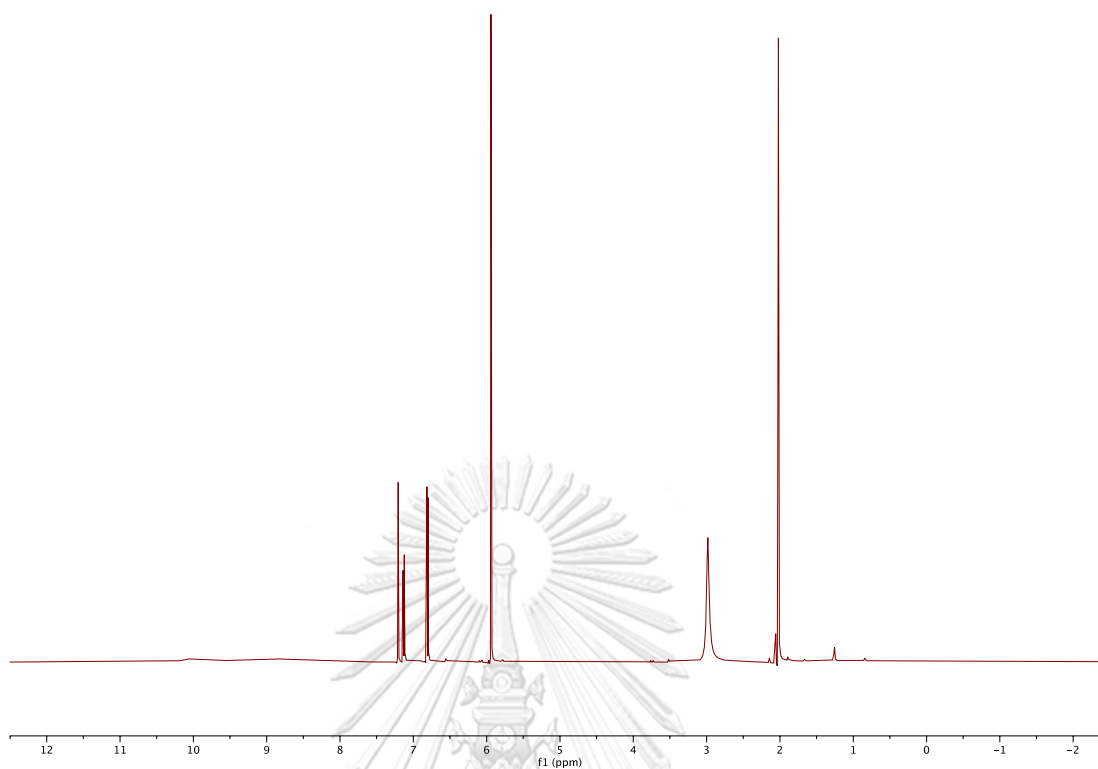


Figure A.14.1 ^1H NMR (400 MHz, acetone- d_6) spectrum of compound 14

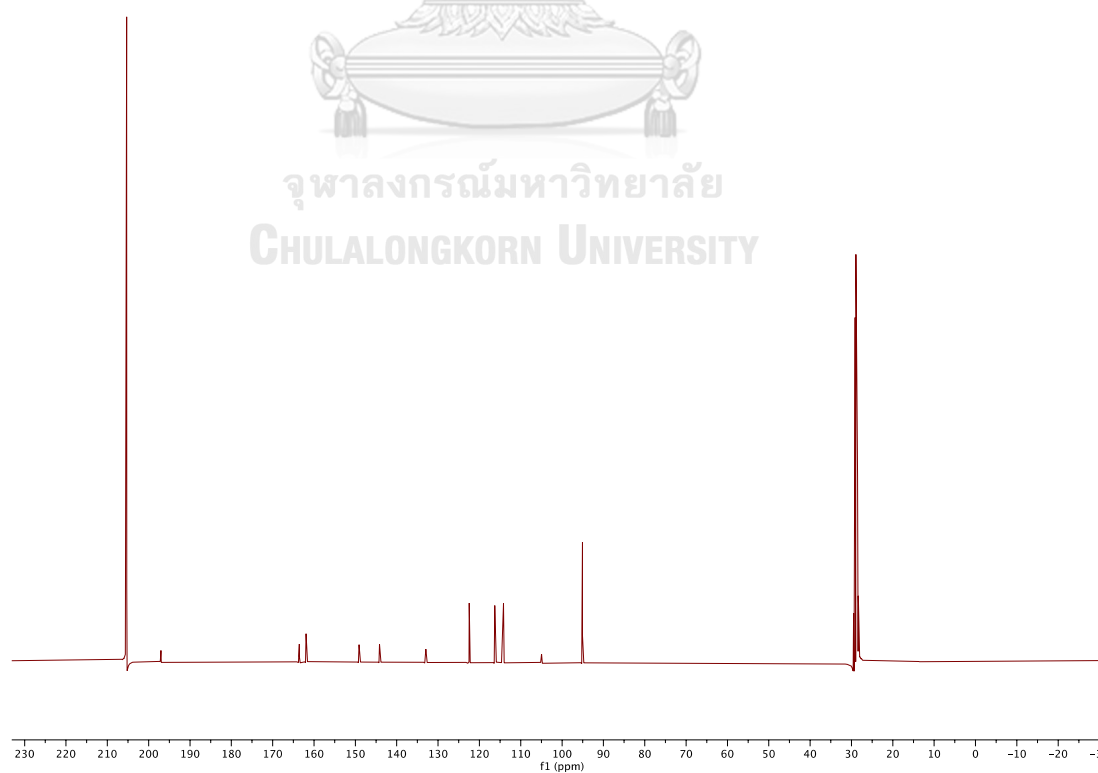


Figure A.14.2 ^{13}C NMR (100 MHz, acetone- d_6) spectrum of compound 14

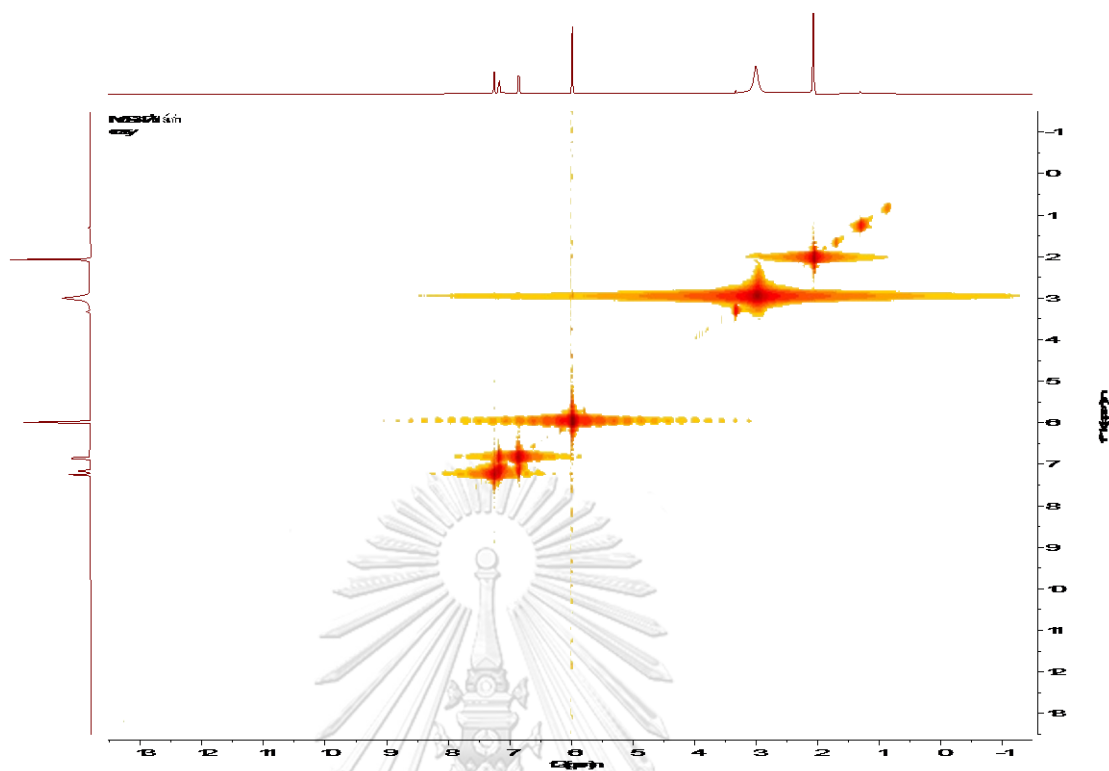


Figure A.14.3 ^1H - ^1H COSY spectrum (acetone- d_6) of compound 14

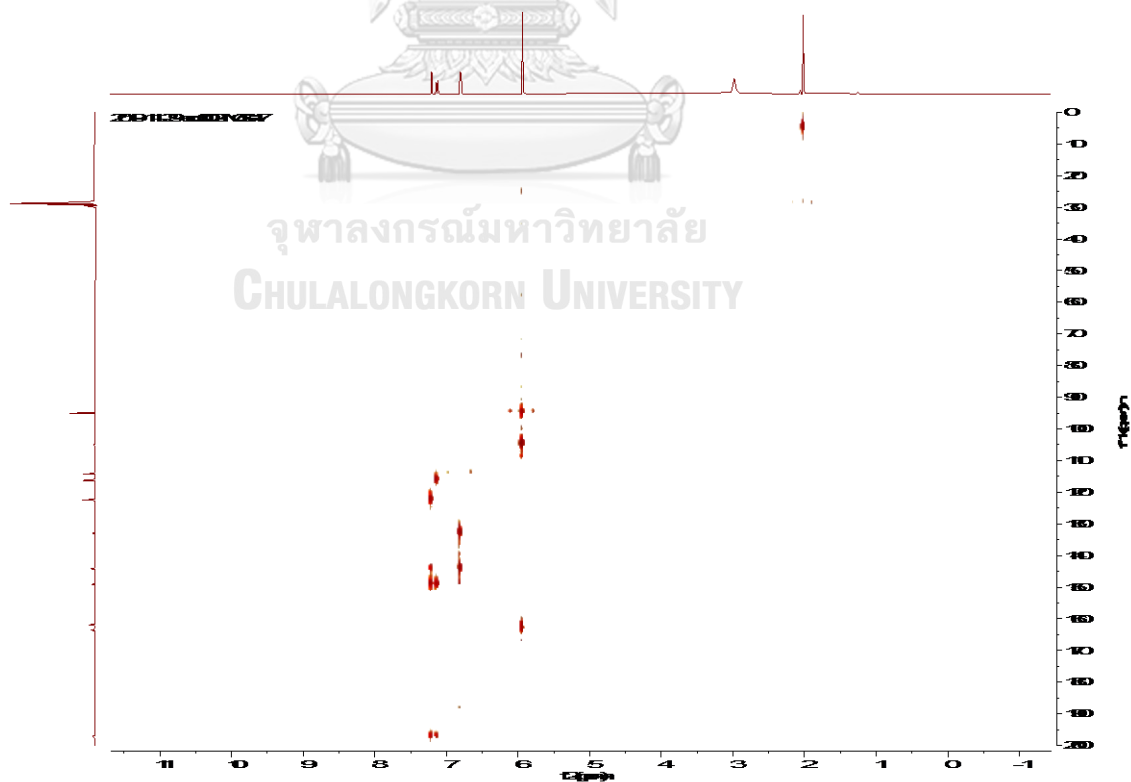


Figure A.14.4 HSQC spectrum (acetone- d_6) of compound 14

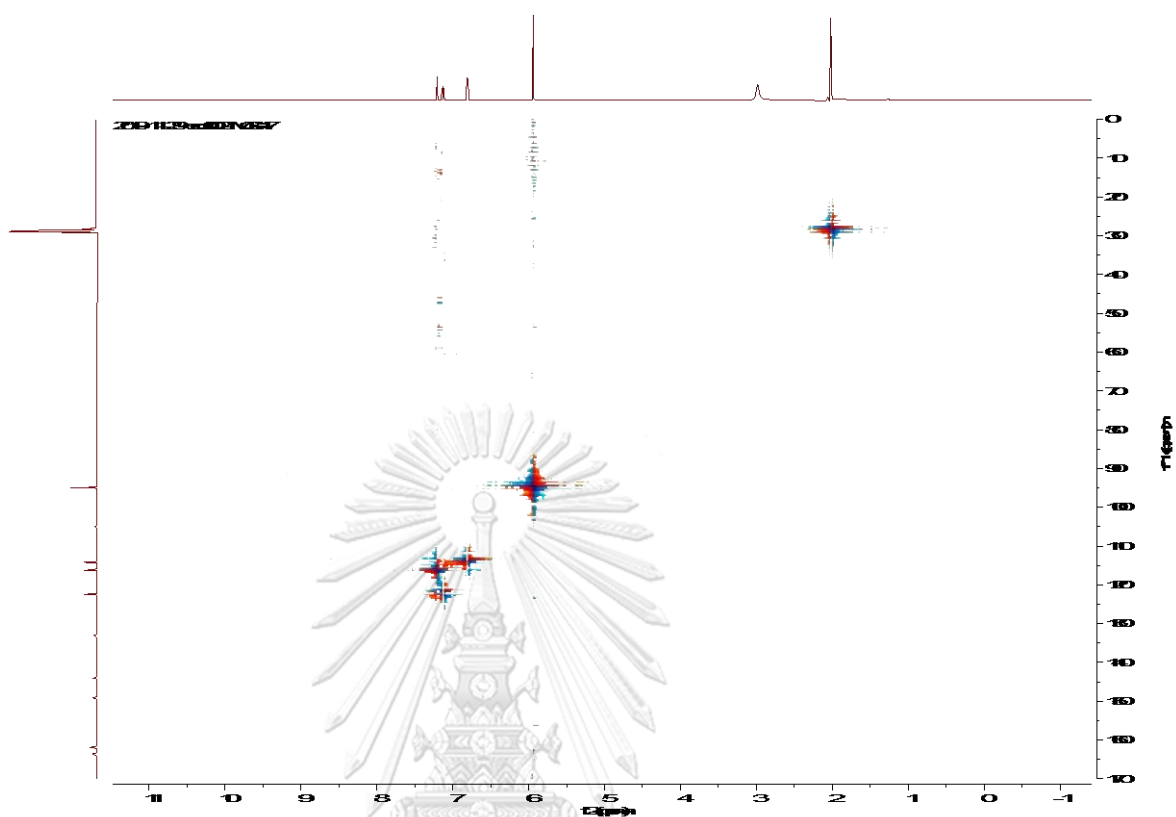


Figure A.14.5 HMBC spectrum (acetone-d6) of compound 14

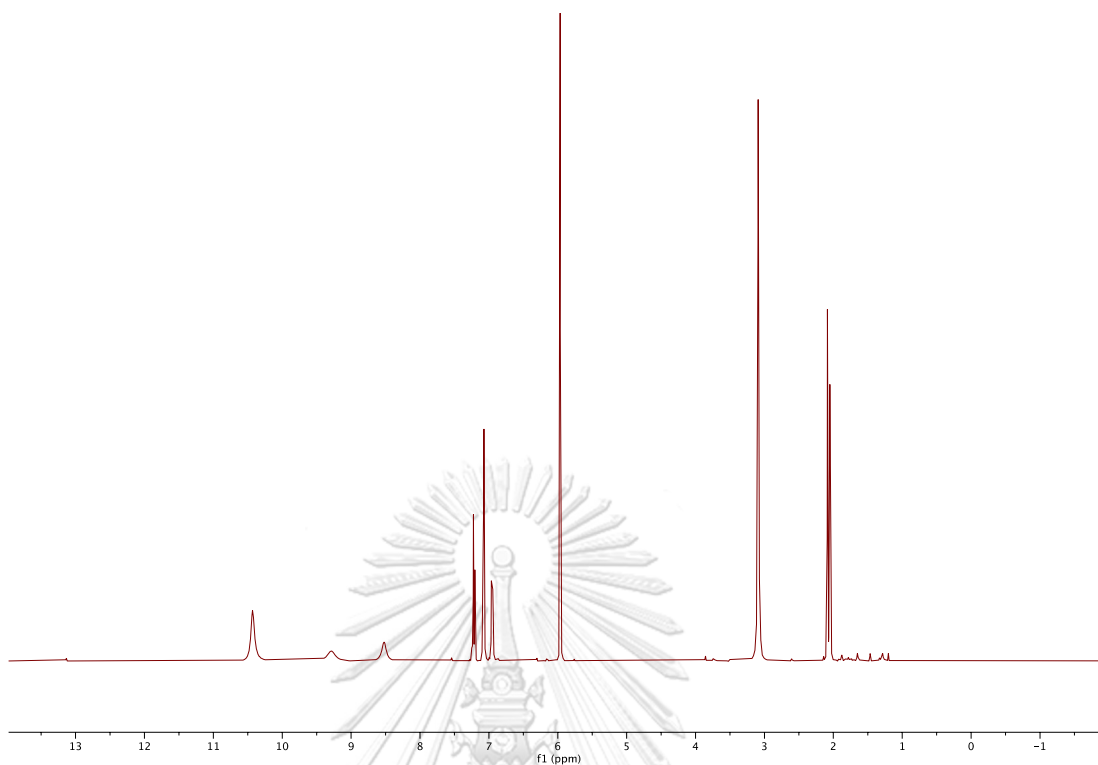


Figure A.15.1 ^1H NMR (400 MHz, acetone- d_6) spectrum of compound **15**

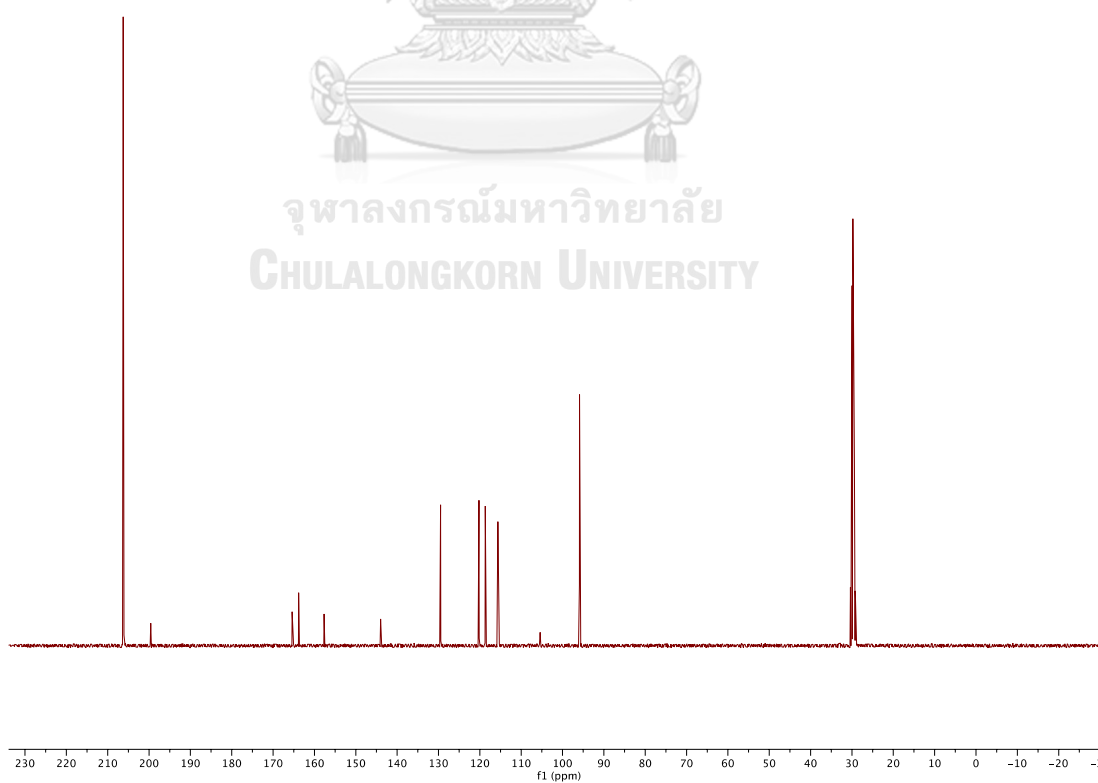


Figure A.15.2 ^{13}C NMR (100 MHz, acetone- d_6) spectrum of compound **15**

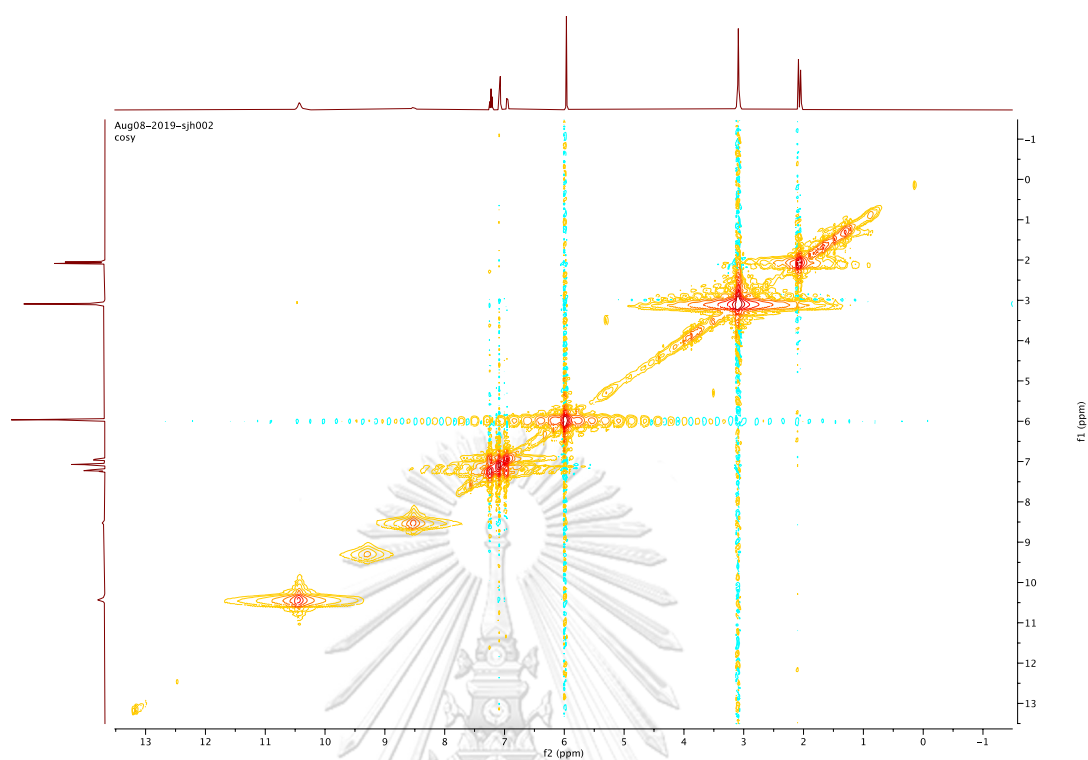


Figure A.15.3 ^1H - ^1H COSY spectrum (acetone- d_6) of compound 15

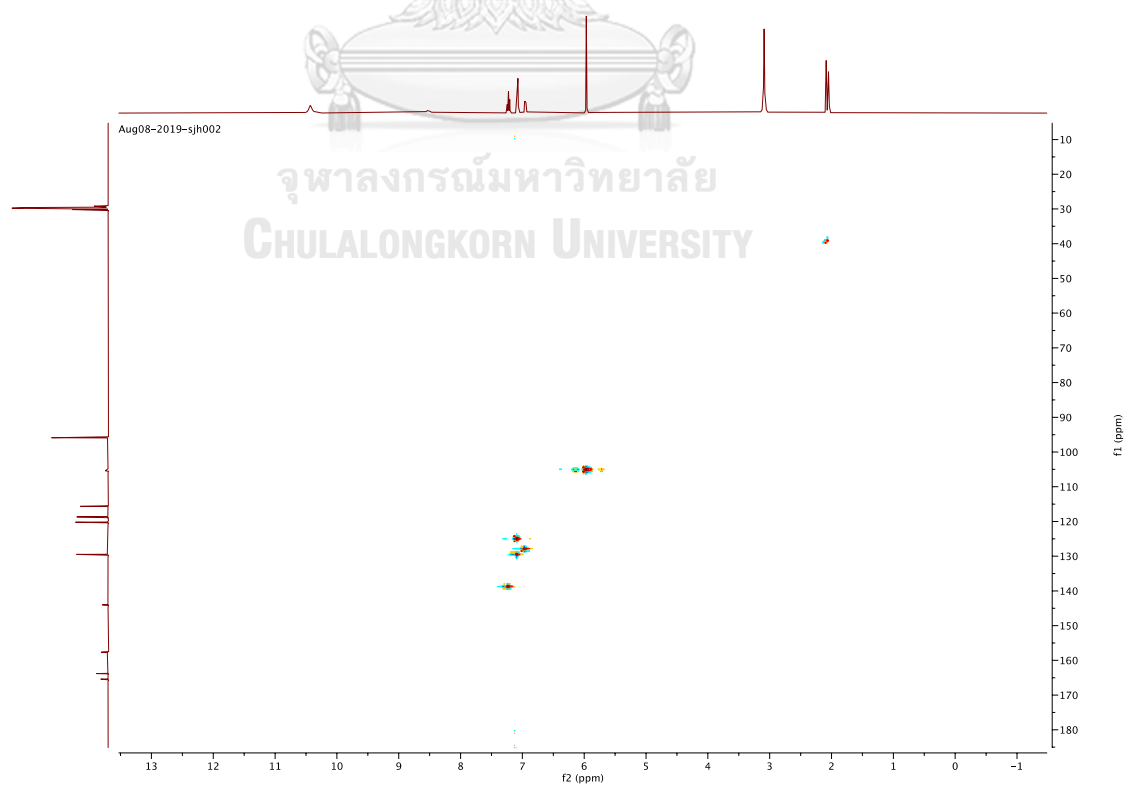
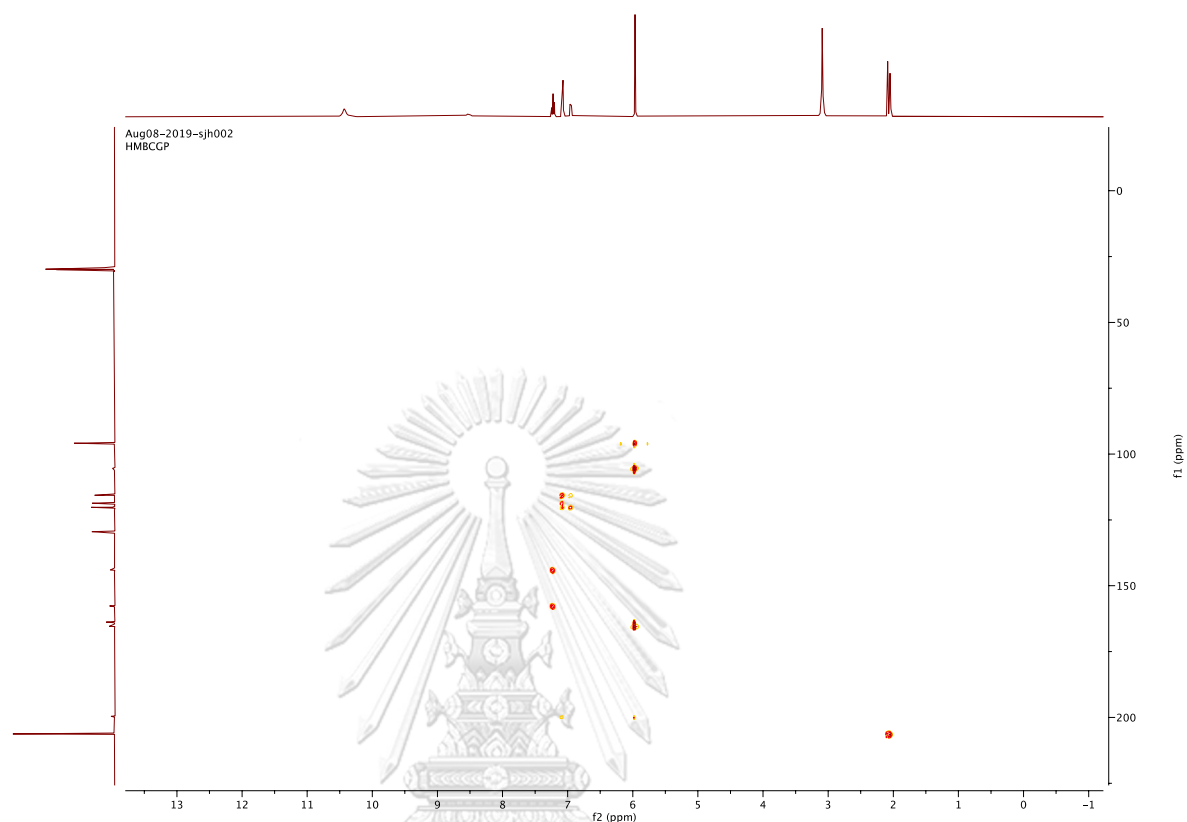


Figure A.15.4 HSQC spectrum (acetone-d₆) of compound 15Figure A.15.5 HMBC spectrum (acetone-d₆) of compound 15

จุฬาลงกรณ์มหาวิทยาลัย
CHULALONGKORN UNIVERSITY

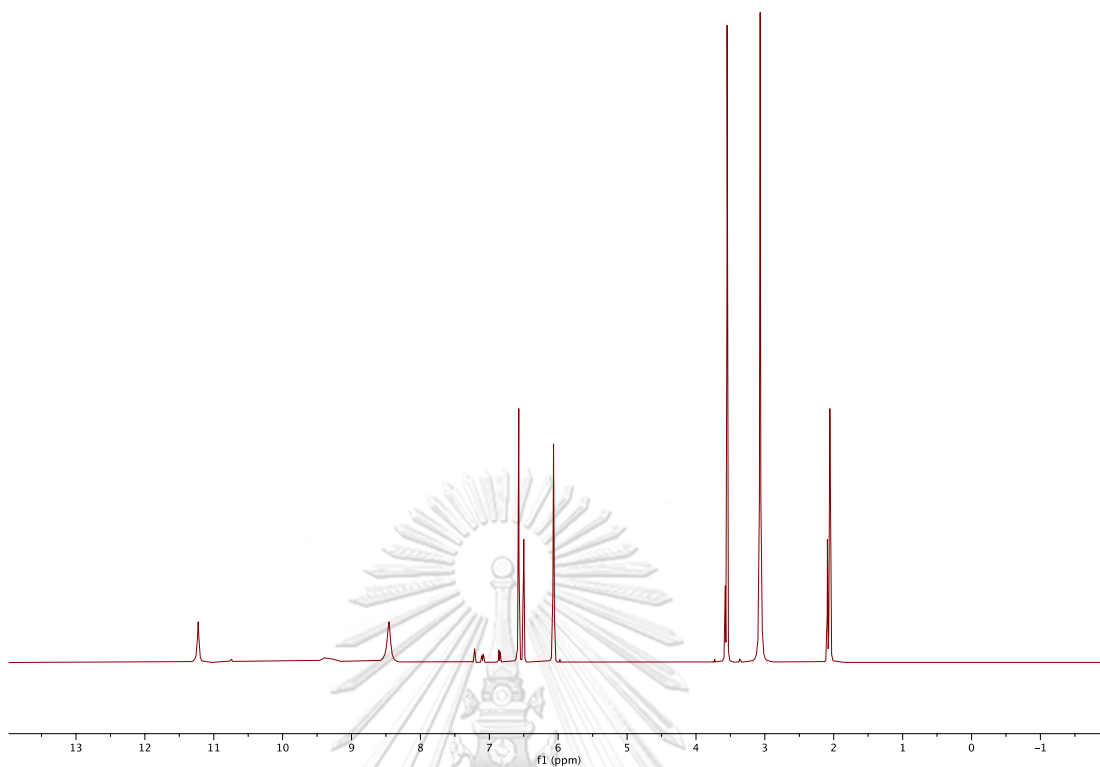


Figure A.16.1 ^1H NMR (400 MHz, acetone- d_6) spectrum of compound **16**

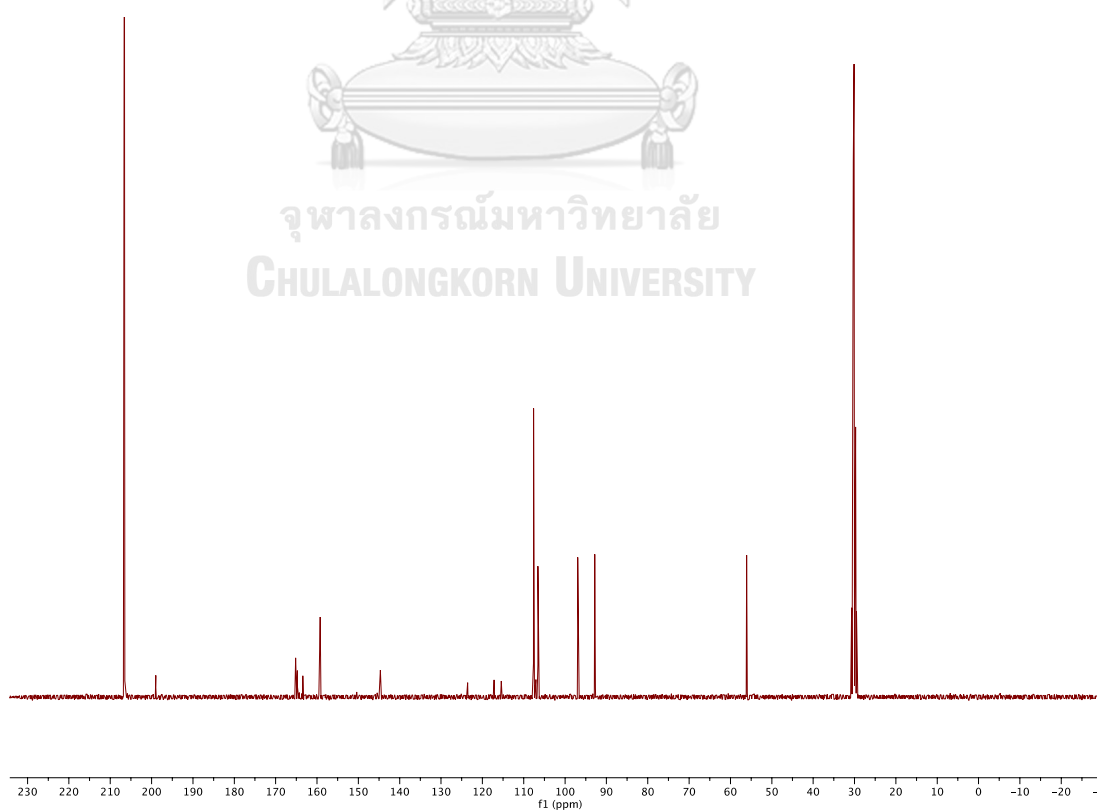


Figure A.16.2 ^{13}C NMR (100 MHz, acetone- d_6) spectrum of compound **16**

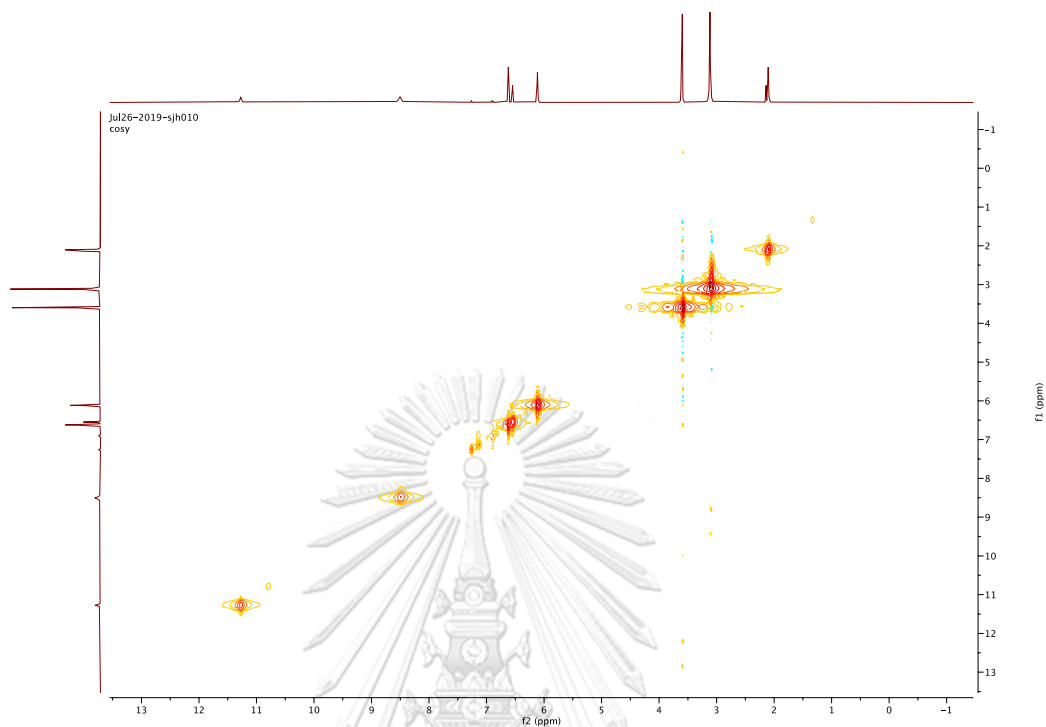


Figure A.16.3 ^1H - ^1H COSY spectrum (acetone- d_6) of compound 16

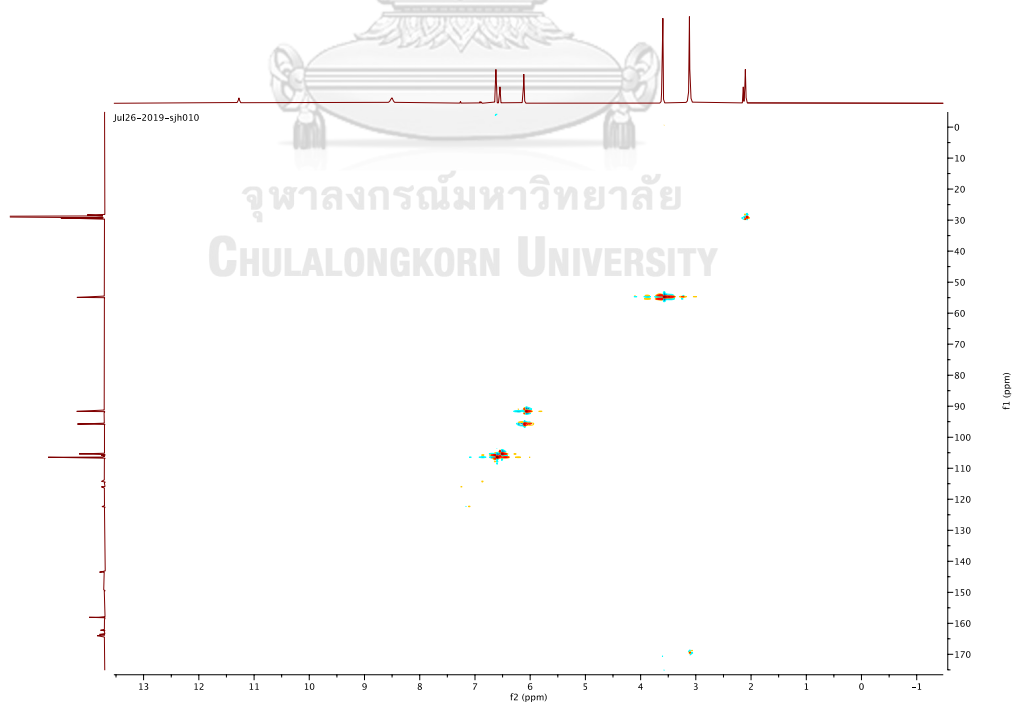


Figure A.16.4 HSQC spectrum (acetone- d_6) of compound 16

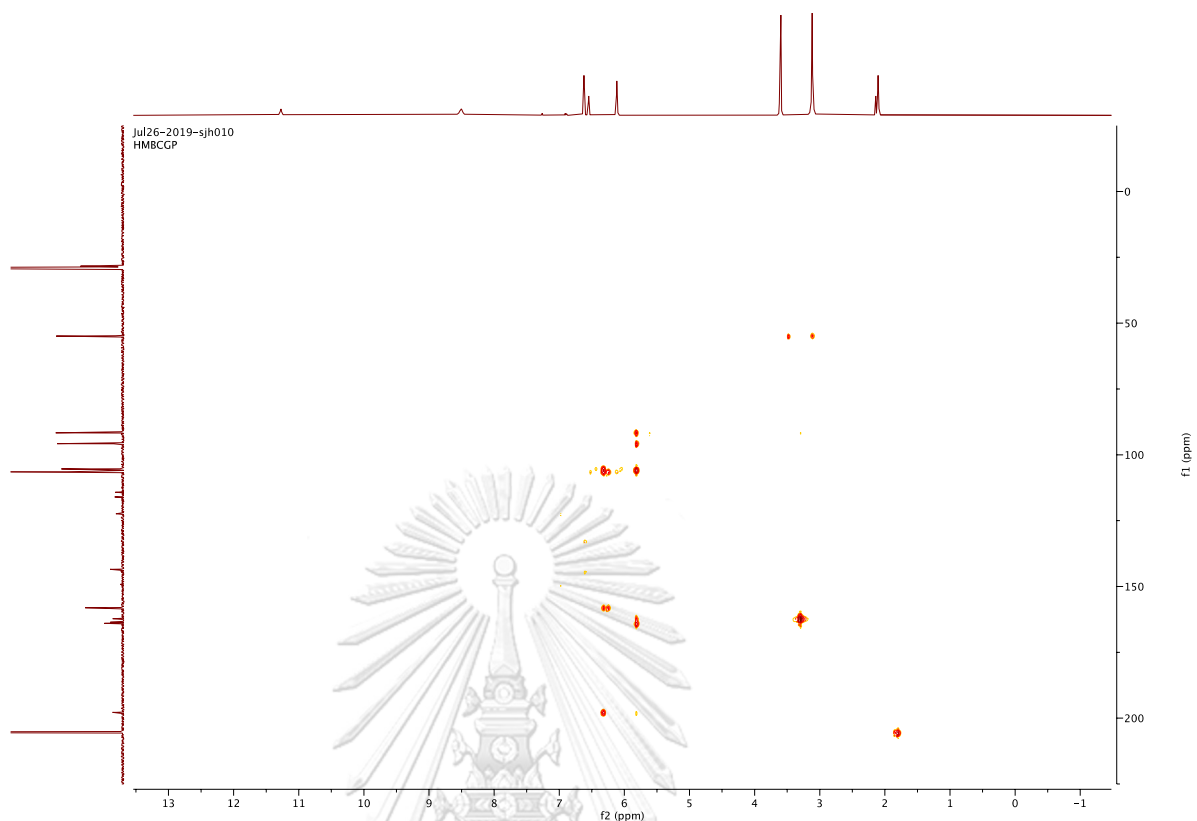


Figure A.16.5 HMBC spectrum (acetone-d₆) of compound 16

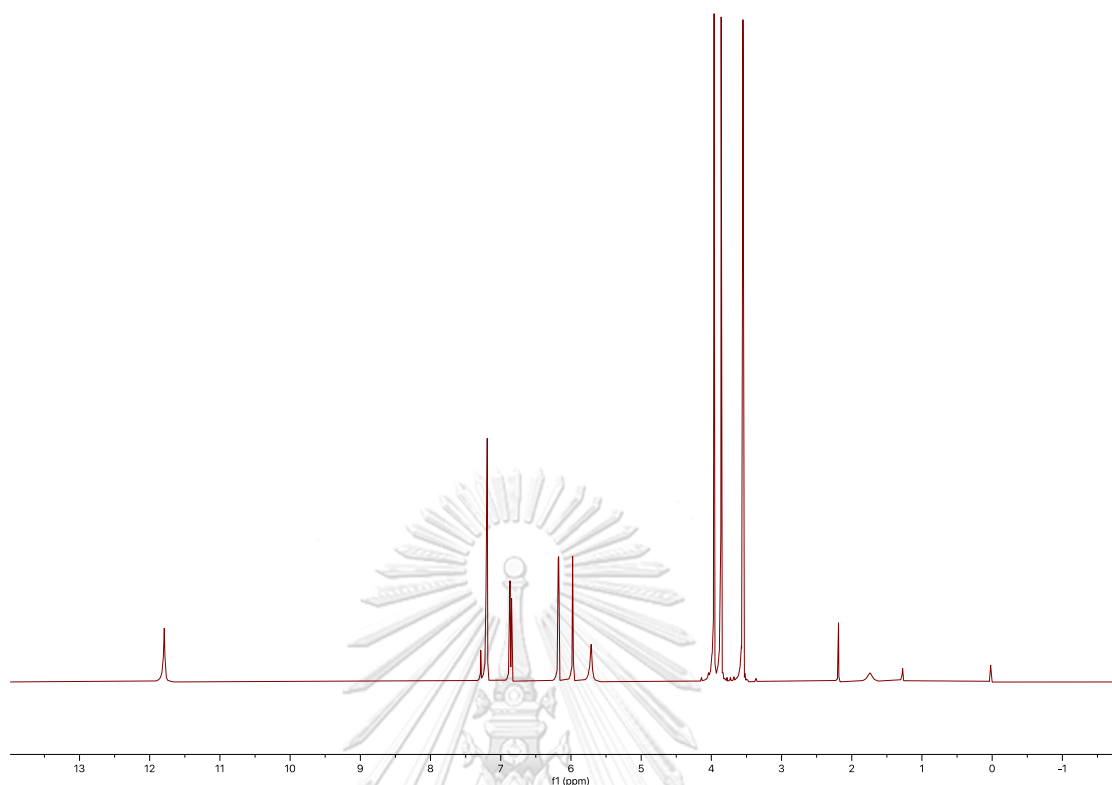


Figure A.17.1 ^1H NMR (400 MHz, CDCl_3) spectrum of compound 17

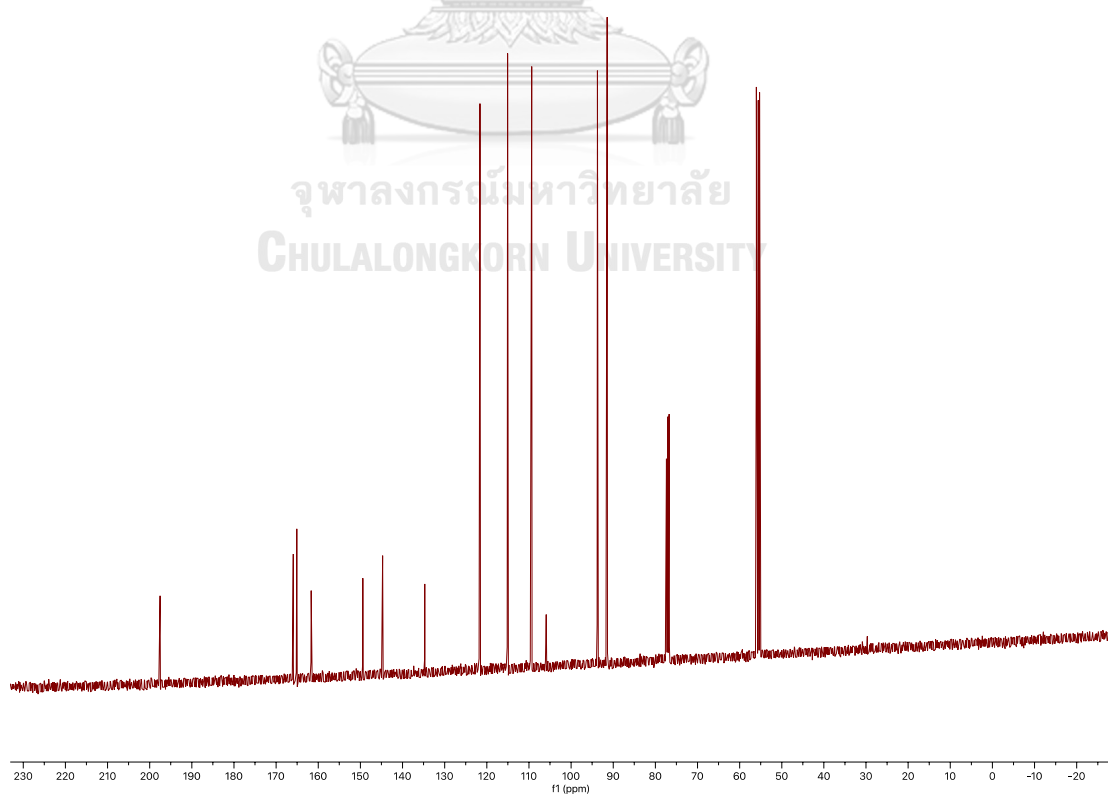


Figure A.17.2 ^{13}C NMR (100 MHz, CDCl_3) spectrum of compound 17

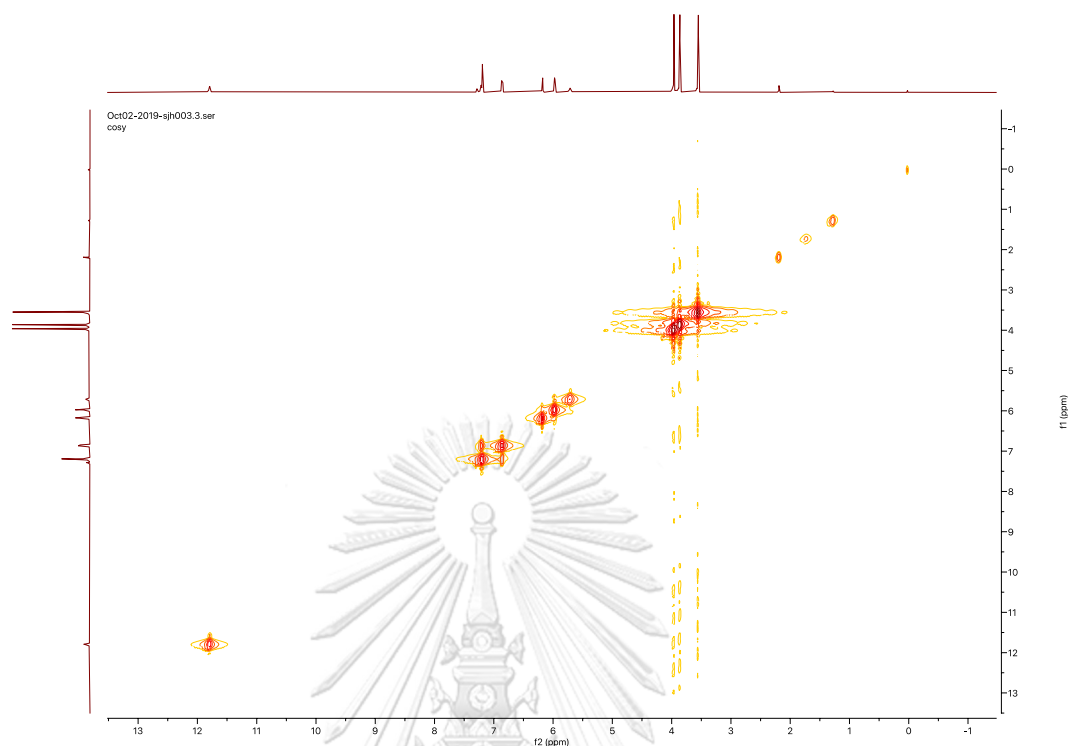


Figure A.17.3 ^1H - ^1H COSY spectrum (CDCl_3) of compound 17

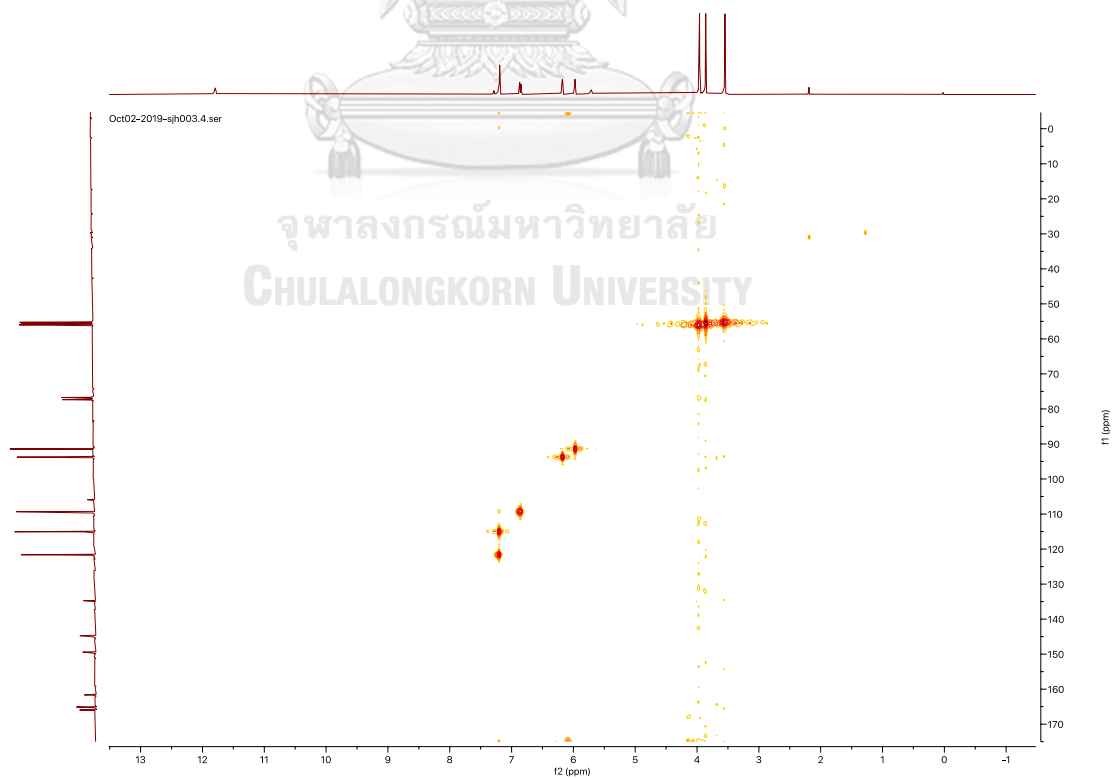


Figure A.17.4 HSQC spectrum (CDCl_3) of compound 17

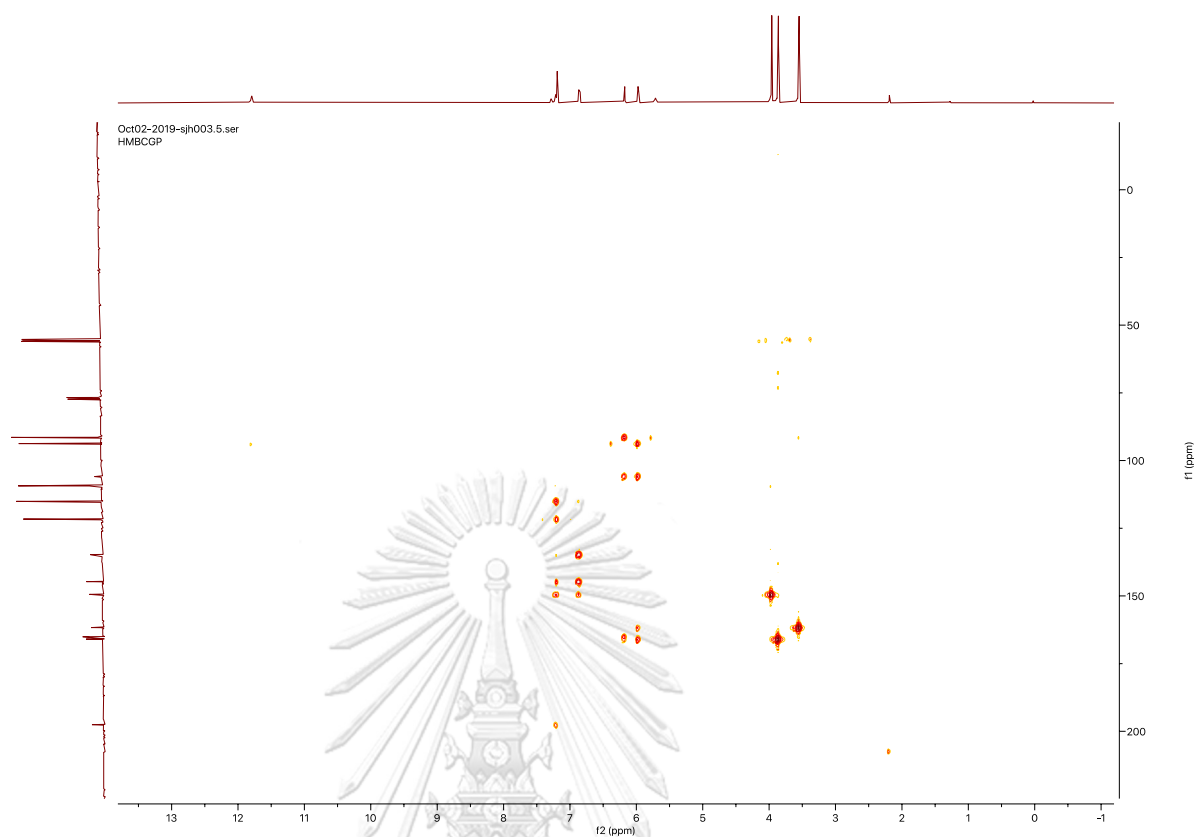


Figure A.17.5 HMBC spectrum (CDCl_3) of compound 17

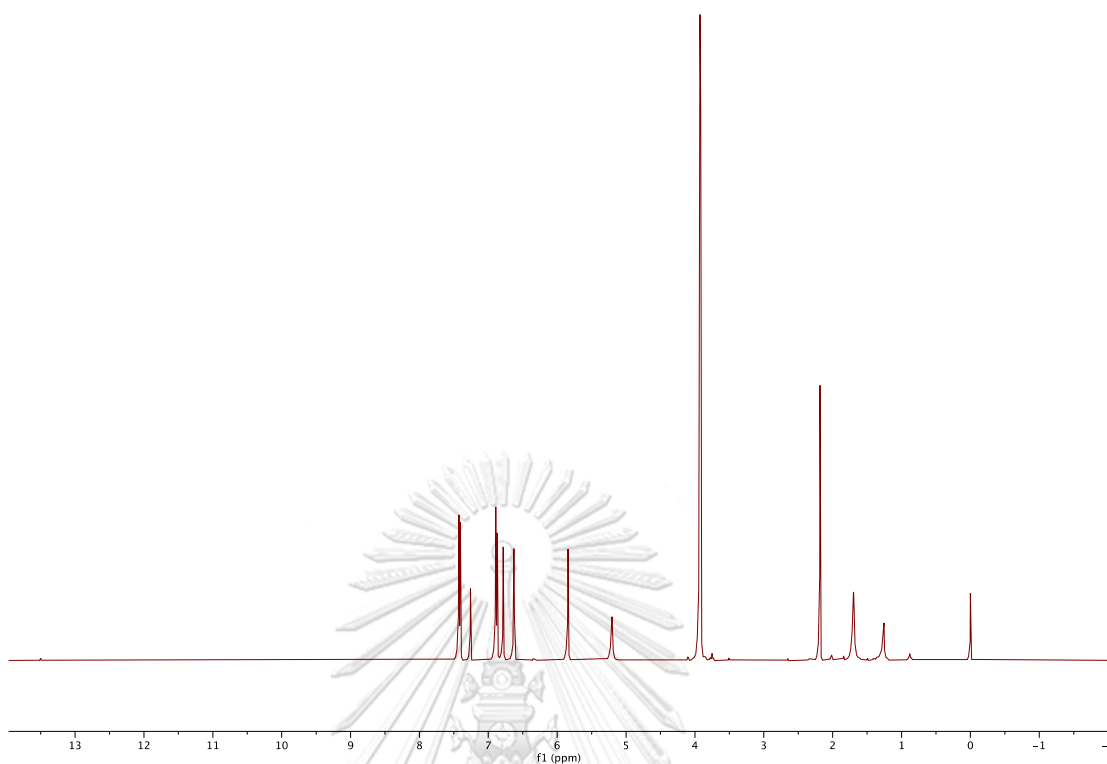


Figure A.18.1 ^1H NMR (400 MHz, CDCl_3) spectrum of compound 18

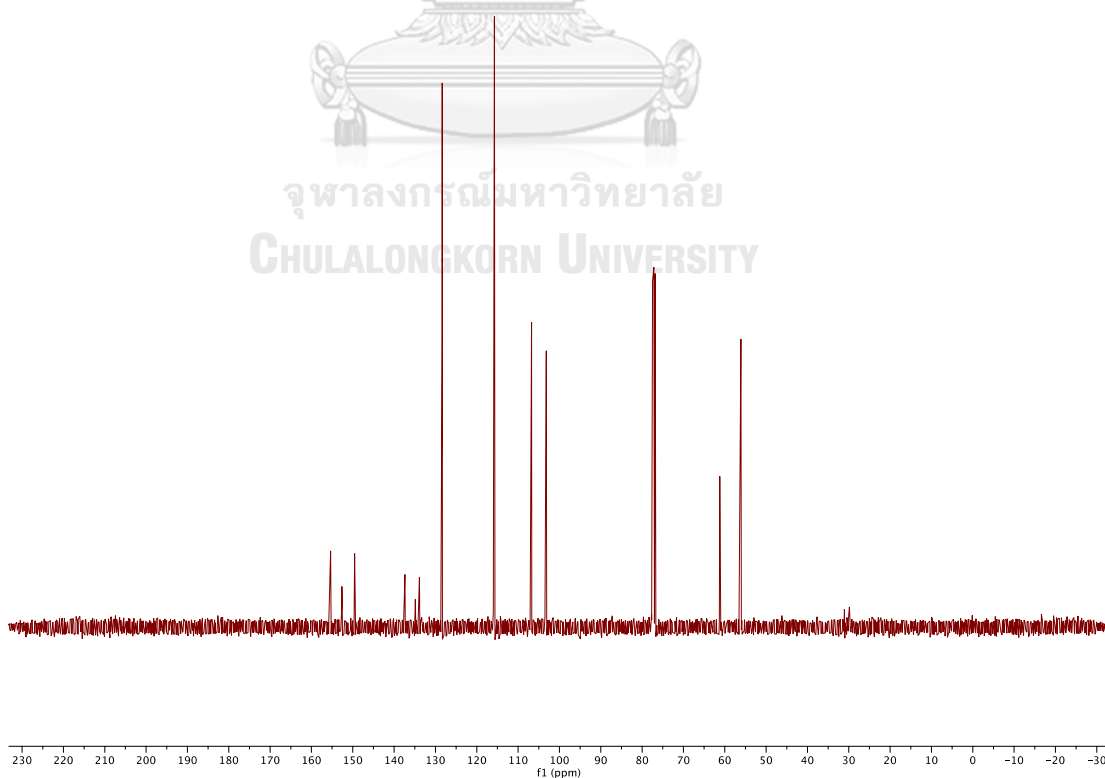


Figure A.18.2 ^{13}C NMR (100 MHz, CDCl_3) spectrum of compound 18

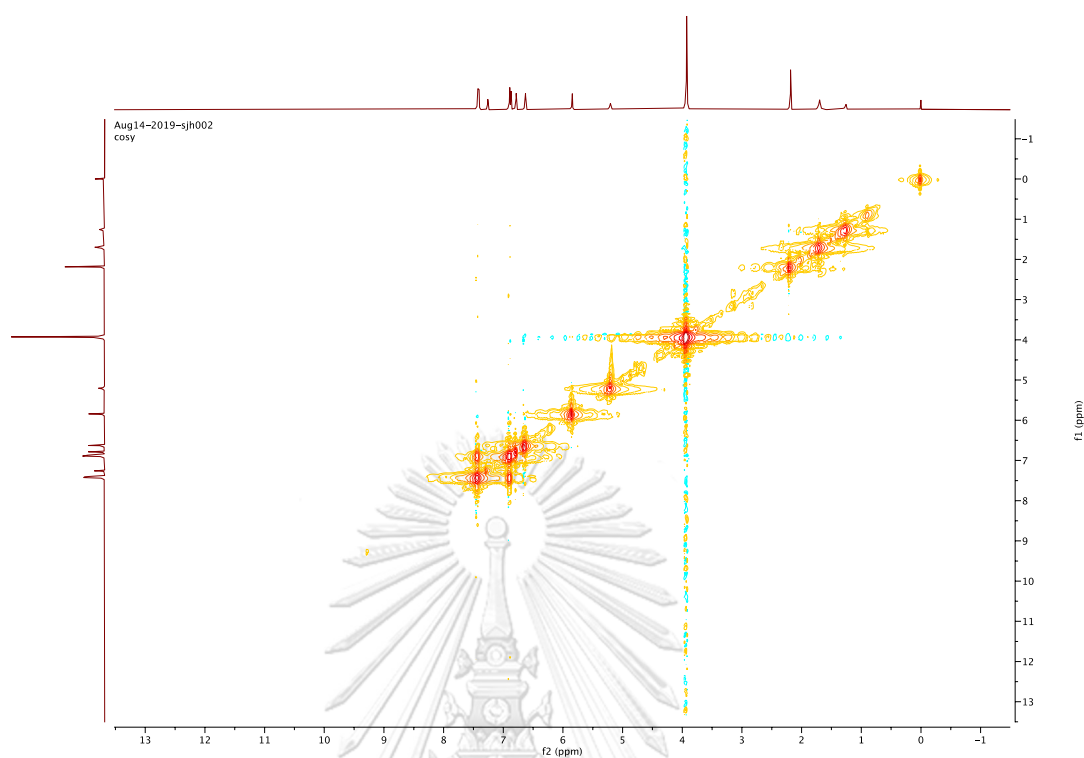


Figure A.18.3 ^1H - ^1H COSY spectrum (CDCl_3) of compound **18**

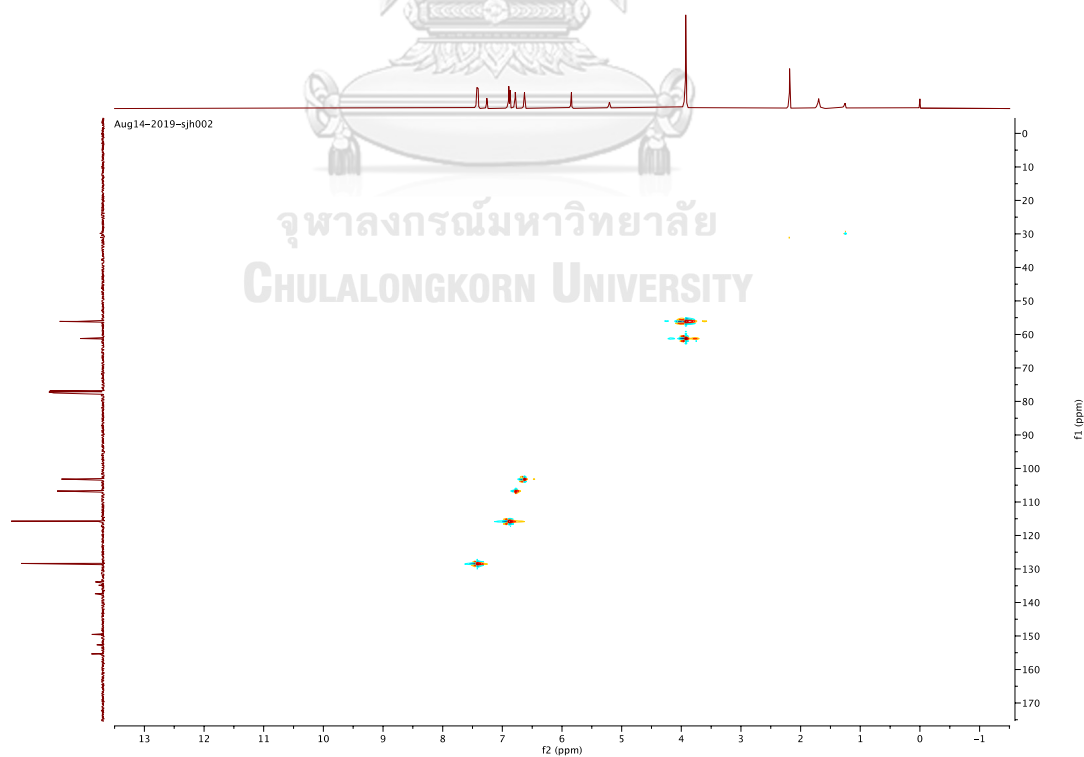


Figure A.18.4 HSQC spectrum (CDCl_3) of compound **18**

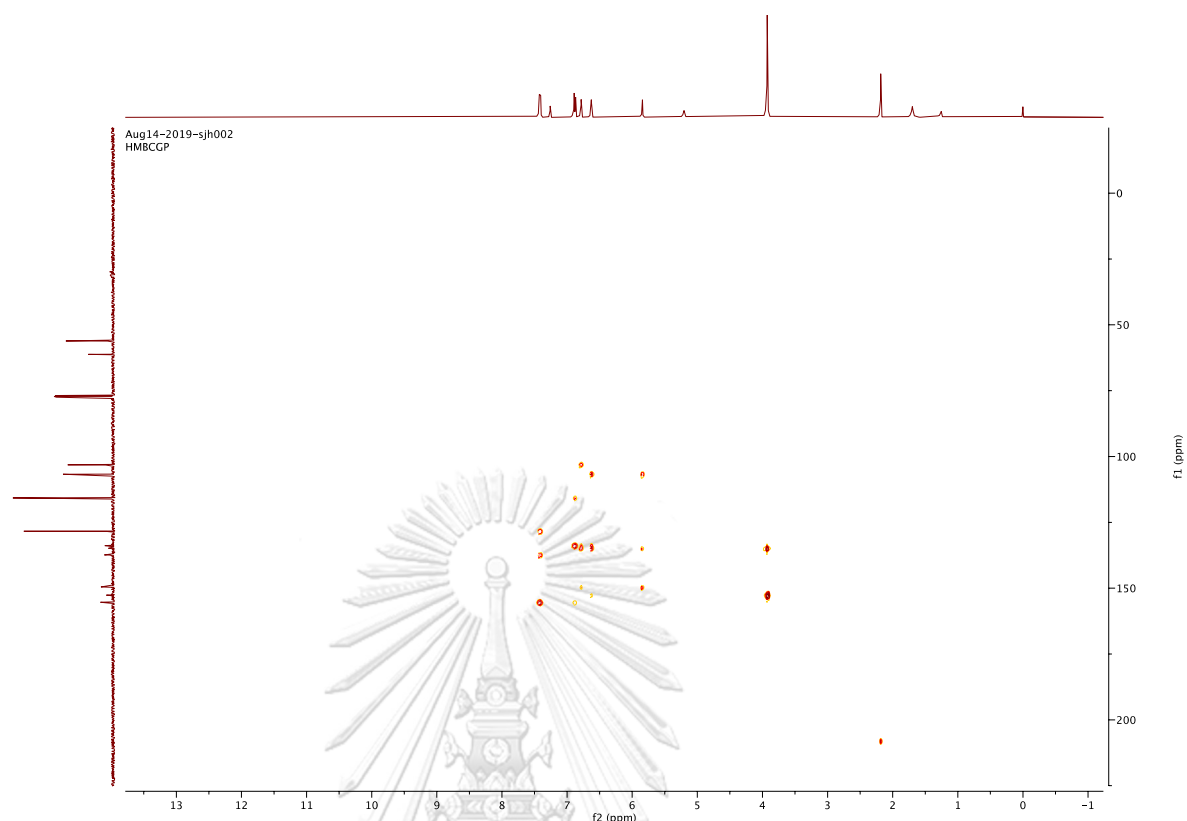


Figure A.18.5 HMBC spectrum (CDCl_3) of compound **18**

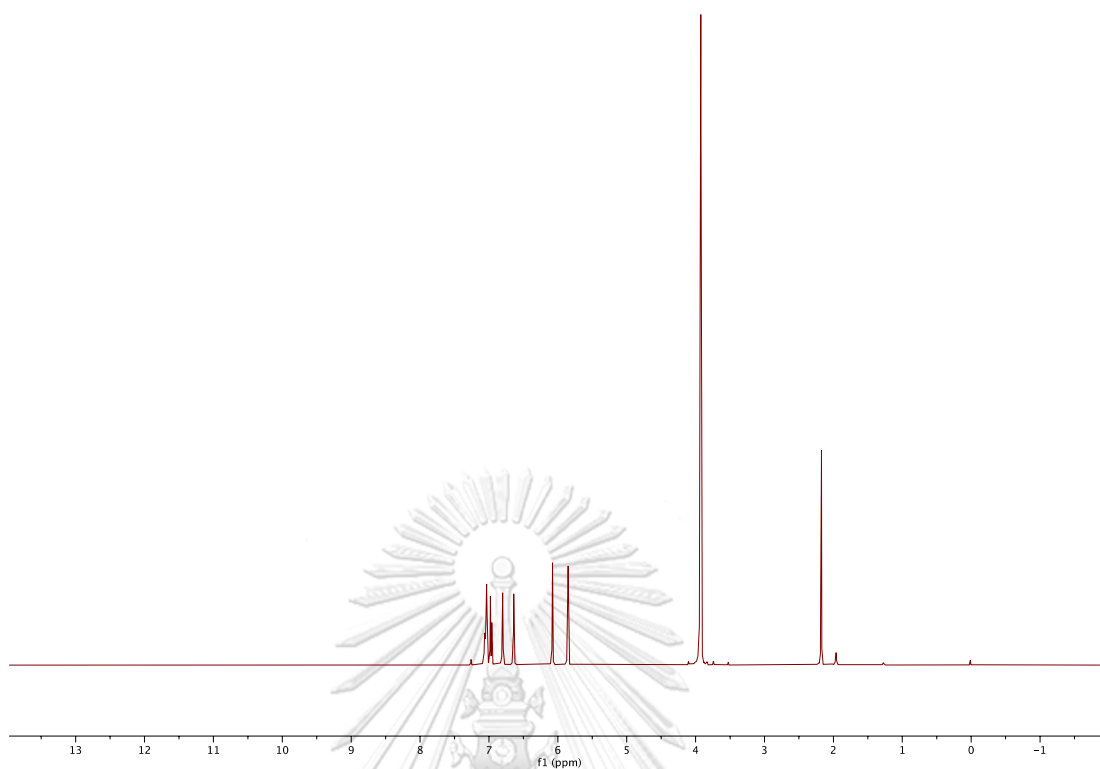


Figure A.19.1 ^1H NMR (400 MHz, CDCl_3) spectrum of compound **19**

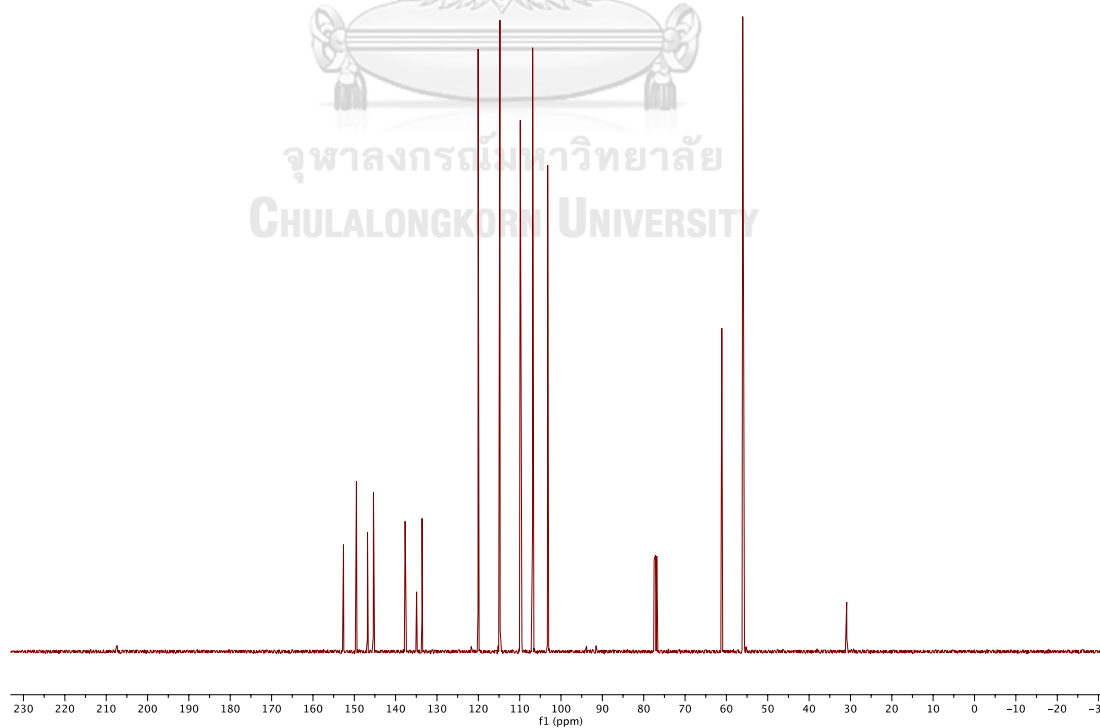


Figure A.19.2 ^{13}C NMR (100 MHz, CDCl_3) spectrum of compound **19**

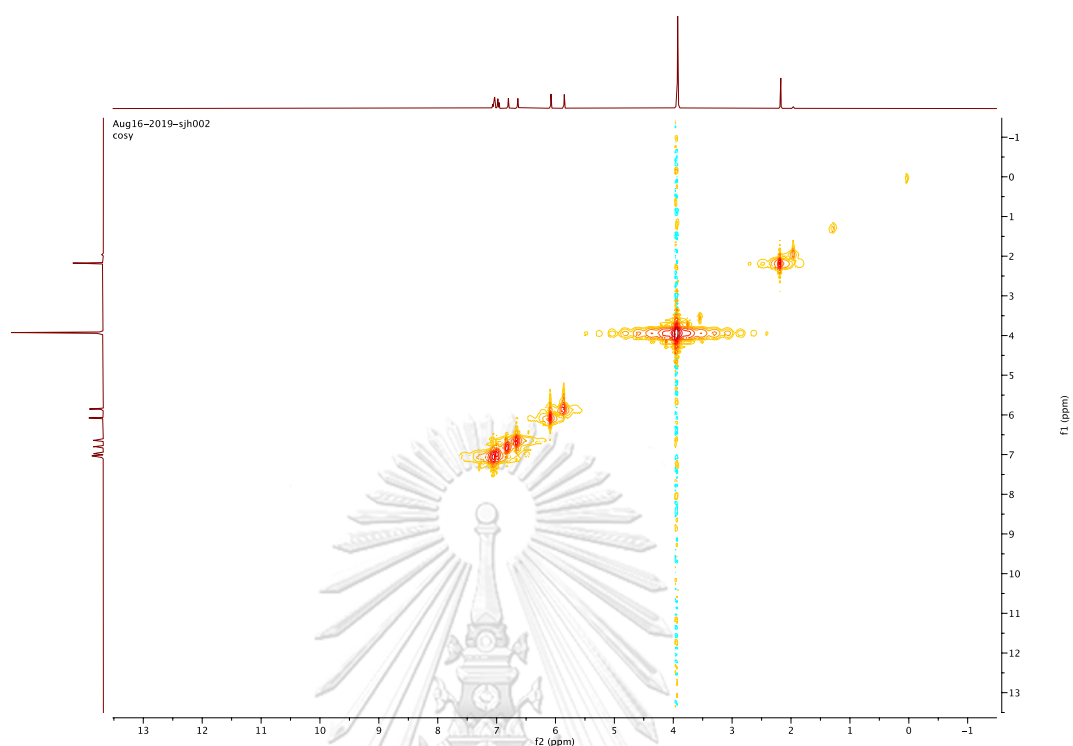


Figure A.19.3 ^1H - ^1H COSY spectrum (CDCl_3) of compound 19

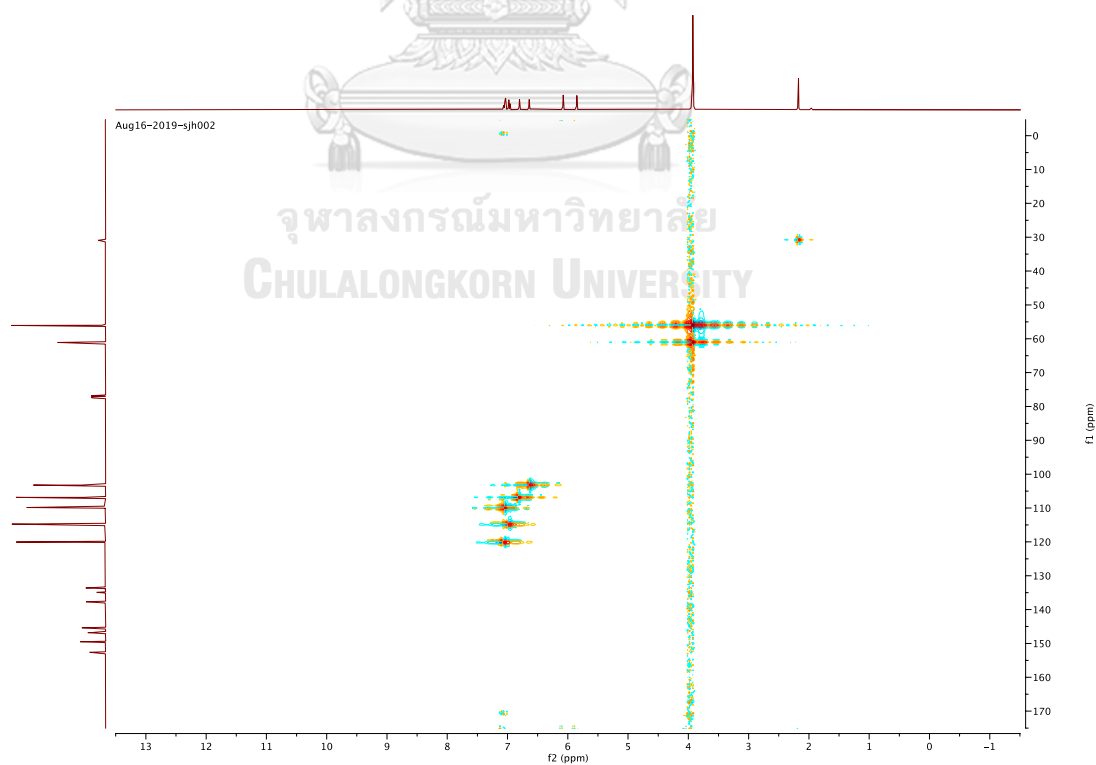


Figure A.19.5 HSQC spectrum (CDCl_3) of compound 19

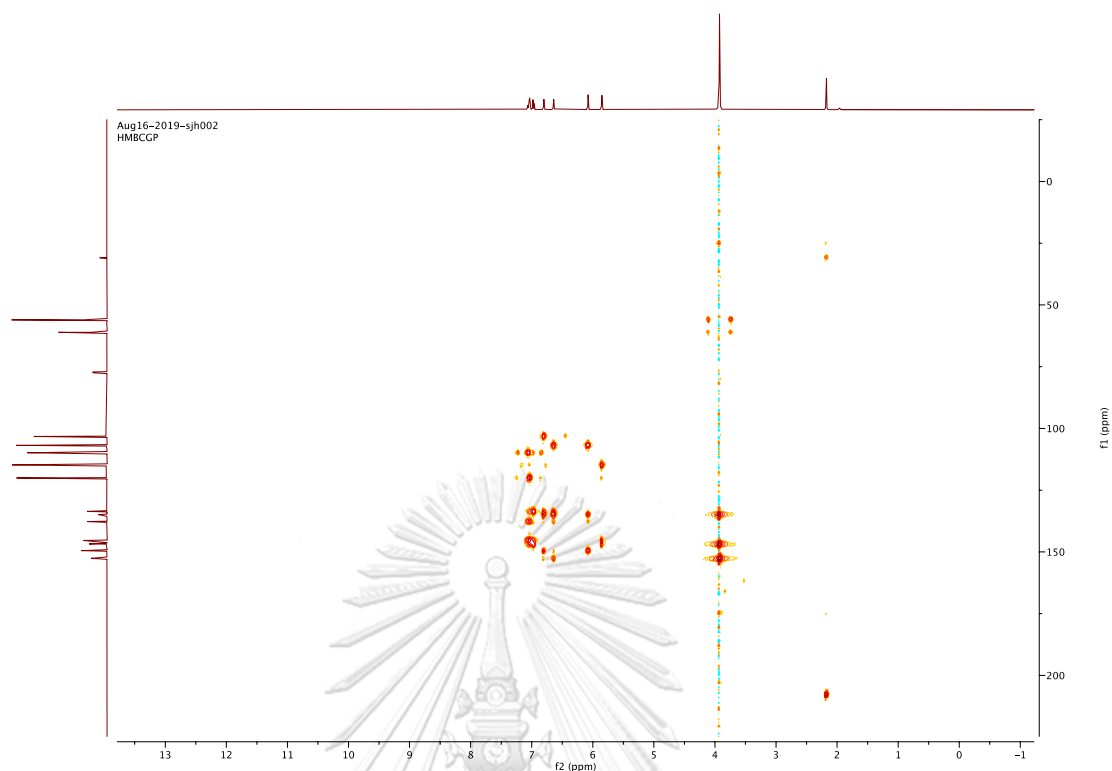


Figure A.19.5 HMBC spectrum (CDCl_3) of compound **19**

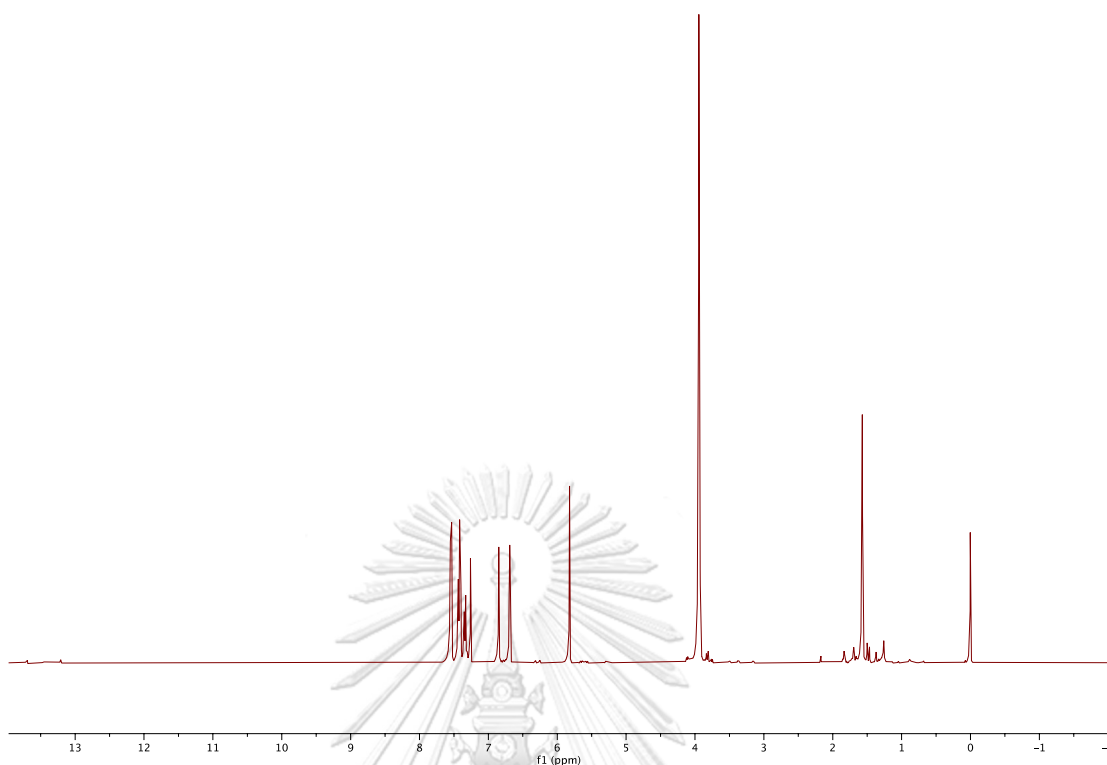


Figure A.20.1 ^1H NMR (400 MHz, CDCl_3) spectrum of compound 20

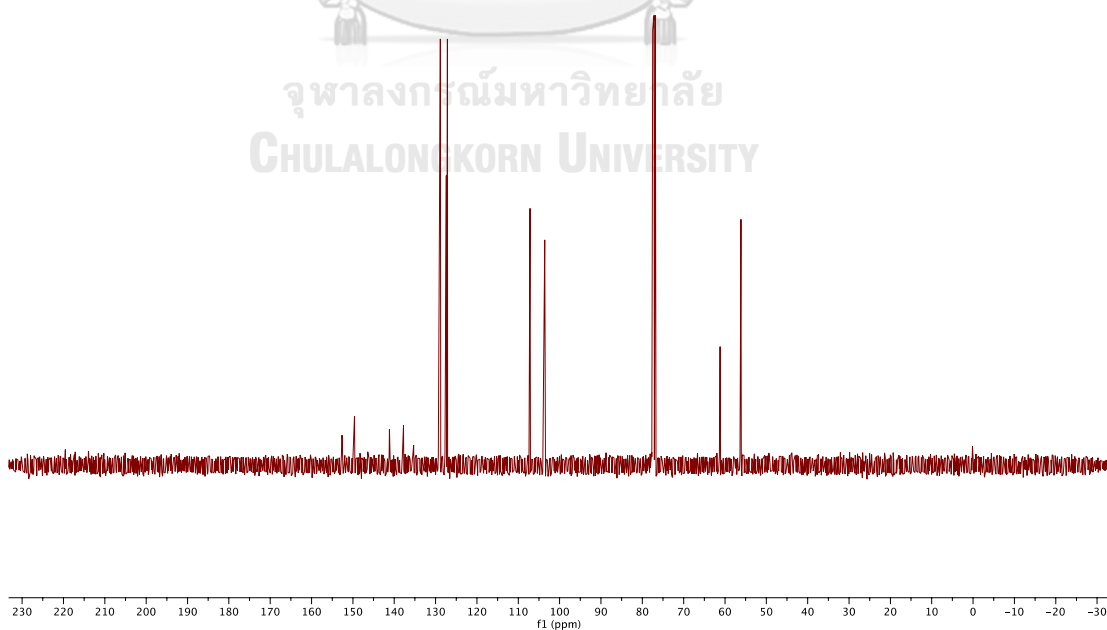


Figure A.20.2 ^{13}C NMR (100 MHz, CDCl_3) spectrum of compound 20

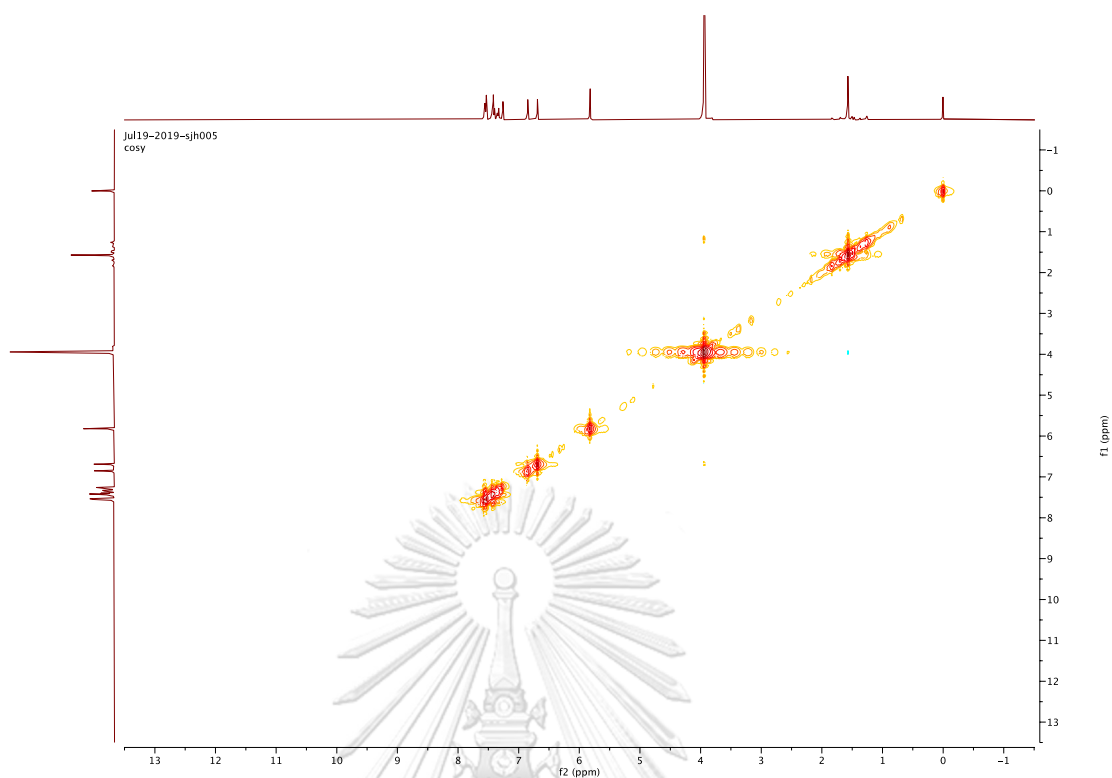


Figure A.20.3 ^1H - ^1H COSY spectrum (CDCl_3) of compound 20

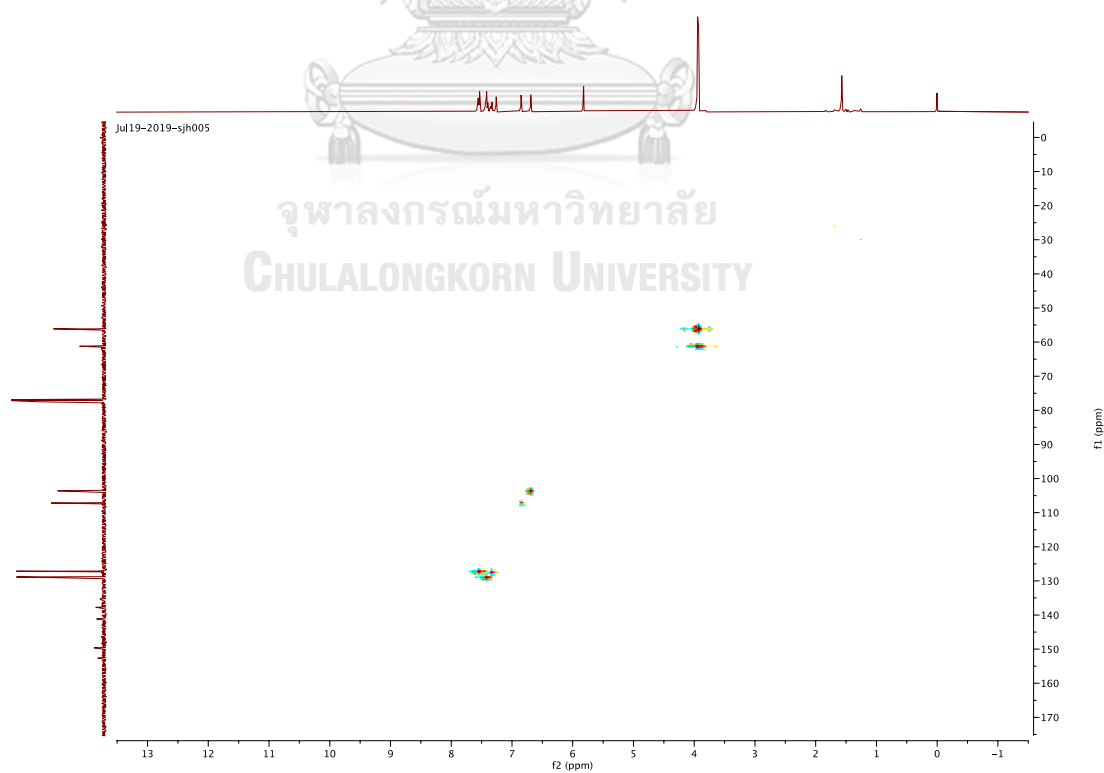


Figure A.20.4 HSQC spectrum (CDCl_3) of compound 20

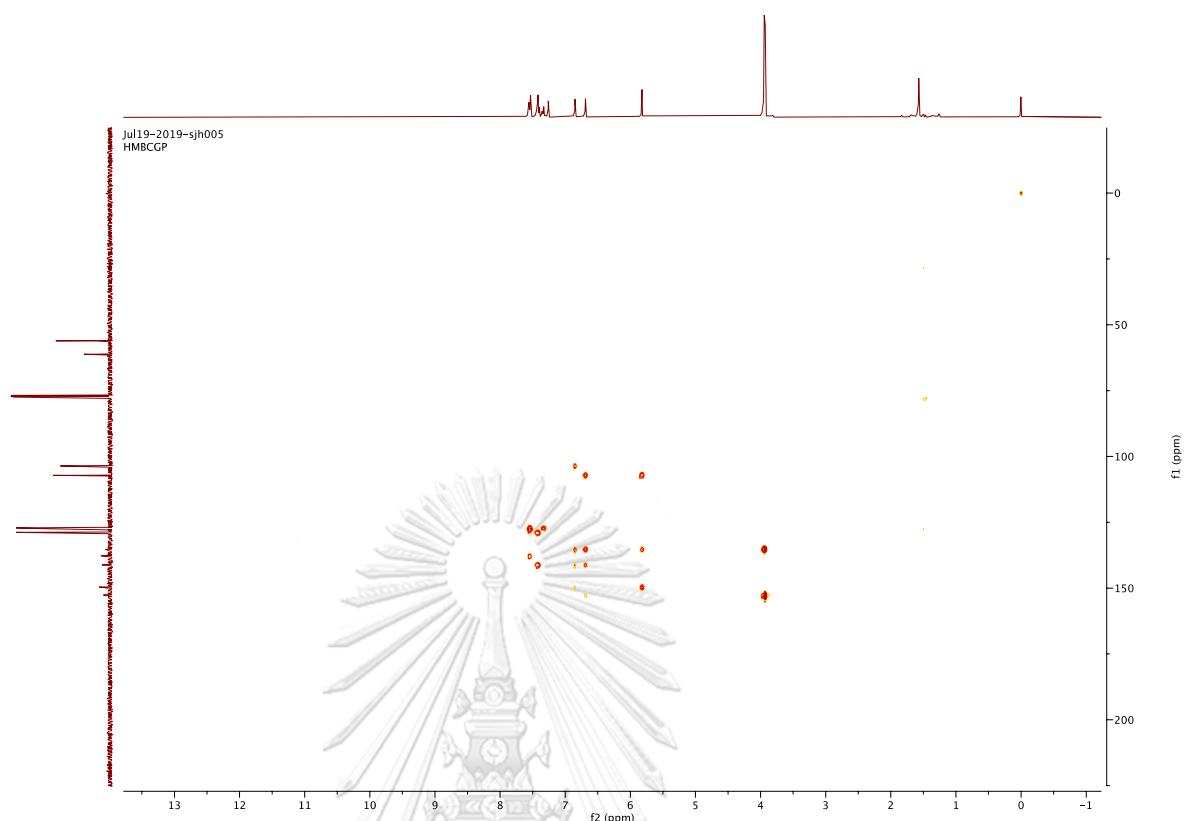


Figure A.20.5 HMBC spectrum (CDCl_3) of compound 20

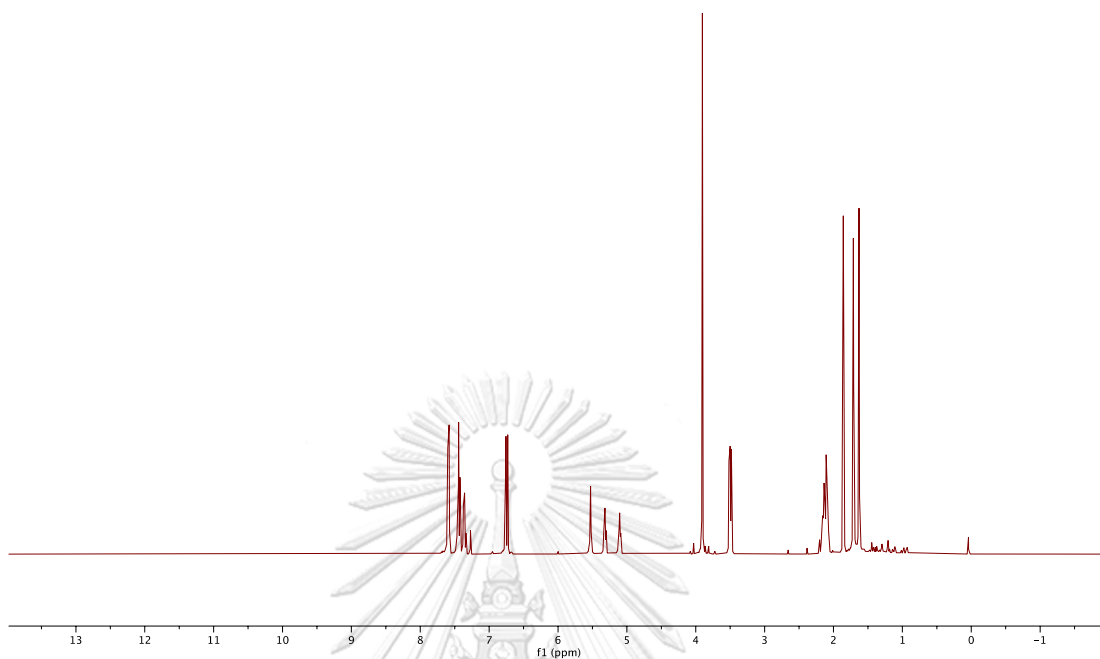


Figure A.21.1 ^1H NMR (400 MHz, CDCl_3) spectrum of compound 21

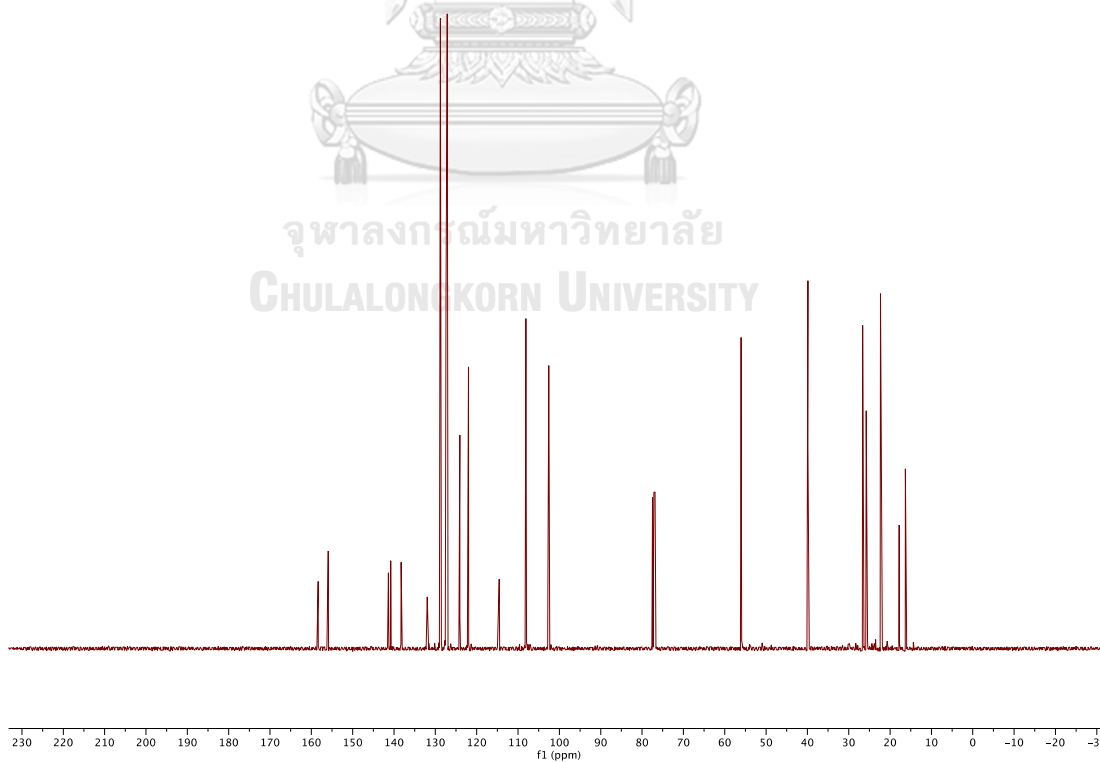


Figure A.21.2 ^{13}C NMR (100 MHz, CDCl_3) spectrum of compound 21

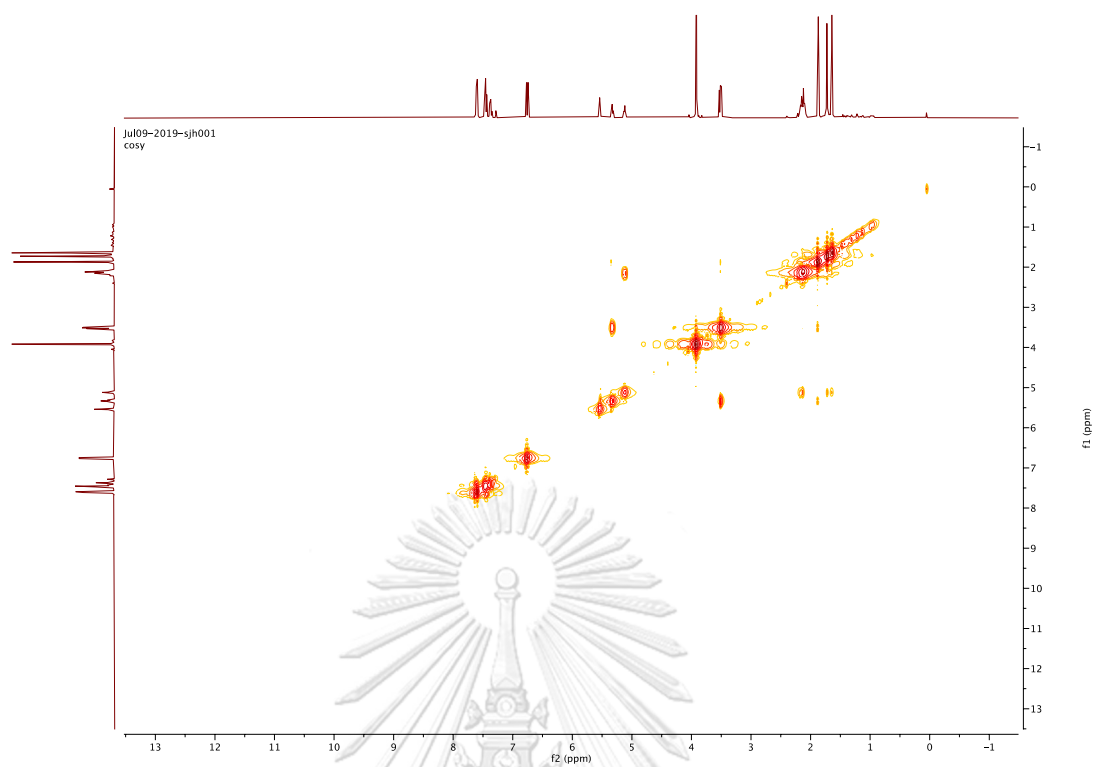


Figure A.21.3 ^1H - ^1H COSY spectrum (CDCl_3) of compound 21

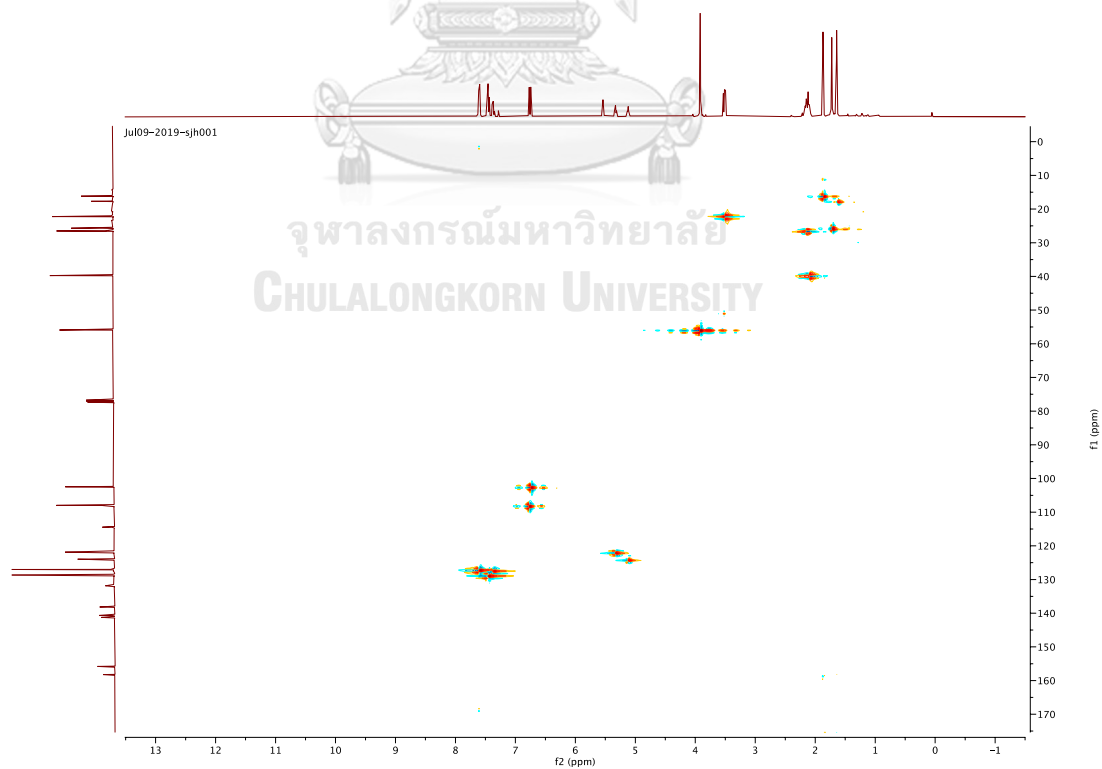


Figure A.21.4 HSQC spectrum (CDCl_3) of compound 21

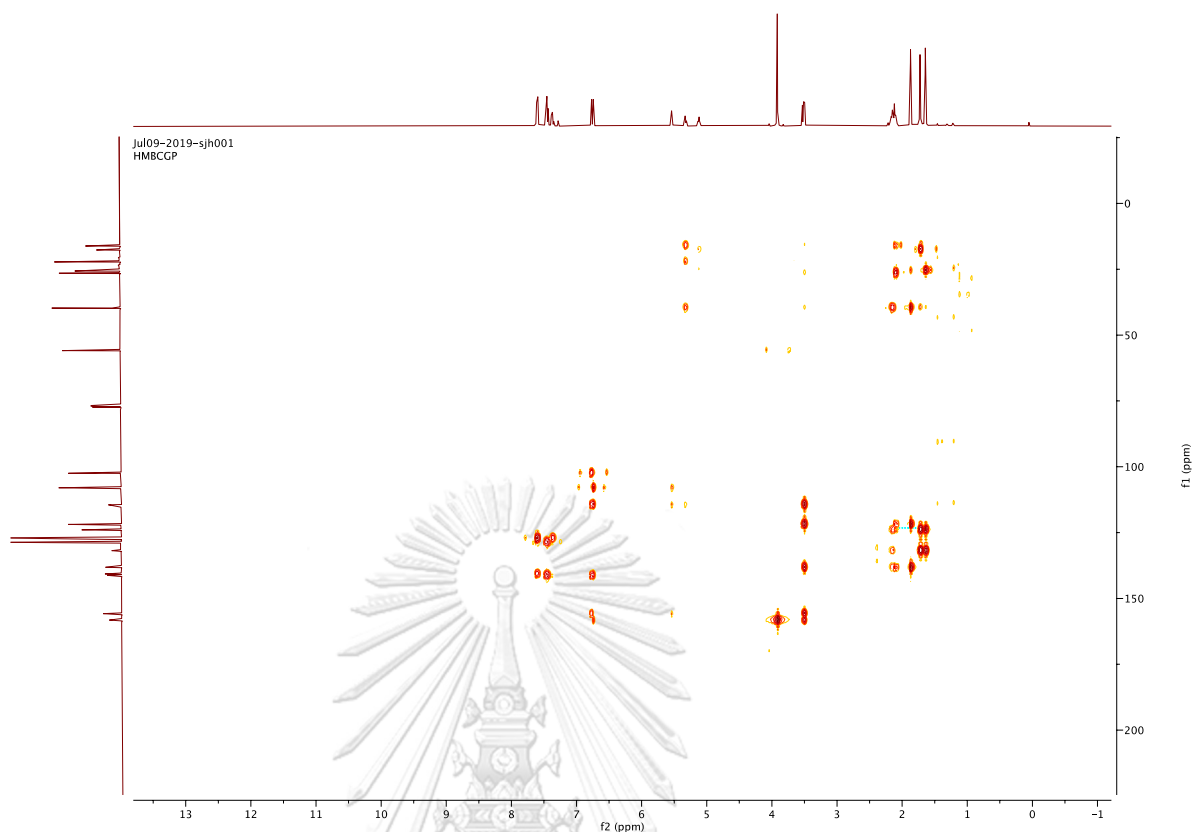


Figure A.21.5 HMBC spectrum (CDCl_3) of compound 21

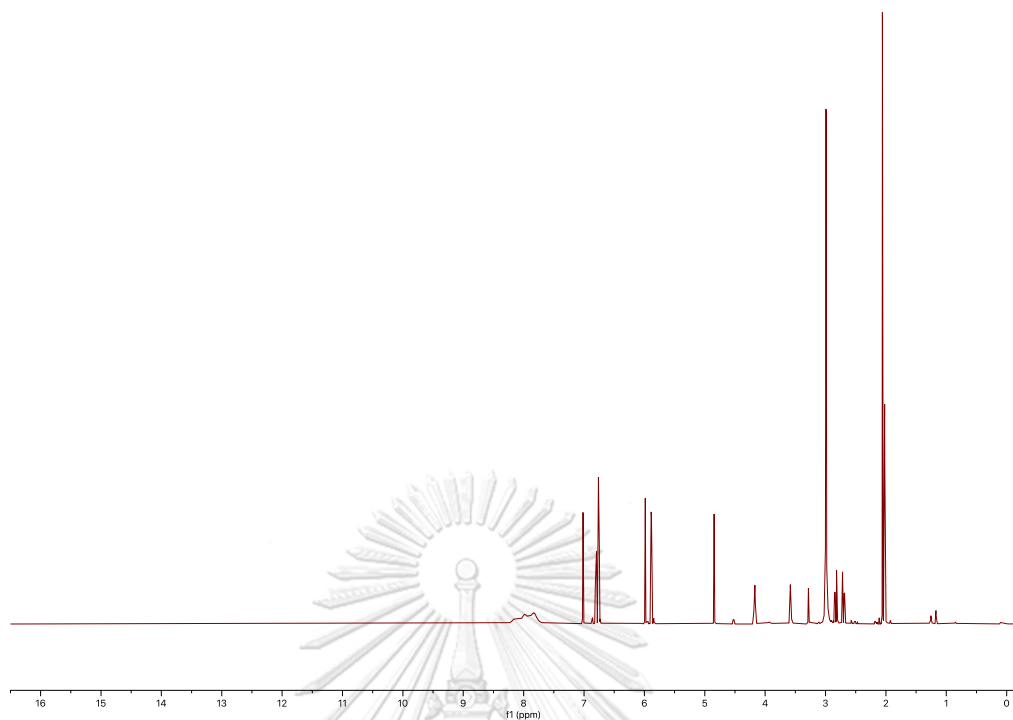


Figure A.22.1 ^1H NMR (400 MHz, acetone- d_6) spectrum of compound **22**

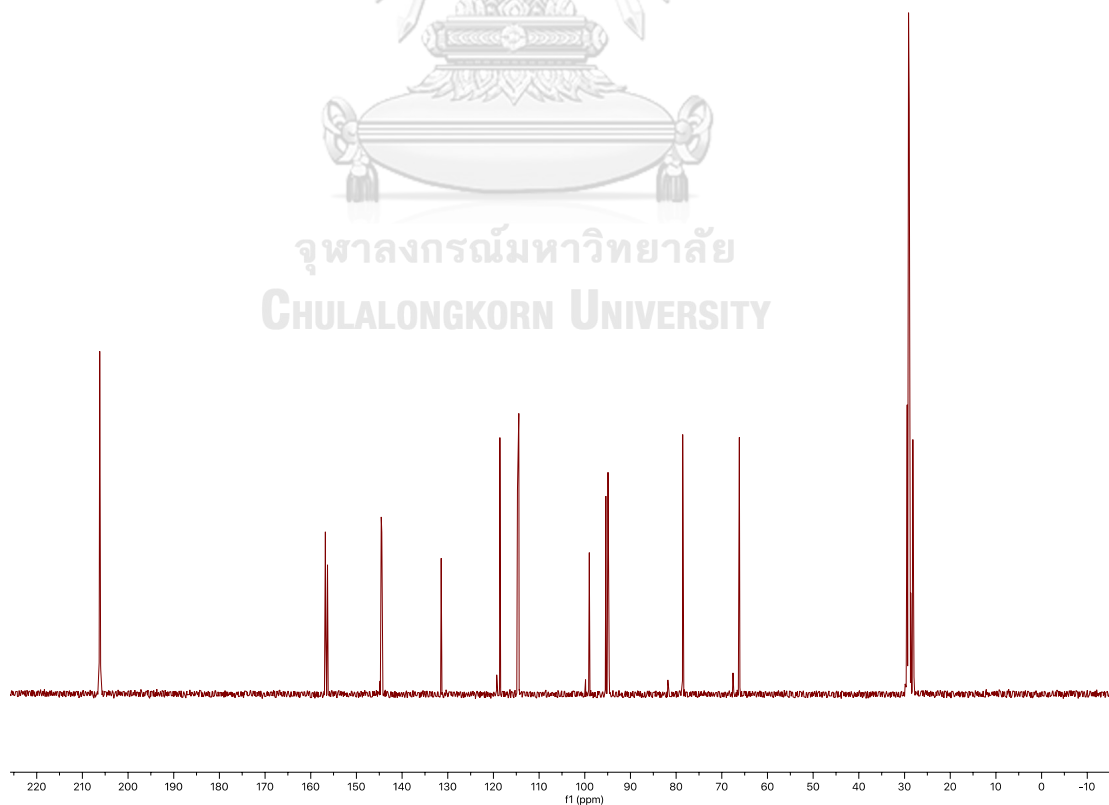


Figure A.22.12 ^{13}C NMR (100 MHz, acetone- d_6) spectrum of compound **22**

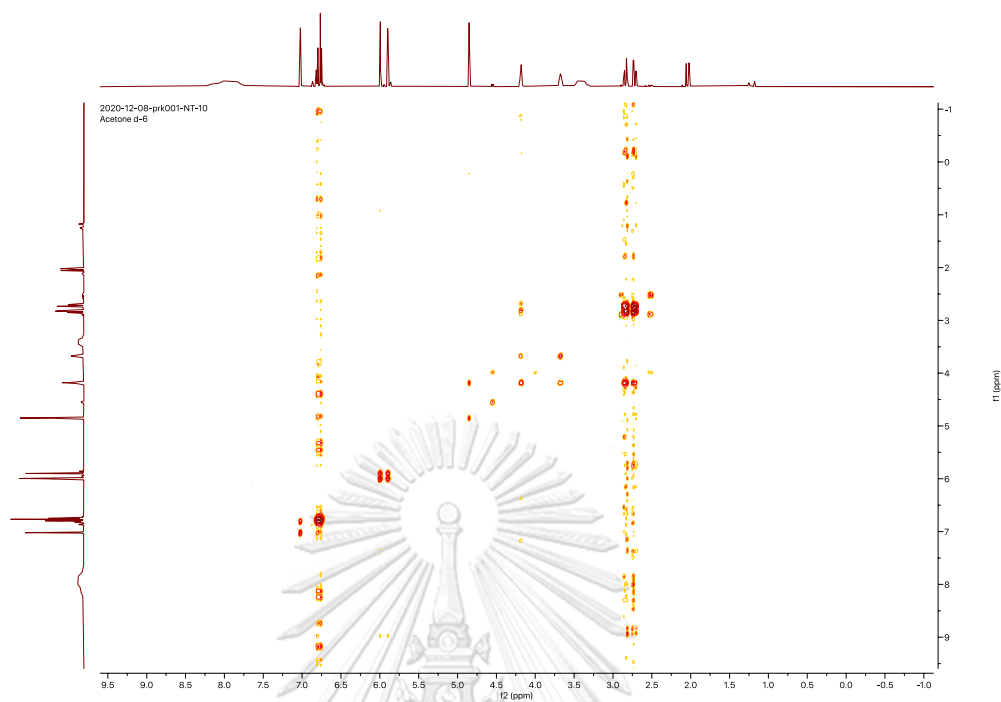


Figure A.22.3 ^1H - ^1H COSY spectrum (acetone-d₆) of compound 22

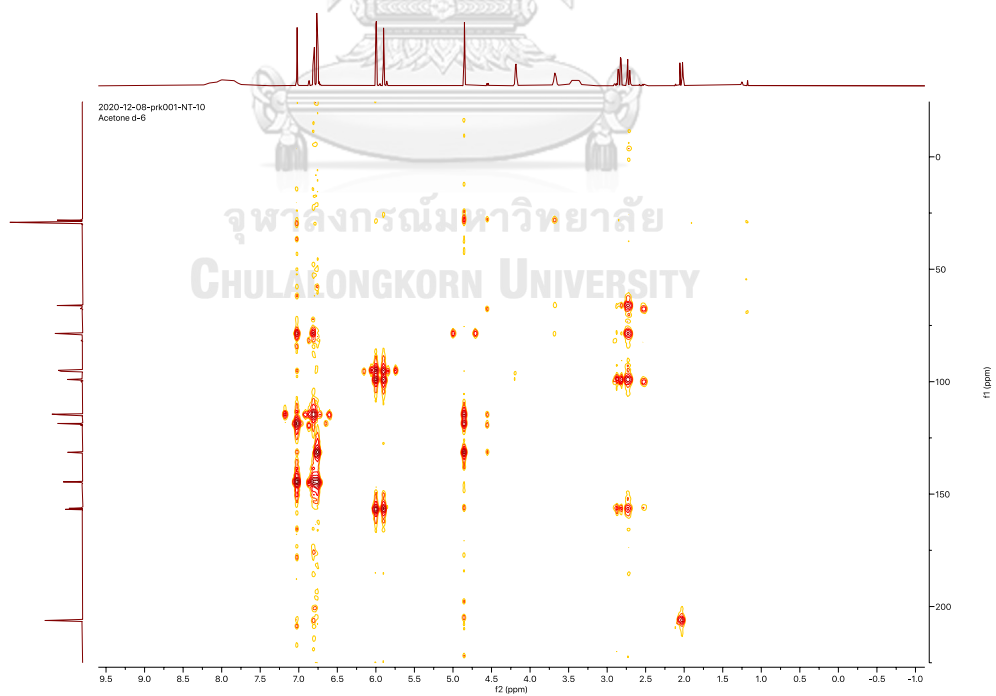


Figure A.22.4 HSQC spectrum (acetone-d₆) of compound 22

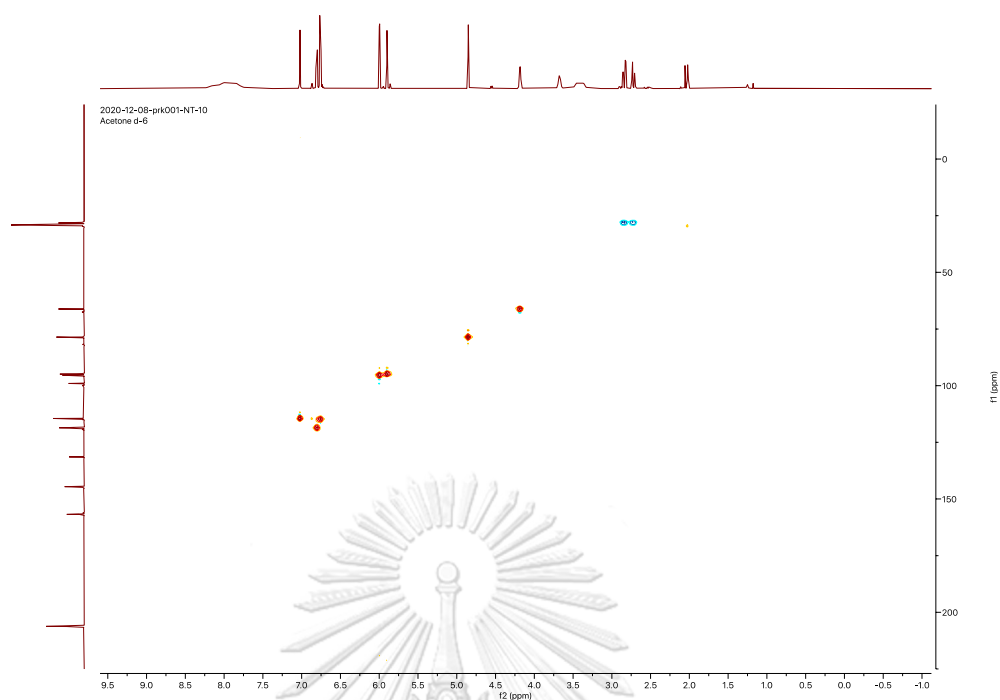


Figure A.22.5 HMBC spectrum (acetone-d₆) of compound 22

Generic Display Report

Analysis Info

Analysis Name D:\Data\Data Service\191217\KP-MGS-8_RA8_01_3555.d
Method nv_pos_6min_profile_wguardcol_50-1500_191021.m
Sample Name KP-MGS-8
Comment

Acquisition Date 12/17/2019 3:28:08 PM

Operator CU.
Instrument micrOTOF-Q II

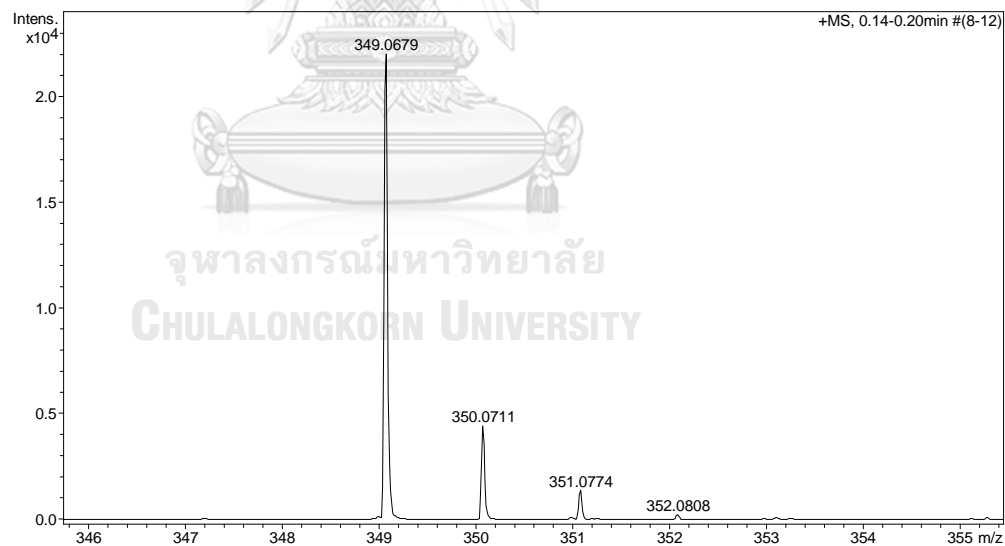
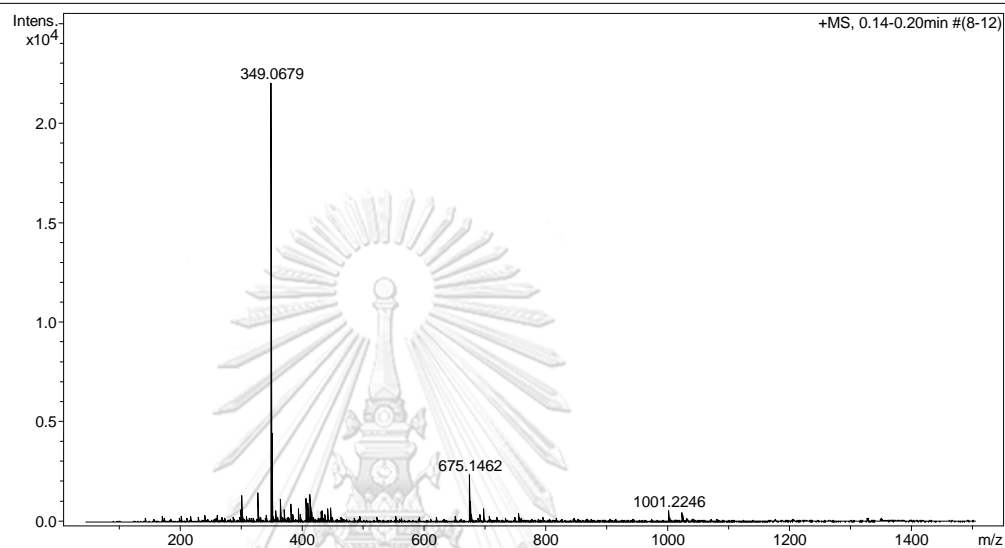


Figure A.20 HRESIMS Mass spectrum of compound 1

Generic Display Report

Analysis Info

Analysis Name D:\Data\Data Service\191217\KP-MGS-16_RB2_01_3557.d
Method nv_pos_6min_profile_wguardcol_50-1500_191021.m
Sample Name KP-MGS-16
Comment

Acquisition Date 12/17/2019 3:41:02 PM

Operator CU.

Instrument micrOTOF-Q II

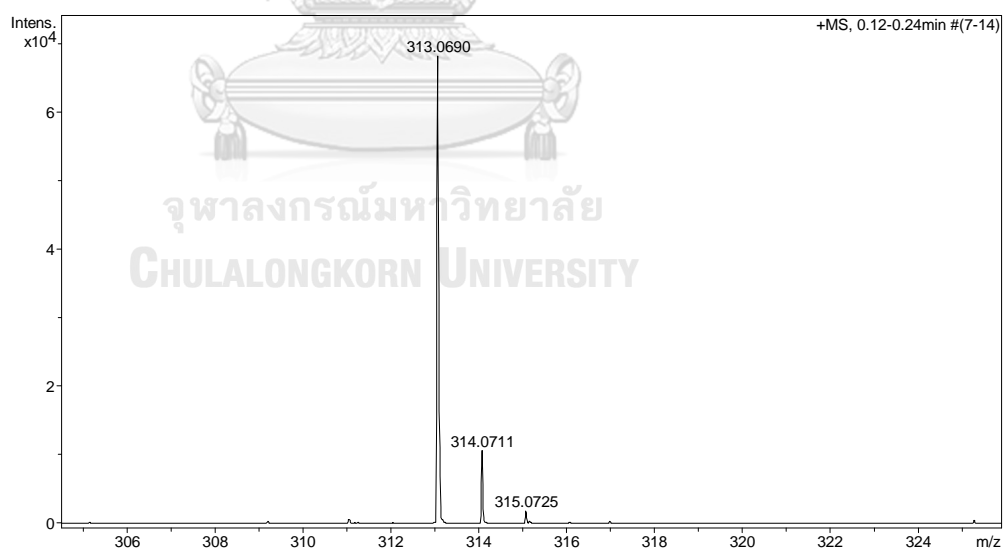
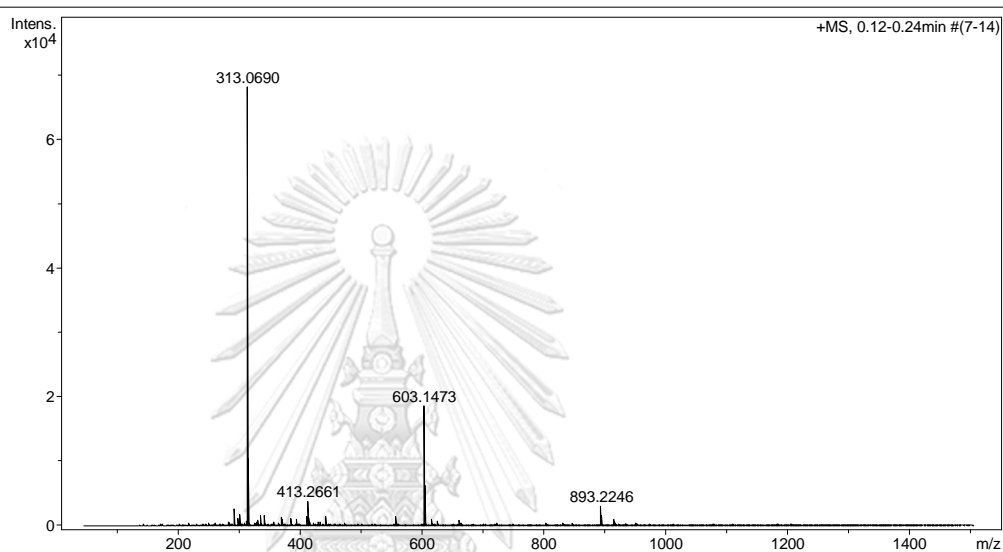


Figure A.22 HRESIMS Mass spectrum of compound 12

Generic Display Report

Analysis Info

Analysis Name D:\Data\Data Service\191217\KP-MGS-18_RB3_01_3558.d
Method nv_pos_6min_profile_wguardcol_50-1500_191021.m
Sample Name KP-MGS-18
Comment

Acquisition Date 12/17/2019 3:47:29 PM

Operator CU.
Instrument micrOTOF-Q II

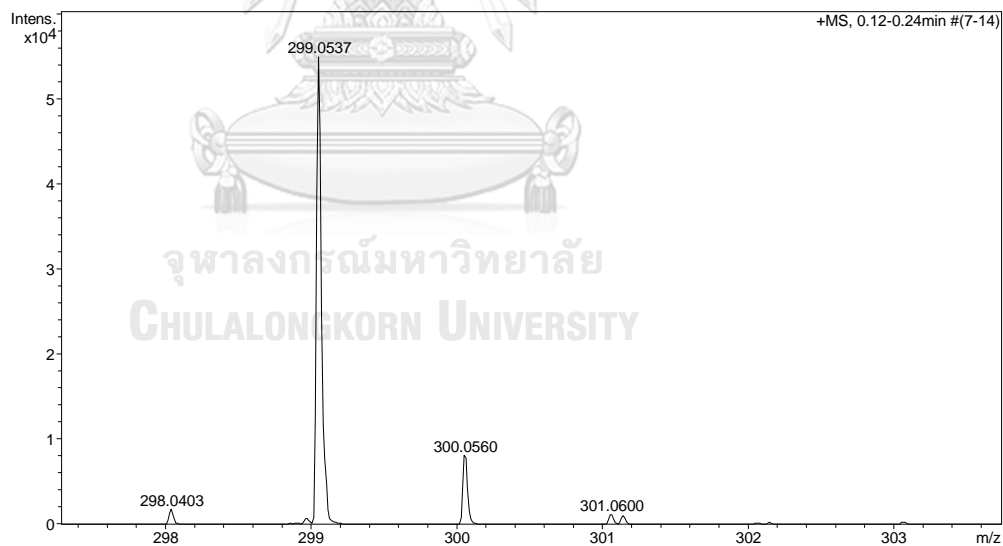
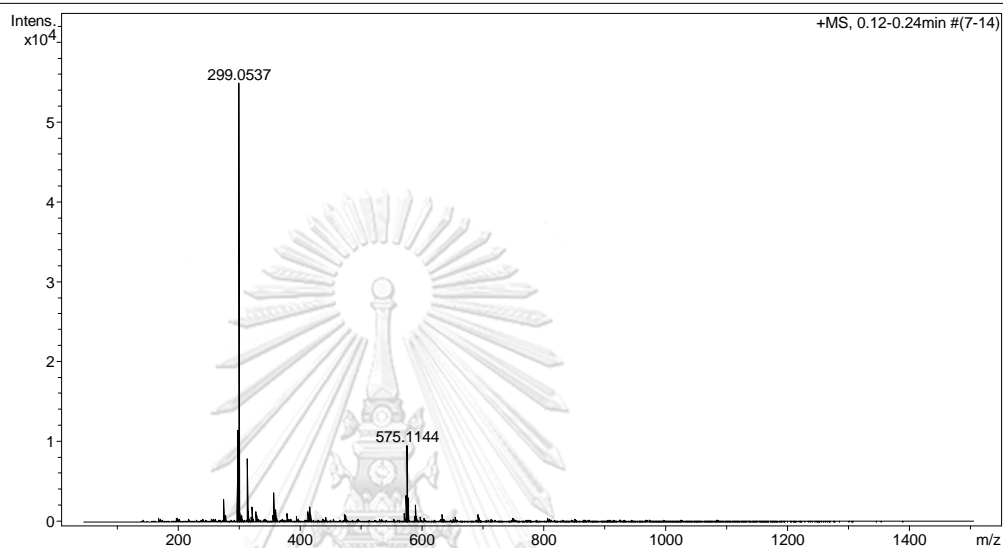


Figure A.23 HRESIMS Mass spectrum of compound 13

Generic Display Report

Analysis Info

Analysis Name D:\Data\Data Service\191217\KP-MGS-10_RB1_01_3556.d
Method nv_pos_6min_profile_wguardcol_50-1500_191021.m
Sample Name KP-MGS-10
Comment

Acquisition Date 12/17/2019 3:34:35 PM

Operator CU.
Instrument micrOTOF-Q II

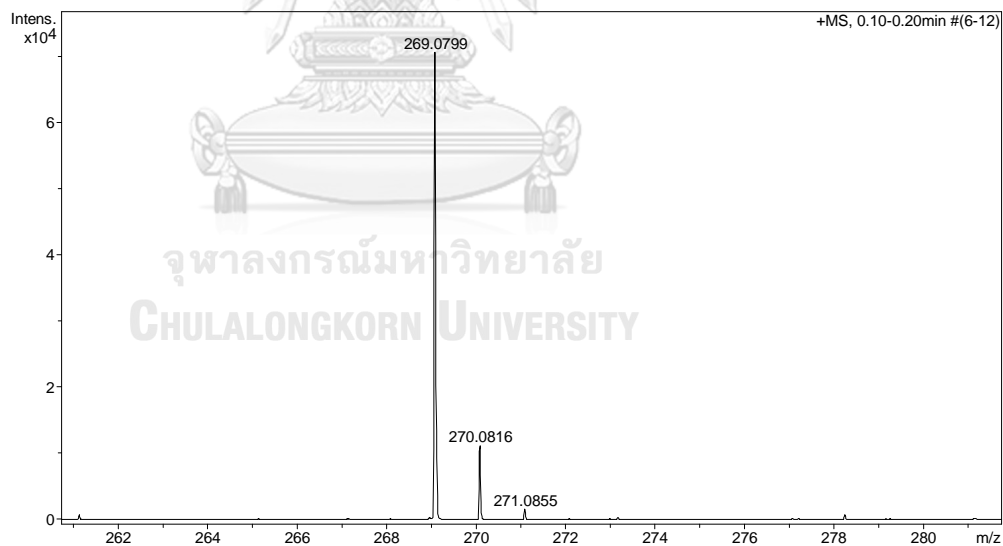
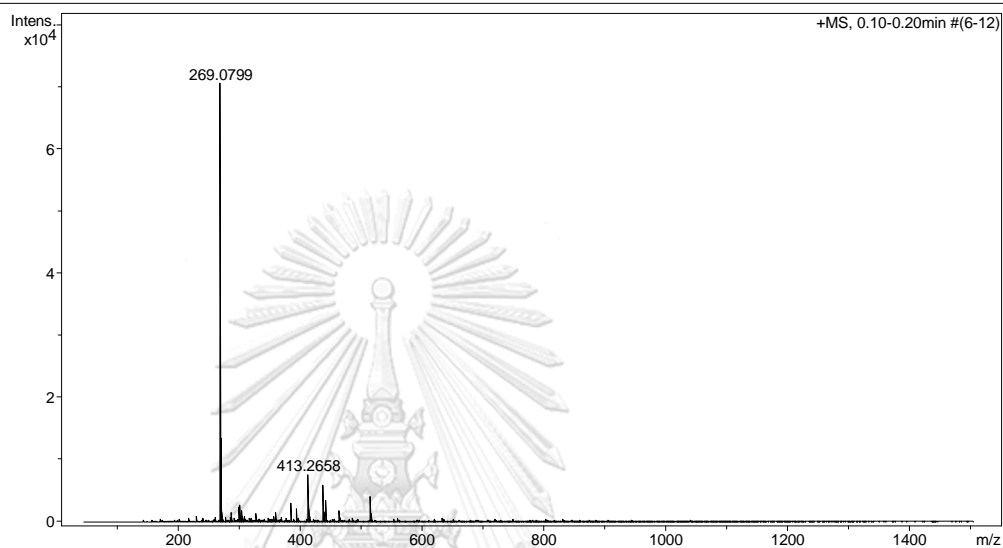


Figure A.21 HRESIMS Mass spectrum of compound 18

VITA

NAME Kedkran Koopklang

DATE OF BIRTH 25 October 1994

PLACE OF BIRTH Bangkok, Thailand

INSTITUTIONS ATTENDED Bachelor degree of Science, Department of Biotechnology,
Mahidol University

HOME ADDRESS 199/202 Manttana-Watcharapol Ramindra Rd. Tareng
Bangkhen Bangkok Thailand 140220

